Multidimensional spectroscopy with quantum light and in optical cavities

Shaul Mukamel ,Frank Schlawin,Konstantin Dorfman

University of California, Irvine

Open Quantum Systems,ICTS, Bangalore July 28, 2017

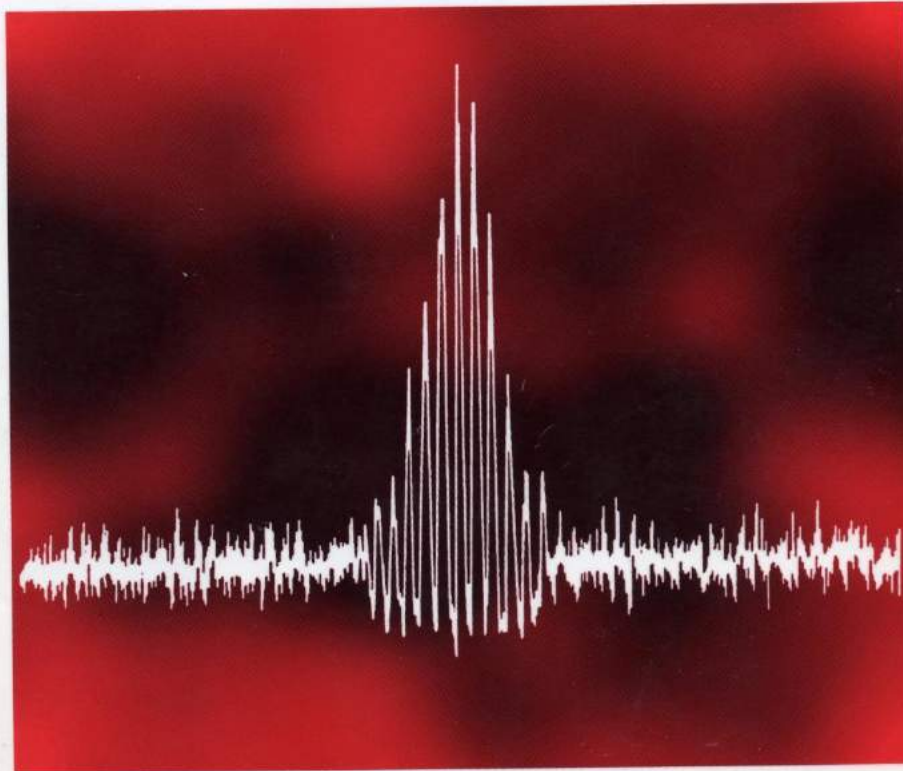# Nonlinear optical signals and spectroscopy with quantum light

Konstantin E. Dorfman,[*] Frank Schlawin,[†] and Shaul Mukamel[‡]

Department of Chemistry and Department of Physics and Astronomy, University of California, Irvine, California 92697, USA

Oxford (1995)

Postdoctoral Opportunities Theoretical and Computational Chemical Physics
UC Irvine, California, Irvine, USA

Research Topics:
a) **Computational Biophysics**
b) **Attosecond X-ray Spectroscopy of Molecules**
c) **Energy and Charge Separation in Photosynthetic Complexes Studied by Nonlinear Spectroscopy**

Professor Shaul Mukamel
Department of Chemistry
1102 Natural Sciences II
University of California, Irvine
Irvine, CA 92697-2025 USA
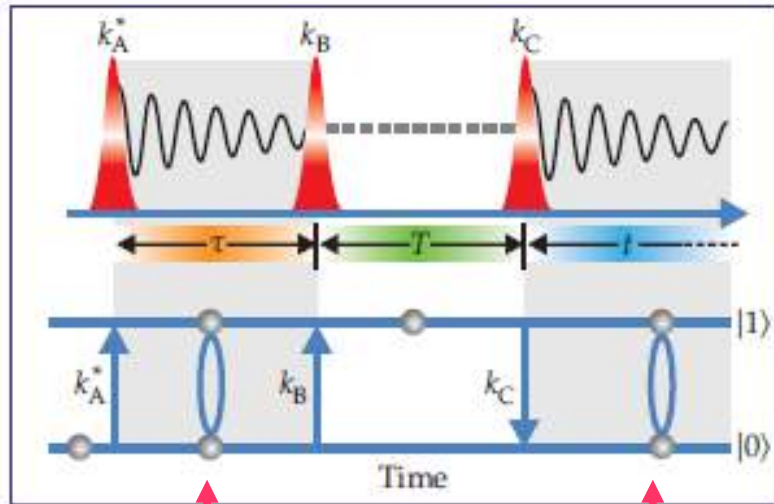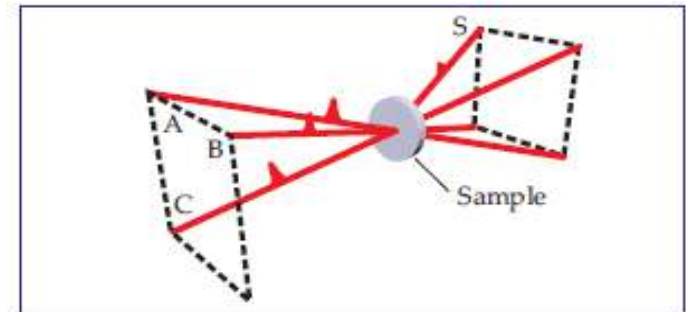**smukamel@uci.edu**

UNIVERSITY of CALIFORNIA · IRVINE

2D spectrum:

Signal (τ, t) ──────▶ Fourier transform

excited state

ground state

Coherent superposition

$\mathbf{k}_s = -\mathbf{k}_A + \mathbf{k}_B + \mathbf{k}_C$

Rephasing spectrum: conjugate pulse arrives 1st

Nonrephasing spectrum: conjugate pulse arrives 2nd

Optical multidimensional coherent SPECTROSCOPY

Steven T. Cundiff and Shaul Mukamel

Techniques developed decades ago for nuclear magnetic resonance and now adapted for the IR, visible, and UV regions of the spectrum are enabling new insights into chemical kinetics and solid-state physics.
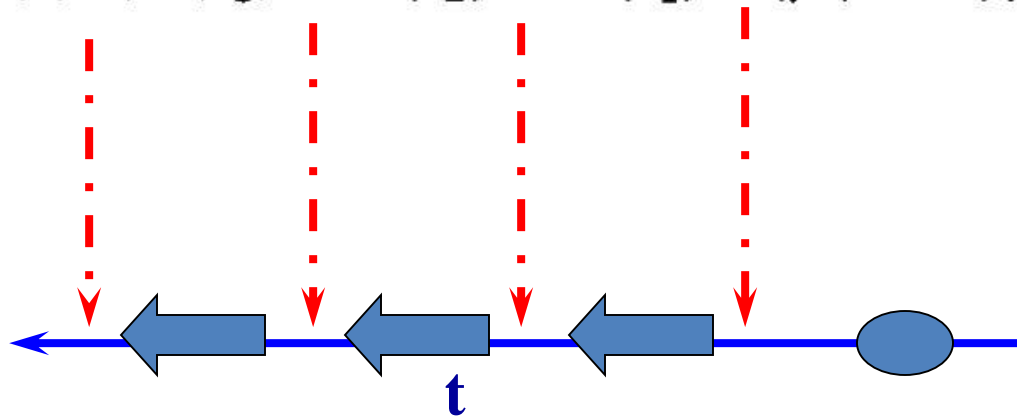
The Nonlinear Response Function

$$P(t) = Tr[V\rho(t)]$$

$$= P^{(1)}(t) + P^{(2)}(t) + P^{(3)}(t) + \cdots$$

$$P^{(3)}(t) = \int_0^\infty dt_3 \int_0^\infty dt_2 \int_0^\infty dt_1 S^{(3)}(t_3, t_2, t_1)$$

$$\times E(t - t_3) E(t - t_3 - t_2) E(t - t_3 - t_2 - t_1)$$

$$S^{(3)}(t_3, t_2, t_1) = \left(\frac{i}{\hbar}\right)^3 \langle\langle V | \mathscr{G}(t_3) \mathscr{V} \mathscr{G}(t_2) \mathscr{V} \mathscr{G}(t_1) \mathscr{V} | \rho(-\infty) \rangle\rangle$$
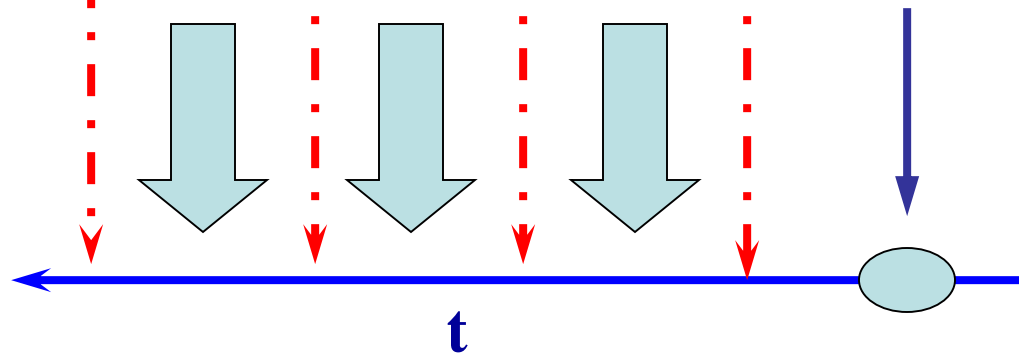
t

The Nonlinear Response Functions;classical light

$$P(\mathbf{r}, t) = P^{(1)}(\mathbf{r}, t) + P^{(2)}(\mathbf{r}, t) + P^{(3)}(\mathbf{r}, t) + ...$$

Nonlinear polarization $\quad P^{(n)}(\mathbf{r}, t) \equiv \langle\langle V | \rho^{(n)}(t) \rangle\rangle \equiv Tr[V \rho^{(n)}(t)]$

$$P^{(n)}(\mathbf{r}, t) = \int_0^\infty dt_n \int_0^\infty dt_{n-1} ... \int_0^\infty dt_1 S^{(n)}(t_n, t_{n-1}, ..., t_1)$$
$$\times E(\mathbf{r}, t - t_n) E(\mathbf{r}, t - t_n - t_{n-1}) ... E(\mathbf{r}, t - t_n - t_{n-1} ... - t_1),$$

$$S^{(3)}(t_3, t_2, t_1) = \left(\frac{i}{\hbar}\right)^3 \langle\langle V | \mathscr{G}(t_3) \mathscr{V} \mathscr{G}(t_2) \mathscr{V} \mathscr{G}(t_1) \mathscr{V} | \rho(-\infty) \rangle\rangle$$

t

Double Fourier transform

$$S_I(\Omega_1, t_2, \Omega_3) = \int_0^\infty dt_3 \int_0^\infty dt_1 e^{i\Omega_1 t_1 + i\Omega_3 t_3} S(t_1, t_2, t_3)$$
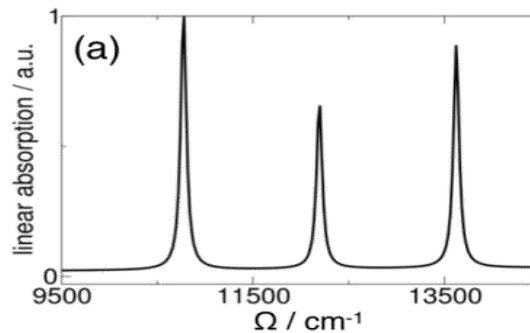
$$S_{III}(t_1, \Omega_2, \Omega_3) = \int_0^\infty dt_3 \int_0^\infty dt_2 e^{i\Omega_2 t_2 + i\Omega_3 t_3} S(t_1, t_2, t_3)$$

- Useful for displaying structural and dynamical information
- Ultrafast (50 fs) time resolution
- Probe intra- and intermolecular interactions
- Spreading transitions in multiple dimensions
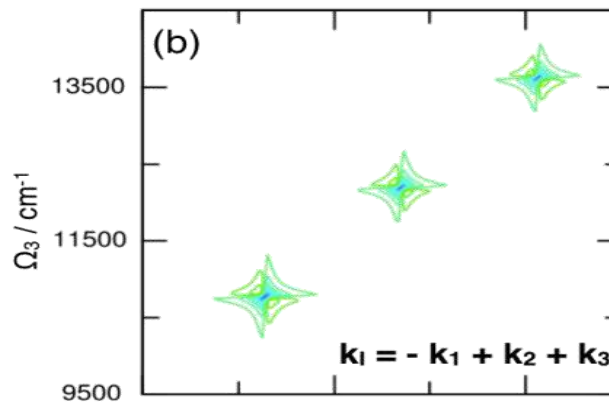- Lineshapes reveal environmental fluctuations

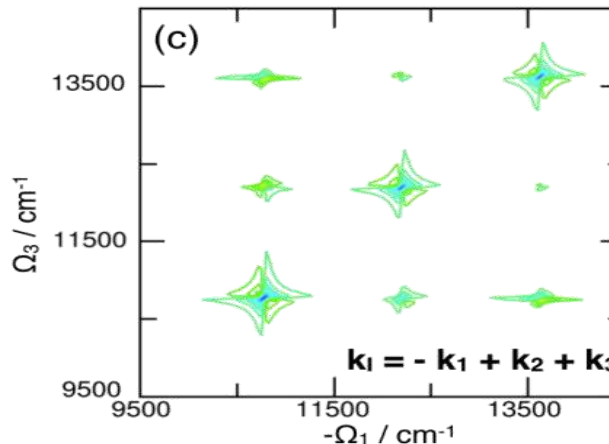# Cross Peaks in Coupled Chromophores

Linear Absorption

Photon Echo of Uncoupled Chromophores
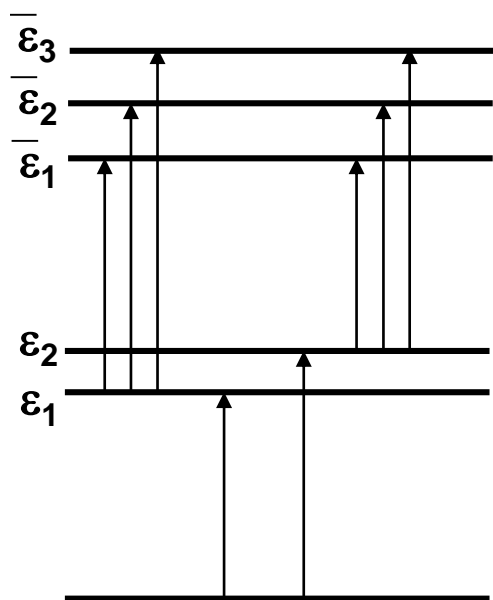
Photon Echo of Coupled Chromophores

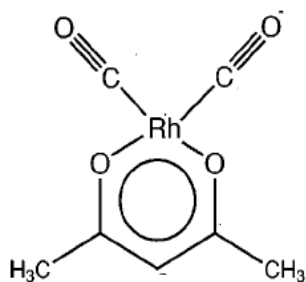
Cross peaks reveal distinct signatures of intermolecular couplings

2D spectra of coupled vibrations

Lineshapes reveal correlated fluctuations

$-1 \leq \eta \leq 1$
$\eta = -1$ Anti-correlated
$\eta = 0$ Uncorrelated
$\eta = 1$ Fully-correlated

$\varepsilon_1 = 2015 \text{ cm}^{-1}$ $\overline{\varepsilon}_1 = 4015 \text{ cm}^{-1}$
$\varepsilon_2 = 2084 \text{ cm}^{-1}$ $\overline{\varepsilon}_2 = 4078 \text{ cm}^{-1}$
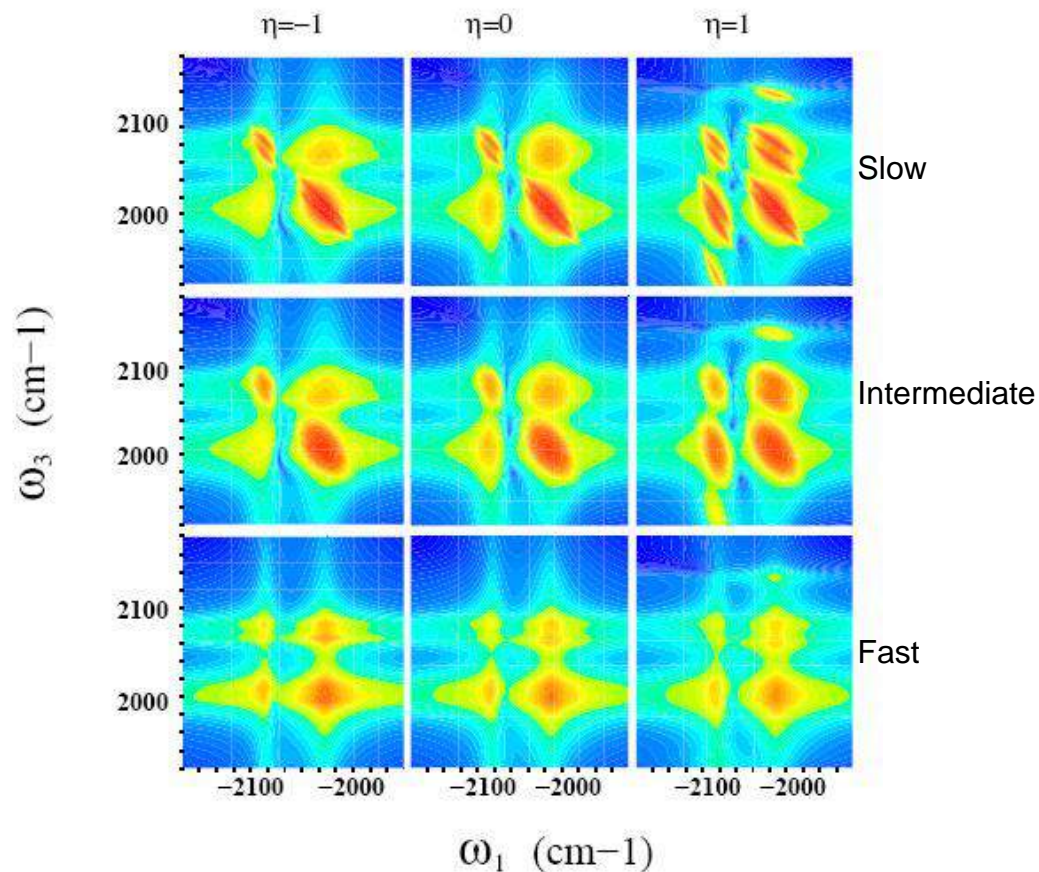 $\overline{\varepsilon}_3 = 4153 \text{ cm}^{-1}$

Wavefunction

Density Matrix

$$\frac{d\psi_j}{dt} = -\frac{i}{\hbar}\sum_m H_{jm}\psi_m$$

$$\frac{d\rho_{jk}}{dt} = -\frac{i}{\hbar}\sum_{m,n}\mathcal{L}_{jk,mn}\rho_{mn}$$

$$\mathcal{L}_{jk,mn} = H_{jm}\delta_{kn} - H_{kn}^{*}\delta_{jm}$$

N-component state vector

$$|\psi\rangle = \sum_j \psi_j |j\rangle$$

N²-component state vector

$$|\rho\rangle\rangle = \sum_{j,k} \rho_{jk} |jk\rangle\rangle$$

The Nonlinear Response to a classical field

Quantum pathways correspond to n field-matter interactions with *m+1* interactions from left and *n-m* interactions from right
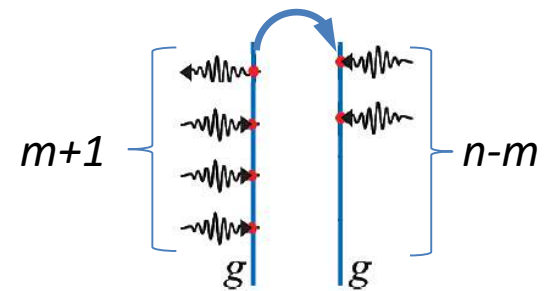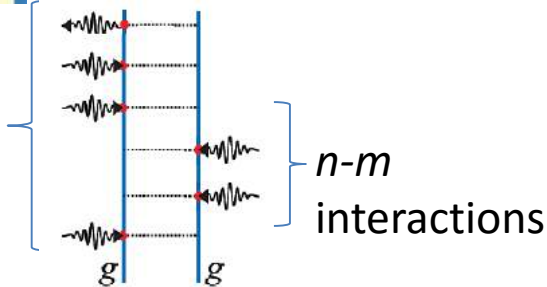
$$\mathbf{S^{(n)}(t)} = \mathrm{Tr}[\mathbf{V}\rho(t)] \qquad \mathbf{S^{(n)}(t)} = \langle \mathbf{\Psi(t)}|\mathbf{V}|\mathbf{\Psi(t)}\rangle$$

<u>2^n Ladder Diagrams</u>   <u>n+1 Loop Diagrams</u>

m+1 interactions   *n-m* interactions

m+1   *n-m*

- Move forward in time
- Density matrix ~N^2 space
- Can eliminate bath (reduced description)
- Keep track of complete time ordering (more terms)

- Move forward and backward in time
- Wave function ~N space
- Must include all degrees of freedom
- Partial time ordering (fewer terms)

Ladder Diagram Rules

1. The diagrams represent all possible interaction configurations
2. Time propagates from bottom – up.
3. Wave-vectors pointing *right* mark $+\mathbf{k}$, *left* - $\mathbf{k}$
4. Wave-vectors, pointing *into* diagram: *absorption*
5. Wave-vectors, pointing *out of* diagram: *emission*
6. Intervals between interactions: t_3, t_2, t_1
7. The state of the density matrix at any time is given by labels on vertical bars.
8. The initial and final states must be *populations.*
9. The response function is a product of density matrix propagations in each interval.
10. The amplitude of the pathway is an ordered product of transition dipoles for each interaction.
11. Odd number of interactions on the right "brings" "-" overall sign.

emission

propagation

absorption
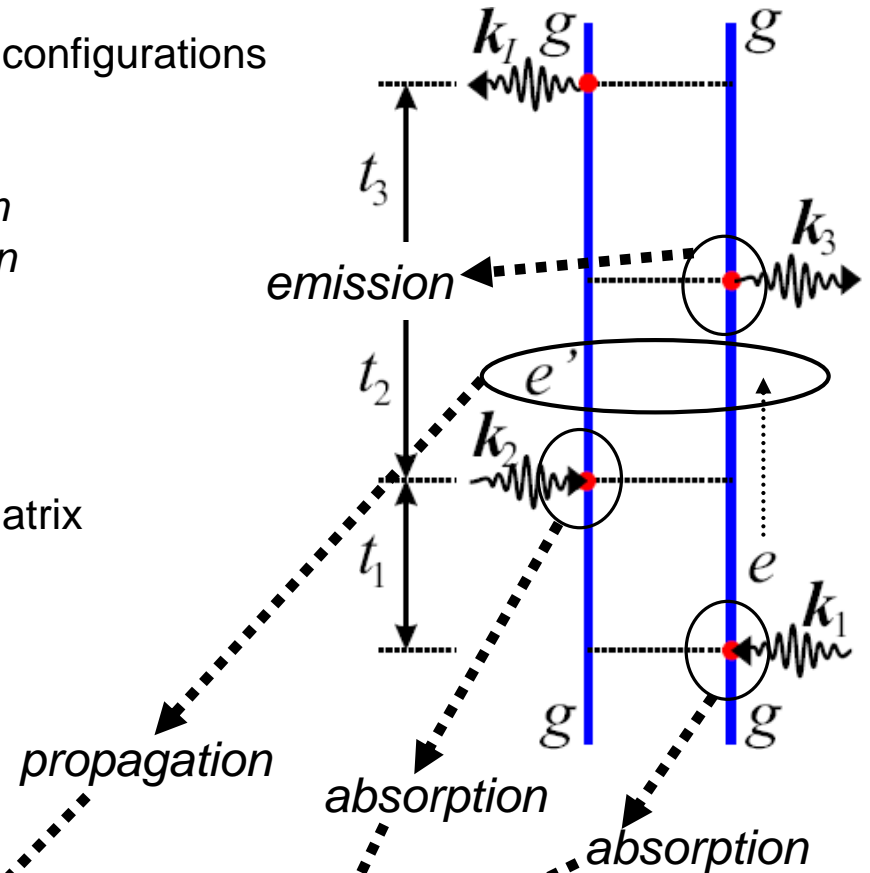
absorption

$$R_i(t_3, t_2, t_1) = \left(\frac{i}{\hbar}\right)^3 \theta(t_1)\theta(t_2)\theta(t_3)\sum_{ee'} \mu_{ge'}\mu_{eg}\mu_{e'g}\mu_{ge}$$

$$\times \exp(-i\omega_{ge}t_1 - i\omega_{e'e}t_2 - i\omega_{e'g}t_3 - \gamma_{ge}t_1 - \gamma_{e'e}t_2 - \gamma_{e'g}t_3)$$
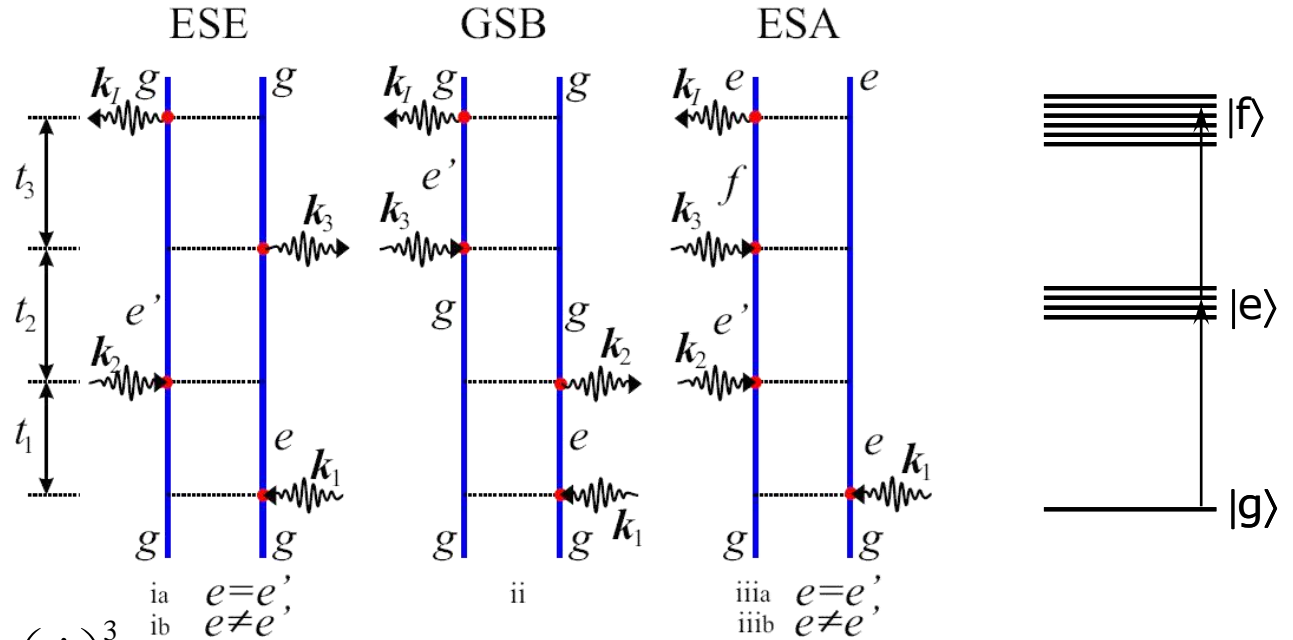
$$k_I = -k_1 + k_2 + k_3$$

ESE   GSB   ESA

ESE: excited state (stimulated) emission

GSB: ground state bleaching

ESA: excited state absorption

$$R_{k_I,\text{i}}^{(SOS)}(t_3,t_2,t_1) = \left(\frac{i}{\hbar}\right)^3 \theta(t_1)\theta(t_2)\theta(t_3)\sum_{ee'} \mu_{ge'}\mu_{eg}\mu_{e'g}\mu_{ge}\exp(-i\xi_{e'g}t_3 - i\xi_{e'e}t_2 - i\xi_{ge}t_1)$$
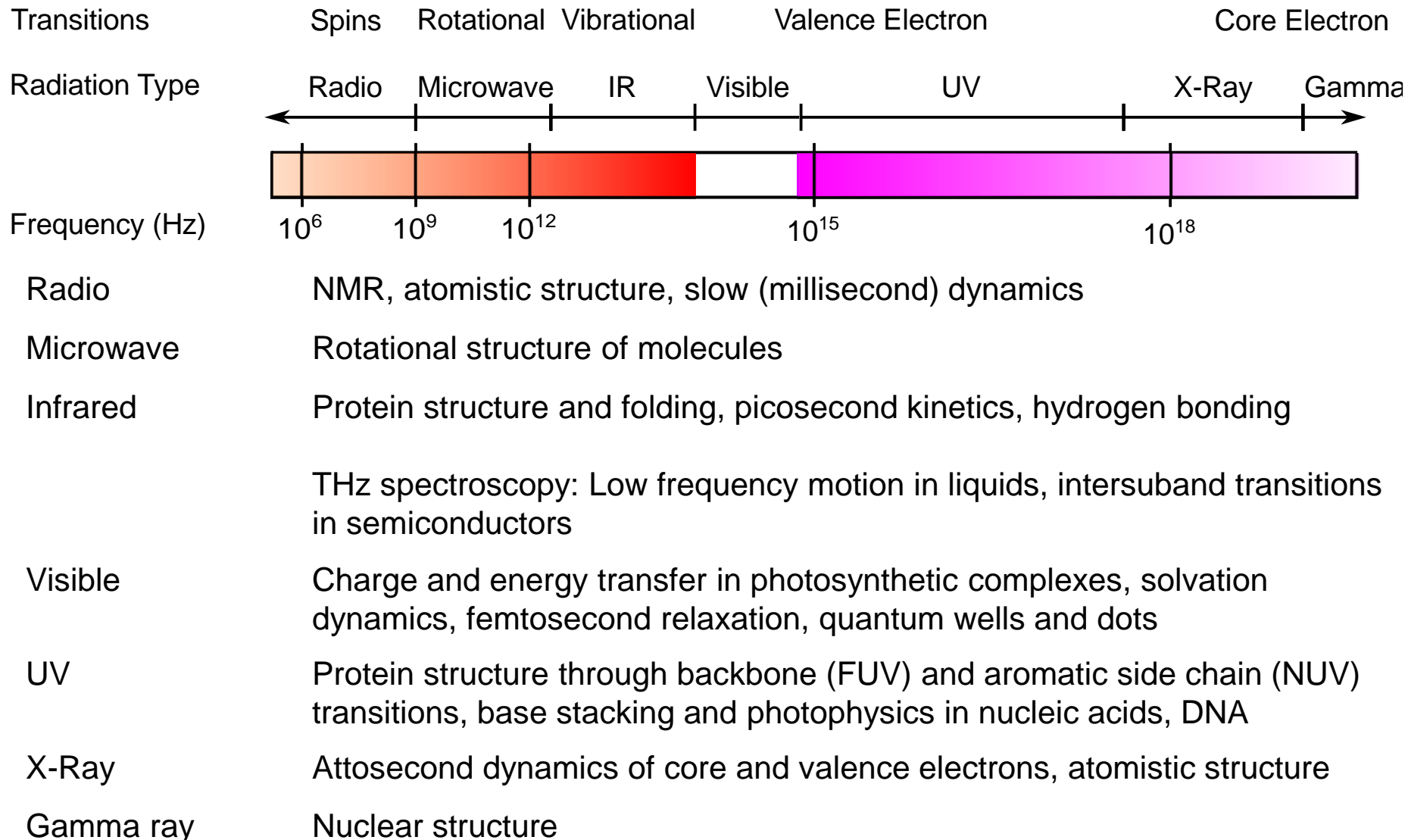
$$R_{k_I,\text{ii}}^{(SOS)}(t_3,t_2,t_1) = \left(\frac{i}{\hbar}\right)^3 \theta(t_1)\theta(t_2)\theta(t_3)\sum_{ee'} \mu_{ge'}\mu_{e'g}\mu_{eg}\mu_{ge}\exp(-i\xi_{e'g}t_3 - i\xi_{ge}t_1)$$

$$R_{k_I,\text{iii}}^{(SOS)}(t_3,t_2,t_1) = -\left(\frac{i}{\hbar}\right)^3 \theta(t_1)\theta(t_2)\theta(t_3)\sum_{ee'f} \mu_{ef}\mu_{fe'}\mu_{e'g}\mu_{ge}\exp(-i\xi_{fe}t_3 - i\xi_{e'e}t_2 - i\xi_{ge}t_1)$$
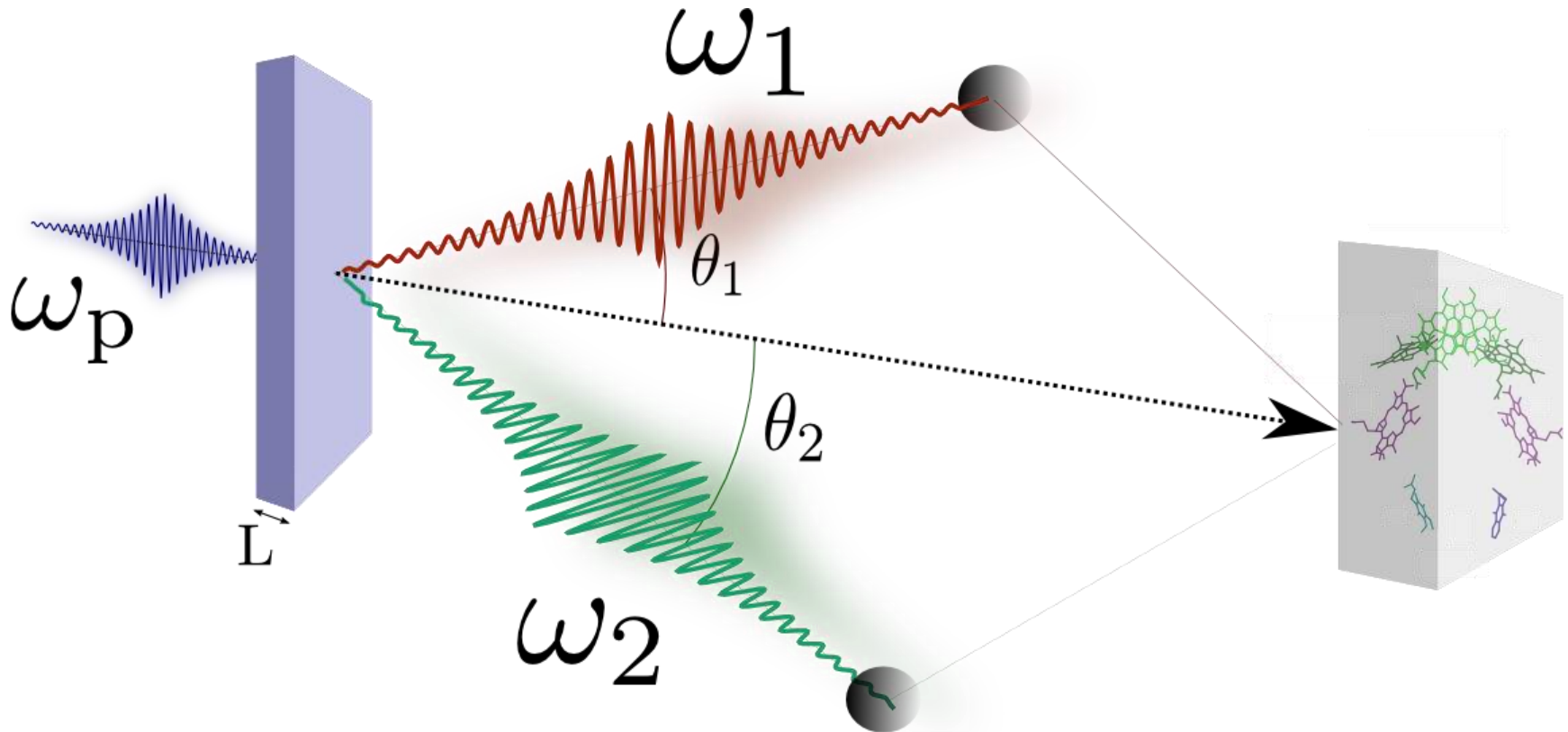
$$\xi_{ab} \equiv \omega_{ab} - i\gamma_{ab}$$

Multidimensional Spectroscopy

Transitions		Spins	Rotational	Vibrational		Valence Electron			Core Electron
Radiation Type		Radio	Microwave	IR	Visible	UV		X-Ray	Gamma

Frequency (Hz) 10^6 10^9 10^{12} 10^{15} 10^{18}

Radio	NMR, atomistic structure, slow (millisecond) dynamics
Microwave	Rotational structure of molecules
Infrared	Protein structure and folding, picosecond kinetics, hydrogen bonding
	THz spectroscopy: Low frequency motion in liquids, intersuband transitions in semiconductors
Visible	Charge and energy transfer in photosynthetic complexes, solvation dynamics, femtosecond relaxation, quantum wells and dots
UV	Protein structure through backbone (FUV) and aromatic side chain (NUV) transitions, base stacking and photophysics in nucleic acids, DNA
X-Ray	Attosecond dynamics of core and valence electrons, atomistic structure
Gamma ray	Nuclear structure

Generation of entangled photon pairs

$$|\psi\rangle = \int d\omega_a \int d\omega_b A_p(\omega_a + \omega_b - \omega_1 - \omega_2) sinc\left(\frac{\Delta k(\omega_a, \omega_b)L}{2}\right) a^\dagger(\omega_a)a^\dagger(\omega_b)|0\rangle$$

A pump photon is down-converted into two entangled photons
in a birefingent crystal, and the photon pair is then directed onto the sample.

Applications of entangled photons

General applications

- Quantum information processing

- Communications

- Lithography

- Metrology

Horodecki, R., Horodecki, P., Horodecki, M. & Horodecki, K. Rev. Mod. Phys. 81, 865–942 (2009).
Lvovsky, A. I. & Raymer, M. G. Rev. Mod. Phys. 81, 299–332 (2009).
Pan, J.-W. et al. Rev. Mod. Phys. 84, 777–838 (2012).
Gisin, N., Ribordy, G., Tittel, W. & Zbinden, H Rev. Mod. Phys. 74, 145–195 (2002).
Boyd, R. W. & Bentley, S. J. J. Modern Opt. 53, 713–718 (2006).
Giovannetti, V., Lloyd, S. & Maccone, L. Nat. Photon. 5, 222–229 (2011).

Spectroscopy applications

- Increased signal strength at low intensity

- New control parameters to disentangle complex spectra

- Control of exciton distribution

M. Kira, S. W. Koch, R. Smith, A. E. Hunter, and S. Cundiff, Nat. Phys. 7, 799 (2011).
J. Javanainen and P. L. Gould, Phys. Rev. A 41, 5088 (1990).
D.-I. Lee and T. Goodson, J. Phys. Chem. B 110, 25582 (2006).
A.   R. Guzman, M. R. Harpham, O. Suzer, M. M. Haley, and T. G. Goodson, J. Am. Chem. Soc. 132, 7840 (2010).
H.-B. Fei, B. M. Jost, S. Popescu, B. E. A. Saleh, and M. C. Teich, Phys. Rev. Lett. 78, 1679 (1997).
J. Peˇrina, Jr., B. E. A. Saleh, andM. C. Teich, Phys. Rev. A 57, 3972 (1998).
B. E. A. Saleh, B. M. Jost, H.-B. Fei, and M. C. Teich, Phys. Rev. Lett. 80, 3483 (1998).
L. Upton, M. Harpham, O. Suzer, M. Richter, S. Mukamel, and T. Goodson, J. Phys. Chem. Lett. 4, 2046 (2013).
H. Oka, J. Chem. Phys. 134, 124313 (2011).
H. Oka, J. Chem. Phys. 135, 164304 (2011).
M. G. Raymer, A. H. Marcus, J. R.Widom, and D. L. P. Vitullo, J. Phys. Chem. B 117, 15559 (2013).

Spectroscopy with quantum light

Entangled-Photon Virtual-State Spectroscopy

Bahaa E. A. Saleh, Bradley M. Jost, Hong-Bing Fei, and Malvin C. Teich*

*Quantum Imaging Laboratory, Department of Electrical and Computer Engineering,
Boston University, Boston, Massachusetts 02215*

25582

THE JOURNAL OF
PHYSICAL B
CHEMISTRY
LETTERS

Entangled Photon Absorption in an Organic Porphyrin Dendrimer

Dong-Ik Lee and Theodore Goodson III*

Department of Chemistry and Applied Physics, University of Michigan, Ann Arbor, Michigan 48109

nature physics

ARTICLES

Quantum spectroscopy with Schrödinger-cat states

M. Kira[1]*, S. W. Koch[1], R. P. Smith[2], A. E. Hunter[2] and S. T. Cundiff[2]

Two photon absorption of quantum light
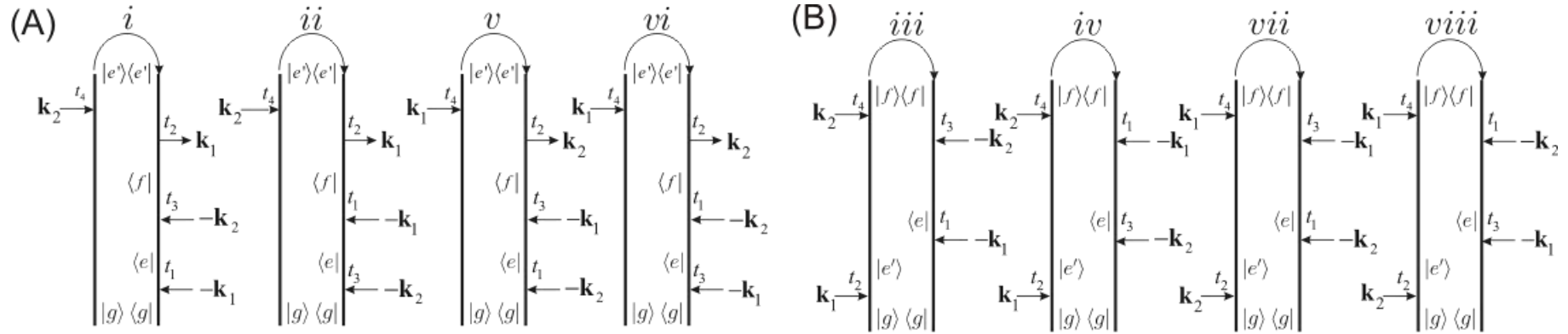
$$S_{TPA}^{Sym}(\omega_1, \omega_2) = \frac{2N\pi}{\Omega} \frac{1}{2T} \int_{-T}^{T} dt_4 \, \mathfrak{J} \frac{i^3}{3!} \int_{-\infty}^{\infty} \int_{-\infty}^{\infty} \int_{-\infty}^{\infty} dt_3 dt_2 dt_1$$

i $[\theta(t_4 t_2)\theta(t_2 t_3)\theta(t_3 t_1)\langle V(t_1)V(t_3)V^\dagger(t_2)V^\dagger(t_4)\rangle\langle E_1^\dagger(t_1)E_2^\dagger(t_3)E_1(t_2)E_2(t_4)\rangle +$

ii $+\theta(t_4 t_2)\theta(t_2 t_1)\theta(t_1 t_3)\langle V(t_3)V(t_1)V^\dagger(t_2)V^\dagger(t_4)\rangle\langle E_2^\dagger(t_3)E_1^\dagger(t_1)E_1(t_2)E_2(t_4)\rangle +$

iii $+\theta(t_4 t_2)\theta(t_4 t_3)\theta(t_3 t_1)\langle V(t_1)V(t_3)V^\dagger(t_4)V^\dagger(t_2)\rangle\langle E_1^\dagger(t_1)E_2^\dagger(t_3)E_2(t_4)E_1(t_2)\rangle +$

iv $+\theta(t_4 t_2)\theta(t_4 t_1)\theta(t_1 t_3)\langle V(t_3)V(t_1)V^\dagger(t_4)V^\dagger(t_2)\rangle\langle E_2^\dagger(t_3)E_1^\dagger(t_1)E_2(t_4)E_1(t_2)\rangle +$

     $+\{\mathbf{k}_1 \leftrightarrow \mathbf{k}_2\}]$

     $v, vi, vii, viii$

UNIVERSITY *of* CALIFORNIA · IRVINE

The third order nonlinear optical signals are governed by a four-point correlation function of the electric field

$$\left\langle E^\dagger(t)E^\dagger(\tau_1)E(\tau_2)E(\tau_3)\right\rangle$$

Classical laser light:

$$= E^*(t)E^*(\tau_1)E(\tau_2)E(\tau_3)$$

gives the classical response function

Entangled photons:

$$= \left\langle\psi\right|E^\dagger(t)E^\dagger(\tau_1)\left|0\right\rangle$$

$$\left\langle 0\right|E(\tau_2)E(\tau_2)\left|\psi\right\rangle$$

Stochastic light:

$$= \left\langle E^\dagger(t)E(\tau_2)\right\rangle\left\langle E^\dagger(\tau_1)E(\tau_3)\right\rangle$$

$$+ \left\langle E^\dagger(t)E(\tau_3)\right\rangle\left\langle E^\dagger(\tau_1)E(\tau_2)\right\rangle$$

- ## Entangled light (parametric down conversion - PDC)

Twin photon state

$$|\psi\rangle = \int_{-\infty}^{\infty} \frac{d\omega_1}{2\pi} \frac{d\omega_2}{2\pi} \Phi(\omega_1, \omega_2) a_{\omega_1}^\dagger a_{\omega_2}^\dagger |0\rangle$$

Two-photon amplitude

$$\Phi(\omega_1, \omega_2) = A_p(\omega_1 + \omega_2)\text{sinc}\left[\frac{\omega_1 - \omega_p}{2}T_{1e} + \frac{\omega_2 - \omega_p}{2}T_{2e}\right] e^{i\frac{\omega_1 - \omega_p}{2}T_{1e} + i\frac{\omega_2 - \omega_p}{2}T_{2e}} + (T_{1e} \leftrightarrow T_{2e})$$
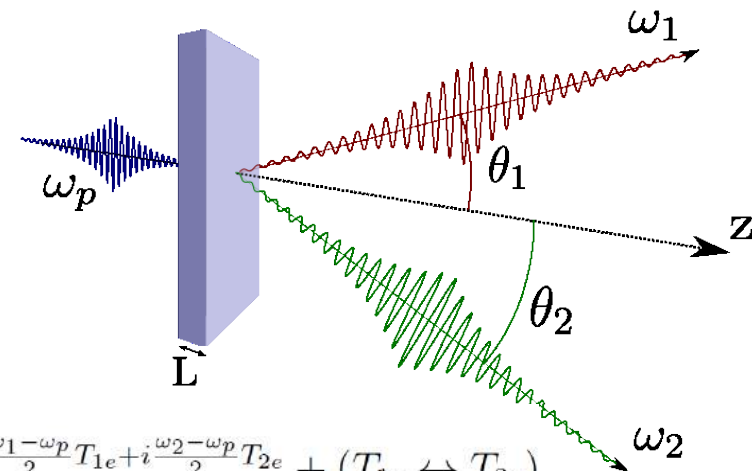
T_{je} time delays acquired by beams during propagation through the nonlinear crystal

$$A_p(\omega) = A_0/[\omega - 2\omega_p + i\sigma_p] \quad \text{Classical pump envelope}$$

$$\langle E^\dagger(\omega_d) E^\dagger(\omega_a + \omega_b - \omega_d) E(\omega_b) E(\omega_a)\rangle = \Phi^*(\omega_a + \omega_b - \omega_d, \omega_d)\Phi(\omega_a, \omega_b)$$

ω_1 , ω_2 broad band and $\omega_1 + \omega_2 = \omega_p$ narrowband

Frequency arguments of different modes are mixed

two photon absorption of entangled light

Two-photon absorption of porphyrin dendrimer with different entanglement times
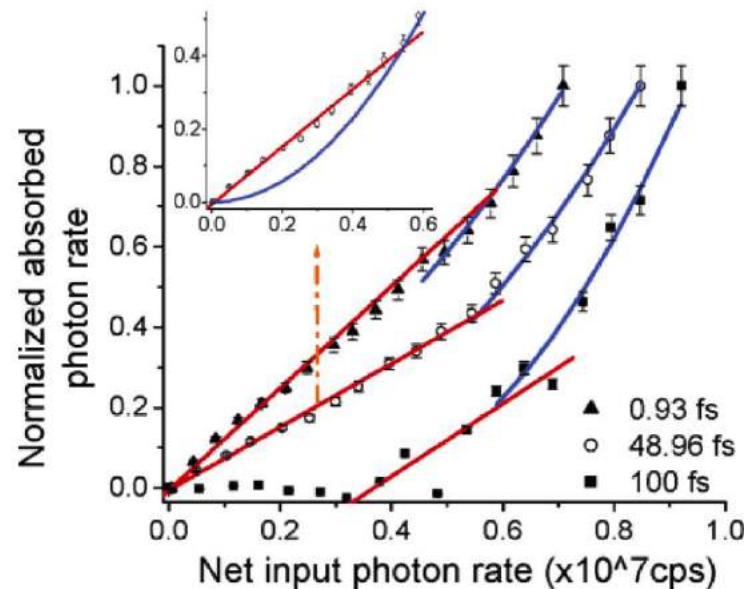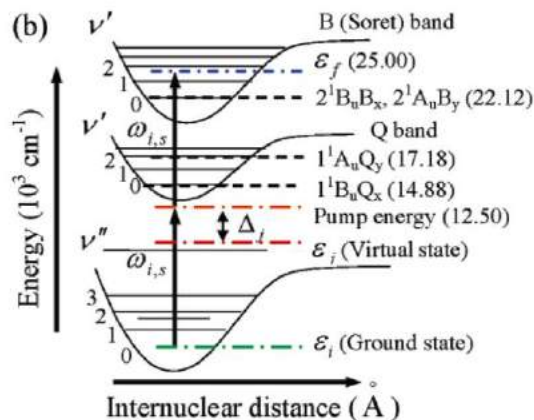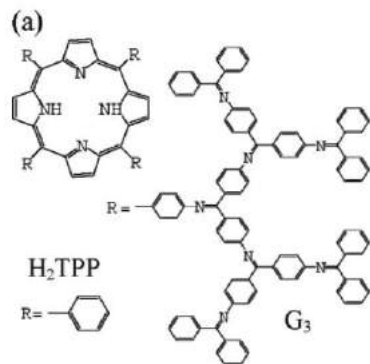
D. Lee and T. Goodson III (2006);

- Photons come in pairs generated simultaneously
- At low intensity the photon pairs are temporally well separated, and the absorption induced by light beam composed by two photons of the same pair (entangled).
- At higher intensities it becomes statistically more plausible for the two photons to come from different pairs, which are not entangled, and the classical quadratic scaling is recovered.

B.E.A. Saleh, A.F. Abouraddy, A.V. Sergienko, and M.C. Teich (2000);
B. Dayan, A. Pe'er, A.A. Friesem, Y. Silberberg (2005);

Nonlinear Optical Signals

$$\langle 0 | E(\omega') E(\omega) | \psi \rangle \propto e^{-(\omega - \omega' - \delta\omega)^2 T^2} e^{-(\omega + \omega' - \omega_1 - \omega_2)^2 / \sigma^2}$$

A.B. U'Ren, K. Banaszek and I.A. Walmsley, Quantum Info. Comput. (2003)

$\propto 1/T$

$\propto \sigma$

9000   11 000   13 000   15 000   22 000   24 000   26 000

Signal-/Idler-spectrum $\omega_{1/2}$ Pump frequency ω_p
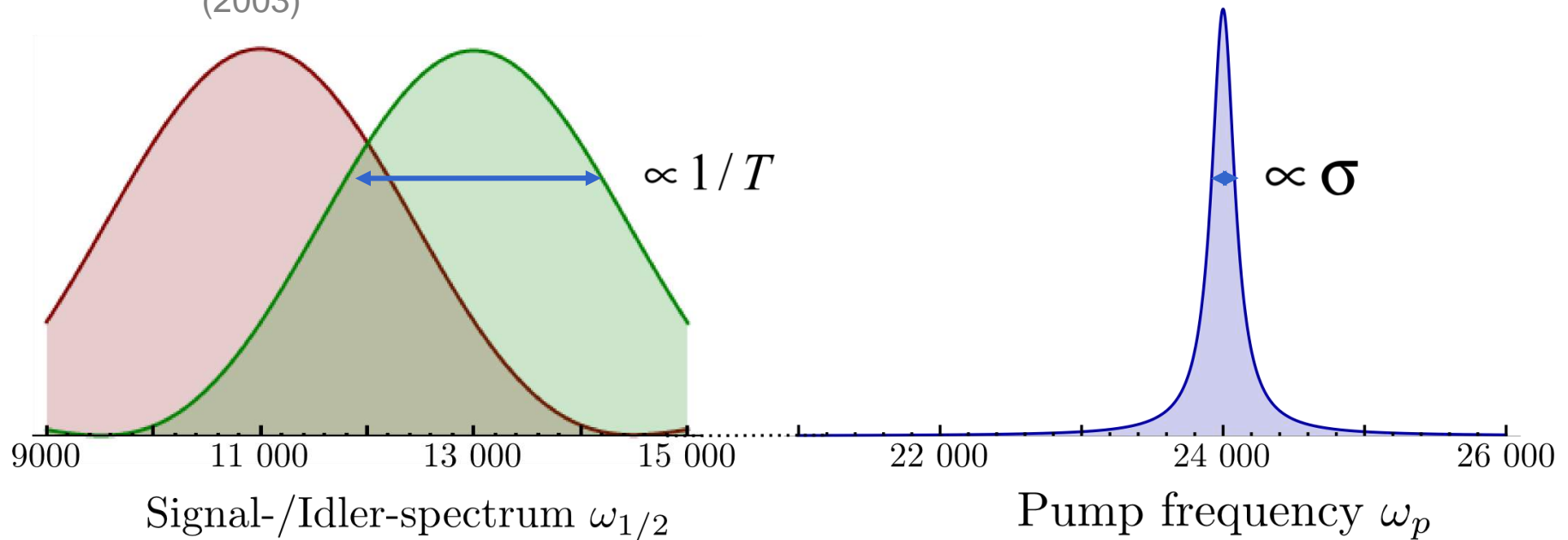
Bandwidth of the individual beams may be very broad
– given by the "entanglement time" T

The sum of frequencies of an entangled pair is given by the width
of the pump pulse, and may be a lot smaller than the bandwidth of the beams.

Correlation function of entangled photons

The two photon frequencies are strongly anti-correlated:

$$\langle 0|E(\omega')E(\omega)|\psi\rangle$$
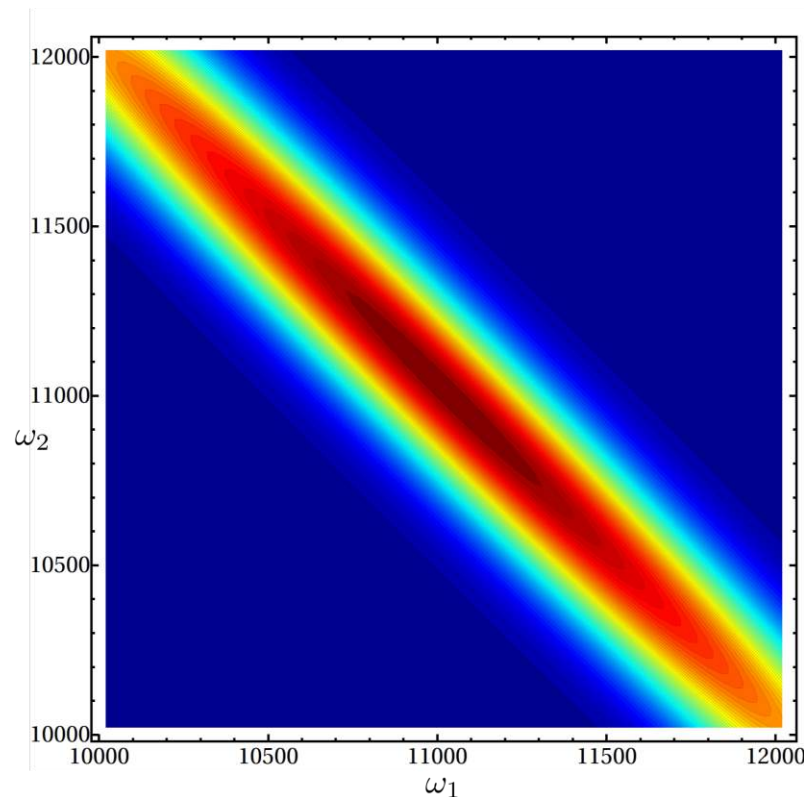
$$\propto e^{-(\omega-\omega'-\delta\omega)^2 T^2}$$

$$\times e^{-(\omega+\omega'-\omega_1-\omega_2)^2/\sigma^2}$$

Correlation function of entangled photons

The two photon frequencies are strongly anti-correlated:

the individual beams are very broadband,

but their sum of their
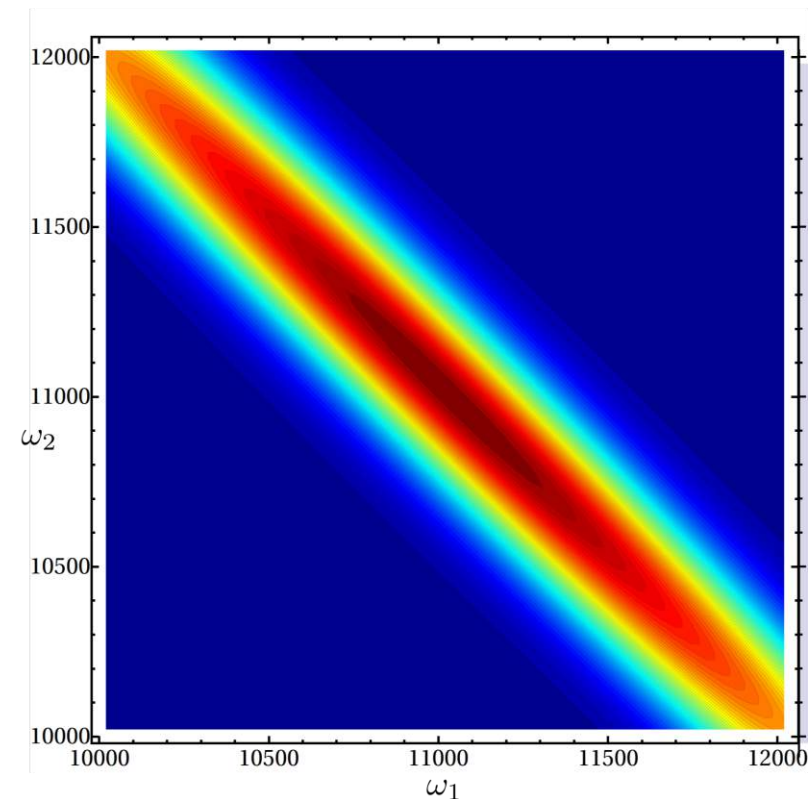
defined.

$$\langle 0 | E(\omega') E(\omega) | \psi \rangle$$

$$\propto e^{-(\omega - \omega' - \delta\omega)^2 T^2}$$

$$\times e^{-(\omega + \omega' - \omega_1 - \omega_2)^2 / \sigma^2}$$

Correlation function of entangled photons

The two photon frequencies are strongly anti-correlated:

the individual beams have a broad bandwidth,

but the sum of their frequencies is sharply defined.

$$\langle 0|E(\omega')E(\omega)|\psi\rangle$$
$$\propto e^{-(\omega-\omega'-\delta\omega)^2 T^2}$$
$$\times e^{-(\omega+\omega'-\omega_1-\omega_2)^2/\sigma^2}$$
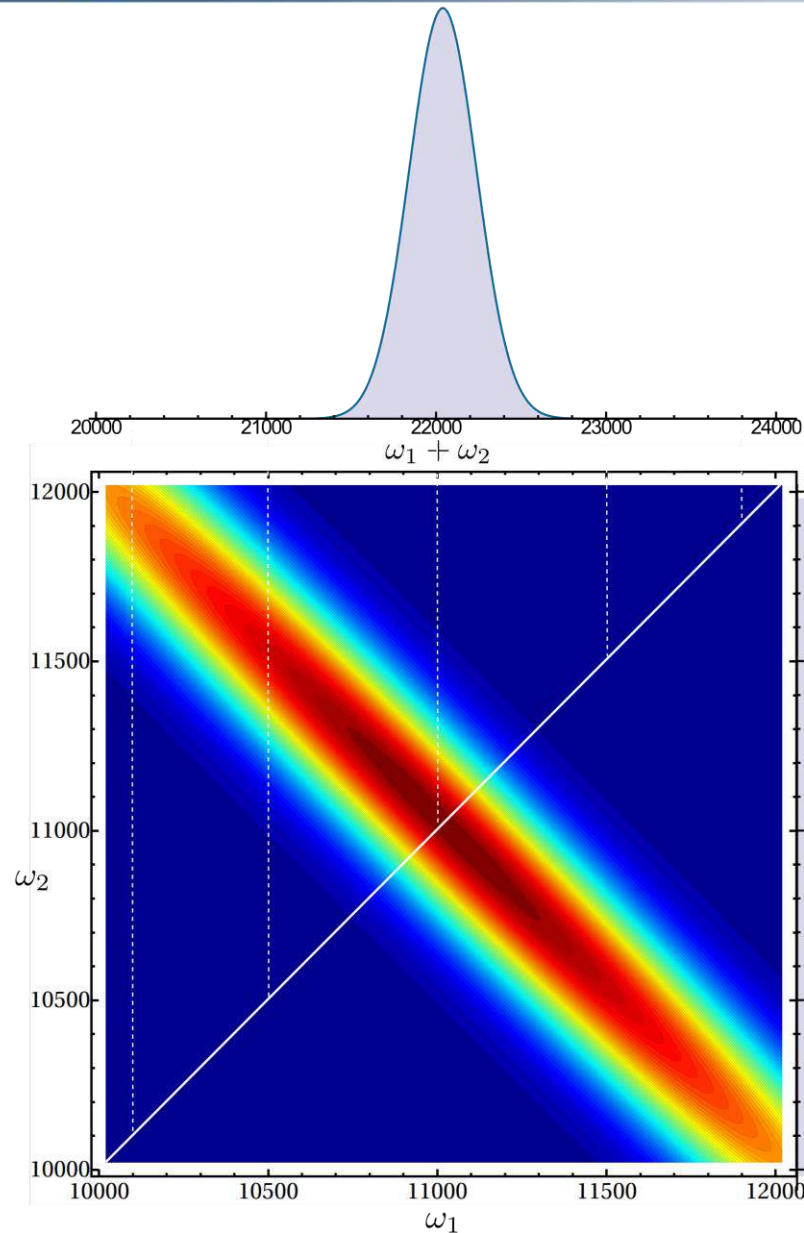
Manipulating two- exciton states in Photosynthetic complexes with entangled light

Two-photon absorption with Quantum light

The crossover can be investigated in a simple three-level system. Again, we calculate the population in the doubly-excited state:

$$p_f(t; \Gamma) = \left\langle \mathcal{T} B_f(t) \exp\left[-\frac{i}{\hbar} \int^t d\tau H_{int}(\tau) \right] \right\rangle$$

$$B_f(t) = |f(t)\rangle\langle f(t)|$$

$$H_{int}(t) = E(t)V^\dagger(t) + h.c.$$

To leading order, it is given by the unrestricted loop diagram:

$$p_f(t; \Gamma) = \left(-\frac{i}{\hbar}\right)^4 \int_{-\infty}^{\infty} d\tau_4 \int_{-\infty}^{\infty} d\tau_3 \int_{-\infty}^{\infty} d\tau_2 \int_{-\infty}^{\infty} d\tau_1 \left\langle \mathcal{T} B_f(t) V(\tau_4) V(\tau_3) V^\dagger(\tau_2) V^\dagger(\tau_1) \right\rangle$$

$$\times \left\langle \mathcal{T} E^\dagger(\tau_4) E^\dagger(\tau_3) E(\tau_2) E(\tau_1) \right\rangle$$

The pump-probe signal with quantum fields

Third-order frequency-dispersed pump-probe signals are given by the third-order polarization of the matter induced by quantum light

$$S_{TPA}(\omega, \Gamma) = \frac{2}{\hbar}\Im\langle E^\dagger(\omega)P^{(3)}(\omega)\rangle$$

$$S_1(\omega, \Gamma) = \frac{2}{\hbar}\Im\int d\omega_a \int d\omega_b$$

$$\times\langle VG(\omega)VG(\omega_a + \omega_b)V^\dagger G(\omega_a)V^\dagger\rangle$$

$$\times\langle E^\dagger(\omega)E^\dagger(\omega_a + \omega_b - \omega)E(\omega_b)E(\omega_a)\rangle$$

$$S_2(\omega, \Gamma) = \frac{2}{\hbar}\Im\int d\omega_a \int d\omega_b$$

$$\times\langle VG^\dagger(\omega_a + \omega_b - \omega)VG(\omega_a + \omega_b)V^\dagger G(\omega_a)V^\dagger\rangle$$

$$\times\langle E^\dagger(\omega)E^\dagger(\omega_a + \omega_b - \omega)E(\omega_b)E(\omega_a)\rangle$$
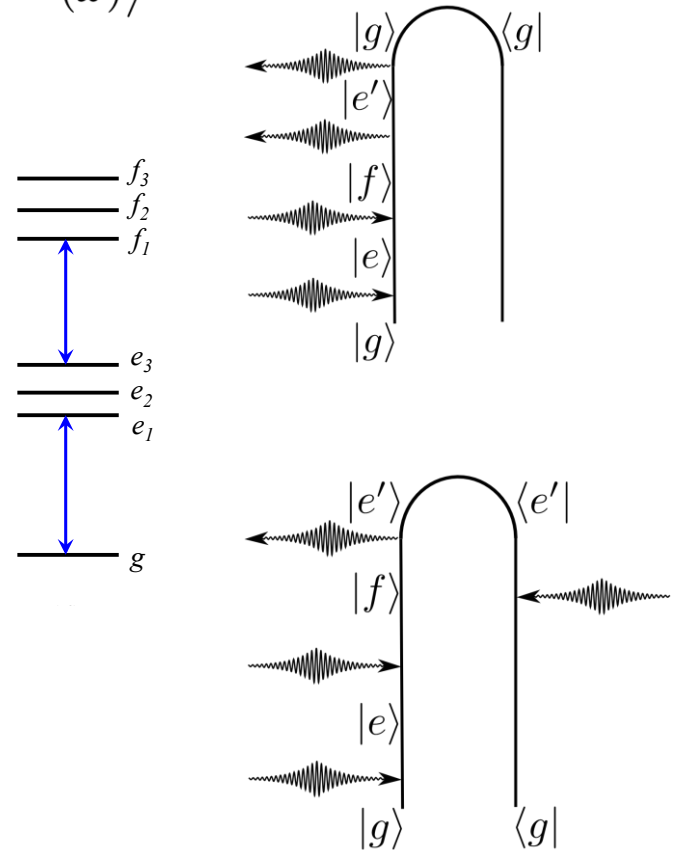
Third-order spectra depend on the <u>four-point</u> correlation function

We can expect to see an influence of entanglement on nonlinear signals!

Application to the Bacterial Reaction Centers
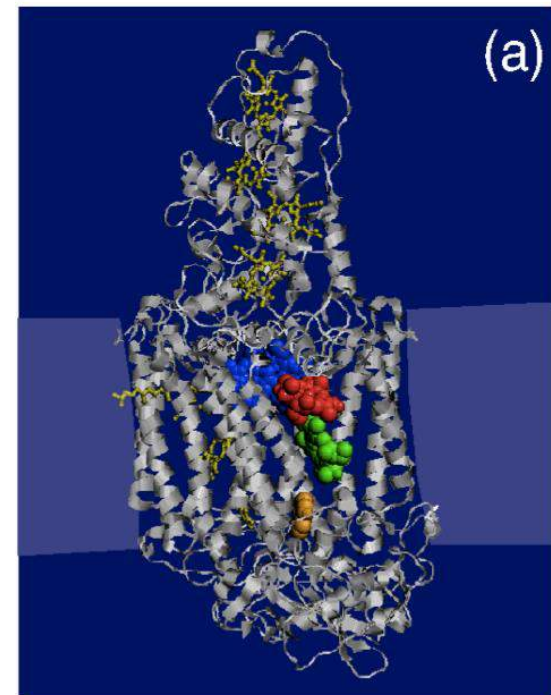
X-ray structures:
Deisenhofer/Michel
Science 1989
Deisenhofer/Epp J. Mol.
Biol.1995
Roszak Science 2003
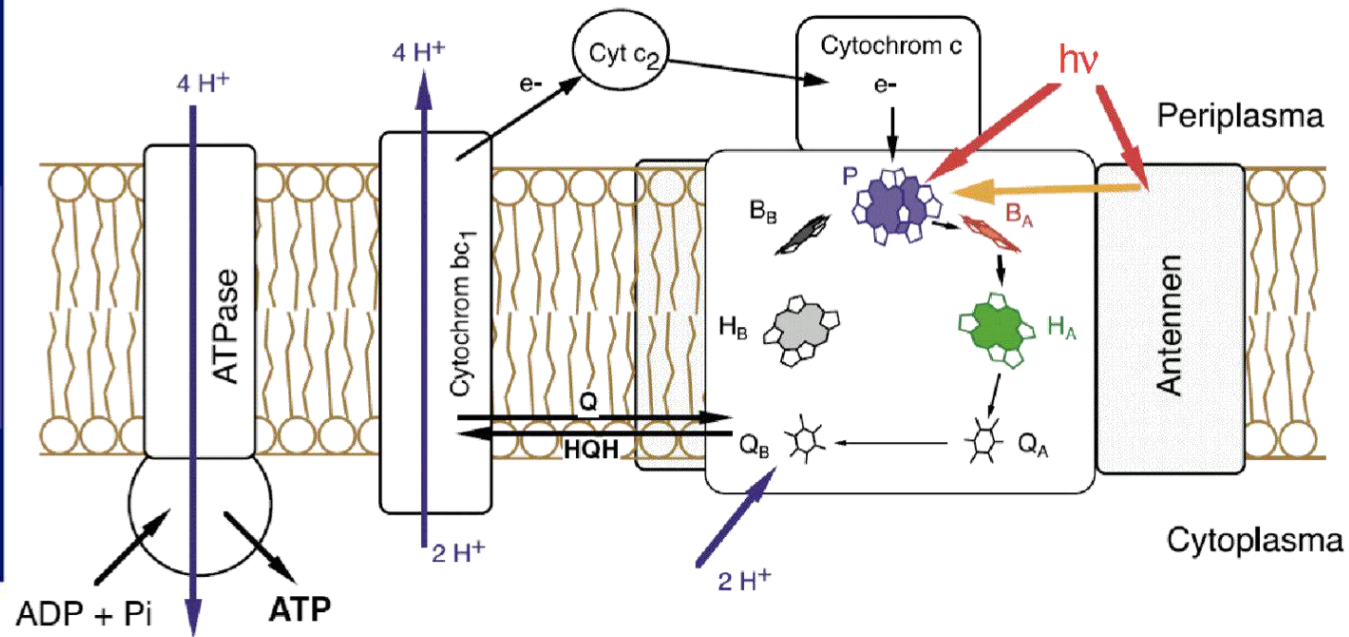
transformation of light energy to chemical energy on a femtosecond to picosecond timescale

photon converson efficiency: > 95 %

2D-spectroscopy: resolve co-factor specific energy relaxation and charge separation

Electron Transfer: Population Dynamics

RC model
(transfer rates in exciton basis)
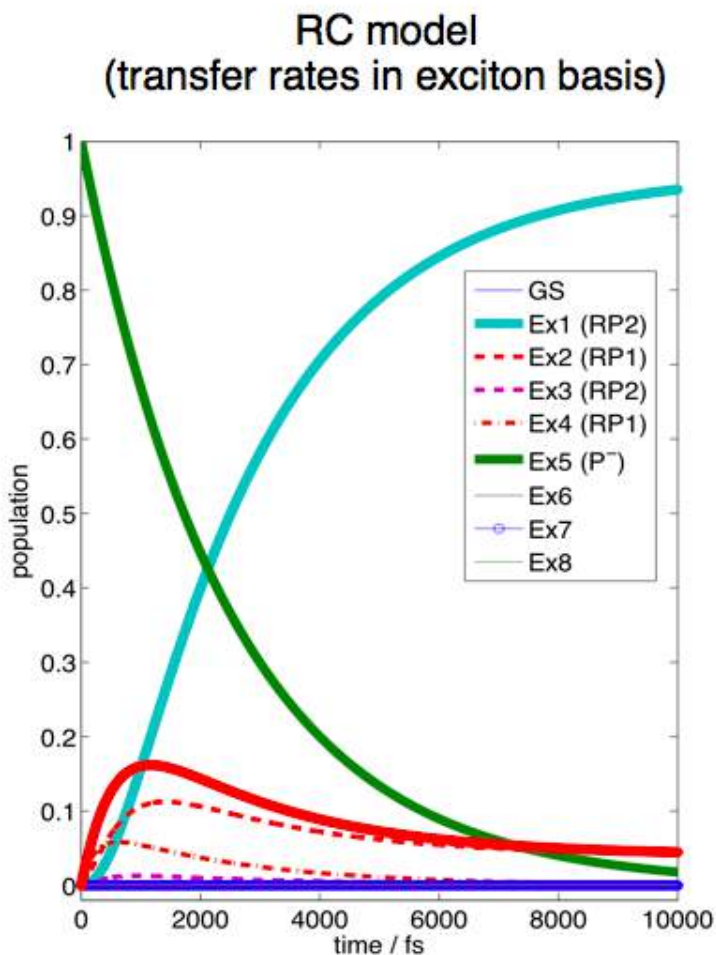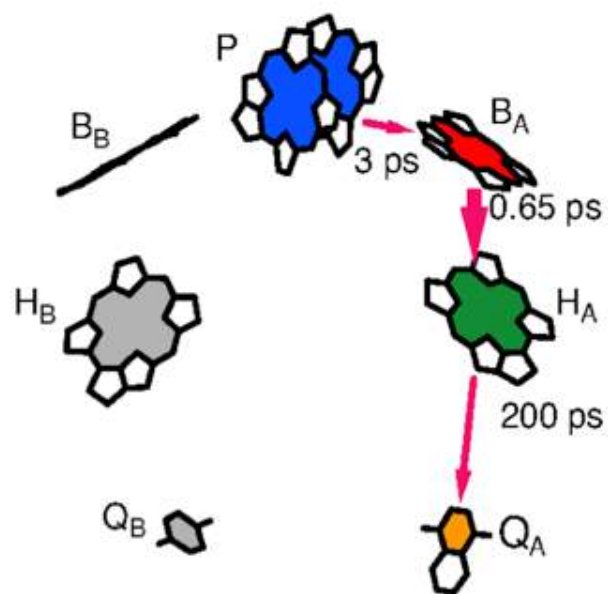
stepwise Electron transfer:
P^- -> BCl_L -> BP_L

initial charge separation: 3 ps

secondary ET: sub-ps

transiently populated RP1 (18 %)

initial state: special pair P^-

Exp:
Holzapfel et al. PNAS, **87**, 5168 (1990)

Application to the bacterial reaction center
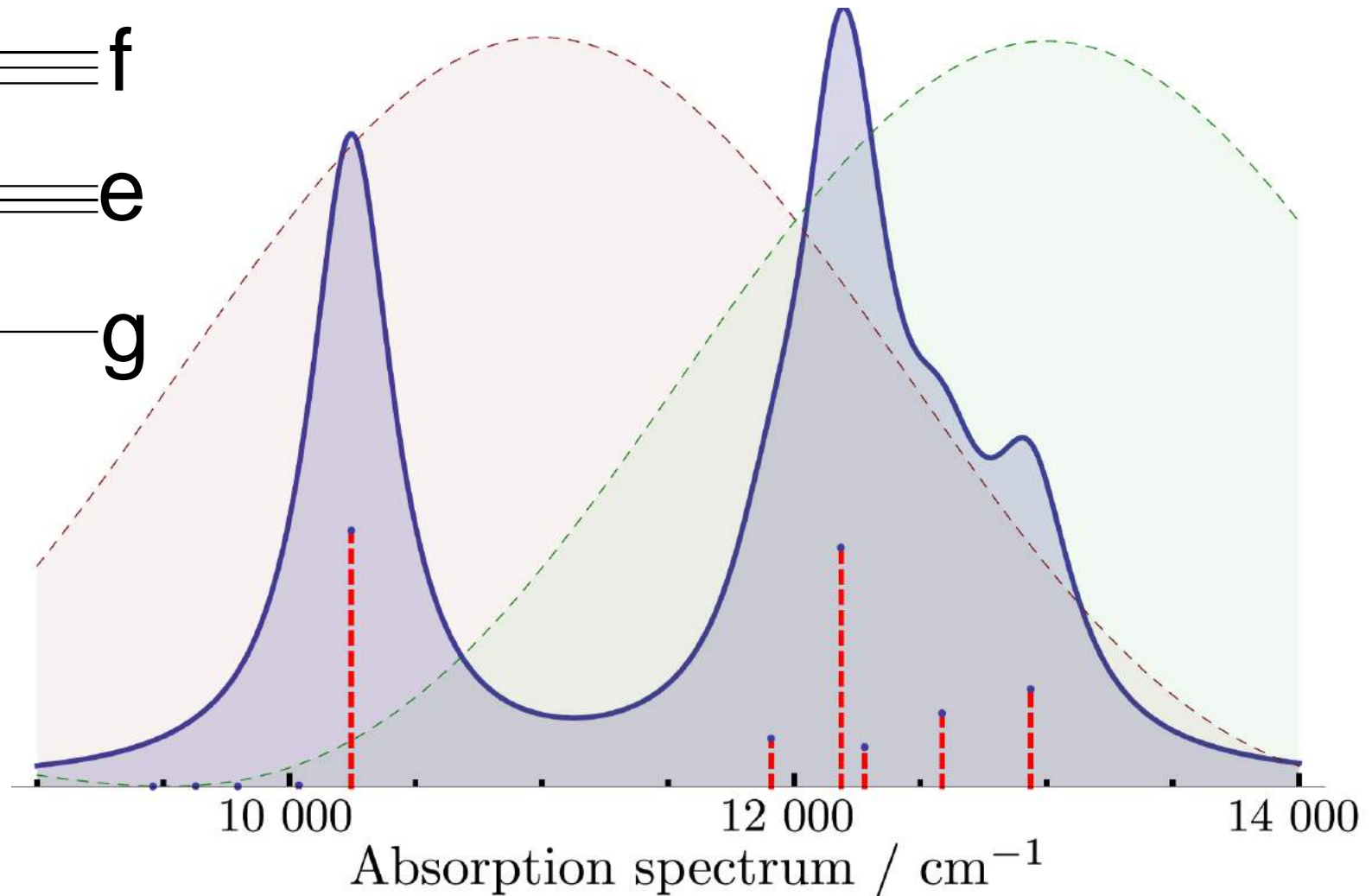
Power spectra of down-converted photons (red and green, dashed)
in comparison to the absorption spectrum of the bacterial reaction center (blue)

$$p_f(t;\Gamma) = \left(-\frac{i}{\hbar}\right)^4 \int_{-\infty}^{\infty} d\tau_4 \int_{-\infty}^{\infty} d\tau_3 \int_{-\infty}^{\infty} d\tau_2 \int_{-\infty}^{\infty} d\tau_1 \left\langle \mathcal{T} B_f(t) V(\tau_4) V(\tau_3) V^\dagger(\tau_2) V^\dagger(\tau_1) \right\rangle$$

$$\times \left\langle \mathcal{T} E^\dagger(\tau_4) E^\dagger(\tau_3) E(\tau_2) E(\tau_1) \right\rangle$$

To describe coupling to an environment, we need break consider three ladder-diagrams (and its complex conjugates):
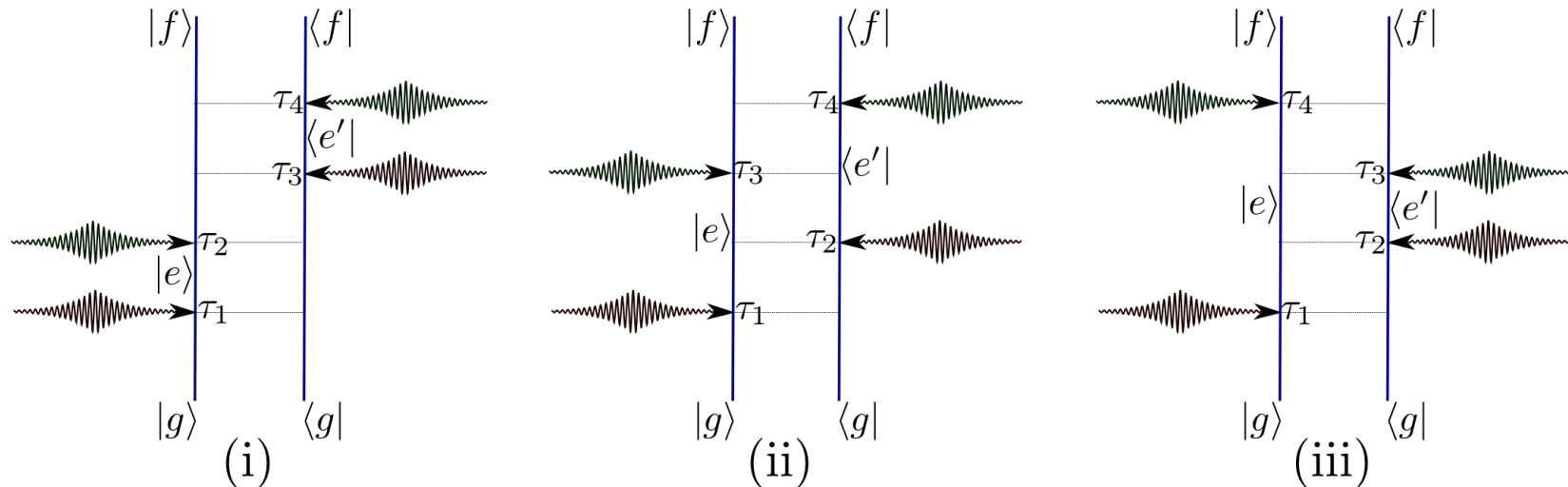
The three diagrams are accompanied by their mirror images, where we exchange left-/right-interactions. These are the complex conjugates, and we can simply evaluate the real value of the three diagrams.

Application to the bacterial reaction center

Single-exciton transport is modeled by a secular Redfield equation:

$$\frac{d}{dt}\varrho_{ee'}(t) = (-i\omega_{ee'} - \gamma_{ee'})\varrho_{ee'}(t) \qquad e \neq e'$$

$$\frac{d}{dt}\varrho_{ee}(t) = \sum_{e'} W_{ee'}\varrho_{e'e'}(t)$$

where the W-superoperator describes population transport.

$$\frac{d}{dt}\varrho_{ff'}(t) = (-i\omega_{ff'} - \gamma_{ff'})\varrho_{ff'}(t)$$

Control of population transport in the reaction center
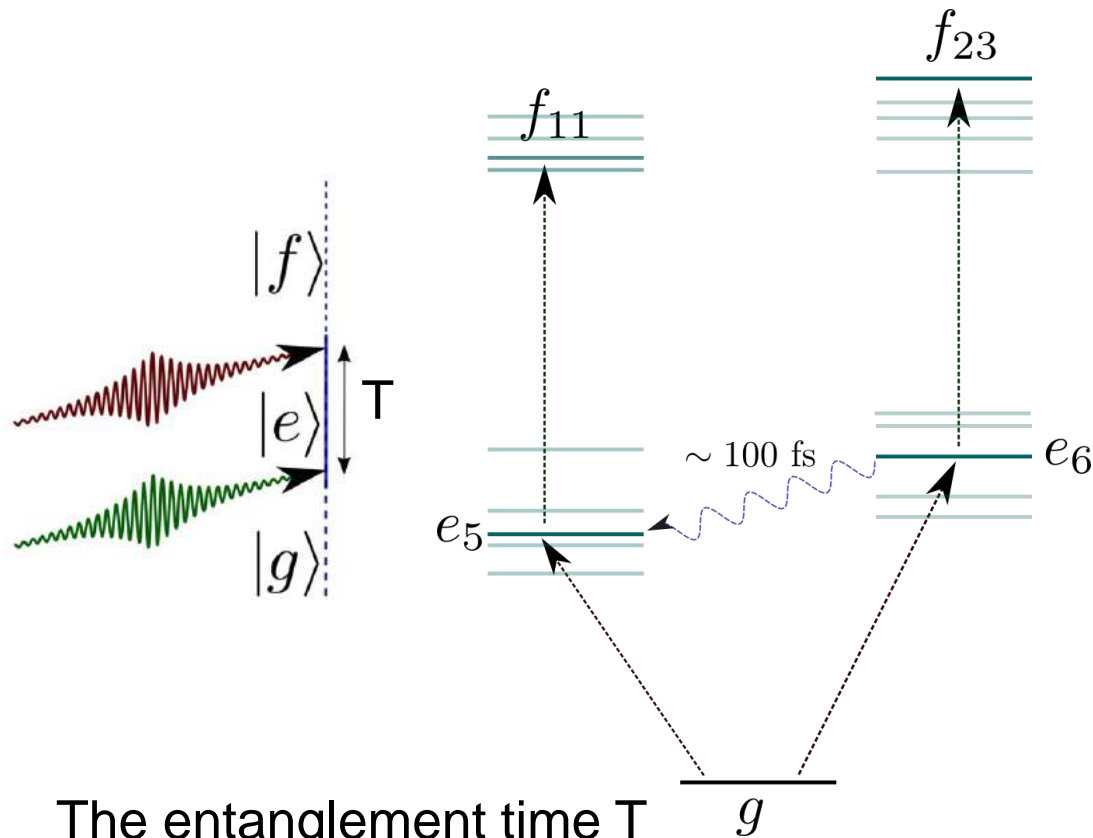
The entanglement time T represents an upper bound on the time the system spends in the single-exciton manifold.
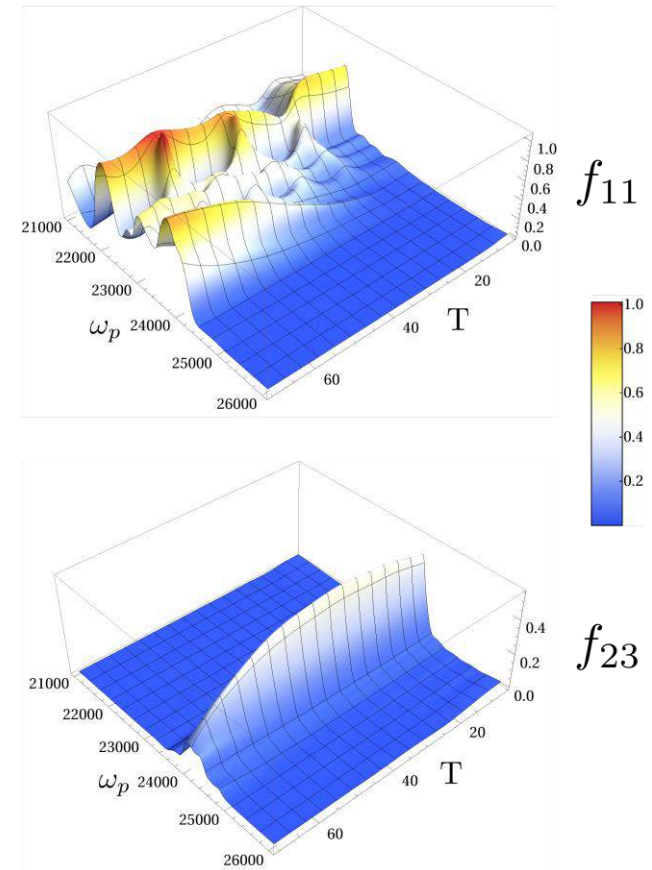
By tuning T, we can control population transport and thus influence two-exciton distributions.

Control of population transport in the reaction center
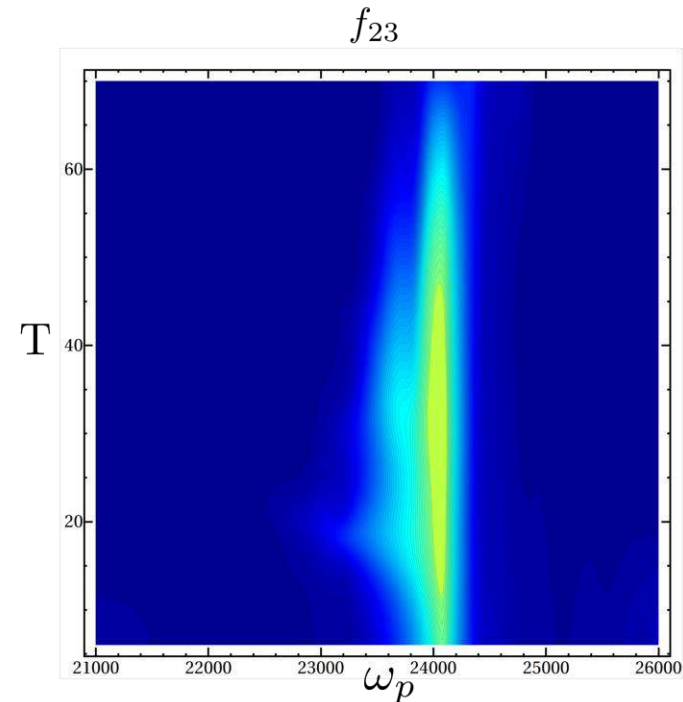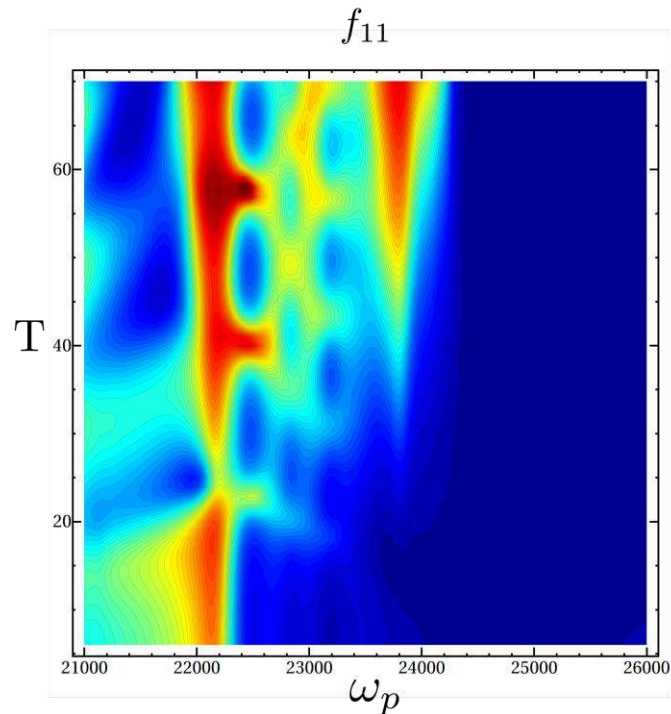
With increasing entanglement time, population transport in the single-exciton manifold opens new excitation pathways e.g., new resonances of state f_{11} appear, while other states such as f_{23} decrease.

Control of population transport in the reaction center
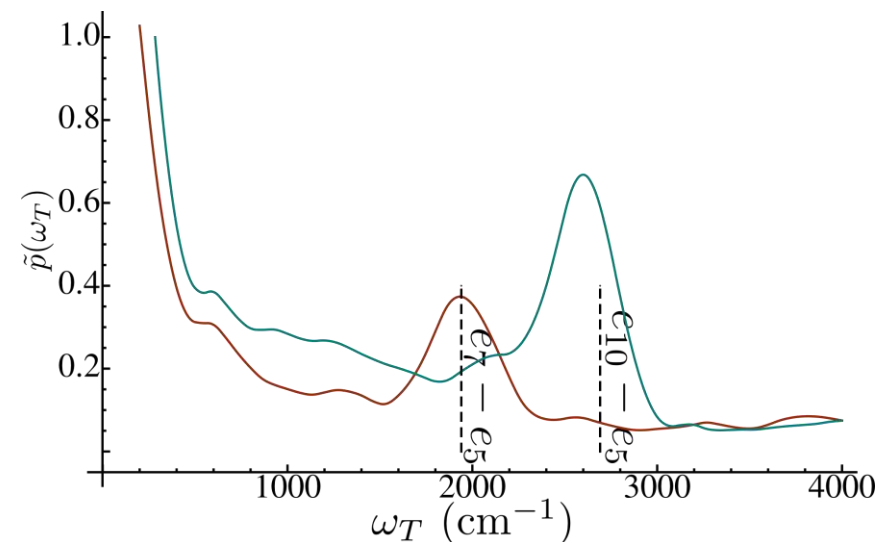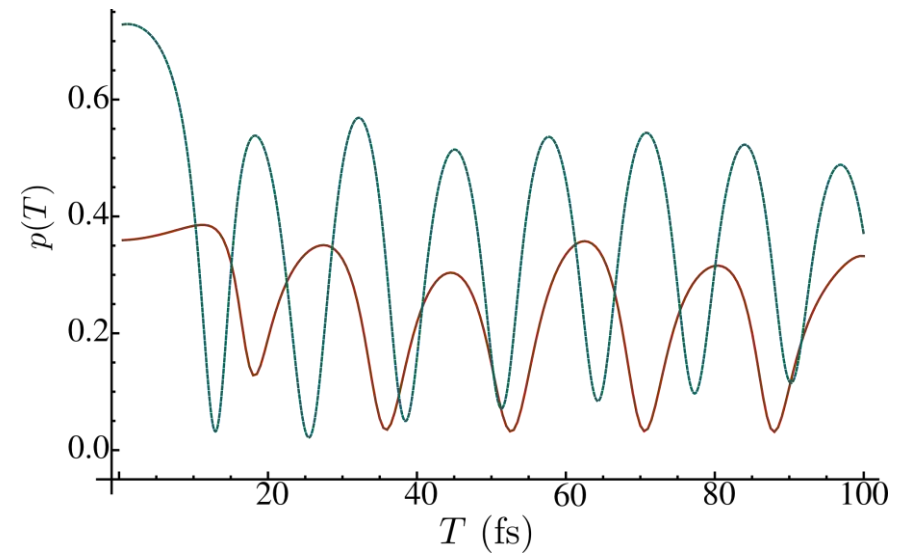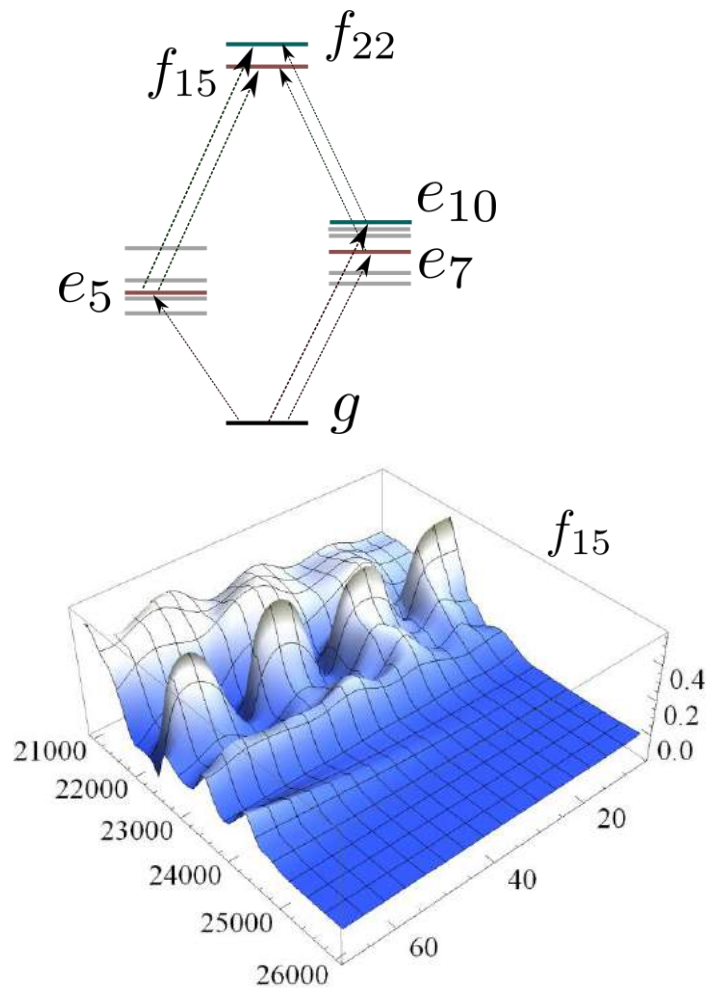
Oscillations in the populations reveal excitation pathways.

Is this degree of control a genuine entanglement effect?

- Frequency correlations are not necessarily a quantum effect
- Can classical light induce similar exciton distributions?
- If not, what is the quintessential advantage of entanglement?

$$e^{-i\omega_1 t} \longrightarrow e^{-i(\omega_1 + \alpha t)t}$$

$$\omega_1$$

$$\omega_2$$

$$e^{-i\omega_2 t} \longrightarrow e^{-i(\omega_2 - \alpha t)t}$$
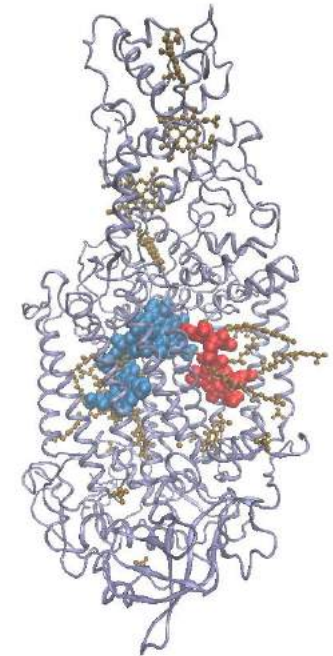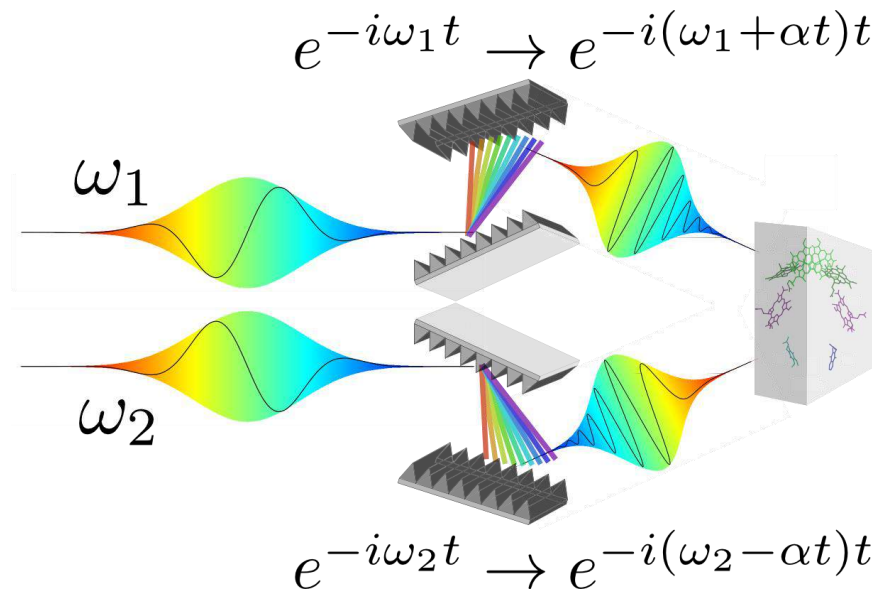
Entangled photons only enter in third-order signals through their four-point correlation function

$$\left\langle E^\dagger(t) E^\dagger(\tau_1) E(\tau_2) E(\tau_3) \right\rangle$$

We can try to mimic this correlation function by classical light!

Mimicking entangled photon pulses by chirped pulses

Gaussian pulses   **Chirped pulse**
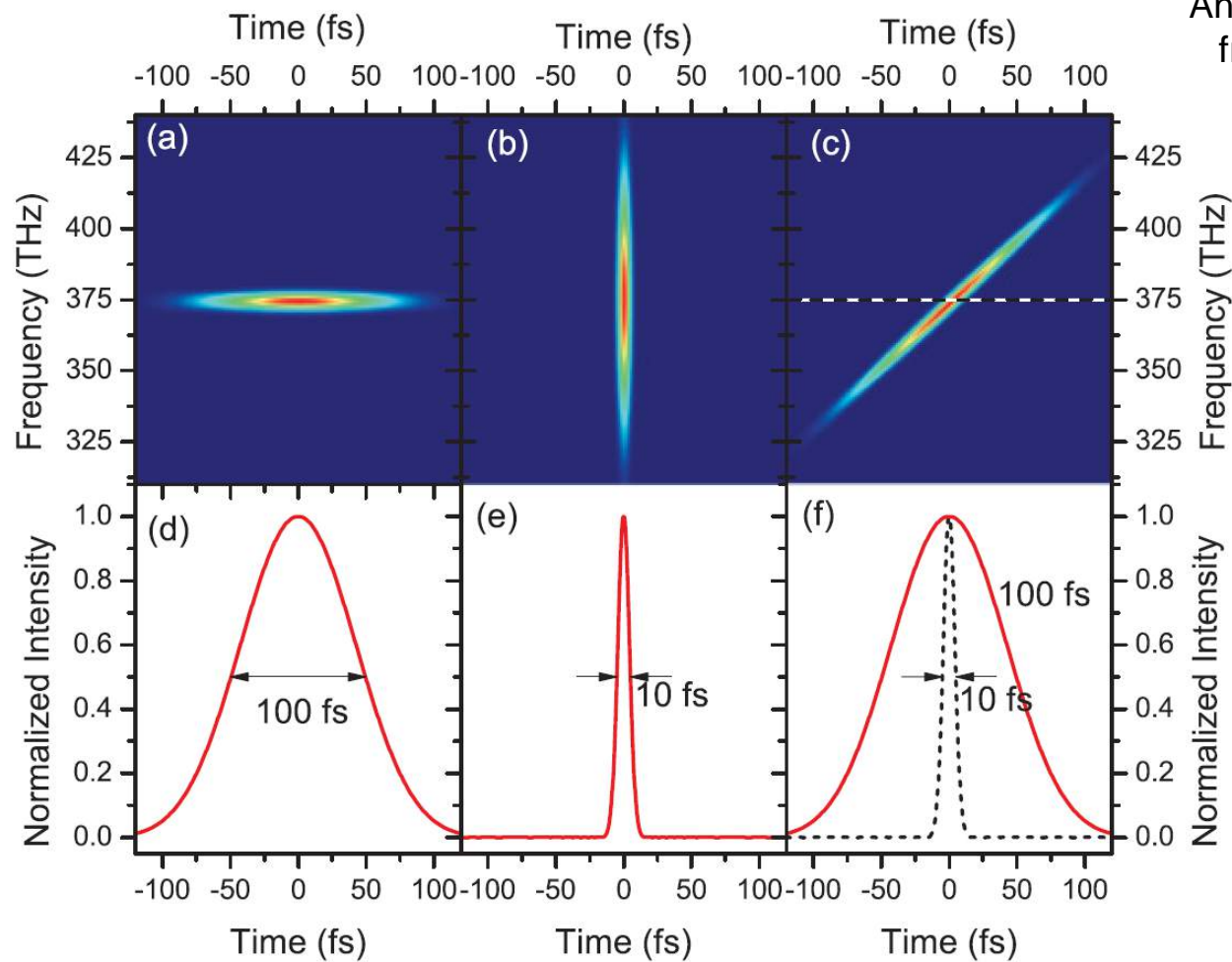
Chirped pulses:
Anti-correlated frequency ramps generate frequency correlations between pulses

$$e^{-i\omega_1 t} \rightarrow e^{-i(\omega_1 + \alpha t)t}$$

ω_1

ω_2

$$e^{-i\omega_2 t} \rightarrow e^{-i(\omega_2 - \alpha t)t}$$
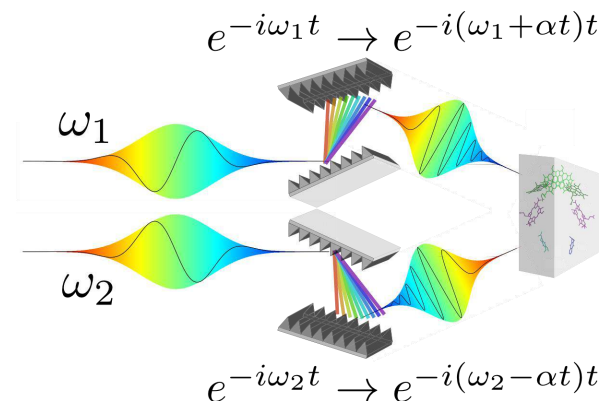
Wigner-functions of two Gaussian pulses (left), and of a chirped pulse (right)

D. Polli et al., Phys. Rev. A **82**, 053809 (2010)

Manipulating distributions of two photon states

Distribution of f-states
vs the pump frequency
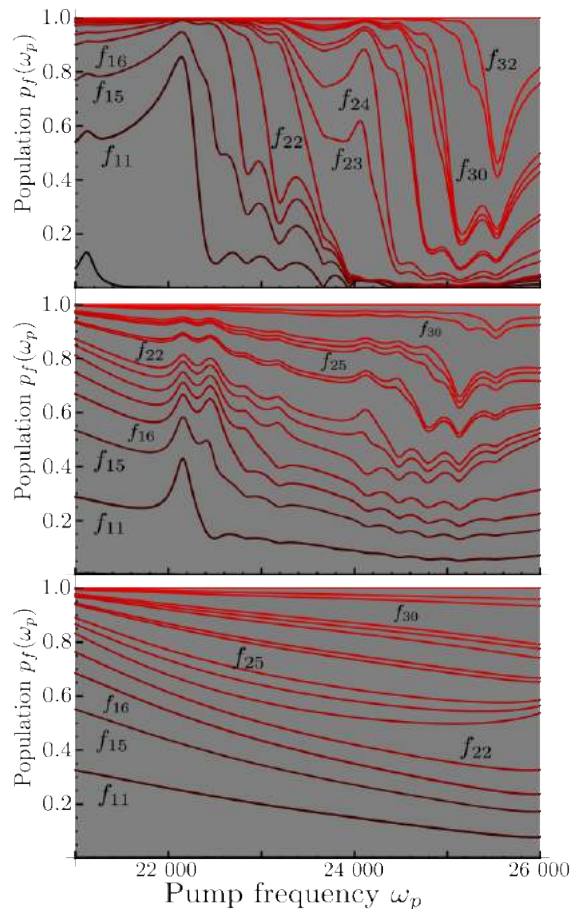
Density matrices created by entangled photons, chirped pulses, and stochastic light.

Entangled photons
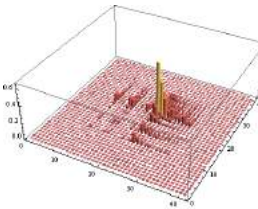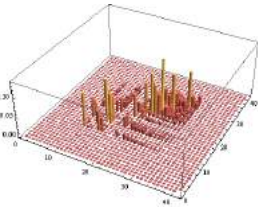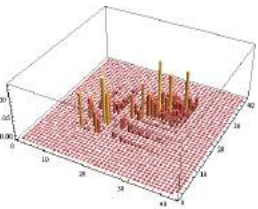
Chirped pulses

Chirped pulses contain incoherent background stemming from autocorrelation of classical pulses, which cannot be suppressed in the current setup.

Stochastic light

F. Schlawin, K.E. Dorfman, B. Fingerhut, and S. Mukamel, Nature Communications \textbf{4}, 1782 (2013).
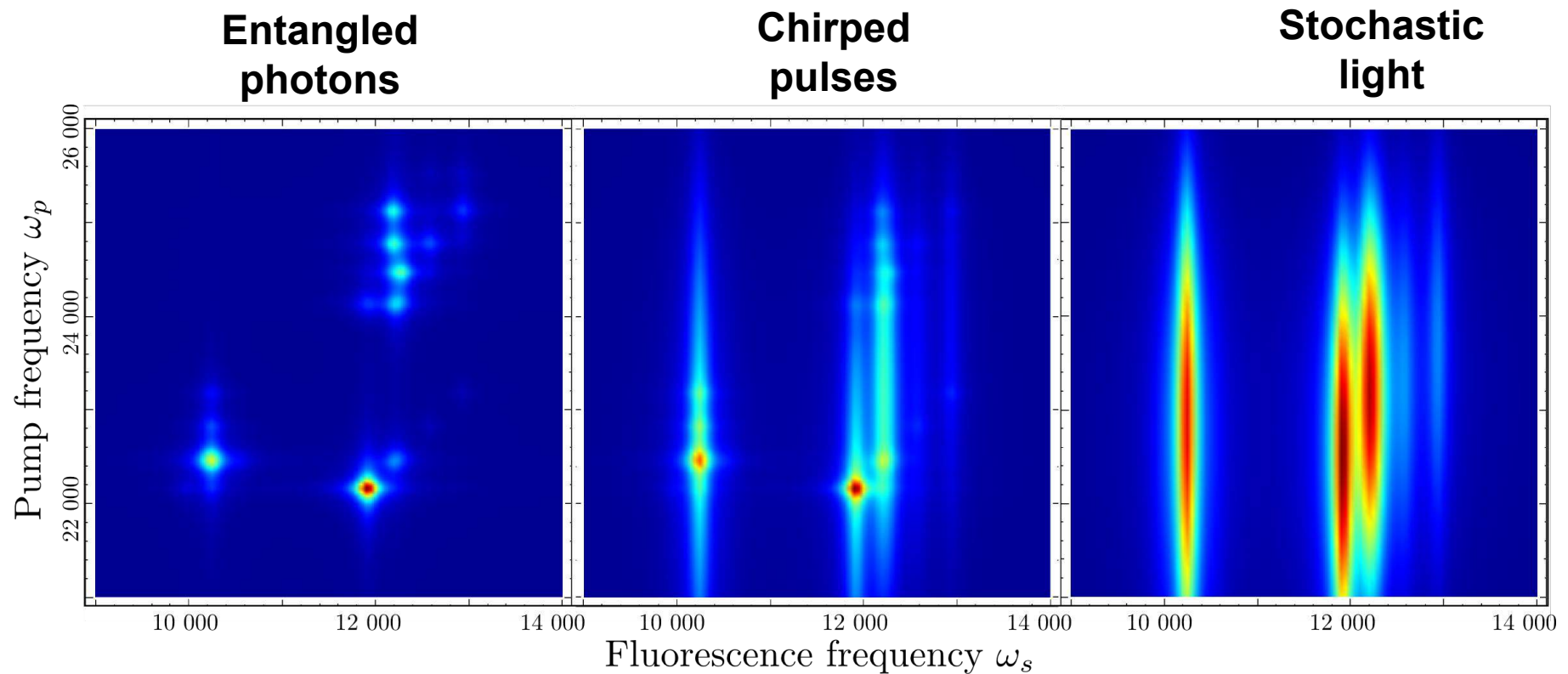
Fluorescence

This degree of control is reflected in the fluorescence signal.
By tuning the pump frequency, we can enhance or suppress
emission from certain states.

Control of population transport - comparison
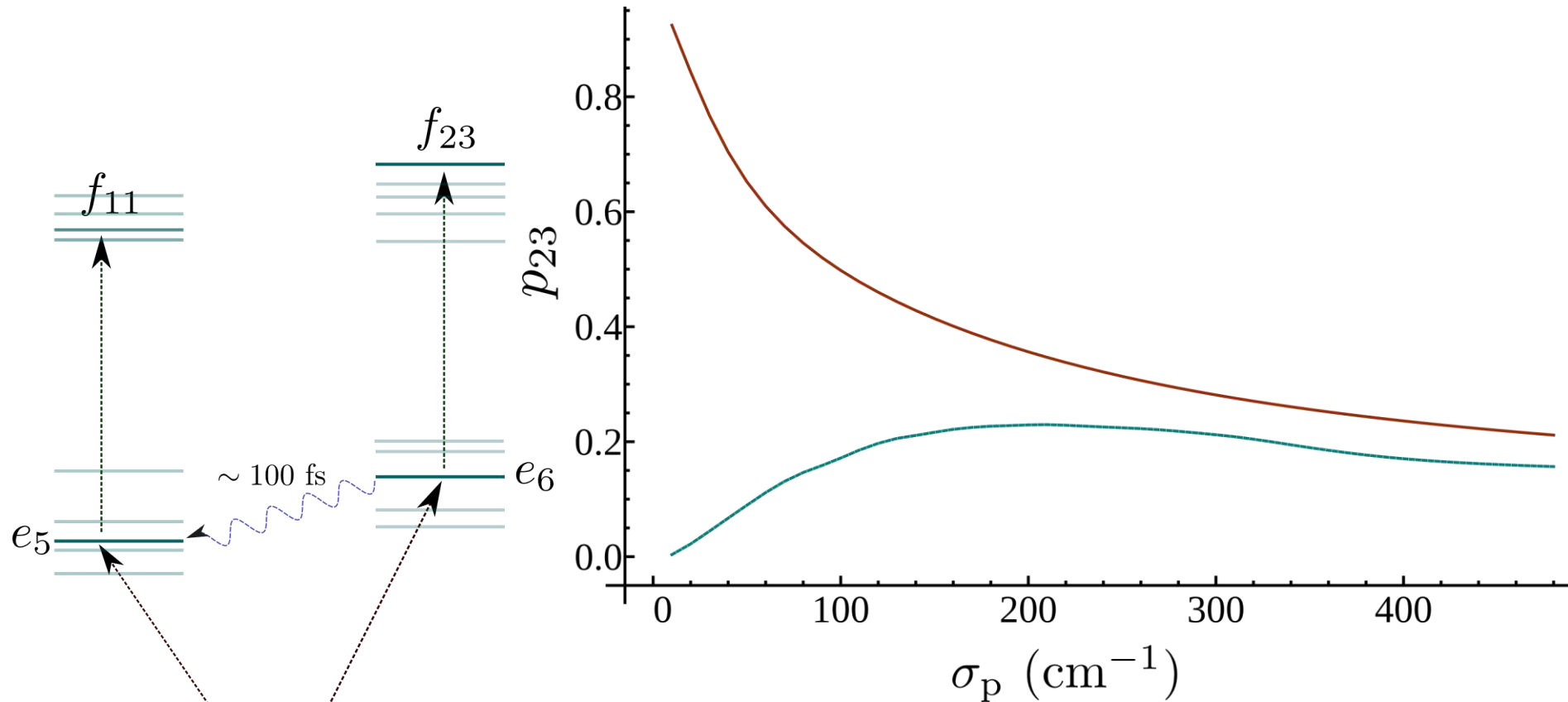
Population in state f_{23} upon excitation by entangled photons (red), and two laser pulses (blue) on resonance with the g-> e and e-> f transitions vs. the pump bandwidth.

Fluorescence measurements

•Exciton distributions can be revealed in fluorescence measurements

•We present simulations of the frequency-resolved fluorescence:

$$S_f(\omega_s; \Gamma) = \sum_{e,f} |\mu_{fe}|^2 p_f(t; \Gamma) \delta(\omega_f - \omega_e - \omega_s)$$
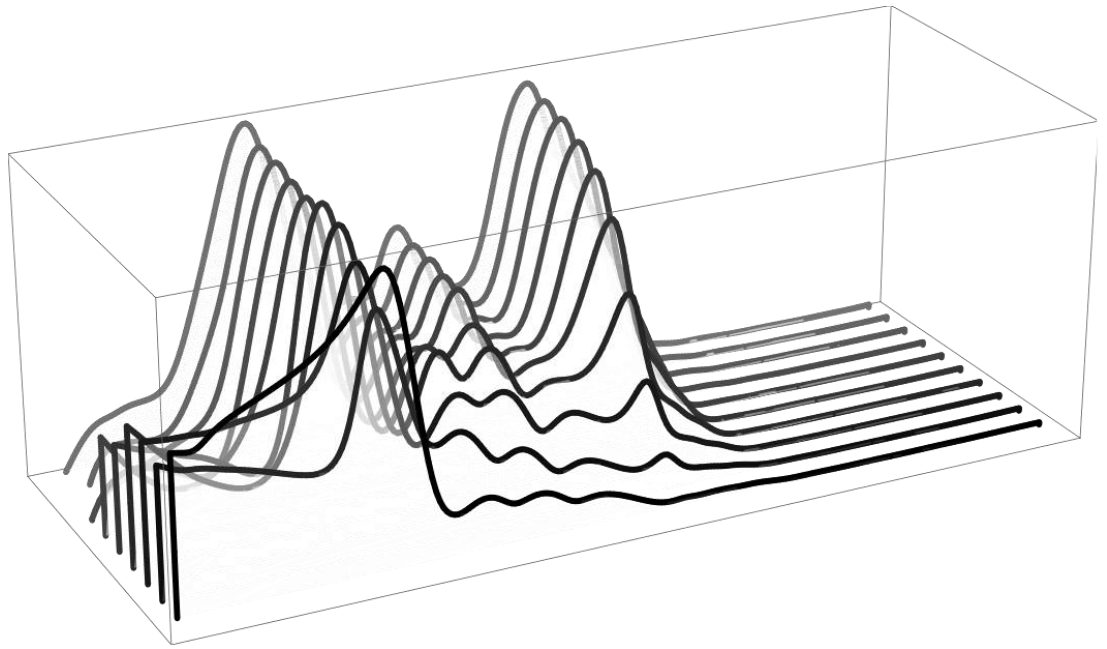
Summary

- Entangled photon pulses offer a unique degree of control on two-exciton distributions of molecular aggregates.

- The spectrum reveals the level structure of the double-exciton manifold, whereas the stochastic or chirped classical light cannot resolve this structure.

- Controlling population transport in the single-exciton manifold can better reveal excitation pathways in the molecular aggregate. This advantage is most pronounced, when the entanglement entropy is also maximal.

Coherent Raman spectroscopy with interferometric detection
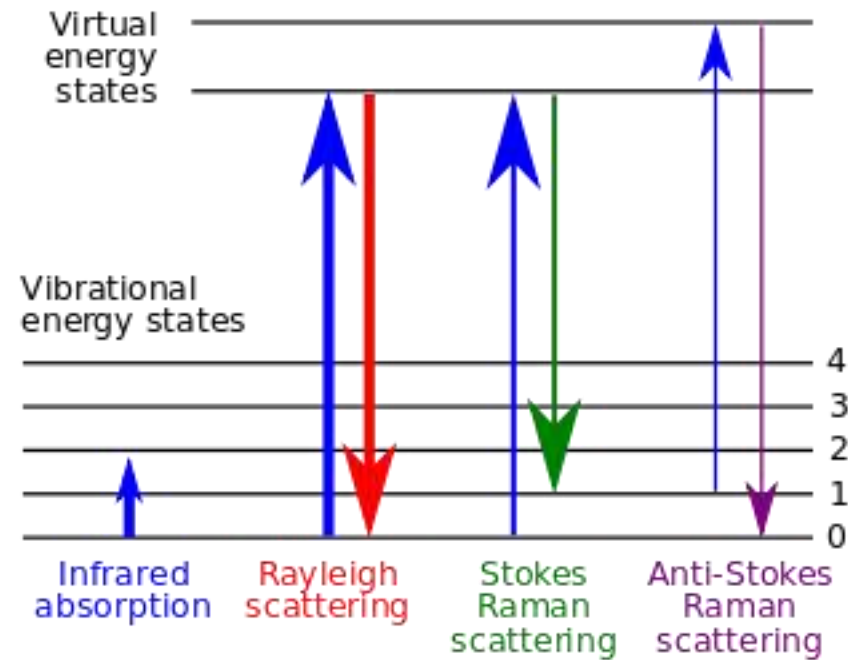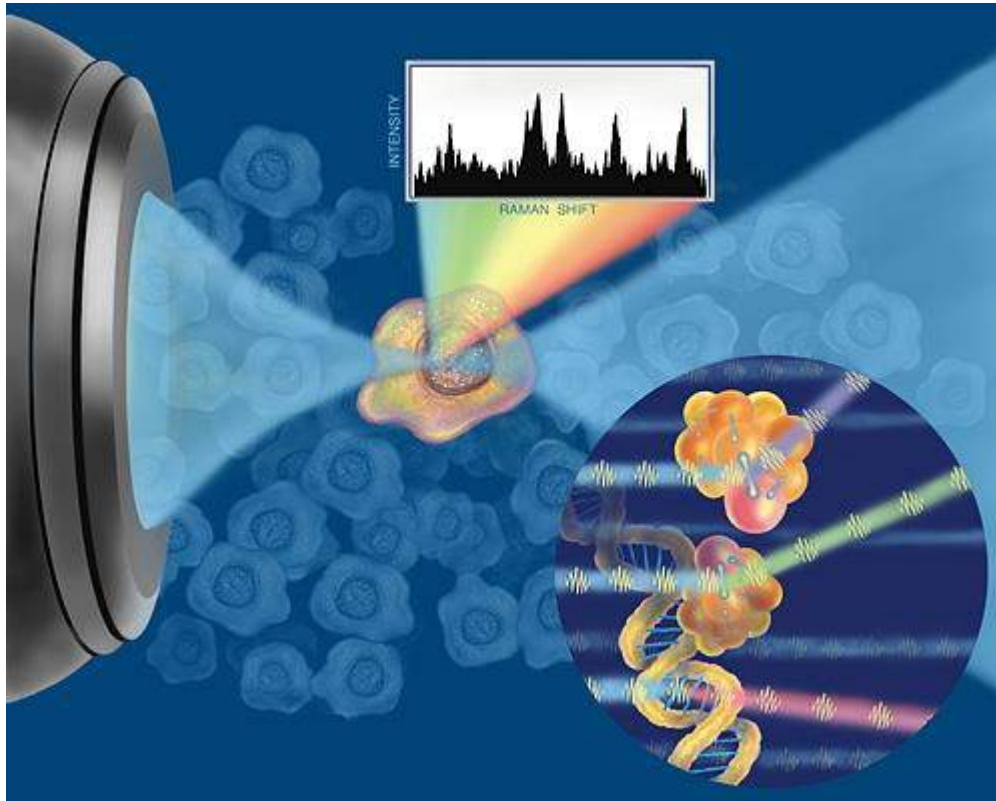
- Ultrafast spectroscopic technique
- Vibrational structures with high temporal 10-fs and spectral ~10cm^{-1} resolution
- Studies of ultrafast electronic dynamics and direct observation of nonstationary vibrational wave-packet motion

Figure (top left) courtesy of T. Huser and D. Taylor UC Davis

Stimulated Raman Signals with Broad-and Narrowband pulses

a Time-resolved FSRS

b FSRS pulse timing

① Actinic pulse
② Raman pulse
③ Probe pulse
←ΔT→
Time
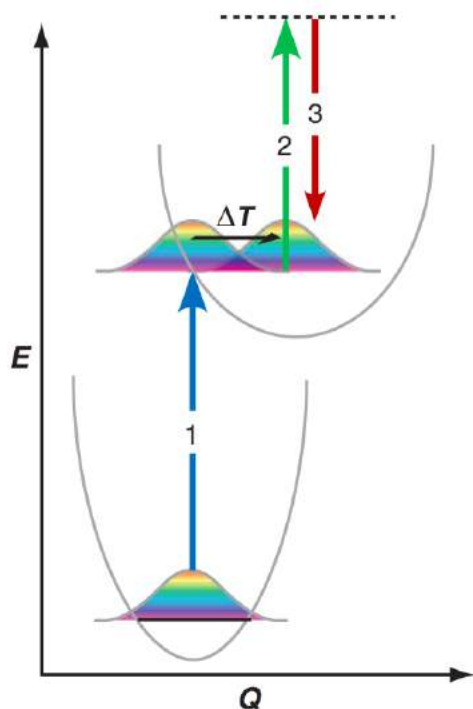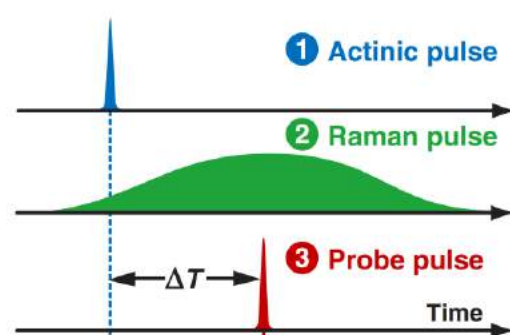
c Energy-level diagram

$|n+1\rangle$
$|n\rangle$
$|n\rangle\langle n|$
$|n+1\rangle\langle n|$
S_1
S_0
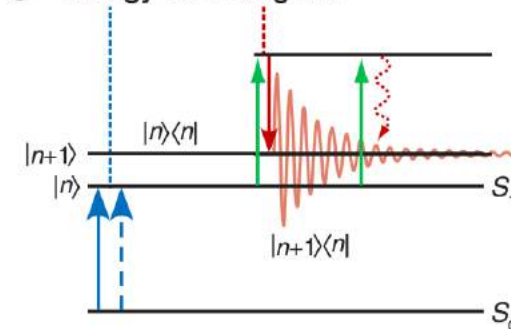
- Ultrashort pulse 1 initiates a chemical reaction in an excited electronic state

- Pulses 2 (narrowband) and 3 (broadband) induce a Raman transition.

•The spectral resolution ($\Delta\omega$) is determined by the monochromator into which the signal is dispersed

•The apparent time resolution (Δt) is determined by the delay time T between broadband pulses $\boldsymbol{k}_1$ and $\boldsymbol{k}_3$

•Apparently there is no lower limit to the product $\Delta\omega\Delta t$

•Does the technique offer perfect snapshots of the changing vibrational frequency ω_{ca} **at** time T?

R. Mathies Annual Review of Physical Chemistry 58, 461 (2007),
T. Tahara Yellow protein: The Journal of Physical Chemistry Letters **3**, 2025 (2012),
pNA, pDNA: P. Gilch, Optics Communications 202, 209 (2002),
CO_2: M. Dantus, Journal of Raman Spectroscopy 41, 1194 (2010),
Bacterial endospores: M. Scully Science 316, 265 (2007),
Cell imaging: Sunney Xie Phys. Rev. Lett. 82, 4142 (May 1999),
Multiplex CARS: J.-X. Cheng, J. Phys. Chem. B 106, 8493 (2002)
M. Müller, J. Phys. Chem. B 106, 3715 (2002)

Stimulated Raman Signal:

$\mathcal{E}_3$

$\mathcal{E}_p$ $\mathcal{E}_2$

$\tau = 0$ $\tau = T$

measured as probe E3 transmission
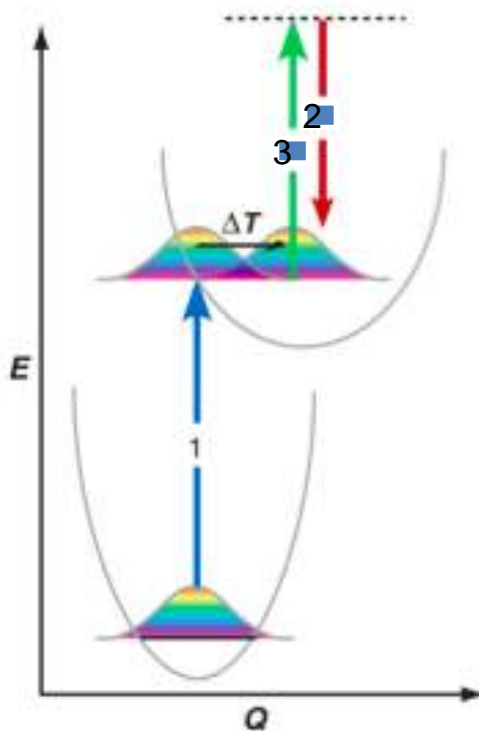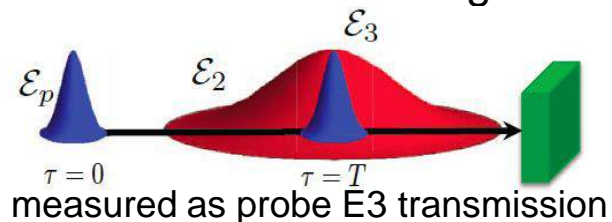
typically:
narrow lines ($\Delta\omega = 10$ cm^{-1})
reported with
high time resolution ($\Delta T = 25$ fs)

B

850 875 920 1210 1240 1265 1535

Batho
1 ps
525 fs
425 fs
375 fs
325 fs
300 fs
275 fs
250 fs
225 fs
200 fs

969 1216 1237 1267 1548

Rho

Stimulated Raman Intensity

800 1000 1200 1400 1600 1800
Raman Shift (cm^{-1})
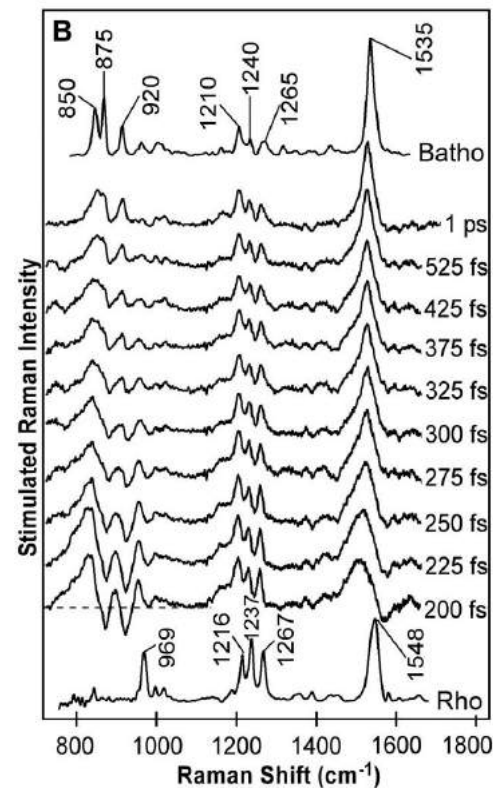
P Kukura et al.
Science 310, 1006 (2005)

Broadband infrared and Raman probes of excited-state vibrational molecular dynamics;

Simulation protocols based on loop diagrams.

K. E. Dorfman, B. P. Fingerhut, S. Mukamel, Phys. Chem. Chem. Phys. **15**, 12348 (2013).

Spectroscopy & Interferometry

Biphoton spectroscopy in a strongly nondegenerate regime of SPDC

A.A. Kalachev, D.A. Kalashnikov, A.A. Kalinkin, T.G. Mitrofanova, A.V. Shkalikov, and V.V. Samartsev *

Kazan Physical-Technical Institute, Russian Academy of Science, 10, Sibirsky trakt str., Kazan 420029, Russia

LETTERS

Quantum-inspired interferometry with chirped laser pulses

R. KALTENBAEK*, J. LAVOIE, D. N. BIGGERSTAFF AND K. J. RESCH*

Institute for Quantum Computing and Department of Physics and Astronomy, University of Waterloo, Waterloo, N2L 3G1, Canada
*e-mail: rkaltenb@iqc.ca; kresch@iqc.ca

New Journal of Physics
The open–access journal for physics

Probing multimode squeezing with correlation functions

Andreas Christ[1,2,3], Kaisa Laiho[2], Andreas Eckstein[2], Katiúscia N Cassemiro[2] and Christine Silberhorn[1,2]

[1] Applied Physics, University of Paderborn, Warburger Straße 100, 33098 Paderborn, Germany
[2] Max Planck Institute for the Science of Light, Günther-Scharowsky Straße 1/Bau 24, 91058 Erlangen, Germany
E-mail: Andreas.Christ@uni-paderborn.de

SCIENTIFIC REPORTS

OPEN

Dispersion-cancelled biological imaging with quantum-inspired interferometry

M. D. Mazurek[1*], K. M. Schreiter[1*], R. Prevedel[1,2], R. Kaltenbaek[1,3] & K. J. Resch[1]

[1]Institute for Quantum Computing and Department of Physics & Astronomy, University of Waterloo, Waterloo, ON N2L 3G1 CANADA, [2]Research Institute of Molecular Pathology (IMP) & Max F. Perutz Laboratories, University of Vienna, Dr. Bohr Gasse 7-9, 1030 Vienna, Austria, [3]Vienna Center for Quantum Science and Technology, Faculty of Physics, University of Vienna, Vienna, Austria.

SUBJECT AREAS:
NONLINEAR OPTICS
ULTRAFAST PHOTONICS
IMAGING AND SENSING
BIOPHOTONICS

Femtosecond Stimulated Raman Spectroscopy (FSRS) with classical light and frequency dispersed detection
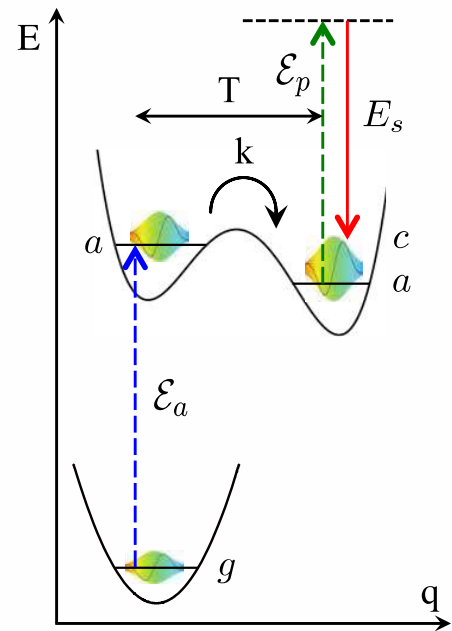
Frequency dispersed detection of Classical probe pulse $\mathcal{E}_s$
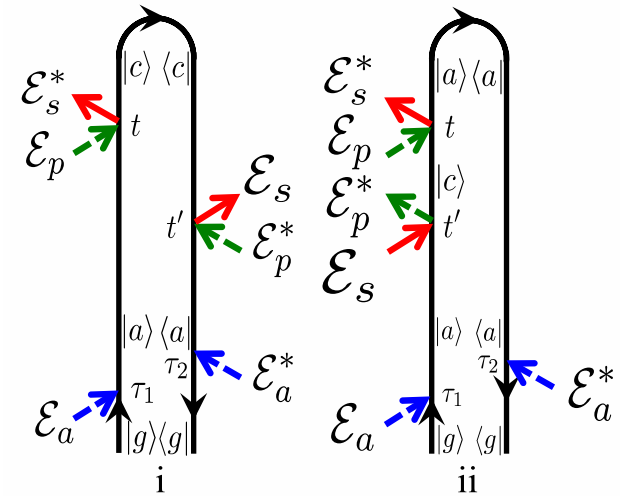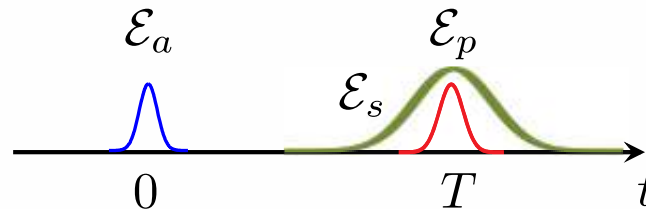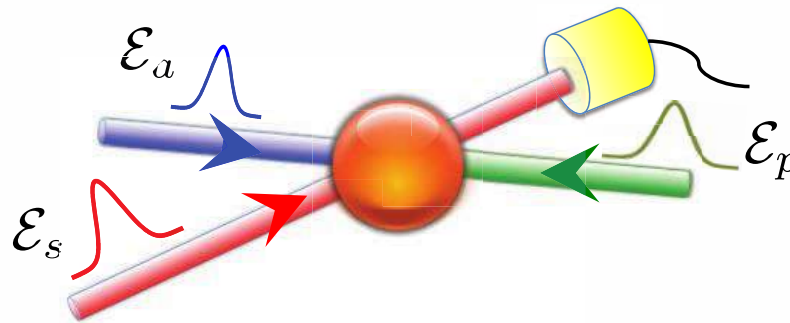
Understanding the Raman spectra

Loss and gain signals in broadband stimulated-Raman spectra: Theoretical analysis

Upendra Harbola and Siva Umapathy
Inorganic and Physical Chemistry, Indian Institute of Sciences, Bangalore, Karnataka 560012, India
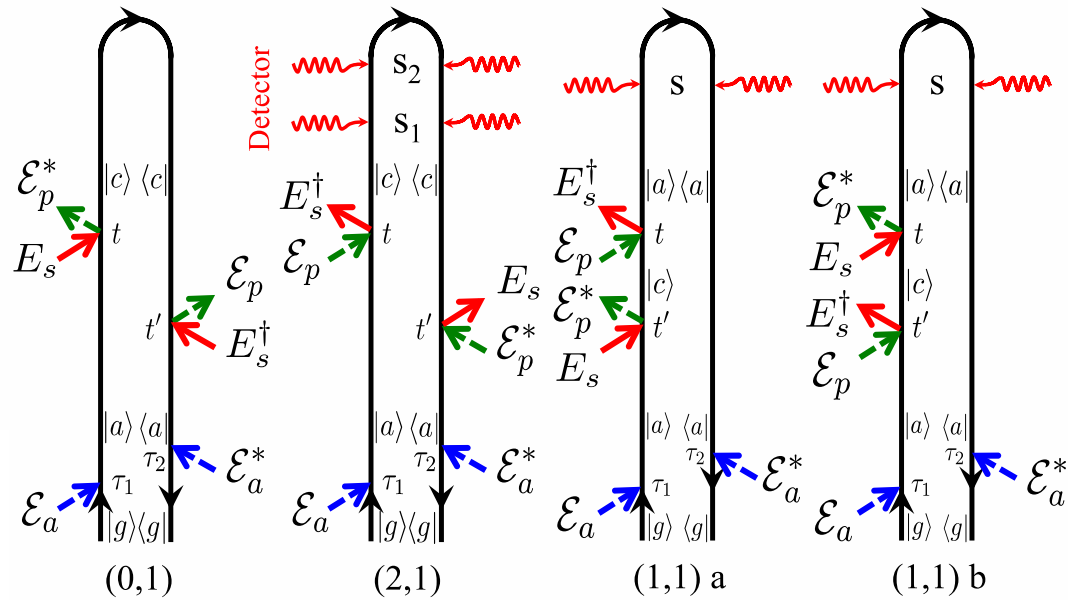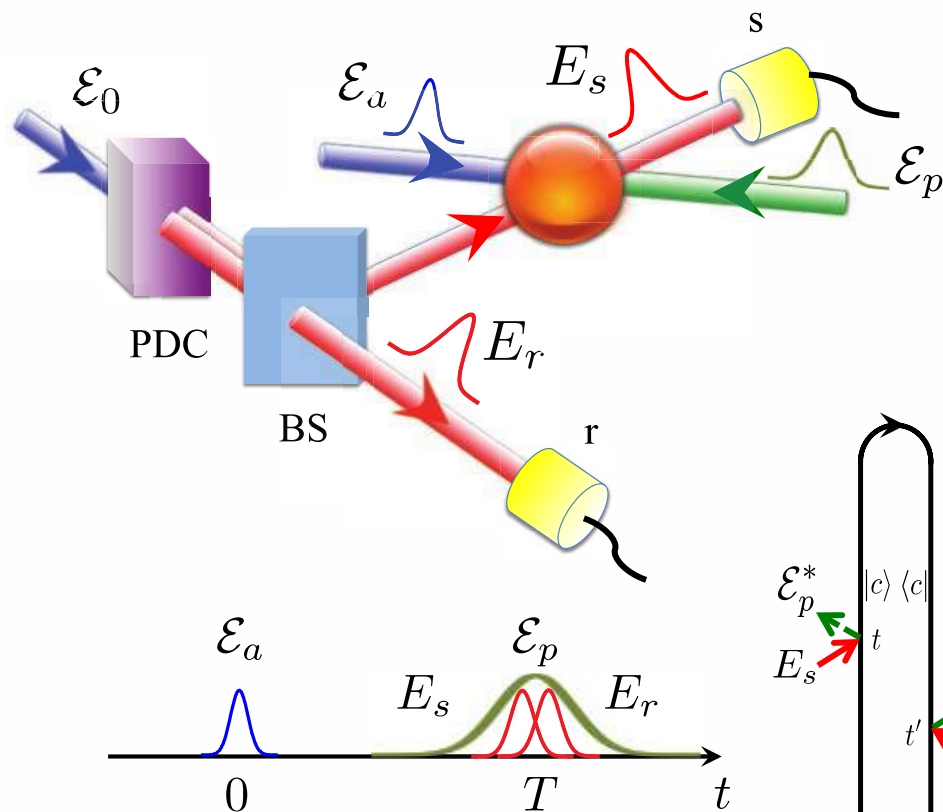
Shaul Mukamel
Department of Chemistry, University of California, Irvine, California 92697-2025, USA
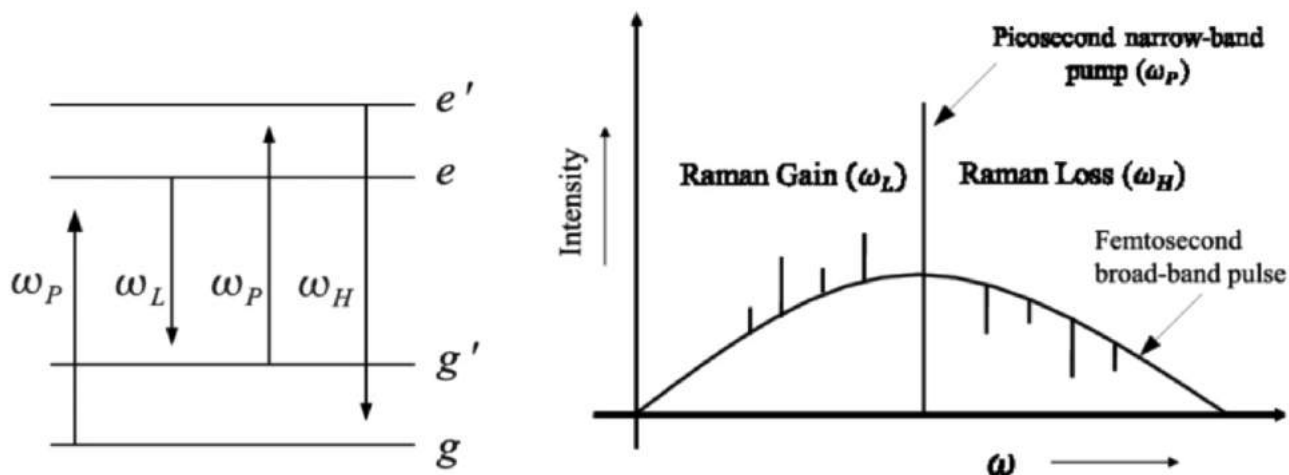
Classification (Total 8 signals):

- Gain (peak) or loss (dip)
- Red- or blue- relative to narrow pump
- Stokes or Antistokes (if excited state Raman)

Interferometric Femtosecond Stimulated Raman Spectroscopy (IFSRS) with entangled photons

Interferometric Femtosecond Stimulated Raman Spectroscopy (IFSRS) with entangled photons
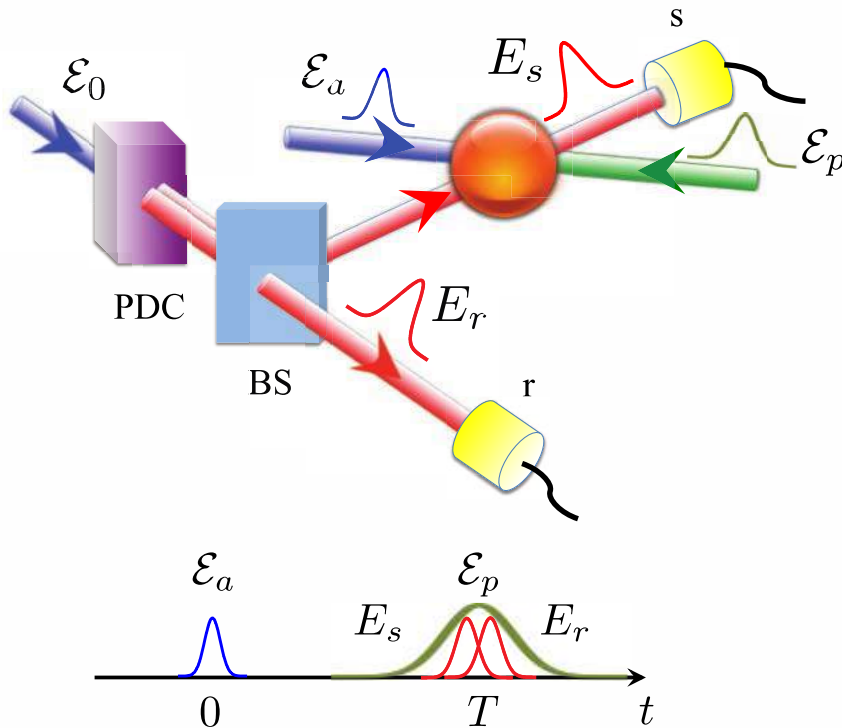
Benefits of using interferometric detection:
In a noninterferometric measurement the temporal and spectral resolution are controlled by the probe pulse envelope

Interferometric measurement allow to detect conjugate variables in two different detectors such that e.g. time gating of the first photon completely determine the time of arrival of the second photon and the frequency gating of the second photon determines the frequency of the first photon.

Time time correlation between photons is controlled by entanglement time (crystal length) frequency correlations are controlled by the bandwidth of the classical pump that creates a pair of entangled photons.

IFSRS with entangled light
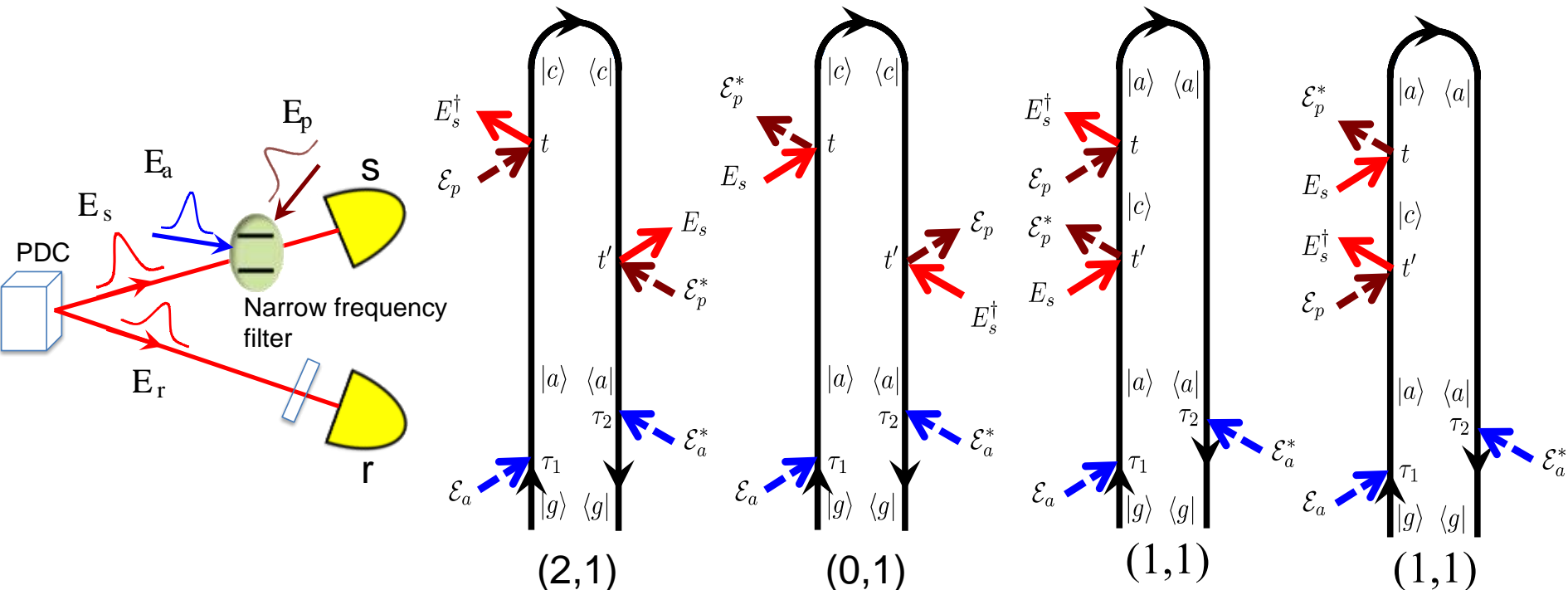
Classification by number of photons detected (N_s, N_r)

$$S_{IFSRS}^{(N_s,1)}(\bar{\omega}_{s_1}, ..., \bar{\omega}_{s_{N_s}}, \bar{\omega}_r, \Gamma_i) =$$

$$\langle \mathcal{T} E_r^{\dagger}(\bar{\omega}_r) E_r(\bar{\omega}_r) \prod_{j=1}^{N_s} E_s^{\dagger}(\bar{\omega}_{s_j}) E_s(\bar{\omega}_{s_j}) e^{-\frac{i}{\hbar} \int_{-\infty}^{\infty} H'_{-}(\tau)d\tau} \rangle$$

Interferometric detection. The detection window is multipoint correlation function of the averaged over the quantum state of light

IFSRS with entangled light (0,1)

$\mathcal{E}_p^*$

E_s

$|c\rangle \quad \langle c|$

t

t'

$\mathcal{E}_p$

$E_s^\dagger$

$|a\rangle \quad \langle a|$

τ_2

$\mathcal{E}_a^*$

τ_1

$\mathcal{E}_a$

$|g\rangle \quad \langle g|$

$(0,1)$
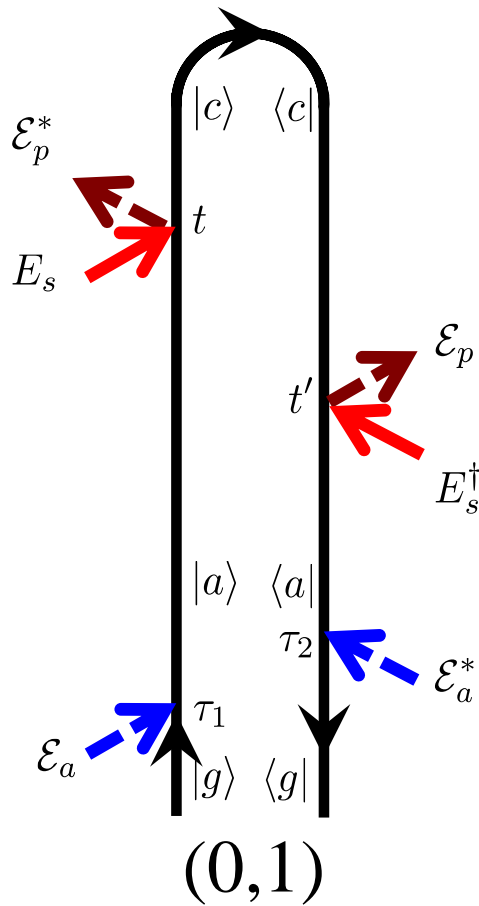
Frequency gated detection of photon in detector r
No detection of the photon in detector s
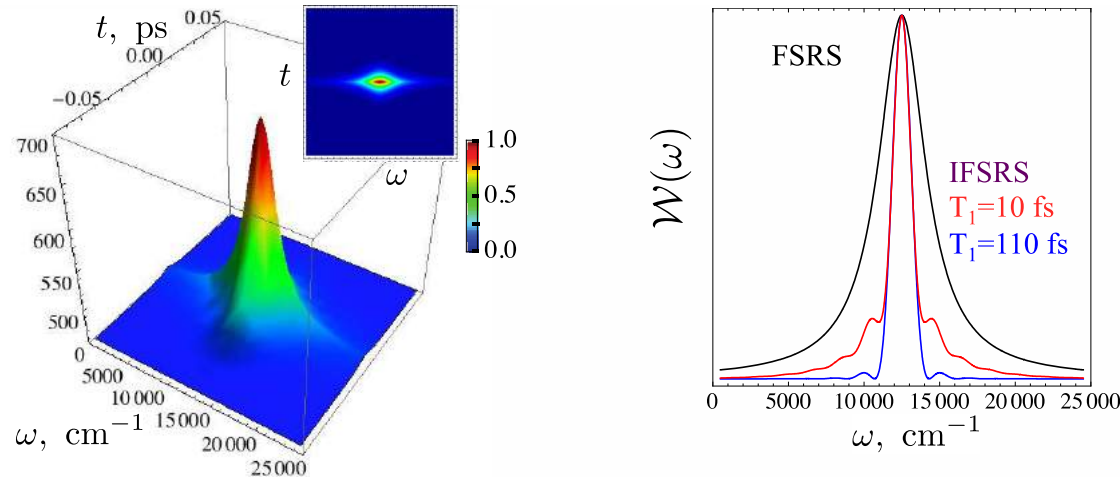which opens at sharp $\bar{t}_s$

Four point correlation function of the matter is windowed by
The four-point correlation function of the entangled field

$$S^{(0,1)}(\bar{t}_s, \bar{\omega}_r; T) = \frac{1}{\hbar^4} \int_{-\infty}^{\bar{t}_s} dt \int_{-\infty}^{\bar{t}_s} dt' \int_{-\infty}^{t} d\tau_1 \int_{-\infty}^{t'} d\tau_2 \mathcal{E}_p(t') \mathcal{E}_p^*(t) \mathcal{E}_a(\tau_1) \mathcal{E}_a^*(\tau_2)$$

$$\times \langle \mathcal{T} E_s^\dagger(t') E_r^\dagger(\bar{\omega}_s) E_r(\bar{\omega}_r) E_s(t) \rangle \langle \mathcal{T} V(\tau_2) \alpha(t') \alpha(t) V^\dagger(\tau_1) \rangle$$

IFSRS with entangled light (2,1)
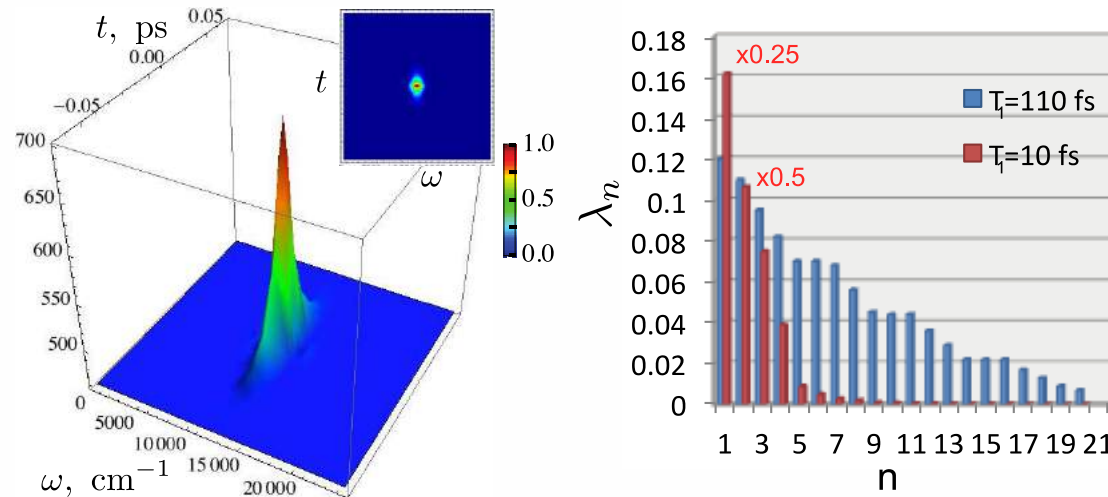
$|c\rangle \quad \langle c|$

$E_s^\dagger$

$\mathcal{E}_p$

t

E_s

t'

$\mathcal{E}_p^*$

$|a\rangle \quad \langle a|$

τ_2

$\mathcal{E}_a^*$

τ_1

$\mathcal{E}_a$

$|g\rangle \quad \langle g|$

$(2,1)$

Frequency gated detection of photon in detector r
Two photons are detected at detector s
which opens at sharp $\bar{t}_{s_1}$ and $\bar{t}_{s_2}$ where $\bar{t}_{s_1} < \bar{t}_{s_2}$

Four point correlation function of the matter is windowed by
The eight-point correlation function of the entangled field

$$S^{(2,1)}(\bar{t}_{s_1}, \bar{t}_{s_2}, \bar{\omega}_r; T) = \frac{1}{\hbar^4} \int_{-\infty}^{\bar{t}_{s_1}} dt \int_{-\infty}^{\bar{t}_{s_1}} dt' \int_{-\infty}^{t} d\tau_1 \int_{-\infty}^{t'} d\tau_2 \mathcal{E}_p(t)\mathcal{E}_p^*(t')\mathcal{E}_a(\tau_1)\mathcal{E}_a^*(\tau_2)$$

$$\times \langle \mathcal{T} E_s(t') E_s^\dagger(\bar{t}_{s_1}) E_s^\dagger(\bar{t}_{s_2}) E_r^\dagger(\bar{\omega}_s) E_r(\bar{\omega}_r) E_s(\bar{t}_{s_2}) E_s(\bar{t}_{s_1}) E_s^\dagger(t)\rangle \langle \mathcal{T} V(\tau_2)\alpha(t')\alpha(t)V^\dagger(\tau_1)\rangle$$

UNIVERSITY of CALIFORNIA · IRVINE

$E_s^\dagger$

$\mathcal{E}_p$

$\mathcal{E}_p^*$

E_s

$|a\rangle \quad \langle a|$

t

$|c\rangle$

t'

$|a\rangle \quad \langle a|$

τ_2

τ_1

$\mathcal{E}_a^*$

$\mathcal{E}_a$

$|g\rangle \quad \langle g|$

$(1,1)$

Frequency gated detection of photon in detector r
One photons is detected at detector s
which opens at sharp $\bar{t}_s$

Four point correlation function of the matter is windowed by
The six-point correlation function of the entangled field

$$S^{(1,1)}(\bar{t}_s, \bar{\omega}_r; T) = -\frac{1}{\hbar^4} \int_{-\infty}^{\bar{t}_s} dt \int_{-\infty}^{t} dt' \int_{-\infty}^{t'} d\tau_1 \int_{-\infty}^{\bar{t}_s} d\tau_2 \mathcal{E}_p(t') \mathcal{E}_p^*(t) \mathcal{E}_a(\tau_1) \mathcal{E}_a^*(\tau_2)$$

$$\times \langle \mathcal{T} E_s^\dagger(\bar{t}_s) E_r^\dagger(\bar{\omega}_s) E_r(\bar{\omega}_r) E_s(\bar{t}_s) E_s(t) E_s^\dagger(t') \rangle \langle \mathcal{T} V(\tau_2) \alpha(t) \alpha(t') V^\dagger(\tau_1) \rangle$$

$\mathcal{E}_p^*$

E_s

$E_s^\dagger$

$\mathcal{E}_p$

$\mathcal{E}_a$

$|a\rangle \quad \langle a|$

t

$|c\rangle$

t'

$|a\rangle \quad \langle a|$

τ_2

τ_1

$\mathcal{E}_a^*$

$|g\rangle \quad \langle g|$

$(1,1)$

Frequency gated detection of photon in detector r
One photons is detected at detector s
which opens at sharp $\bar{t}_s$

Four point correlation function of the matter is windowed by
The six-point correlation function of the entangled field

$$S^{(1,1)}(\bar{t}_s, \bar{\omega}_r; T) = -\frac{1}{\hbar^4} \int_{-\infty}^{\bar{t}_s} dt \int_{-\infty}^{t} dt' \int_{-\infty}^{t'} d\tau_1 \int_{-\infty}^{\bar{t}_s} d\tau_2 \mathcal{E}_p(t)\mathcal{E}_p^*(t')\mathcal{E}_a(\tau_1)\mathcal{E}_a^*(\tau_2)$$

$$\times \langle \mathcal{T} E_s^\dagger(\bar{t}_s) E_r^\dagger(\bar{\omega}_s) E_r(\bar{\omega}_r) E_s(\bar{t}_s) E_s^\dagger(t) E_s(t') \rangle \langle \mathcal{T} V(\tau_2)\alpha(t)\alpha(t')V^\dagger(\tau_1) \rangle$$

Classical vs Entangled light detection window

Wigner function for classical and quantum light

$$W_s(\omega, t) = \int_{-\infty}^{\infty} \frac{d\Delta}{2\pi} \mathcal{E}_s^*(\omega) \mathcal{E}_s(\omega + \Delta) e^{-i\Delta t}$$

$$W_q(\omega, t; \bar{\omega}_r) = \int_{-\infty}^{\infty} \frac{d\Delta}{2\pi} \Phi^*(\omega, \bar{\omega}_r) \Phi(\omega + \Delta, \bar{\omega}_r) e^{-i\Delta t}$$

Two-photon state

$$|\psi\rangle = |0\rangle + \int_{-\infty}^{\infty} d\omega_s d\omega_r \Phi(\omega_s, \omega_r) a_{\omega_s}^\dagger a_{\omega_r}^\dagger |0\rangle$$

Schmidt decomposition

$$\Phi(\omega_s, \omega_r) = \sum_n \sqrt{\lambda_n} \psi_n(\omega_s) \phi_n(\omega_r)$$

Many terms in expansion corresponds to inseparable state

Entangled twin photon state provides higher spectral resolution

IFSRS for time evolving vibration

Slow dynamics and long dephasing

Separate measurement of
blue- and red- parts of the spectra

Fast dynamics and short dephasing
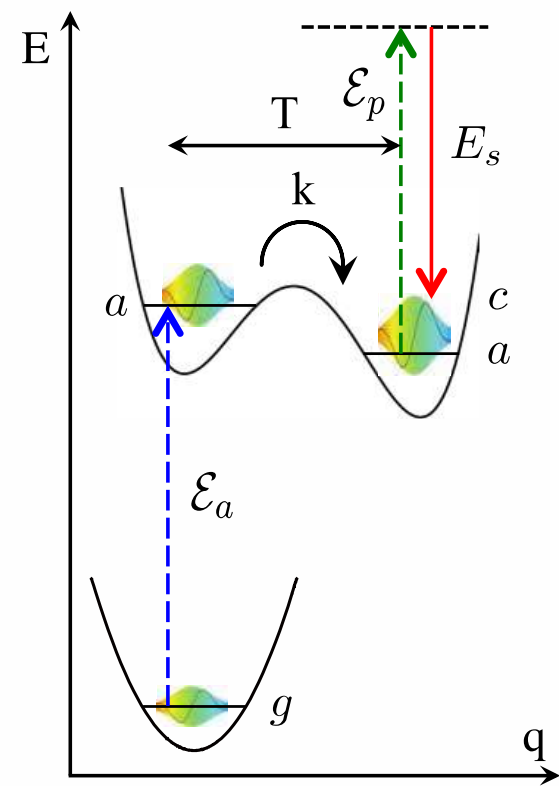
Entangled light provides
High spectral resolution
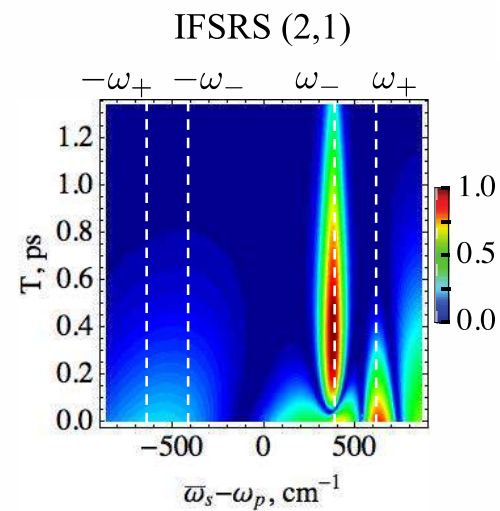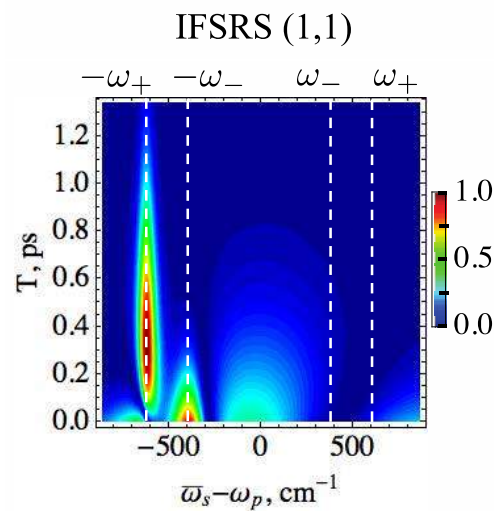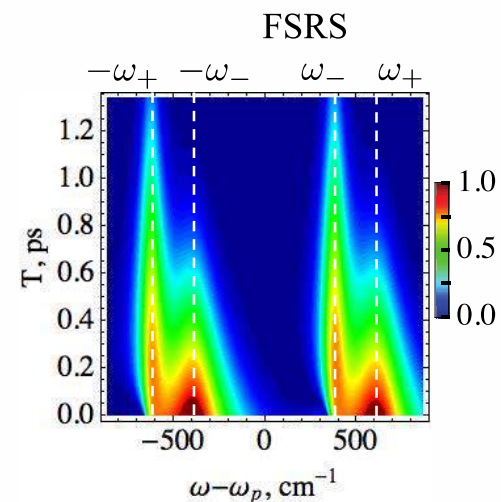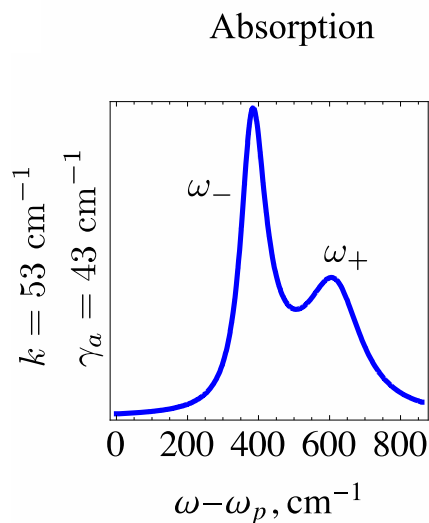
Role of entanglement

General two-photon state

$$|\psi\rangle = |0\rangle + \int_{-\infty}^{\infty} d\omega_s d\omega_r \Phi(\omega_s, \omega_r) a_{\omega_s}^\dagger a_{\omega_r}^\dagger |0\rangle$$

Entangled twin photon state

$$\Phi(\omega_s, \omega_r) = \mathcal{E}_0(\omega_s + \omega_r) \sum_{i \neq j = 1}^{2}$$

$$\times \text{sinc}\left(\omega_{s0} T_i / 2 + \omega_{r0} T_j / 2\right) e^{i\omega_{s0} T_i / 2 + i\omega_{r0} T_j / 2}$$

(high spectral and temporal resolution)

Correlated separable (disentangled) state

$$\rho_{cor} = \int_{-\infty}^{\infty} d\omega_s d\omega_r |\Phi(\omega_s, \omega_r)|^2 |1_{\omega_s}, 1_{\omega_r}\rangle\langle 1_{\omega_s}, 1_{\omega_r}|$$

(high spectral, low temporal resolution)

Uncorrelated separable state

$$\Phi_{uncor}(\omega_s, \omega_r) = \Phi_s(\omega_s)\Phi_r(\omega_r)$$

(Low spectral resolution as in classical FSRS)
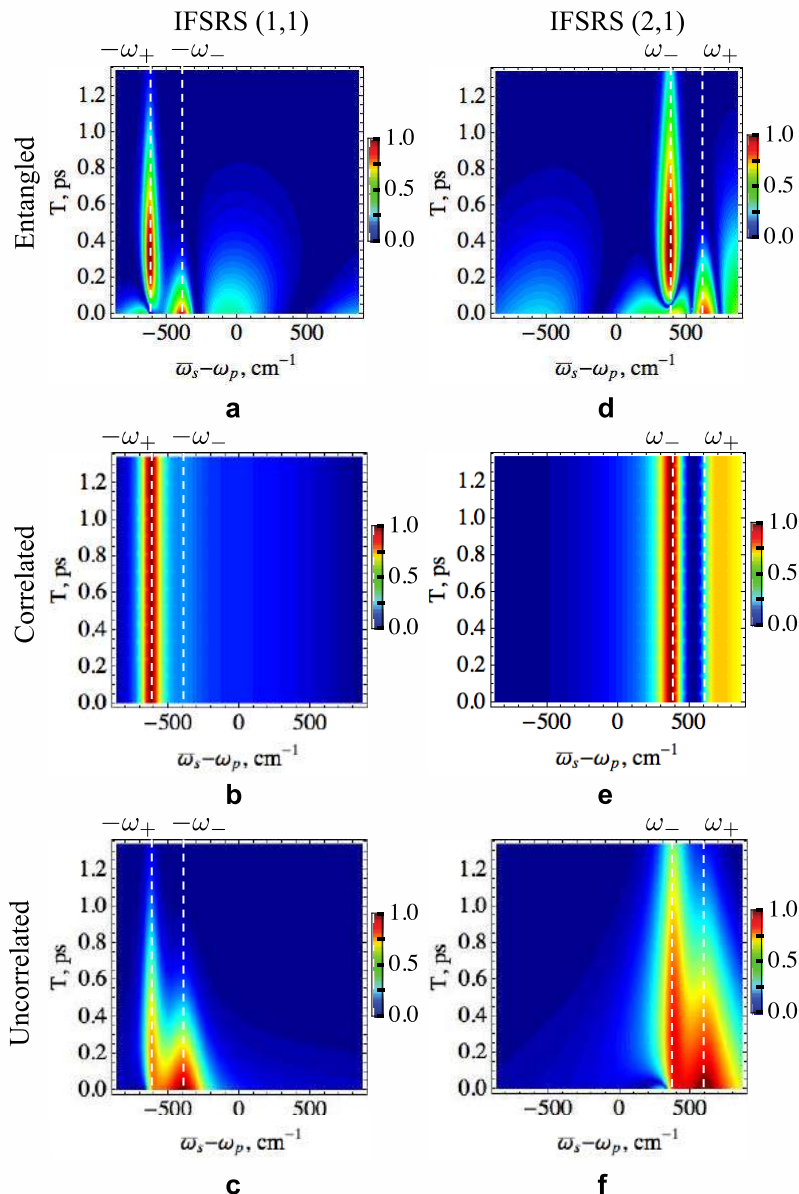
Summary

- Bath dynamics can be investigated and controlled by using entangled light

- Elaborate time-and-frequency gated detection allow to preserve quantum interference in the presence of the bath

- Raman resonances in femtosecond stimulated Raman spectroscopy (FSRS) can be studied and manipulated by using interferometric detection of a pair of entangled photons, one (signal) interacts with the molecule and acts as the broadband probe and the detection of other (idler) provides a nondestructive measurement of the probe.

- Raman gain and loss signals can be detected separately, which is not possible with classical light.

- The resolution of Raman resonances can be improved reducing bath induced broadening

Broadband Raman X ray probes of nonadiabatic dynamics

Shaul Mukamel, Konstantin E. Dorfman, Benjamin P. Fingerhut

X-ray Free Electron Lasers

• P. Luchini and H. Motz. *Undulators and Free-electron Lasers*(Oxford University Press, USA, 1990)
• Nat. Phot., 4(12):802–803, December 2010
• P. Emma, *et. al.* Nat. Phot. **4**, 641 (2010)

~60eV

Nature Comm. 3:1100 (2012) DOI: 10.1038/ncomms2108

$E_{X\text{-}Ray}$ 279.17 eV
$\lambda_{X\text{-}Ray}$ 4.2023 nm
$N_{photons}$ 15.37 E12

Stanford LCLS X-ray Free Electron Laser

https://slacportal.slac.stanford.edu/sites/lcls_public/Pages/status.aspx
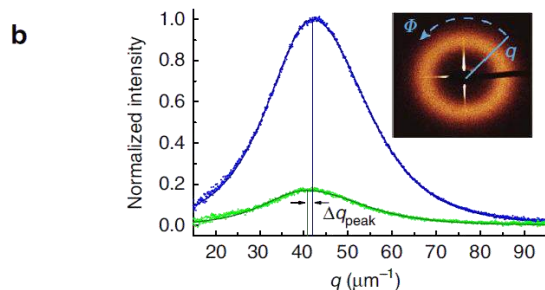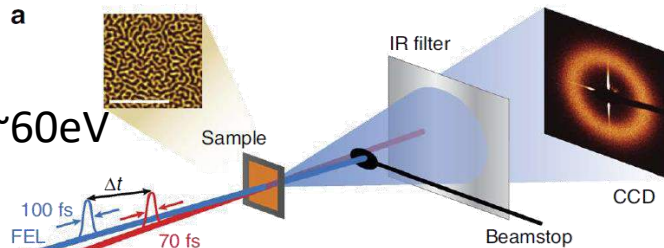
http://flash.desy.de/photon_science/
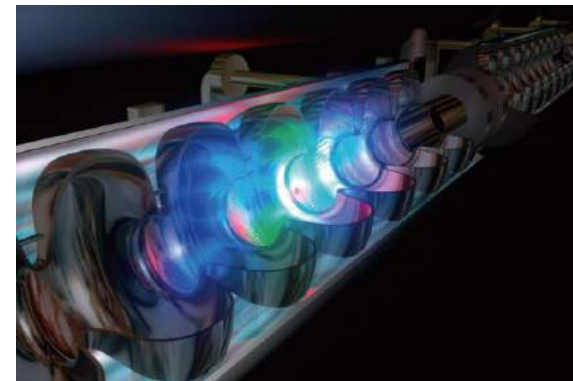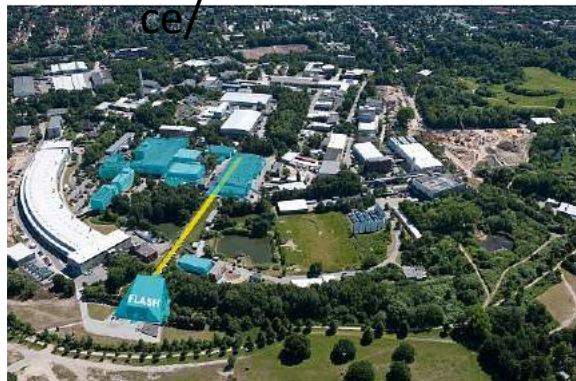
http://flash.desy.de/sites2009/site_vuvfel/content/e395/e2188/FLASH-Broschrefrs_web.pdf

High-Harmonic Generation Sources
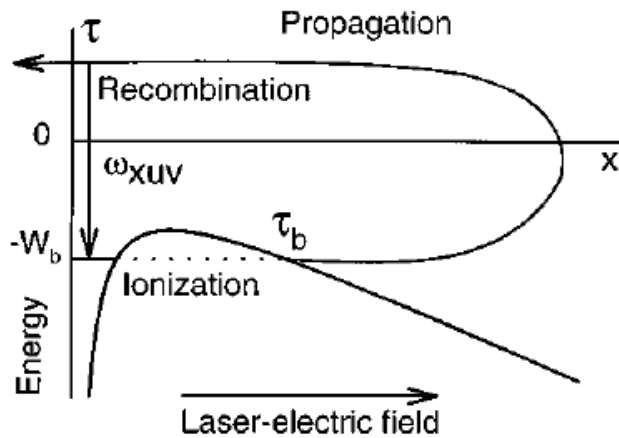
•Schematic depiction of HHG process.
•T. Brabec and F. Krausz. "Intense few-cycle laser fields: Frontiers of nonlinear optics." *Rev. Mod. Phys.* 72.2 (2000): 545.
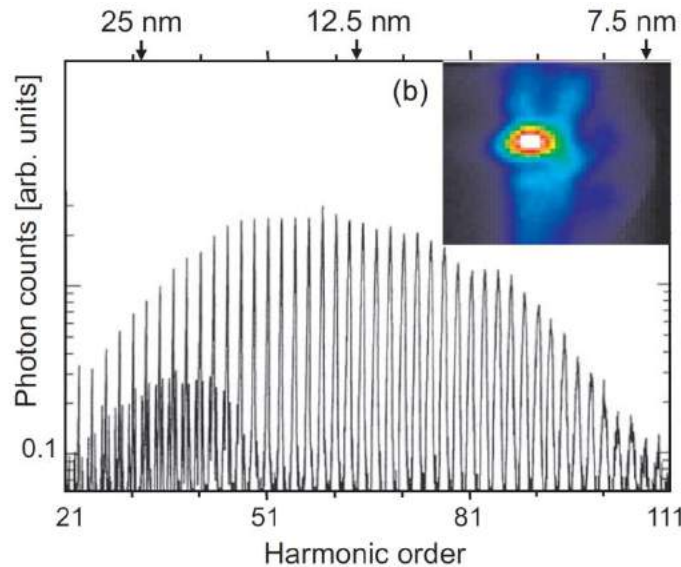
•Spectral distribution of HHG (inset: spatial intensity profile)
•F. Krausz and M. Ivanov. "Attosecond physics." *Rev. Mod. Phys.* 81.1 (2009): 163.

•Schematic of AS-1 beamline at Max Planck Institute of Quantum Optics
•F. Krausz and M. Ivanov. "Attosecond physics." *Rev. Mod. Phys.* 81.1 (2009): 163.

•Time-Dependent electron density of simple atom in HHG (taken from website of Ultrafast X-ray group at University of Southampton http://www.orc.soton.ac.uk/xray.html)
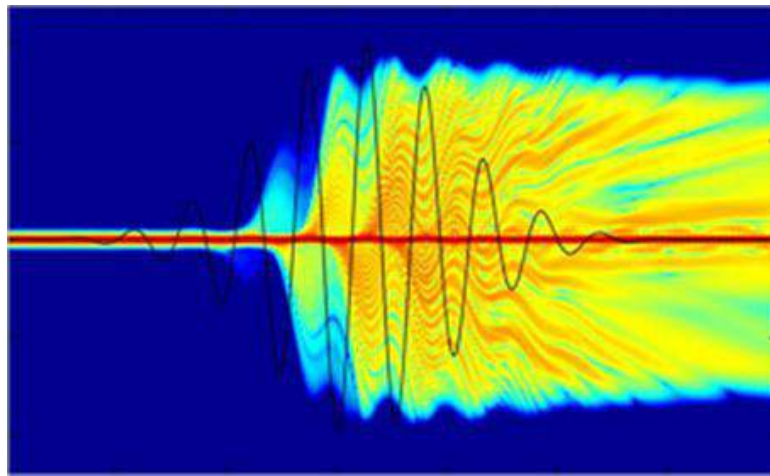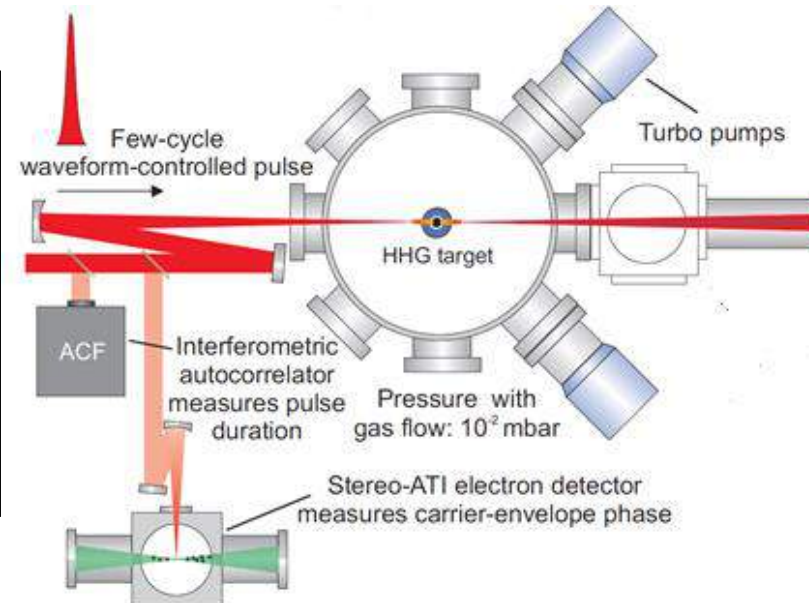
Conical intersections (CoIr
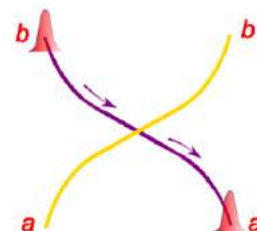
- A fundamental concept for chemical reaction dynamics that controls the rates and yields of photochemical processes

- Points where the molecule reaches a geometry for which potential energy surfaces of different electronic states come close in energy and may even become degenerate.

- Born-Oppenheimer approximation breaks down.

- The electronic and nuclear motions are strongly coupled

- Direct characterization of CoIns is essential to the understanding of ultrafast photo-induced chemical reactions.

- Direct detection of this ultrafast event is still lacking, only indirect circumstantial evidence exists.

Review books: Domcke, W., Yarkony, D. R., and Koppel, H., editors.
Conical Intersections: Electronic Structure, Dynamics & Spectroscopy. World scientific (2004).
Conical Intersections: Theory, Computation and Experiment. World scientific (2011)

68

Conical Intersections (CoIns)

- Responsible for fast, radiationless decay

- Very common in polyatomic molecules

- Important in bio-molecules

- Protects DNA from UV-damage

- Not directly probed

- Inferred from fast rates
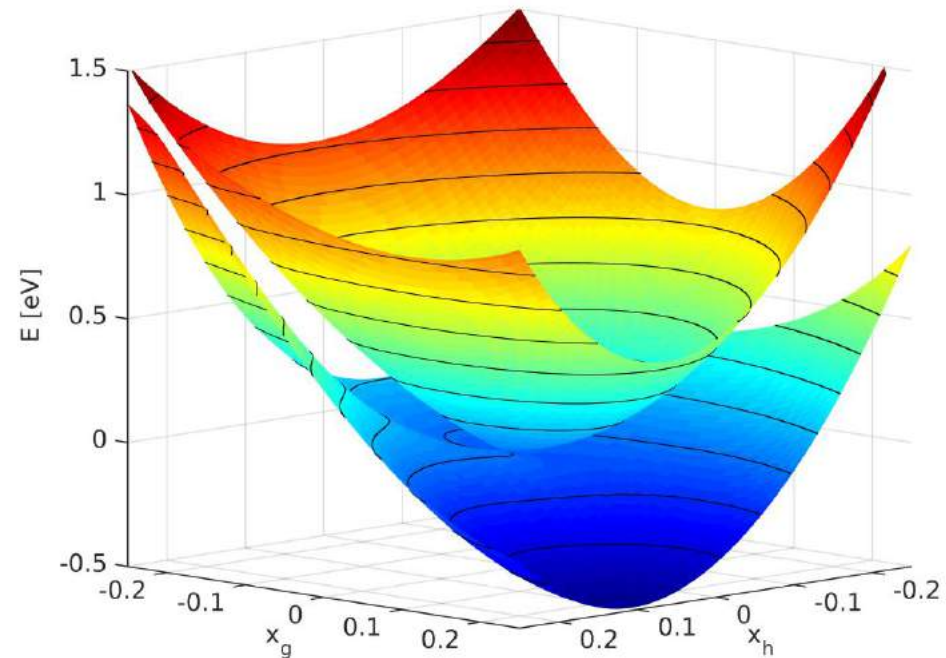
Conical Intersections

- Requires 3 atoms or more

- Point of degeneracy

- Branching space, 2 vib. DOF:

  gradient difference vector (g)

  non-adiabatic coupling vector (h)

- N-2 dim. seam space
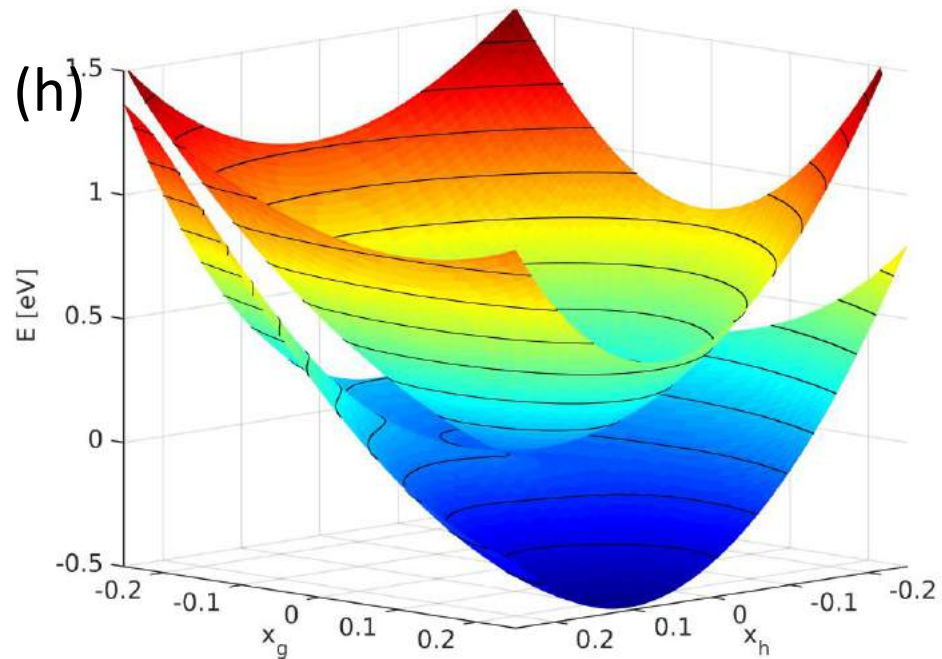
Spectroscopic Signatures of CoIns

- Conventional Methods are based on Populatiom dynamics

- Infrared/Optical pulses

- Change of vibrational Frequencies

- Transient Absorption

- Challenge: rapidly decreasing energy gap

    → huge bandwidth needed

- Solution X-ray pulses (FEL, HHG sources)

Catching Conical Intersections in the Act

Monitoring Transient Electronic Coherences by Attosecond X-Ray Raman Signals

TRUECARS

Transient Redistribution of Ultrafast Electronic

Coherences in Attosecond Raman Signals

- → attoseconds, several eV bandwidth

- → sensitive to coherences, background free

Coherent Signatures of Conical Intersections in Ultrafast X-Ray Spectroscopy

Markus Kowalewski, Kochise Bennett, Konstantin Dorfman,

Shaul Mukamel
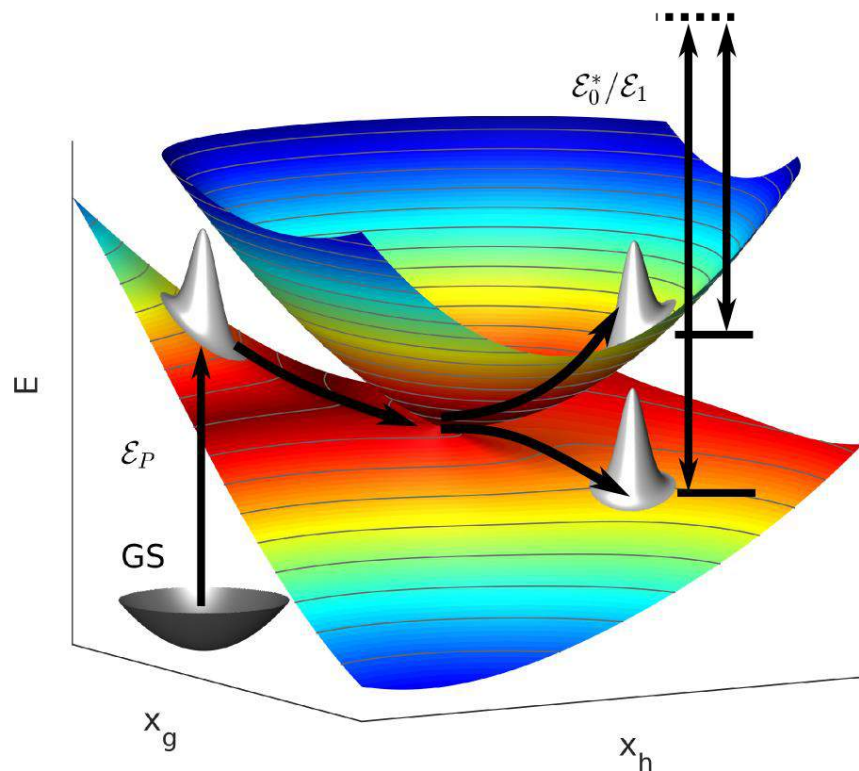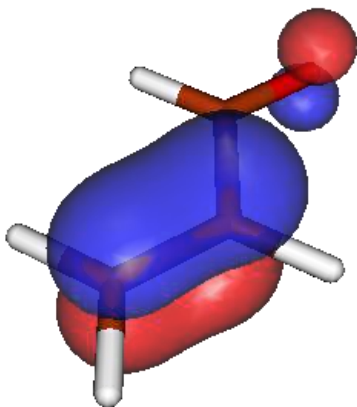
The FSRS Signal

- UV excitation launches dynamics

- Raman probe: broad/narrow
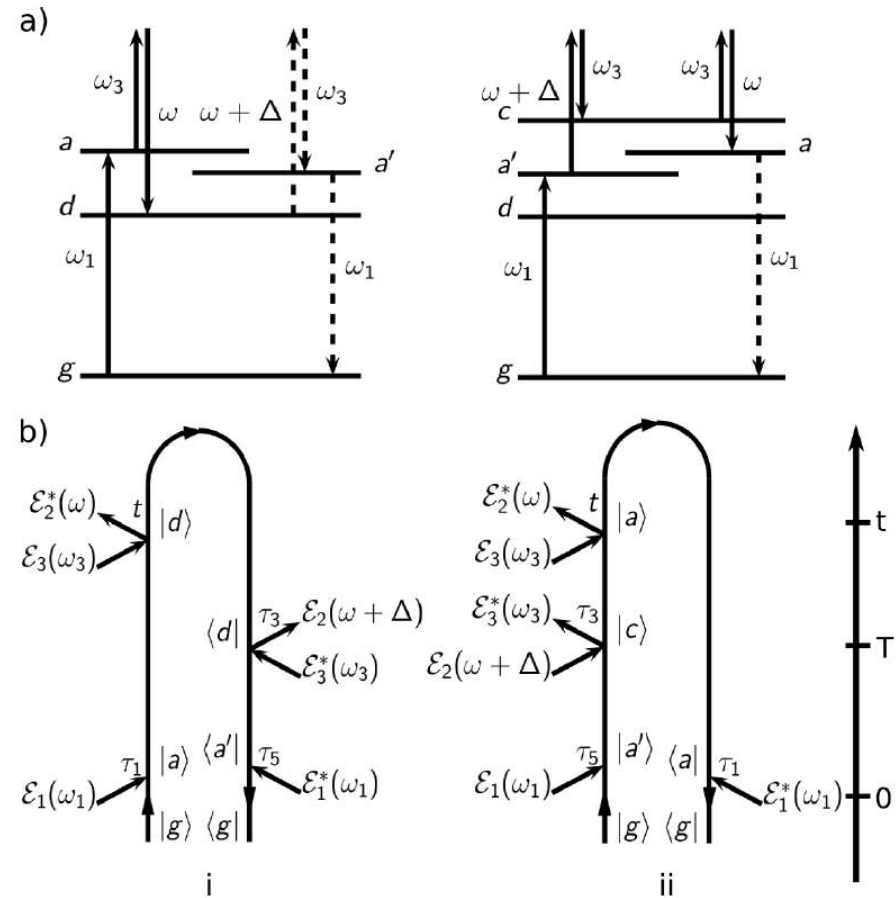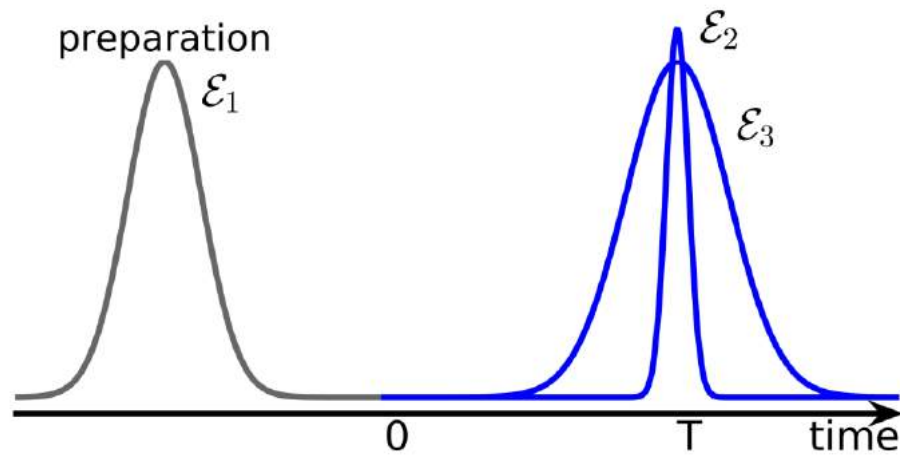
TRUECARS

- A preparation process (gray box) leaves the system in a nonstationary state.
- A hybrid pulse with broadband () and narrowband () components probes the dynamics.
- The frequency-dispersed transmission of the broadband component is plotted versus the delay time
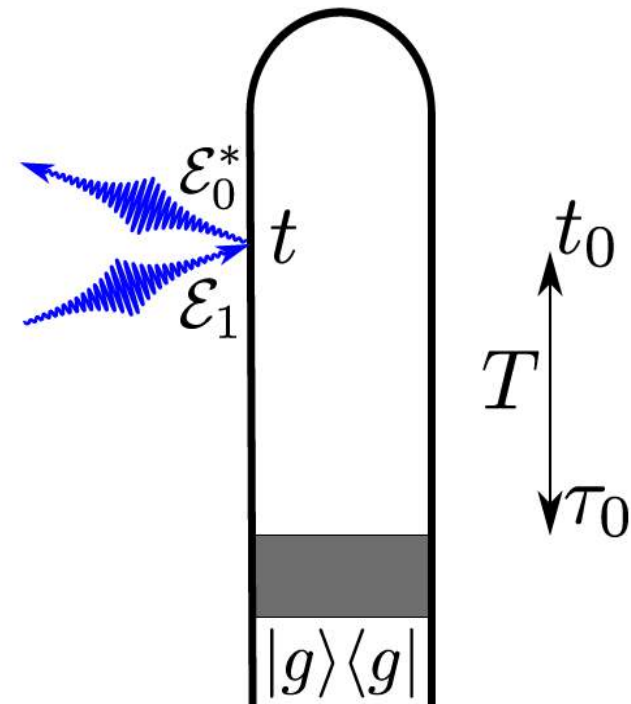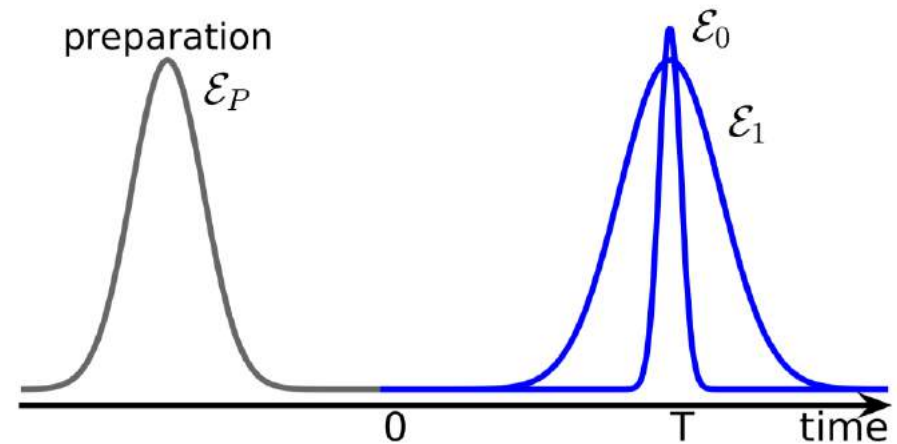
TRUECARS vs SXRS

• TRUECARS is linear (left) and provides background-free measurement of electronic coherence. TCRR depends on relative phase and requires phase-control to observe.
• SRS is quadratic (right) and contains contributions due to populations. The field phases come in pairs and cancel.
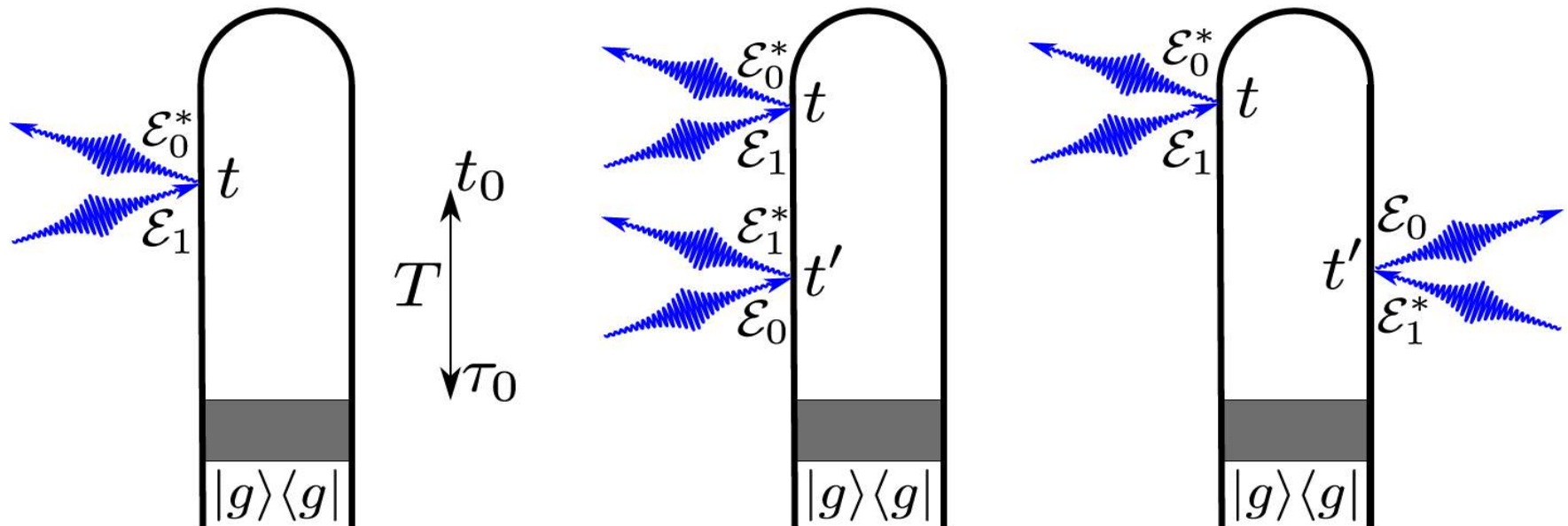
TRUECARS – Similar to CARS (Half CARS)

• CARS (right): Electronic coherence generated with a pair of pulses and probed with a second pair after a fixed delay.
• TRUECARS (left): A nonstationary state is prepared and electronic coherence is generated internally through the propagation
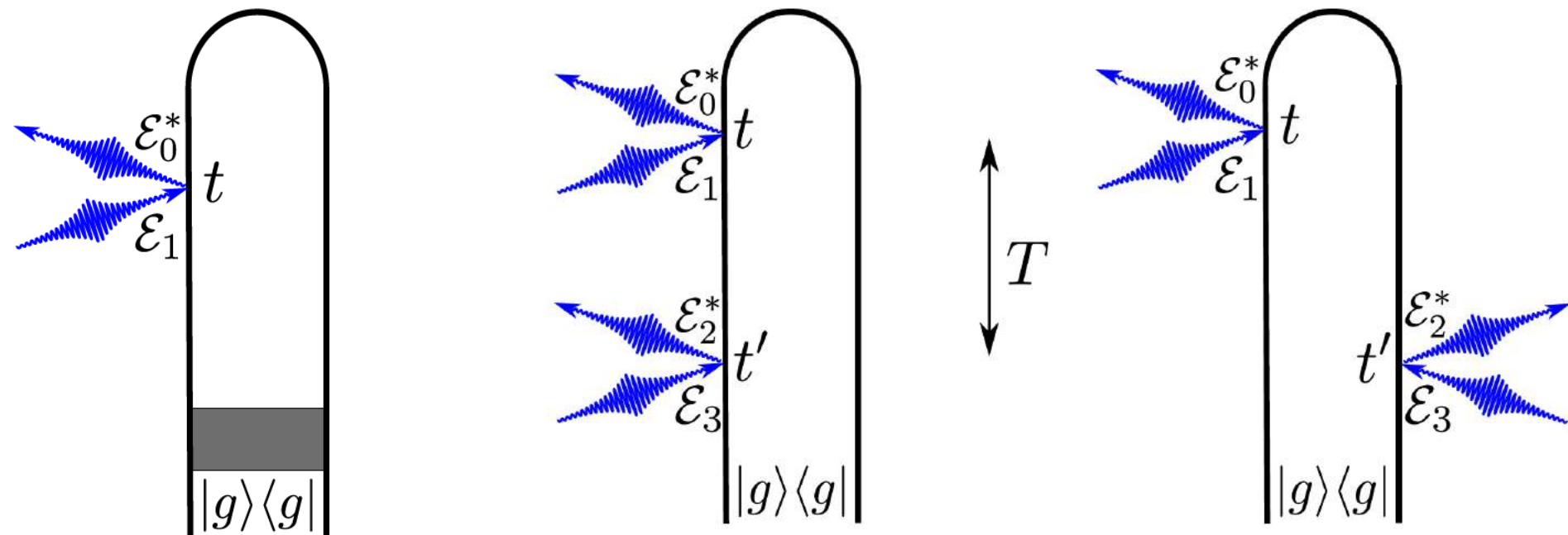
TRUECARS

- Initial state preparation followed by delay and probe with hybrid broadband (as) narrowband (fs) pulse

- Coherences created by laser pulse or system coupling (CoIn)

- Frequency-dispersed photon number change of broadband pulse is detected

- Signal is off-resonant and Linear in probe

- Energy splitting appears as Raman shift between observed and central pulse frequencies

TRUECARS - Formalism

$$\hat{H}_{\mathrm{mp}}(t) = \hat{\alpha}|\mathcal{E}_0(t) + \mathcal{E}_1(t)|^2$$
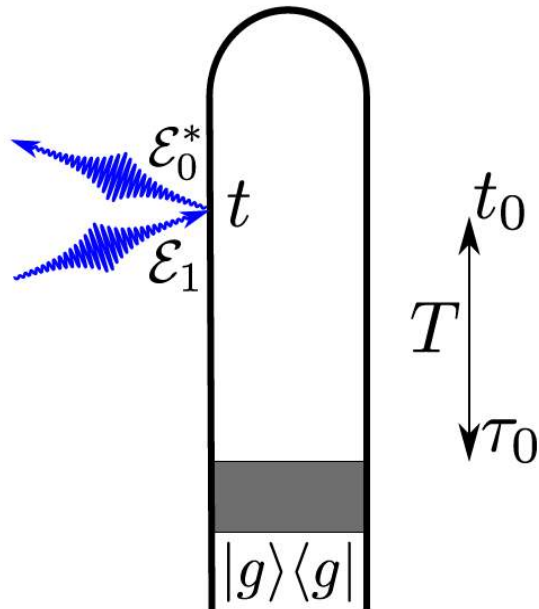
$$S(\omega, T) = 2\Im \int_{-\infty}^{+\infty} \mathrm{d}t\, e^{i\omega(t-T)} \mathcal{E}_0^*(\omega)\mathcal{E}_1(t-T)$$

$$\times \langle\psi(t)|\hat{\alpha}|\psi(t)\rangle$$

TRUECARS - Signal

$$S(\omega, T) = 2\Im \int_{-\infty}^{+\infty} dt\, e^{i\omega(t-T)} \mathcal{E}_0^*(\omega)\mathcal{E}_1(t-T)$$

$$\times \langle\psi(t)|\hat{\alpha}|\psi(t)\rangle$$

Signal depends on x-ray polarizability, electronic coherences:

$$\rho_{el} = \mathrm{Tr}_n(\rho) = \begin{pmatrix} \langle\phi_1|\phi_1\rangle & \langle\phi_1|\phi_2\rangle \\ \langle\phi_2|\phi_1\rangle & \langle\phi_2|\phi_2\rangle \end{pmatrix}$$

$$\alpha(t) = \langle\psi(t)|\hat{\alpha}|\psi(t)\rangle = \langle \begin{pmatrix} \phi_1(t) \\ \phi_2(t) \end{pmatrix} | \begin{pmatrix} 0 & 1 \\ 1 & 0 \end{pmatrix} | \begin{pmatrix} \phi_1(t) \\ \phi_2(t) \end{pmatrix} \rangle = 2\Re\langle\phi_1(t)|\phi_2(t)\rangle$$

Simple Model System

Model resembles wave packet passing through CoIn/avoided crossing:
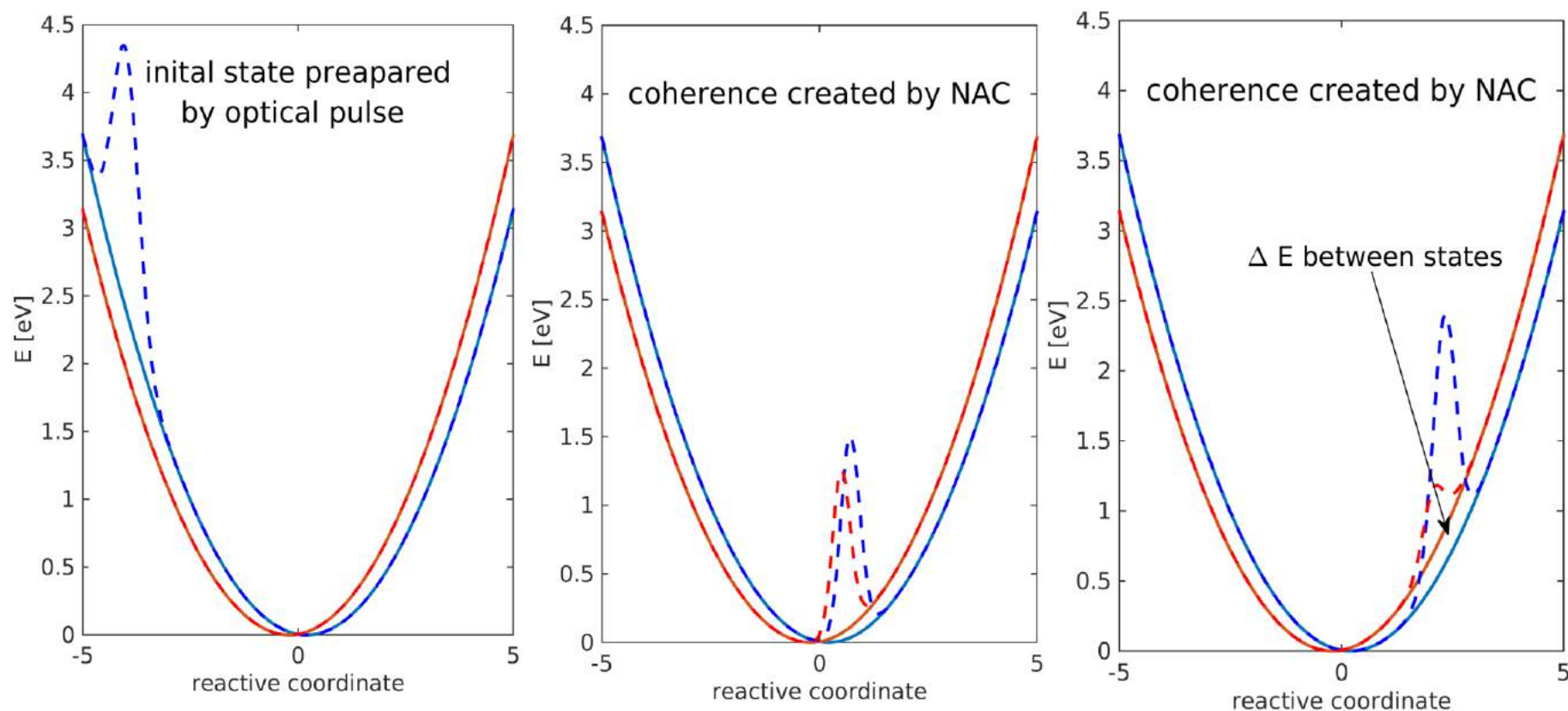
Simple Model System - Hamiltonian

Model Hamiltonian in diabatic represntation

$$H = -\mathbb{1}\frac{1}{2m}\sum_{i\in\{h,g\}}\frac{\mathrm{d}^2}{\mathrm{d}x_i^2} + \begin{pmatrix} H_1(x) & H_{12}(x) \\ H_{12}(x) & H_2(x) \end{pmatrix}$$

Harmonic model

$$H_1 = \frac{1}{2}0.01\left(x - 0.2\right)^2$$

$$H_2 = \frac{1}{2}0.01\left(x + 0.2\right)^2$$

Time stepping (Short Iterative Lanczos)

$$\psi(x, t + \Delta t) = \exp\left(-iH\Delta t\right)\psi(x, t)$$

Gaussian coupling resembles avoided crossing

$$H_{12} = 0.01\exp\left(-x^2\right)$$

TRUECARS Signal

Spectrum resembles the time-dependent splitting
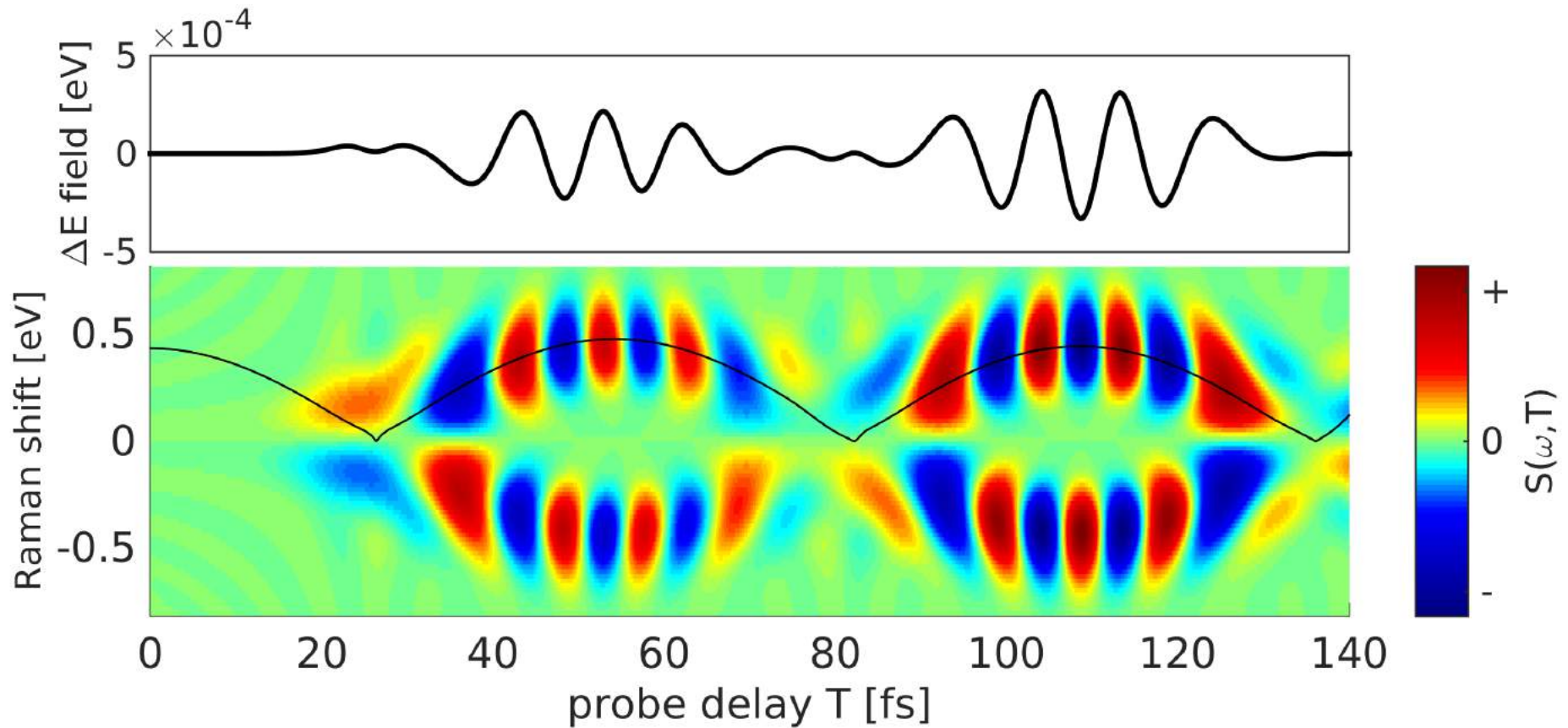
Nonadiabatic dynamics of molecules in optical cavities

Markus Kowalewski, Kochise Bennett, and Shaul Mukamel
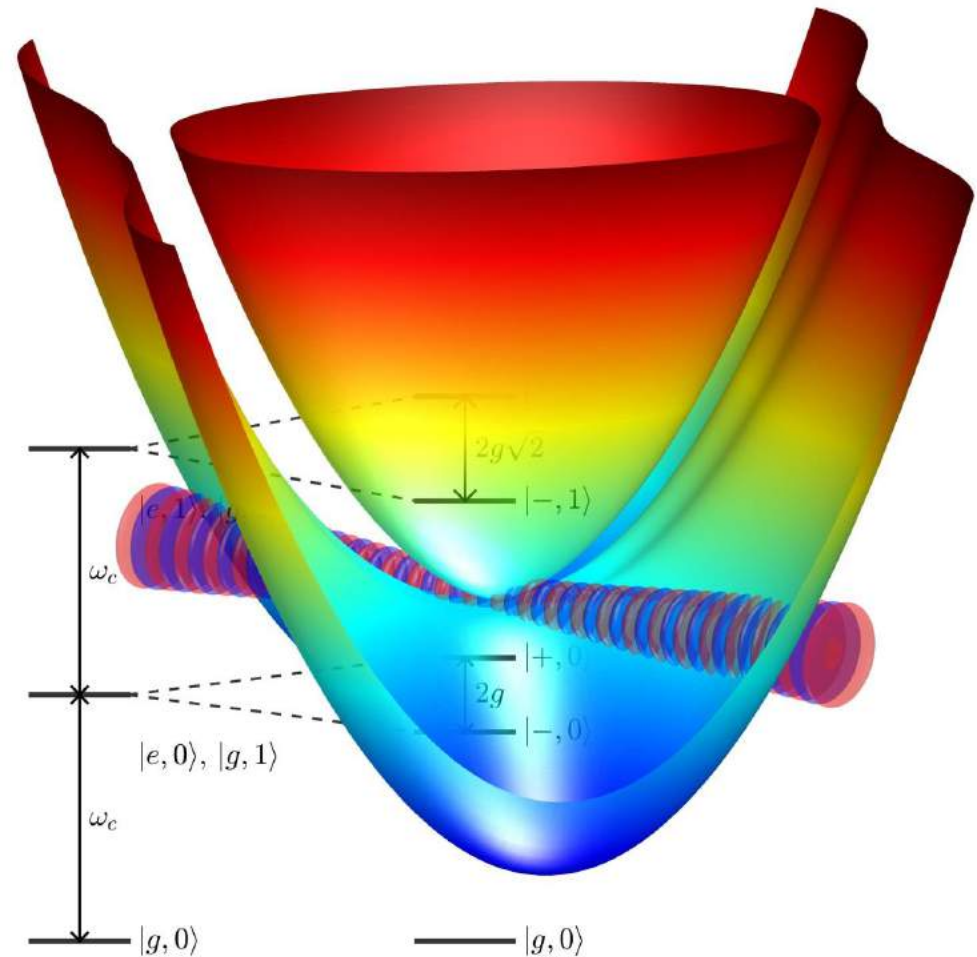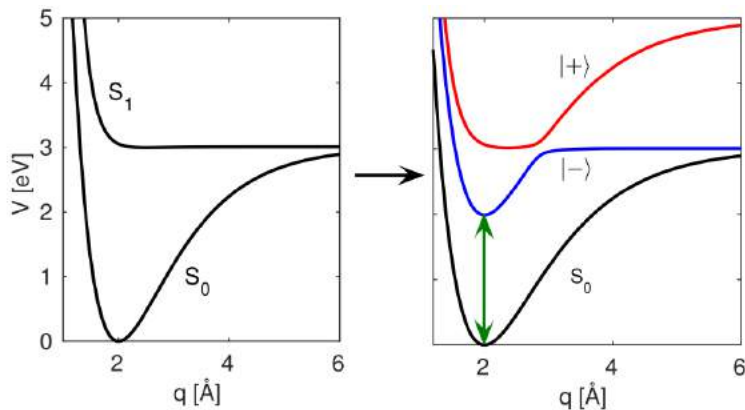
Quantum Field Modifications of Photochemistry and Spectroscopy

Markus Kowalewski, Kochise Bennett, Prasoon Saurabh,

Shaul Mukamel
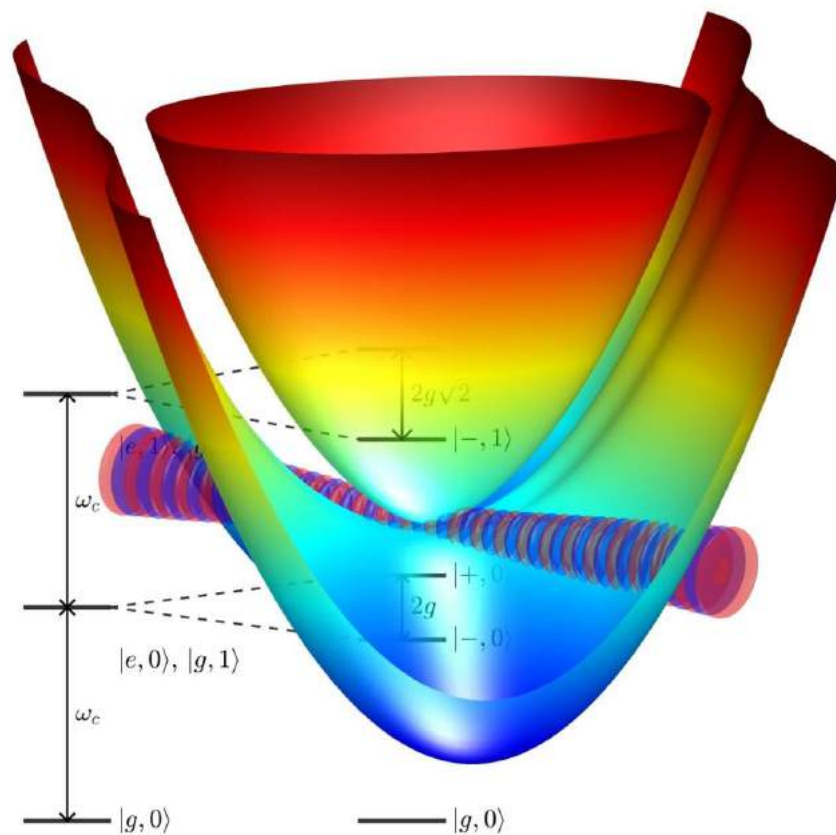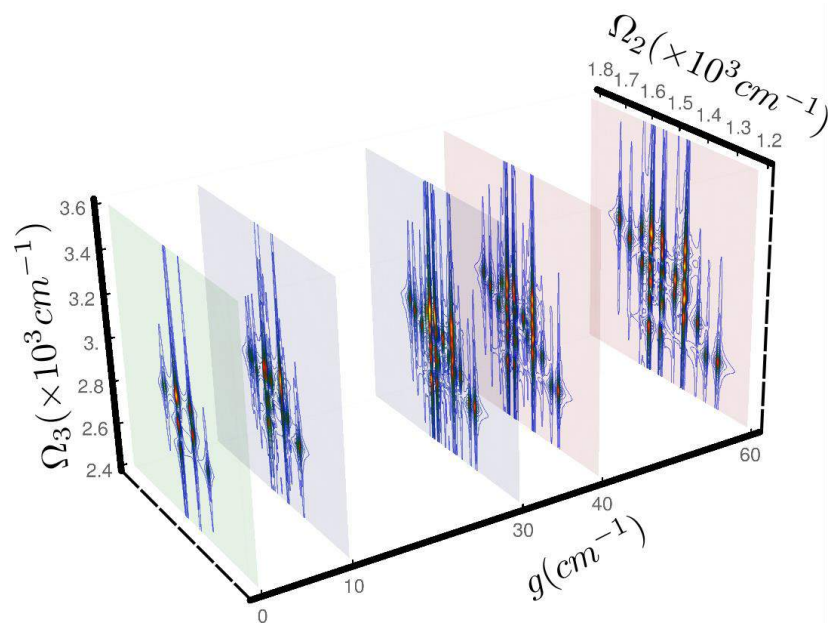
Cavity QED

- Enhancement of stim. Emssion

- Purcell effect

- Cavity QED: Well studied for atoms

- Coupling to Vacuum field

- Quantum nature of the field

γ = Atomic spontaneous decay κ = cavity decay rate
g = Single photon Rabi frequency / 2

$$g = \varepsilon_c \mu_{eg}/2\hbar \qquad \varepsilon_c = \sqrt{\frac{\hbar\omega_c}{V\epsilon_0}},$$

E. M. Purcell, Phys. Rev. **69**, 674 (1946)
H. J. Kimble, Phys. Scripta **T76**, 127 (1998)
S. Haroche, Rev. Mod. Phys. **85**, 1083 (2013)
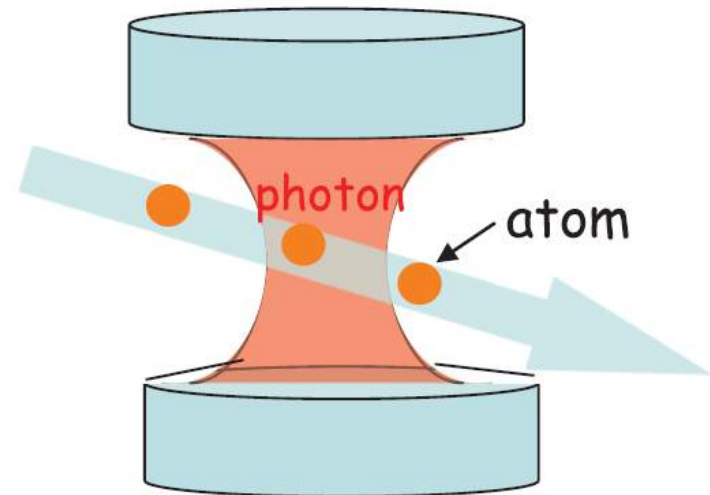
Overview

- Extend JC-model to molecules

- Single molecule model

- Formalism for non-adiabatic quantum dynamics

- Study modification of photochemistry
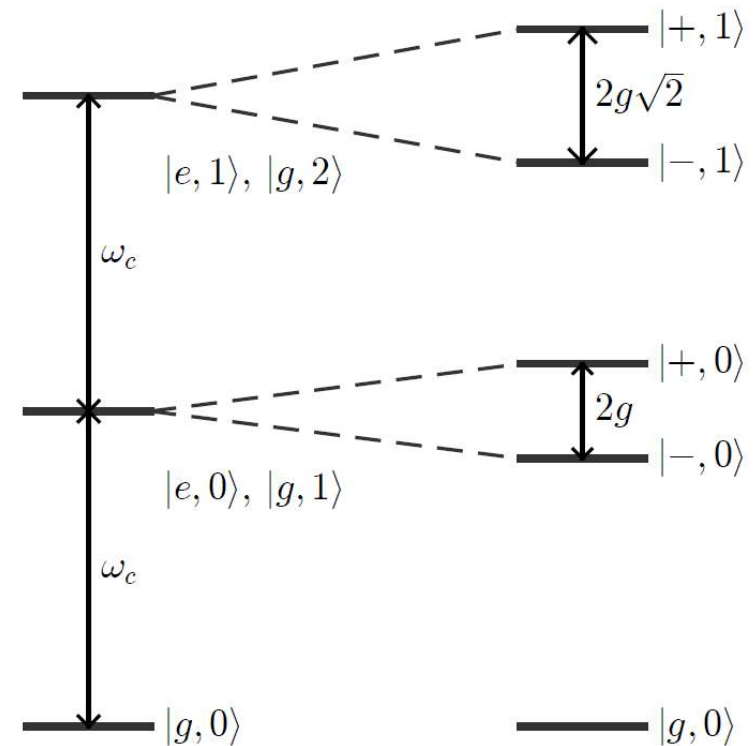
The Jaynes-Cummings Model

- Jaynes-Cummings Hamiltonian

- Quantized Radiation Field

$$H_M = \frac{\hbar}{2}\omega_0 \left(\sigma^\dagger \sigma - \sigma \sigma^\dagger \right)$$

$$H_C = \hbar \omega_c \left(a^\dagger a + \frac{1}{2} \right)$$

$$H_I = \hbar g \left(a^\dagger \sigma + a \sigma^\dagger \right)$$

Solutions: dressed states

$$E_{\pm,n} = \frac{\hbar}{2}\omega_0 + \hbar \omega_c \left(n_c + \frac{1}{2} \right) \pm \frac{\hbar}{2}\Omega_n$$

Ω_n: effective Rabi-frequency

$g = \varepsilon_c \mu / \hbar$: cavity coupling

$$\Omega_n = \sqrt{4g^2(n_c + 1) + \delta_c^2}$$
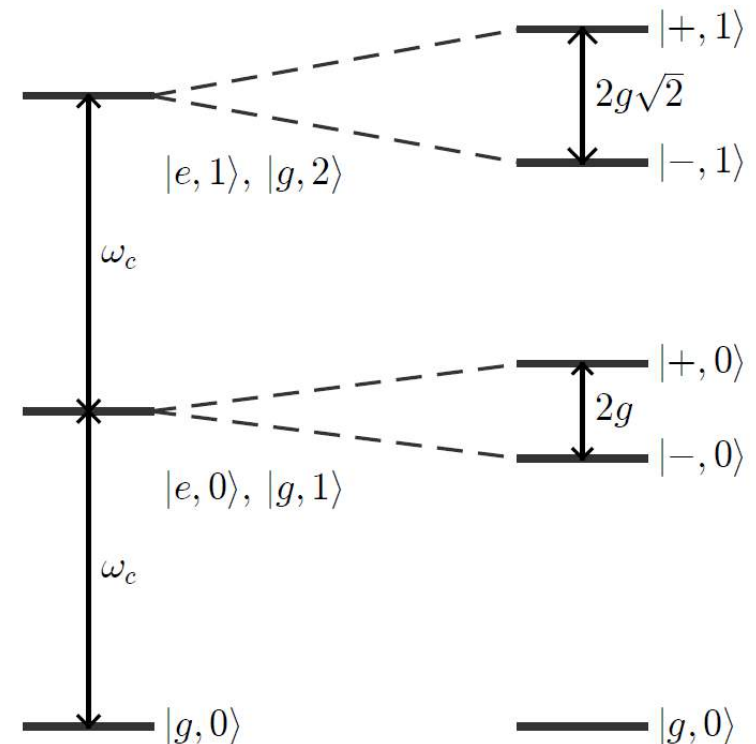
Limits of the Rotating Wave Approximation

Full Hamiltonian:

$$\hat{H}_{ec} = H_e + H_c + H_I = \frac{\hbar\omega_0}{2}(2\hat{\sigma}^\dagger\hat{\sigma} - 1) + \hbar\omega_c\hat{a}^\dagger\hat{a} + \hbar g(\hat{a}^\dagger + \hat{a})(\hat{\sigma}^\dagger + \hat{\sigma})$$

$$\Psi_c = \sum_{n=0}^{M} c_{g,n_c}|g, n_c\rangle + c_{e,n_c}|e, n_c\rangle$$

- Block Structure

- RWA conserves

  excitation number

$$\hat{N} \equiv \hat{n}_c + \hat{\sigma}^\dagger\hat{\sigma}$$

- Blocks mix due to

  Counter-rotating terms

$$\hat{\sigma}^\dagger\hat{a}^\dagger \quad \hat{\sigma}\hat{a}$$

$$
\begin{pmatrix}
N_0 & & (a\sigma) & \\
& \begin{pmatrix} N_1 \end{pmatrix} & & \\
(a^\dagger\sigma^\dagger) & & \begin{pmatrix} N_2 \end{pmatrix} & \\
& \ddots & & \ddots
\end{pmatrix}
$$

Dynamics beyond the RWA - Formalism

Three approaches:

- Diagonalization via Fock states

  - Natural basis within RWA; facilitates analogy

  - Too many states needed at ultrastrong coupling

- Diagonalization via photon-added coherent states

  - Can handle ultrastrong coupling with much fewer states

  - Requires large number of states at low coupling strengths

- Discretize Cavity mode in real space

  - Elegent solution to obtain dynamical quantities and observables

  - Potential surfaces and NACs are never calculated so can't use this picture to interpret

Nonadiabatic Dynamics at Avoided Crossings

- Cavity coupling beyond the rotating wave approximation

- Ultra-strong coupling regime

- Manipulate wave packet branching at avoided crossings/CoIns

- Extended Formalism required

ionic Na $^+$ + I $^-$
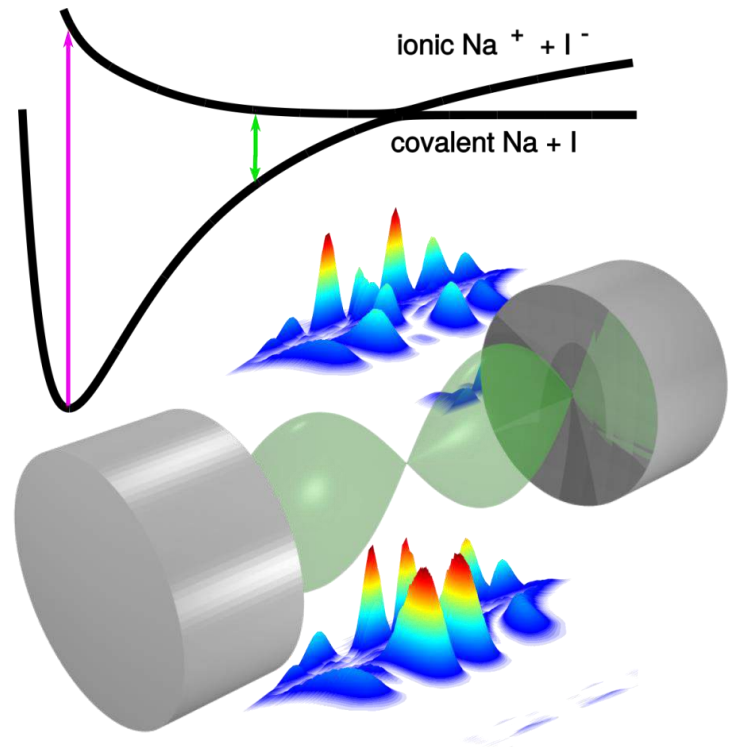
covalent Na + I

Electron Harpooning in Sodium Iodide

Couple cavity to covalent

and ionic state.

Modify branching ration
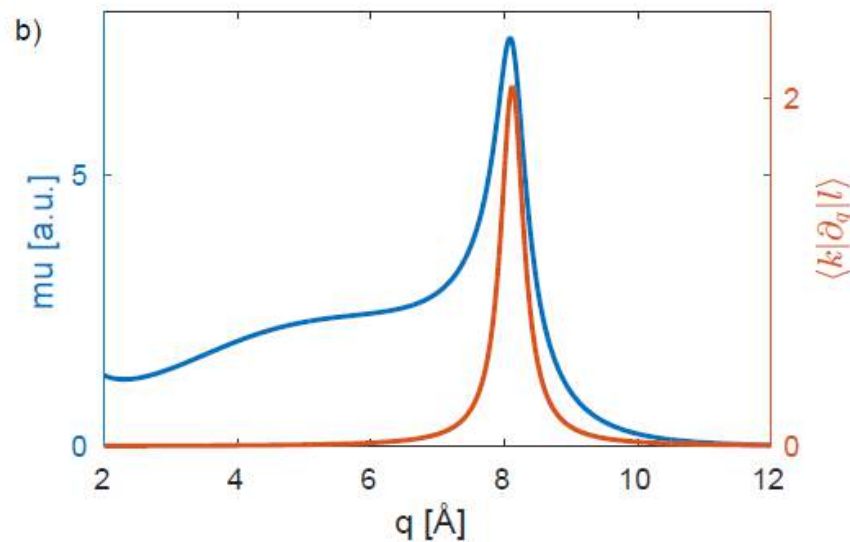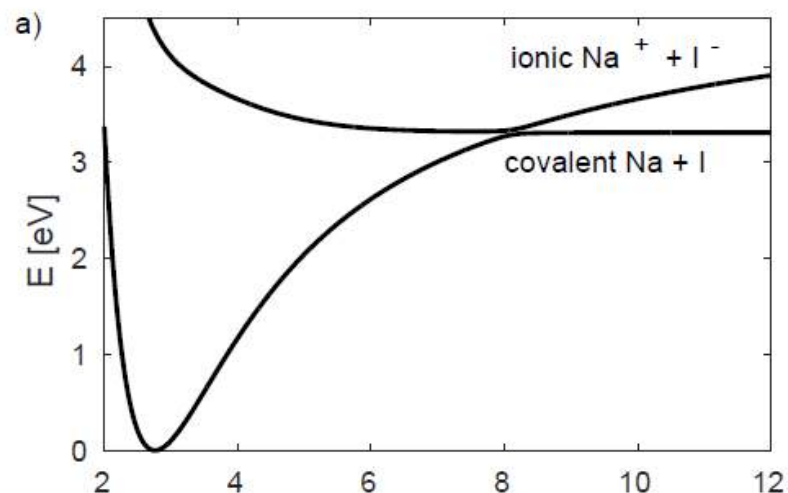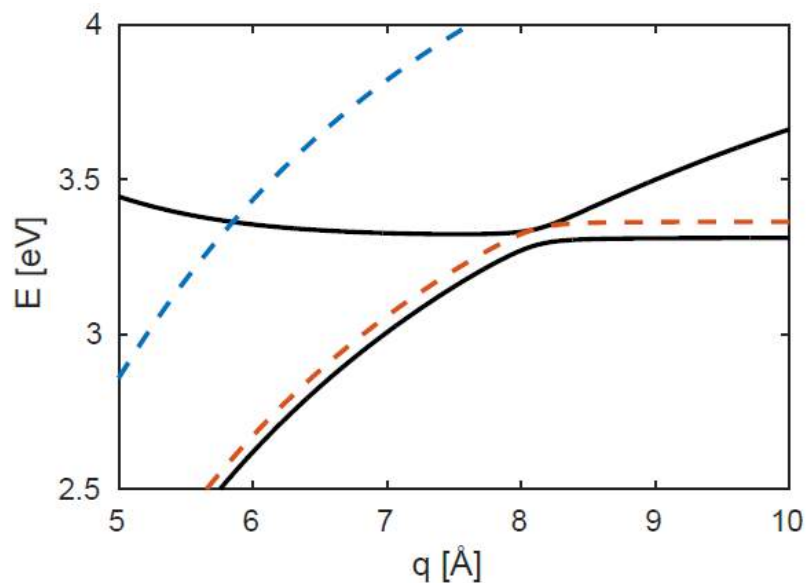
Sodium Iodide

Zewail's landmark experiment
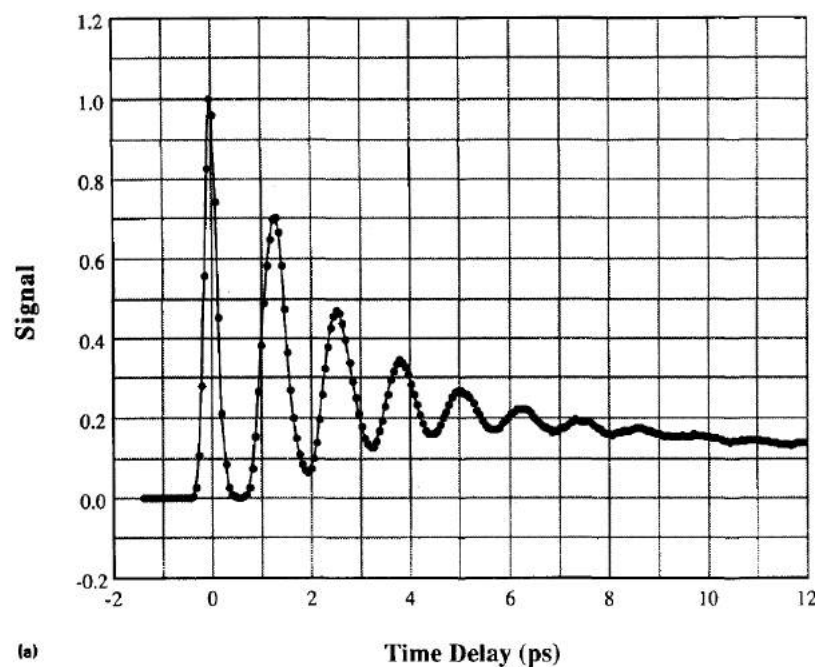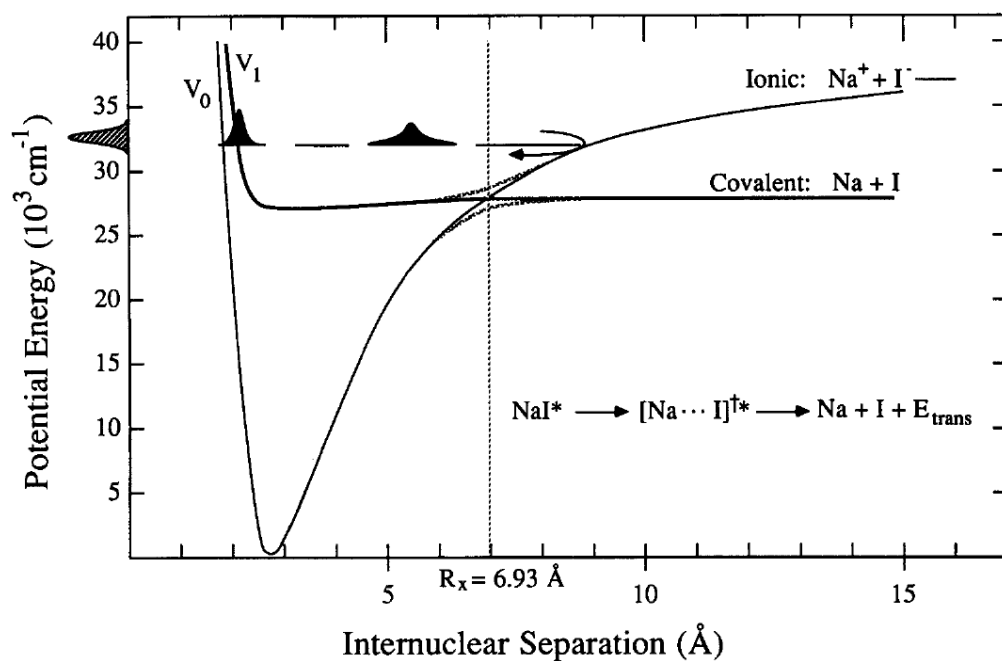
T. S. Rose, M. J. Rosker, and A. H. Zewail, J. Chem. Phys. **91**, 7415 (1989)

Sodium Iodide – Dressed Potential Surfaces
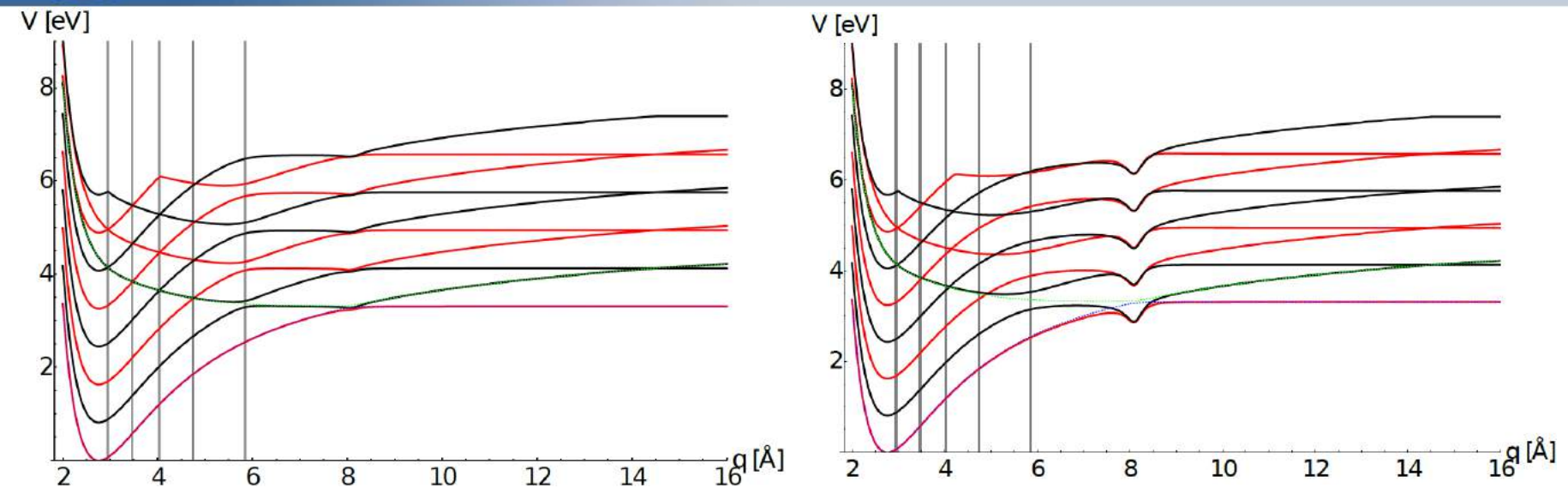
- Positive (red) and negative (black) parity dressed states for gmax=200 and 600meV

- Vertical lines are at n-photon resonances (n=1…5 from right to left)

- Induced NAC spikes at n=odd (same-parity avoided crossings)

- Ultrastrong coupling opens up a dip at the original avoided crossing

  - Can act as a barrier/trap to wavepackets

  - All states connected in this region via transformed NACs

Sodium Iodide - Dynamics

Population dynamics for different coupling strengths
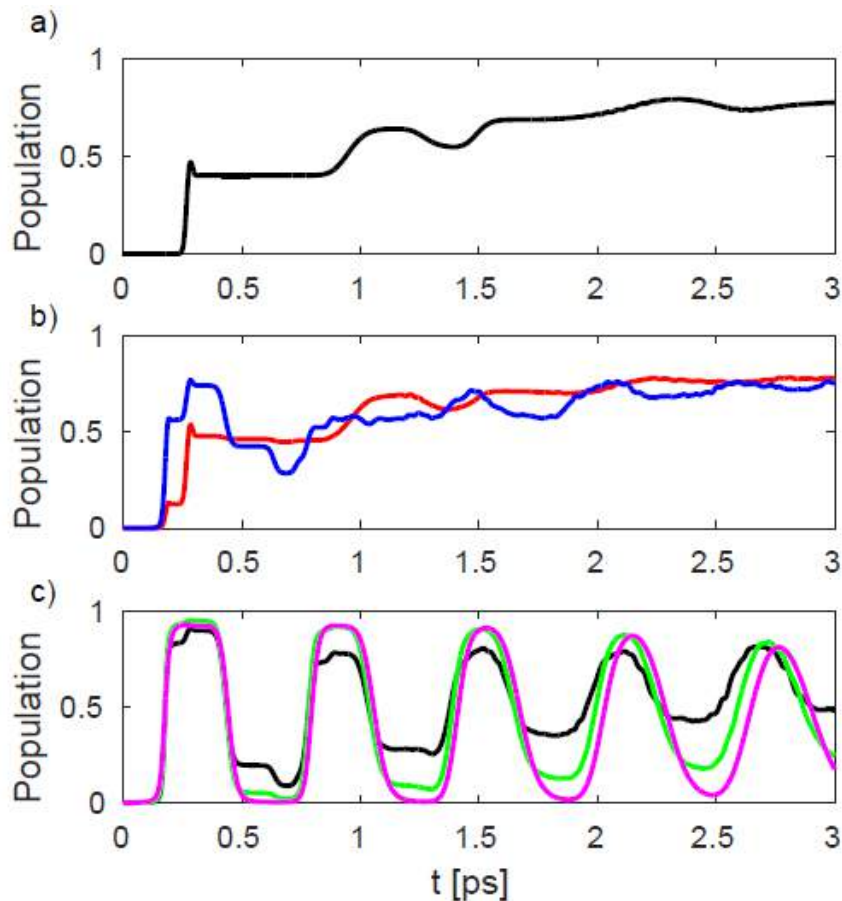
No Cavity

$0.05, 0.13\ \omega_c$

$0.19, 0.25, 0.38\ \omega_c$

M. Kowalewski, K. Bennett, S. Mukamel, J. Phys. Chem. Lett. **7**, 2050 (2016)

Sodium Iodide – Modified Branching Ratio

Dissociation can be suppressed by cavity coupling

Branching

Photon number
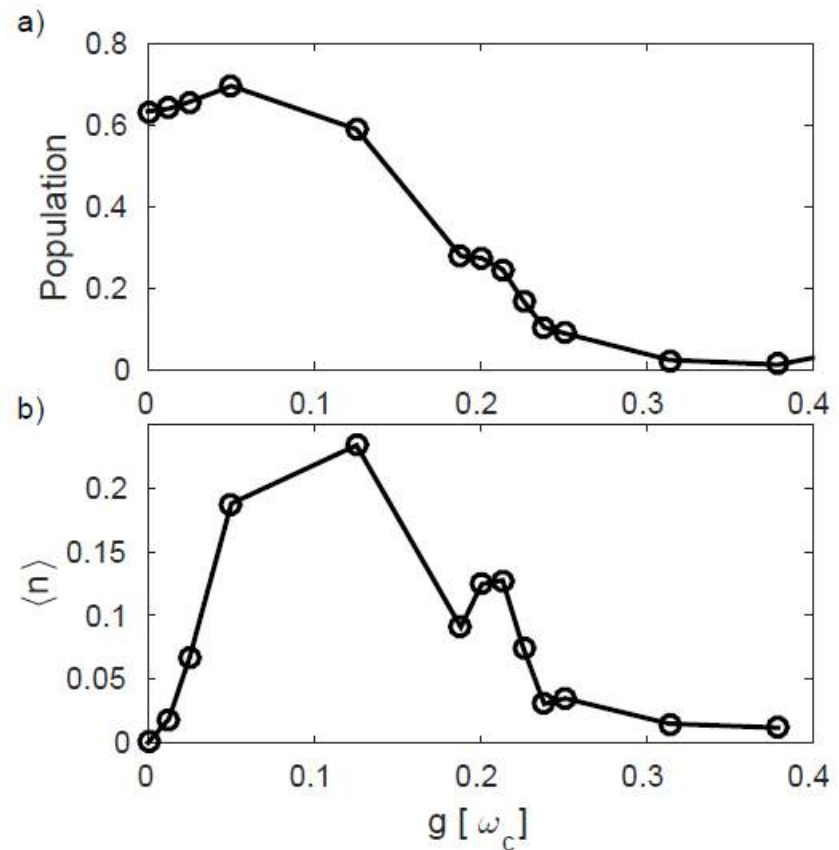
Conclusions

- Strong coupling of single molecules

- Formalism for nonadiabatic quantum dynamics in cavities

- Quantities easily available from Quantum Chemistry

- Photochemical modifications possible

- New kind of light induced conical intersections (PhCoIn)

- Explore collective effects: scaling
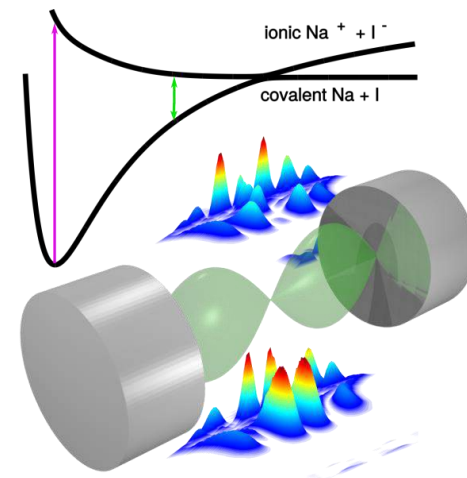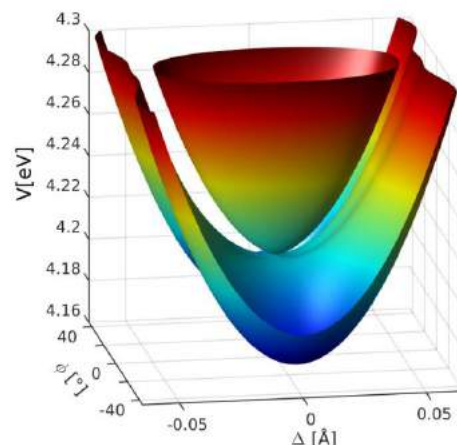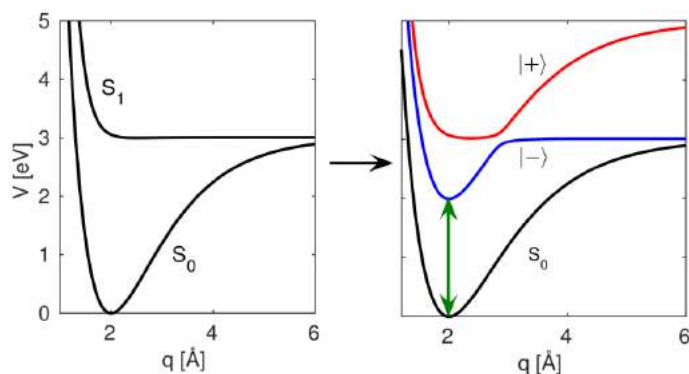
Multidimensional Spectroscopy of Trapped Ions

F. Schlawin, M. Gessner, H. Häffner, S. Mukamel, and A. Buchleitner
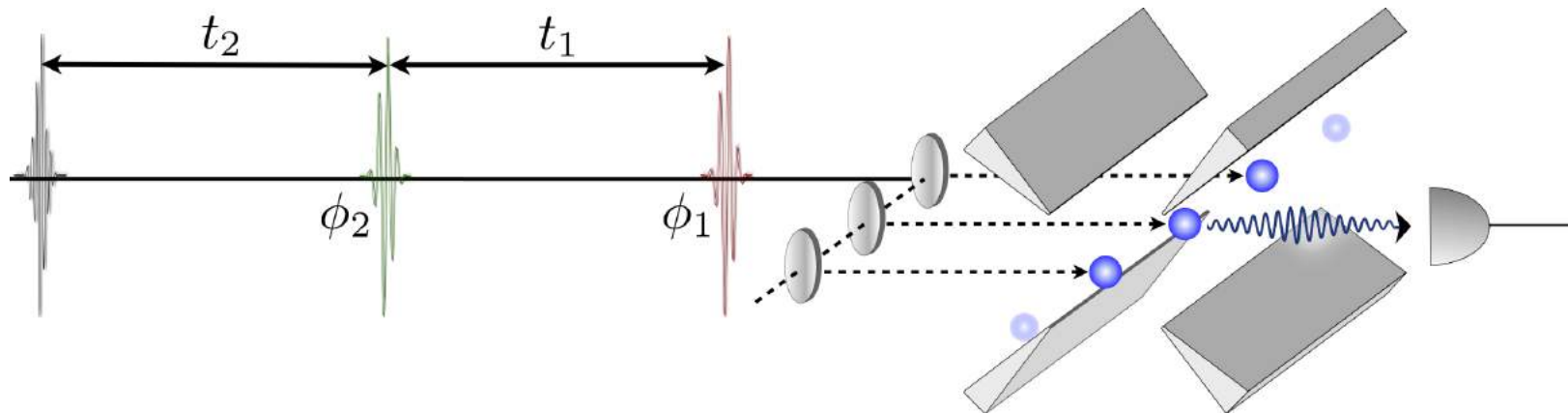
Freiburg, October 9, 2014

Trapped ion crystals
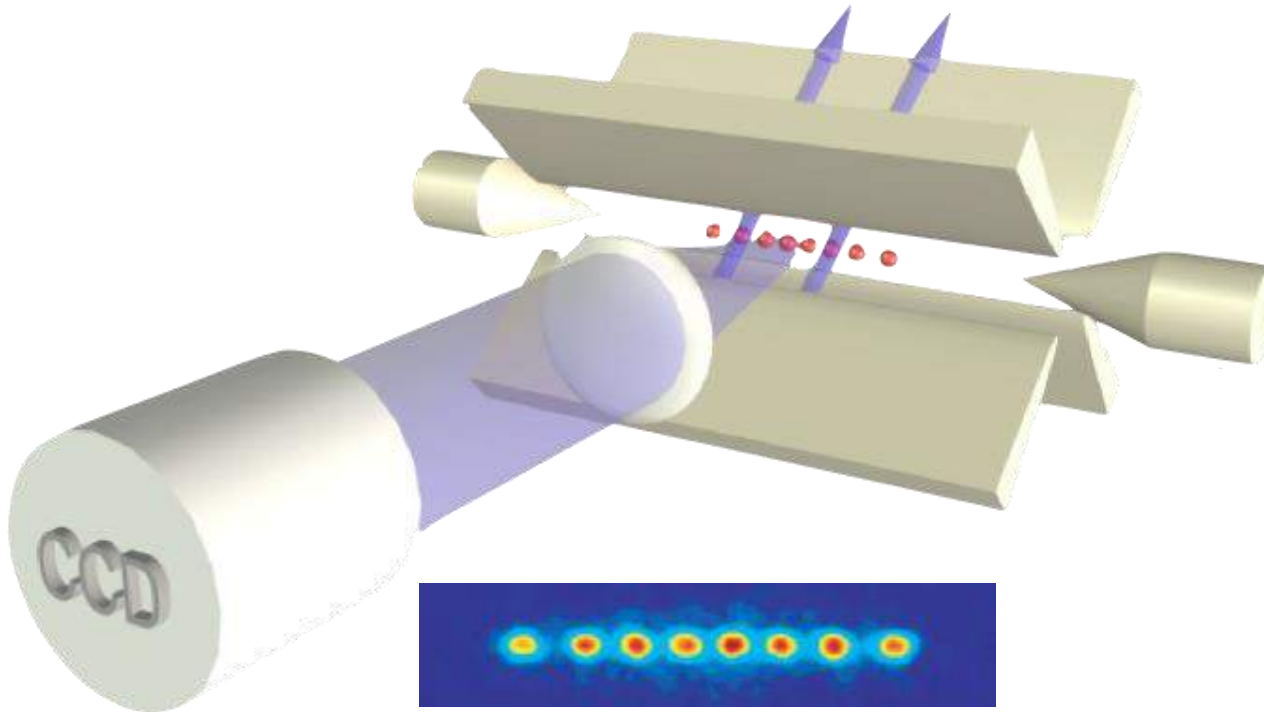
Goal: Develop scalable and flexible method to probe its nonequilibrium physics!

[Image: R. Blatt and D. Wineland, Nature 453, 1008 (2008)]
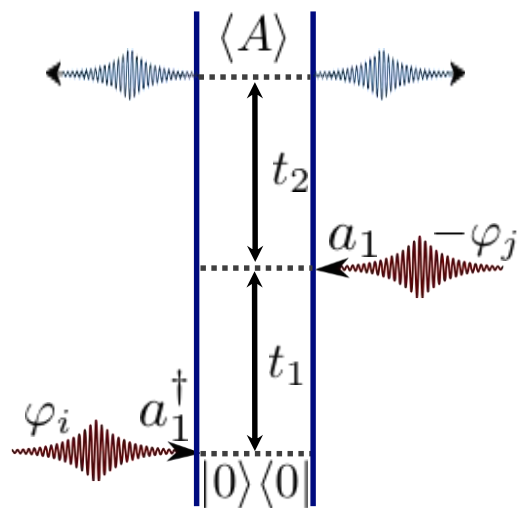
Nonlinear measurement protocols

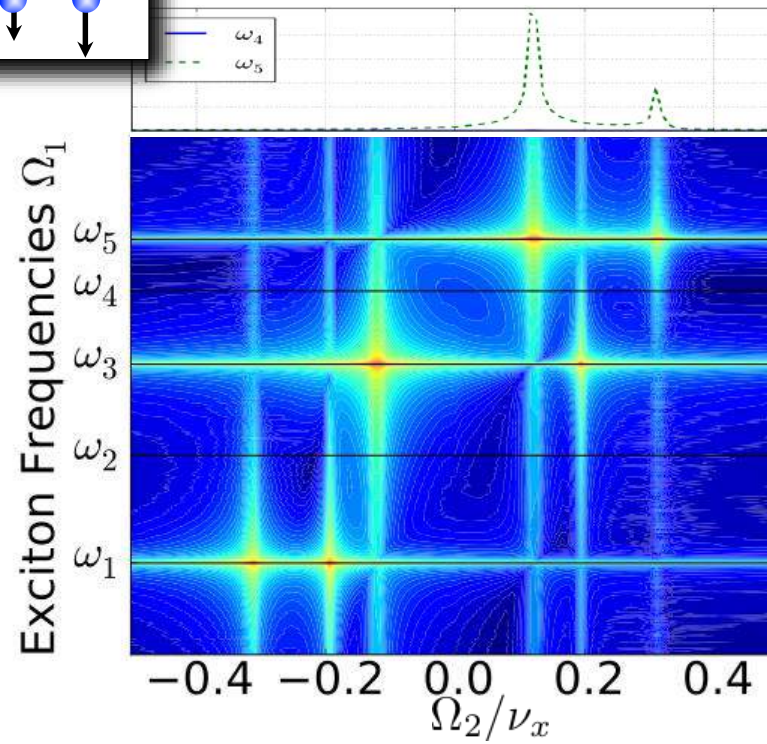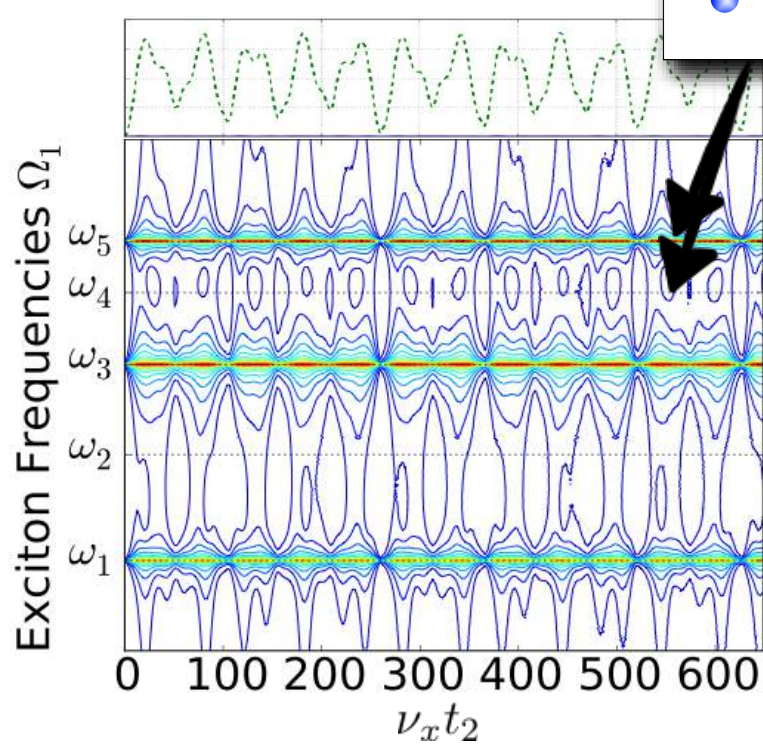Probe system with a sequence of short pulses, scan time delays

Ingredients:

- Local phonon excitation

- Fluorescence readout

- <u>Phase cycling</u>: Pathway selection by control of laser phases
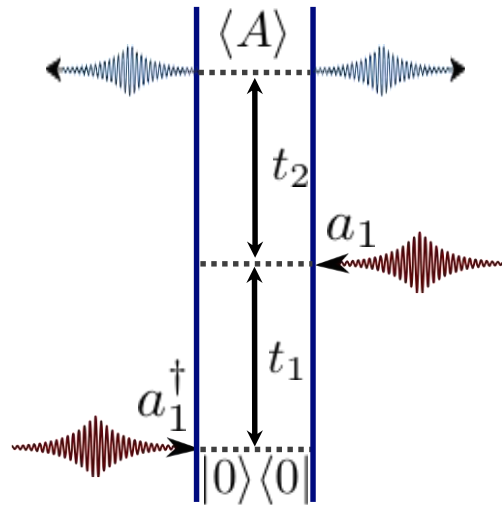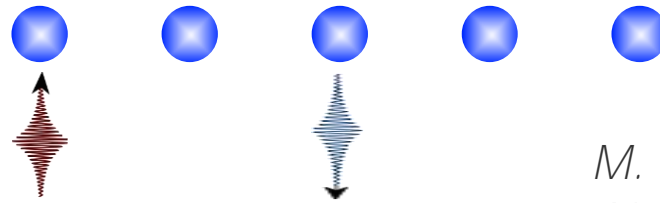
Local phonons in an ion chain

*M. Gessner et al.,
New J. Phys. 16,
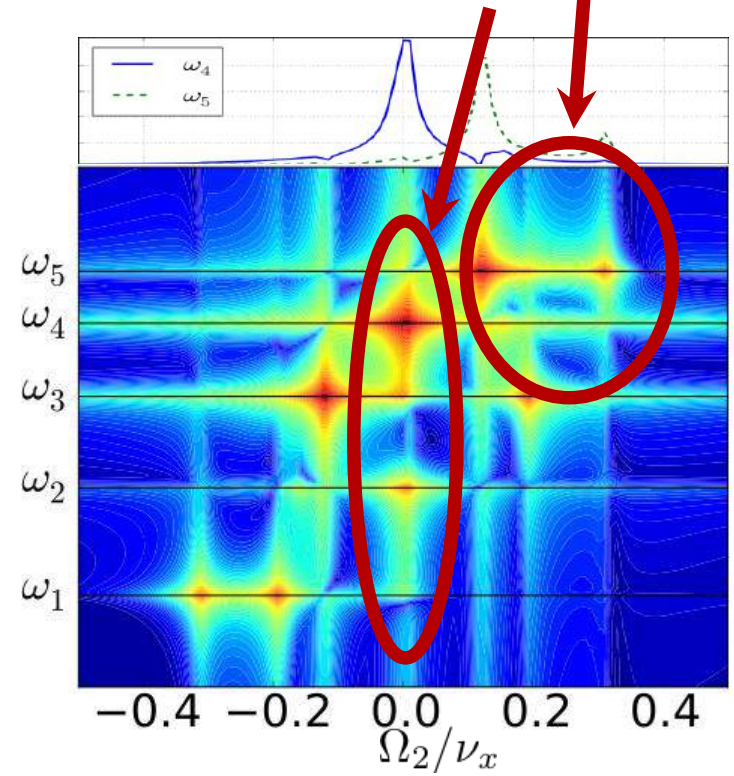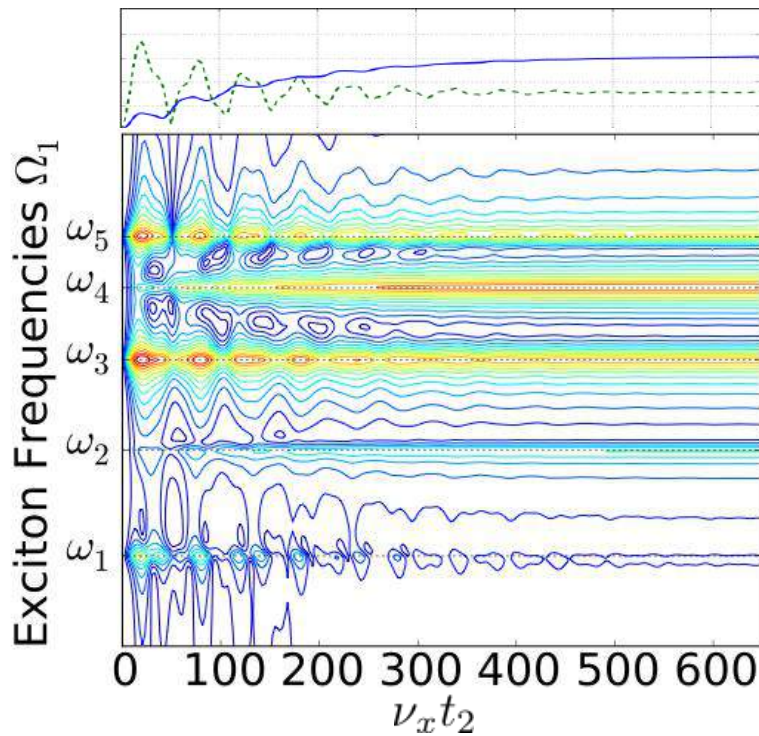092001 (2014)*

Local phonons in an ion chain

Local dephasing: $L_i = \sqrt{\gamma}\, a_i^\dagger a_i$

M. Gessner et al.,
New J. Phys. 16,
092001 (2014)

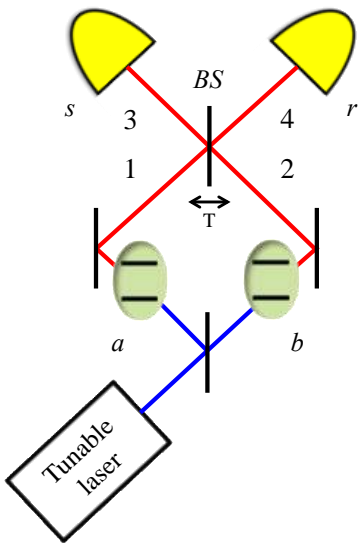Coherent transport
Incoherent transport

Spectral diffusion in quantum emitters measured by photon correlations

Shaul Mukamel and Konstantin E. Dorfman,

University of California, Irvine

Photon coincidence counting (PCC)

$$R_c^{34}(\Gamma_r,\Gamma_s) = \int_{-\infty}^{\infty} dt_s \int_{-\infty}^{\infty} dt_r \left\langle E_3^{(tf)\dagger}(t_r) E_4^{(tf)\dagger}(t_s) E_4^{(tf)}(t_s) E_3^{(tf)}(t_r) \right\rangle$$

1. A pair of photons is generated by two remote two-level chromophores a and b.

2. The photons enter a 50:50 beam splitter and are finally registered by time-and-frequency gated detectors s and r.

3. Possible outcomes:
   - two photons registered in detector s (2,0)
   - two photons registered in detector r (0,2)
   - coincidence: one photon is detected in each (1,1).

4. For classical particles PCC=1/2

5. Indistinguishable photons – we only see (2,0) and (0,2), the PCC vanishes (Hong-Our-Mandel dip).

6. The PCC rate is 1 for distinguishable photons, 0 - indistinguishable.

7. PCC rate less than ½ indicates that photons are indistinguishable.

Spectral diffusion in the emitters decreases the degree of indistinguishability eroding the HOM dip!

Measurement of Subpicosecond Time Intervals between Two Photons by Interference

C. K. Hong, Z. Y. Ou, and L. Mandel

Department of Physics and Astronomy, University of Rochester, Rochester, New York 14627
(Received 10 July 1987)

A fourth-order interference technique has been used to measure the time intervals between two photons, and by implication the length of the photon wave packet, produced in the process of parametric down-conversion. The width of the time-interval distribution, which is largely determined by an interference filter, is found to be about 100 fs, with an accuracy that could, in principle, be less than 1 fs.

$$N_c = C(T^2 + R^2)\left[1 - \frac{2RT}{R^2 + T^2}e^{-(\Delta\omega\,\delta\tau)^2}\right].$$
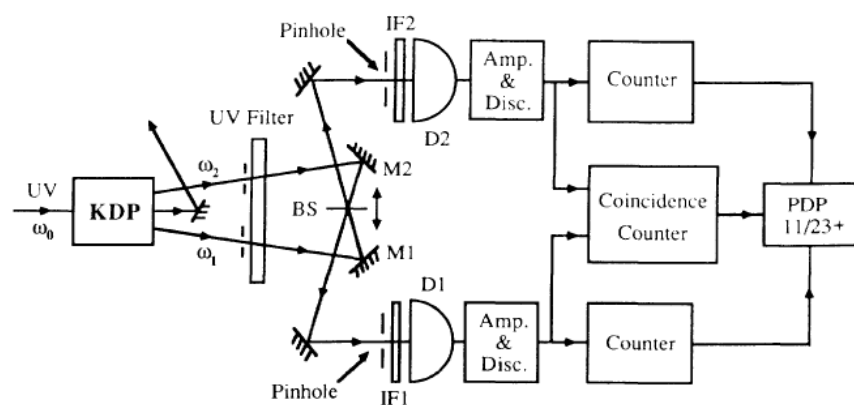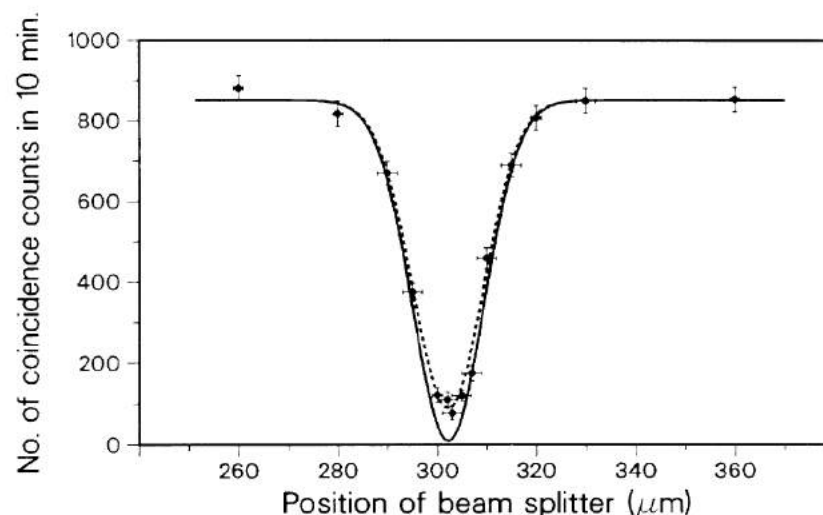

FIG. 1. Outline of the experimental setup.

Quantum Interference of Tunably Indistinguishable Photons from Remote Organic Molecules

R. Lettow,[1] Y. L. A. Rezus,[1] A. Renn,[1] G. Zumofen,[1] E. Ikonen,[2] S. Götzinger,[1] and V. Sandoghdar[1]

[1]Laboratory of Physical Chemistry and optETH, ETH Zurich, CH-8093 Zurich, Switzerland

[2]Metrology Research Institute, Aalto University and Centre for Metrology and Accreditation (MIKES),
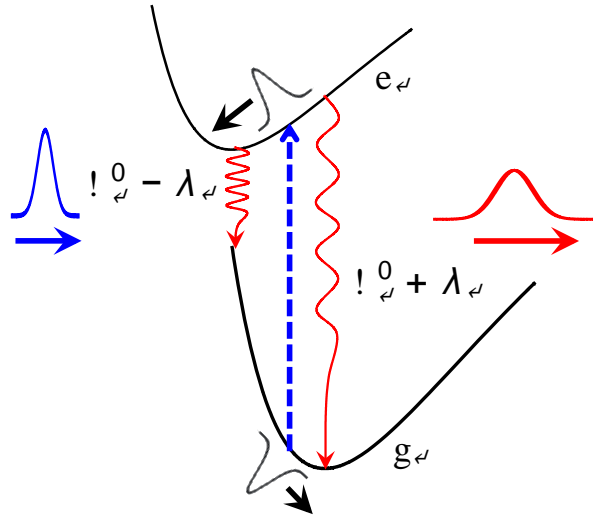P.O. Box 13000, FI-00076 Aalto, Finland
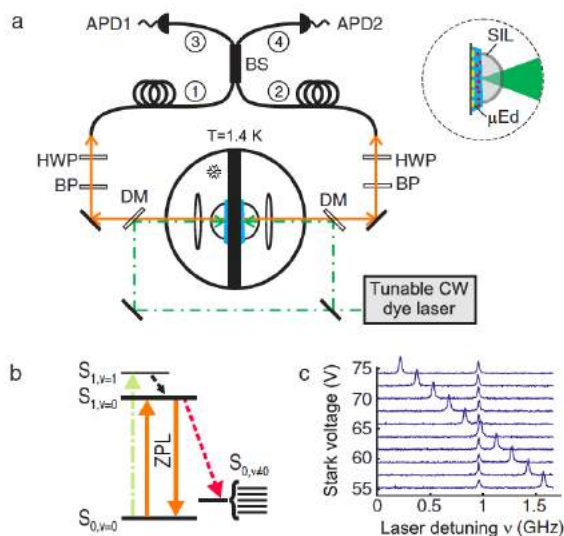
Phenomenologically added broadening
to account for bath (10-100x natural linewidth)
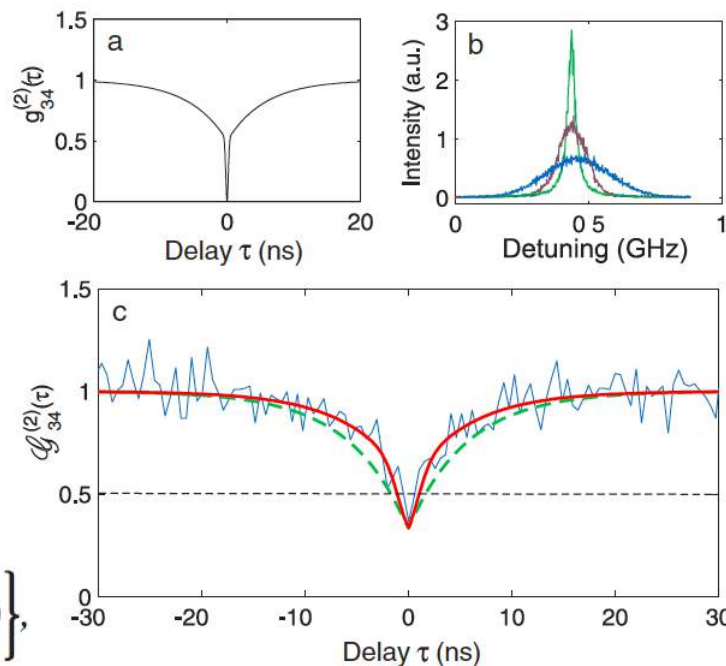
$$G_{34}^{(2)}(\tau) = c_1^2 G_{11}^{(2)}(\tau) + c_2^2 G_{22}^{(2)}(\tau) + 2c_1 c_2$$

$$\times \left\{ 1 - \eta \frac{\langle S_1 \rangle \langle S_2 \rangle}{\langle I_1 \rangle \langle I_2 \rangle} |g_{11}^{(1)}(\tau)||g_{22}^{(1)}(\tau)| \cos(\Delta \omega \tau) \right\},$$

Hamiltonian

$$\hat{H}_\nu^\alpha = \hbar^{-1}\langle\nu_\alpha|\hat{H}|\nu_\alpha\rangle = \epsilon_{\nu_\alpha} + \hat{q}_{\nu\alpha} + \hat{H}_B^\alpha$$

Collective Bath coordinate

$$\hat{q}_{\nu\alpha} = \hbar^{-1}\langle\nu_\alpha|\hat{H}_{SB}|\nu_\alpha\rangle = \sum_k d_{\nu_\alpha\nu_\alpha,k}(\hat{a}_k^\dagger + \hat{a}_k)$$

Lineshape function

$$\beta^{-1} = k_B T$$

$$g_\alpha(t) \equiv g_{\nu_\alpha\nu_\alpha'}(t) = \int \frac{d\omega}{2\pi}\frac{C_{\nu_\alpha\nu_\alpha'}''(\omega)}{\omega^2}\left[\coth\left(\frac{\beta\hbar\omega}{2}\right)(1-\cos\omega t) + i\sin\omega t - i\omega t\right]$$

Bath spectral density

$$C_{\nu_\alpha\nu_\alpha'}''(\omega) = \frac{1}{2}\int_0^\infty dt\, e^{i\omega t}\langle[\hat{q}_{\nu\alpha}(t),\hat{q}_{\nu'\alpha}(0)]\rangle$$
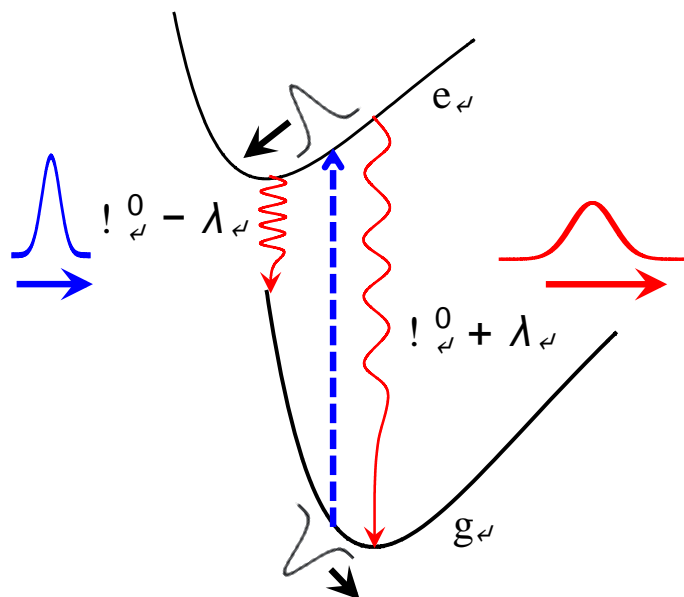
Absorption lineshape

$$\sigma_A(\omega) = \frac{1}{\pi}\sum_{\alpha=a,b}\int_0^\infty dt\, e^{i(\omega-\omega_\alpha)t - g_\alpha(t)}$$

Fluorescence lineshape

$$\sigma_F(\omega) = \frac{1}{\pi}\sum_{\alpha=a,b}\int_0^\infty dt\, e^{i(\omega-\omega_\alpha+2\lambda_\alpha)t - g_\alpha^*(t)}$$

Bath spectral density

$$C''_{\nu_\alpha \nu_\alpha}(\omega) = 2\lambda_\alpha \frac{\omega \Lambda_\alpha}{\omega^2 + \Lambda_\alpha^2}$$

Λ_α - fluctuation relaxation rate

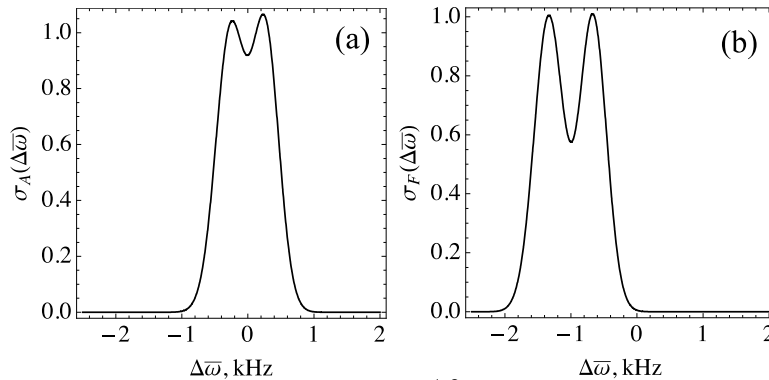λ_α - reorganization energy

$$\Delta_\alpha^2 = 2\lambda_\alpha k_B T / \hbar$$

Linewidth function in high temperature limit $k_B T \gg \hbar \Lambda_\alpha$

$$g_\alpha(t) = \left(\frac{\Delta_\alpha^2}{\Lambda_\alpha^2} - i \frac{\lambda_\alpha}{\Lambda_\alpha} \right) \left(e^{-\Lambda_\alpha t} + \Lambda_\alpha t - 1 \right)$$
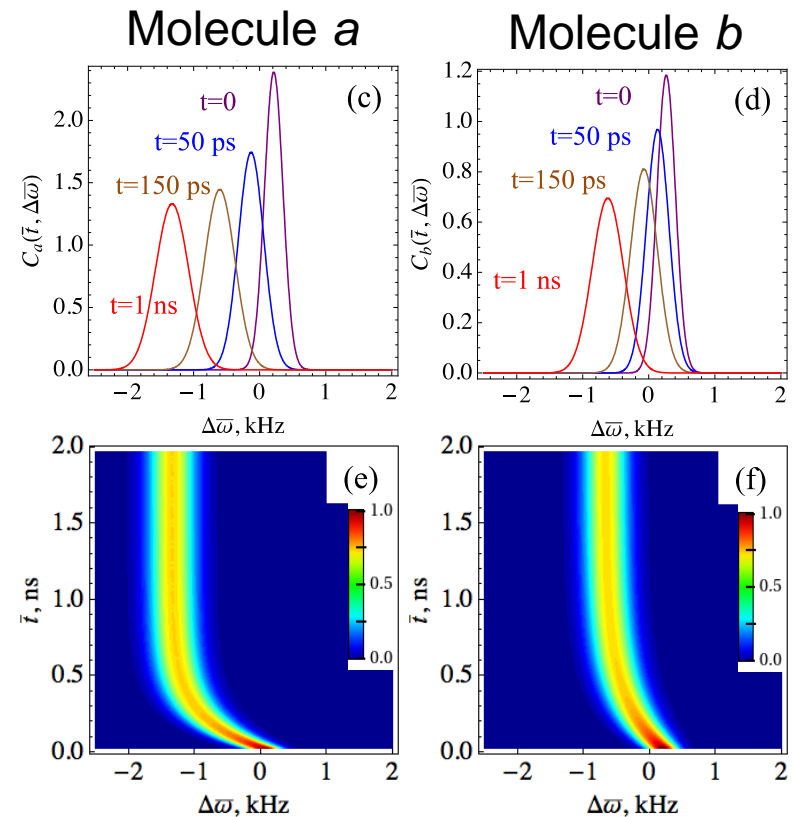
$\Lambda_\alpha \ll \Delta_\alpha$ (slow fluctuations, spectral diffusion)

Absorption lineshape

$$\sigma_A(\omega) = \sum_{\alpha=a,b} (2\pi\Delta_\alpha)^{-1/2} e^{-\frac{(\omega-\omega_\alpha^0-\lambda_\alpha)^2}{2\Delta_\alpha^2}}$$

Fluorescence lineshape

$$\sigma_F(\omega) = \sum_{\alpha=a,b} (2\pi\Delta_\alpha)^{-1/2} e^{-\frac{(\omega-\omega_\alpha^0+\lambda_\alpha)^2}{2\Delta_\alpha^2}}$$
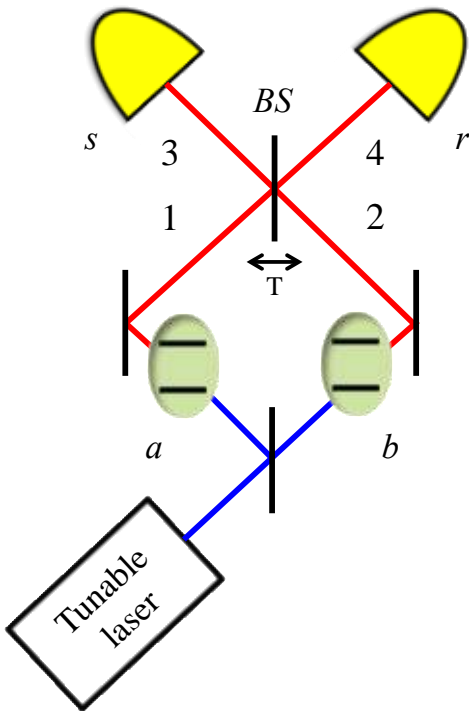
Time-and-frequency-resolved fluorescence follow narrowband excitation (hole burning)

$$C_\alpha^j(t,\omega) = C_{\alpha 0}^j(t) e^{-\frac{(\omega_p-\omega_\alpha^0-\lambda_a)^2}{2\tilde{\sigma}_{p\alpha}^2} - \frac{(\omega-\tilde{\omega}_\alpha(t))^2}{2\tilde{\sigma}_\alpha^{j2}(t)}}$$

Coincidence counting signal

$$R_c^{34}(\Gamma_r, \Gamma_s) = \int_{-\infty}^{\infty} dt_s \int_{-\infty}^{\infty} dt_r \langle E_3^{(tf)\dagger}(t_r) E_4^{(tf)\dagger}(t_s) E_4^{(tf)}(t_s) E_3^{(tf)}(t_r) \rangle$$

Output-input for a 50:50 beam splitter

$$E_3(t) = \frac{E_1(t) - iE_2(t+T)}{\sqrt{2}}, \quad E_4(t) = \frac{E_2(t) - iE_1(t-T)}{\sqrt{2}}$$

Time-and-frequency resolved field

$$E^{(tf)}(\bar{t}, \bar{\omega}; r_D, t) = \int_{-\infty}^{\infty} dt' F_f(t-t', \bar{\omega}) F_t(t', \bar{t}) E(r_S, t')$$
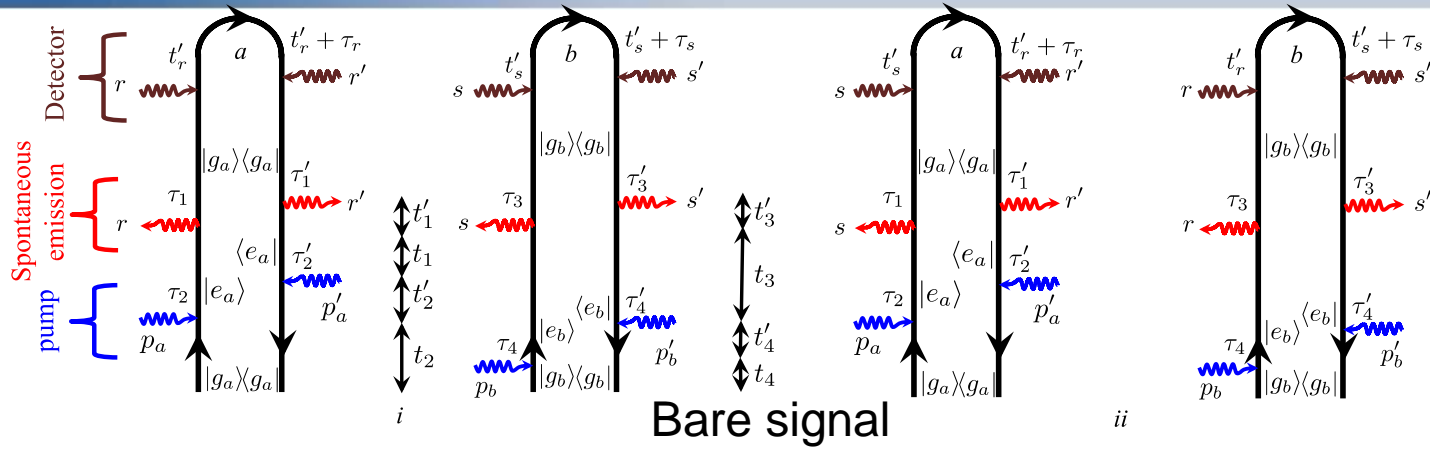
Frequency gate

Time gate

Detector spectrogram   Bare signal

$$R_c^{34}(\Gamma_r, \Gamma_s; T) = \frac{1}{(2\pi)^2} \int_{-\infty}^{\infty} d^2\Gamma_r' d^2\Gamma_s' [W_D^{(r)}(\Gamma_r, \Gamma_r'; 0) W_D^{(s)}(\Gamma_s, \Gamma_s', 0) R_B^{(i)}(\Gamma_r', \Gamma_s') +$$

$$W_D^{(r)}(\Gamma_r, \Gamma_r'; -T) W_D^{(s)}(\Gamma_s, \Gamma_s', T) R_B^{(ii)}(\Gamma_r', \Gamma_s')] + (s \leftrightarrow r, T \leftrightarrow -T).$$

Microscopic calculation of the bare signal

Bare signal

$$R_B^{(i)}(t'_s, \omega'_s; t'_r, \omega'_r) = \mathcal{D}^2(\omega_a)\mathcal{D}^2(\omega_b)\int_{-\infty}^{\infty}d\tau_p d\tau'_p d\tau_s d\tau_r e^{-i\omega'_s\tau_s - i\omega'_r\tau_r}\int_{-\infty}^{\infty}dt_p dt'_p$$

$$\times \mathcal{E}_p^*(t_p - \tau_p - \bar{t}_p, r_a)\mathcal{E}_p(t_p - \bar{t}_p, r_a)\mathcal{E}_p^*(t'_p - \tau'_p, r_b)\mathcal{E}_p(t'_p, r_b)$$

$$\times F_a(t_p - \tau_p, t'_r + \tau_r, t'_r, t_p)F_b(t'_p - \tau'_p, t'_s + \tau_s, t'_s, t'_p),$$

$$R_B^{(ii)}(t'_s, \omega'_s; t'_r, \omega'_r) = -\mathcal{D}^2(\omega_a)\mathcal{D}^2(\omega_b)\int_{-\infty}^{\infty}d\tau_p d\tau'_p d\tau_s d\tau_r e^{-i\omega'_s\tau_s - i\omega'_r\tau_r}\int_{-\infty}^{\infty}dt_p dt'_p$$

$$\times \mathcal{E}_p^*(t_p - \tau_p - \bar{t}_p, r_a)\mathcal{E}_p(t_p - \bar{t}_p, r_a)\mathcal{E}_p^*(t'_p - \tau'_p, r_b)\mathcal{E}_p(t'_p, r_b)$$

$$\times F_a(t_p - \tau_p, t'_r + \tau_r, t'_s, t_p)F_b(t'_p - \tau'_p, t'_s + \tau_s, t'_r, t'_p)$$

Four-point matter correlation function

$$F_\alpha(t_1, t_2, t_3, t_4) = \langle V(t_1)V^\dagger(t_2)V(t_3)V^\dagger(t_4)\rangle_\alpha = |\mu_\alpha|^4 e^{-i\omega_\alpha(t_1 - t_2 + t_3 - t_4)}e^{\Phi_\alpha(t_1, t_2, t_3, t_4)}$$
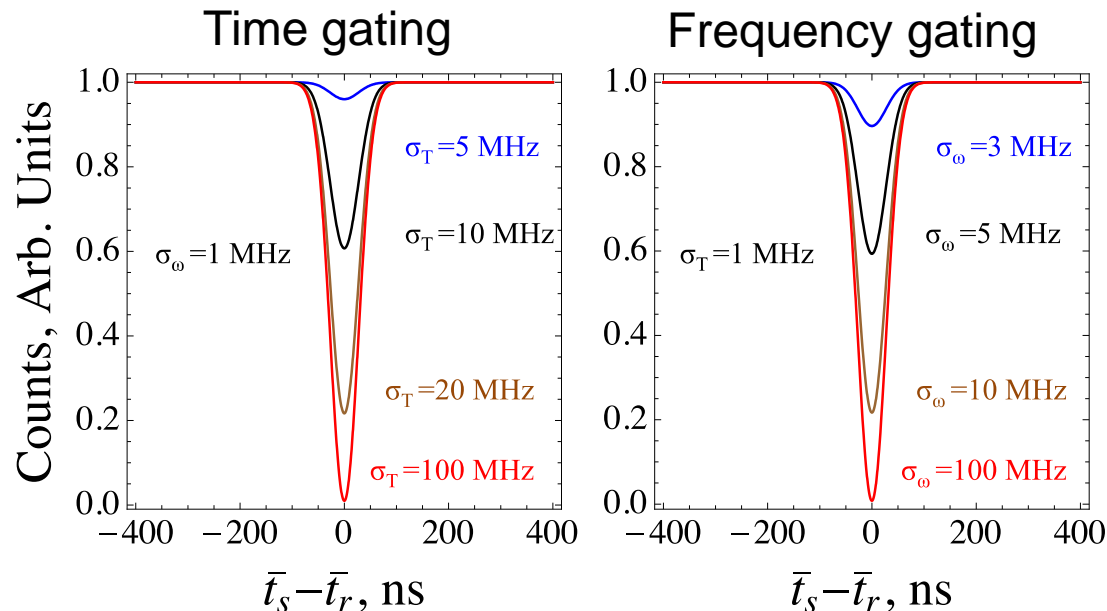
$$\Phi_\alpha(t_1, t_2, t_3, t_4) = -g_\alpha(t_1 - t_2) - g_\alpha(t_3 - t_4) + g_\alpha(t_1 - t_3) - g_\alpha(t_2 - t_3) + g_\alpha(t_2 - t_4) - g_\alpha(t_1 - t_4)$$

Time-and-frequency resolved PCC

Distinguishability due to detection alone; No spectral diffusion

$$R_c^{34}(\tau;T) \sim 1 - \eta\cos(\omega_{ab}t_d + \Omega_\tau T)e^{-\frac{1}{2}\sigma_\tau^2 T^2 - \frac{1}{2}(\Delta_a^2 + \Delta_b^2)t_d^2}$$

Time gating

Frequency gating

$t_d = \bar{t}_s - \bar{t}_r$ time delay between detector times
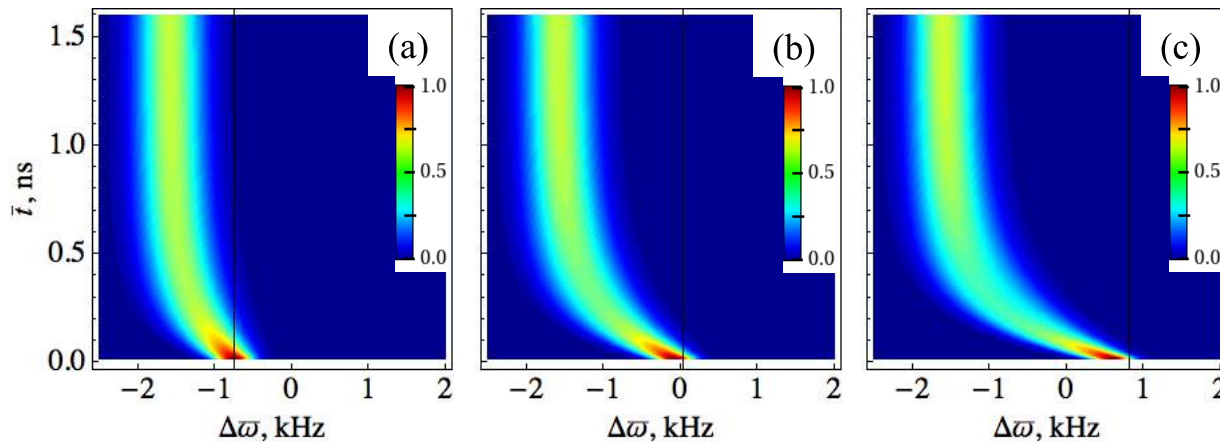
cT asymmetry between position of the beam splitter

PCC with spectral diffusion

Varying the pump frequency ω_p
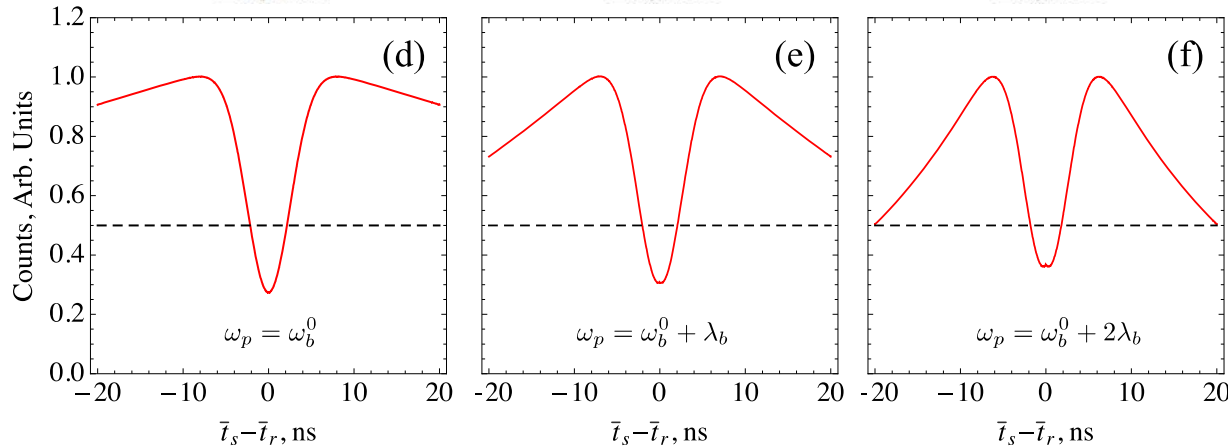
$$\omega_p = \omega_b^0 \qquad \omega_p = \omega_b^0 + \lambda_b \qquad \omega_p = \omega_b^0 + 2\lambda_b$$

Time-and-frequency resolved fluorescence

$$\Delta\bar{\omega} = \omega - \tfrac{1}{2}(\omega_a + \omega_b)$$

PCC signal

Less distinguishable

More distinguishable

PCC for various parameters

Fluorescence contribution

$$R_c^{34}(\Gamma_r, \Gamma_s; T) = R_0 C_a^r(\Gamma_r) C_b^s(\Gamma_s) \times$$
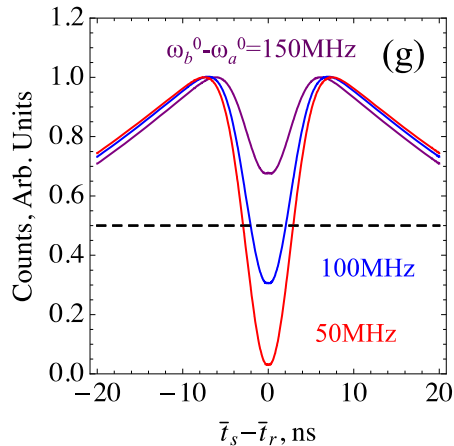
$$C_\alpha^j(t, \omega) = C_{\alpha 0}^j(t) e^{-\frac{(\omega_p - \omega_\alpha^0 - \lambda_a)^2}{2\tilde{\sigma}_{p\alpha}^2} - \frac{(\omega - \tilde{\omega}_\alpha(t))^2}{2\tilde{\sigma}_\alpha^{j2}(t)}}$$
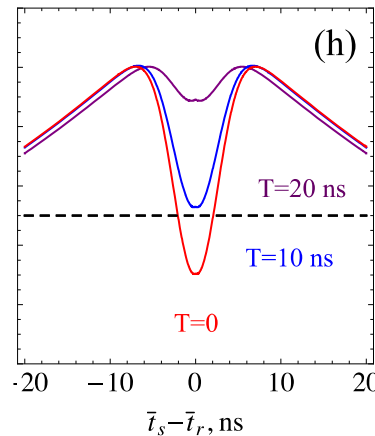
$$\left[1 - \frac{I_a^r(\Gamma_r, \bar{t}_s, -T) I_b^s(\bar{t}_r, \Gamma_s, T)}{C_a^r(\Gamma_r) C_b^s(\Gamma_s)} \cos U(\Gamma_r, \Gamma_s; T) e^{-\tilde{\Gamma}(\bar{t}_s - \bar{t}_r)} \right]$$

Quantum Interference contribution

$$+ (a \leftrightarrow b, T \leftrightarrow -T),$$

$$I_\alpha^j(\Gamma_1, t_2, \tau) = I_{\alpha 0}^j(t_1, t_2) e^{-\frac{\omega_{ab}^2}{4\sigma_T^{j2}} - \frac{1}{4}\sigma_{\tau\alpha}^j(t_1, t_2)^2 \tau^2}$$

$$\times e^{-\frac{(\omega_p - \omega_{p\alpha}^j(t_1, t_2))^2}{2\sigma_{p\alpha}^{j2}(t_1, t_2)}} e^{-\frac{(\omega_1 - \omega_\alpha^j(t_1, t_2))^2}{2\sigma_\alpha^{j2}(t_1, t_2)}},$$
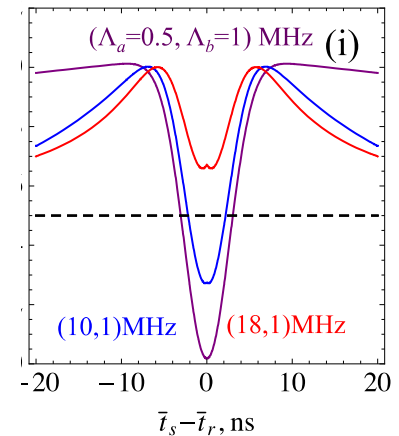
Difference between transition frequencies

Position of the beam splitter (delay between photon detection)

Spectral diffusion rate (for fixed linewidth)

For larger discrepancy between transition frequencies HOM dip becomes smaller

For larger asymmetry in the position of the beamsplitter HOM dip becomes smaller

For larger discrepancy between spectral diffusion rates HOM dip becomes smaller

Summary

- We developed microscopic theory for generation and control of the indistinguishability of the photons generated by two independent molecules coupled to the bath

- Elaborate time-and-frequency gated detection allows to preserve quantum interference between photons

- Microscopic bath model allow to simulate real molecules and their manipulation of the single photons

We extended the studies of Sangdoghdar et al.by including

- Microscopic model for the detection using time-and-frequency resolved photon counting provide novel control knobs for the quantum interference of the photons

- Microscopic model for bath induced fluctuations that erode the quantum interference of the photons allows to simulate real quantum emitters beyond 2-level qubit model without adding phenomenological noise effects.
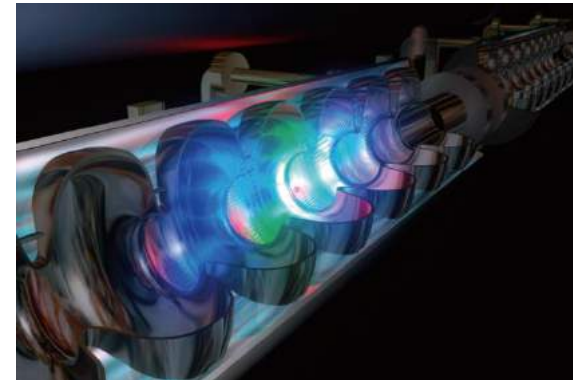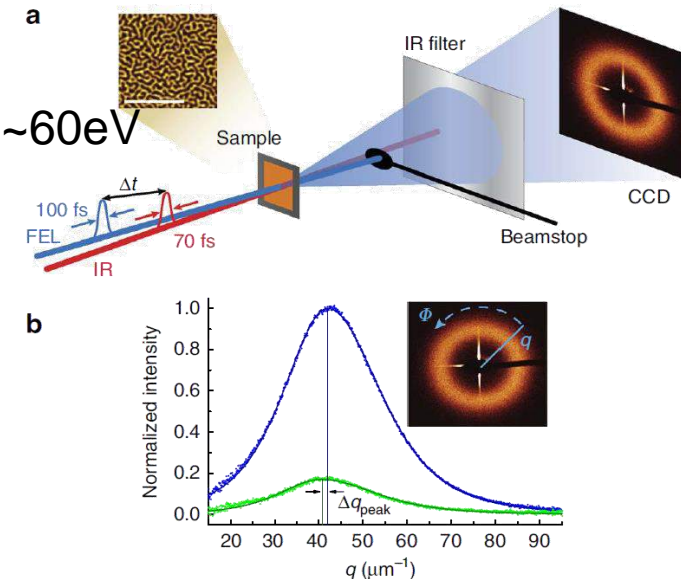
X-ray Free Electron Lasers
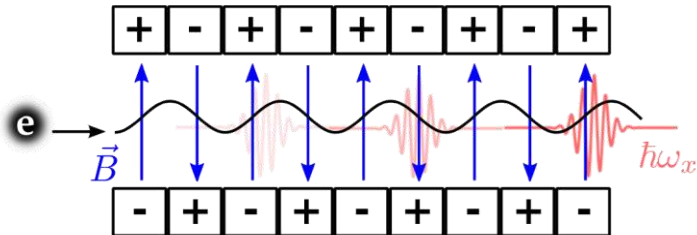
e $\rightarrow$ $\vec{B}$ $\hbar\omega_x$

• P. Luchini and H. Motz. *Undulators and Free-electron Lasers*(Oxford University Press, USA, 1990)
• Nat. Phot., 4(12):802–803, December 2010
• P. Emma, *et. al.* Nat. Phot. **4**, 641 (2010)

$E_{X\text{-}Ray}$ 279.17 eV
$\lambda_{X\text{-}Ray}$ 4.2023 nm
$N_{photons}$ 15.37 E12

Stanford LCLS X-ray Free Electron Laser

https://slacportal.slac.stanford.edu/sites/lcls_public/Pages/status.aspx

~60eV

a

IR filter

Sample

Δt
100 fs
FEL
70 fs
IR
Beamstop

CCD

b

Normalized intensity
1.0
0.8
0.6
0.4
0.2
0.0

Φ
q

Δq_{peak}

20 30 40 50 60 70 80 90
q (μm^{-1})

http://flash.desy.de/photon_science/

Nature Comm. 3:1100 (2012)
DOI: 10.1038/ncomms2108

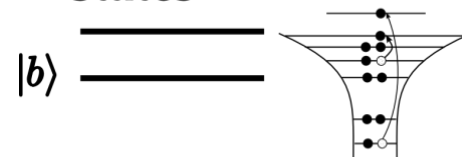http://flash.desy.de/sites2009/site_vuvfel/content/e395/e2188/FLASH-Broschrefrs_web.pdf

Raman Scattering: Vibrations vs. Electrons

Femtosecond Optical Spectroscopy of vibrations

Attosecond X-ray Spectrosocpy of electrons

Fast electronic system acts as a yardstick for measuring the dynamics of the slow vibrational system

core excited states

$|b\rangle$
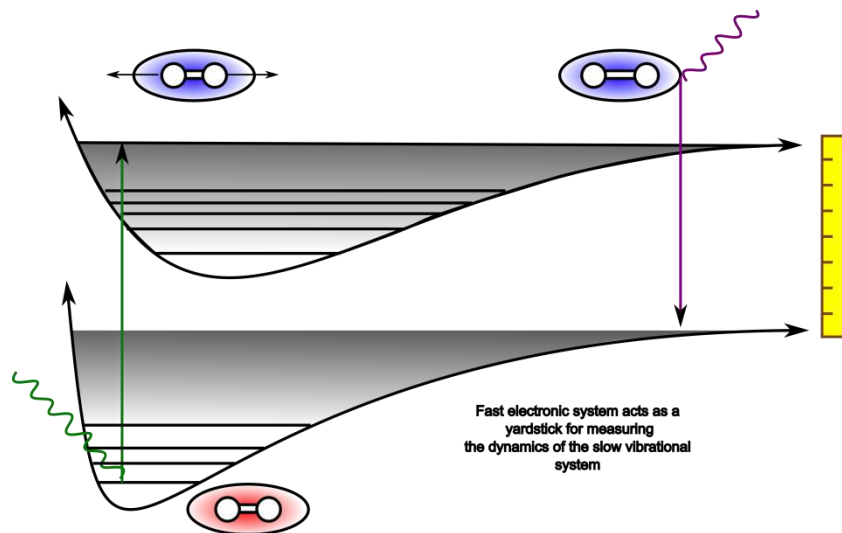
Slow valence excitations coupled to fast core excitations

$|c\rangle$

$|a\rangle$

valence excited states

Dynamics of the slow system (vibrational or valence elctron) are probed by excited via transitory excitation of the fast system (valence or core electron).

The Polarizability

Conventional Raman

$$\alpha = \alpha_0 + \sum_i \frac{\partial \alpha}{\partial Q_i} Q_i + \sum_{ij} \frac{1}{2} \frac{\partial^2 \alpha}{\partial Q_i \partial Q_j} Q_i Q_j + \dots$$

$$Q_i = \sqrt{\frac{\hbar}{2 m_i \omega_i}} (a_i^\dagger + a_i)$$

Boson creation and annihilation operators for vibrations

X-Ray Raman (RIXS)

$$\alpha = \alpha_0 + \sum_{i,j} K_{ij} c_i^\dagger c_j + \sum_{i,j,r,s} K_{ijrs} c_i^\dagger c_j c_r^\dagger c_s + \dots$$

$$c_i^\dagger (c_j)$$

Fermi creation (annihilation) operators of valence orbitals

Raman Scattering: Vibrations vs. Electrons –(2)

	UV/Vis	X-ray
Pulse Duration:	~10fs	~100as
Energies:	1-10eV	+100eV
Dynamics:	probes nuclear dynamics on different valence PESs.	probes valence excitations with different core occupations
Decay Mechanisms:	Fluorescence, IVR	Fluorescence, Auger
Slow System: Low Frequencies	vibrations	valence electrons
Fast System: High Frequencies	valence electrons	core-electrons
Absorption	Infrared	XANES

VPES
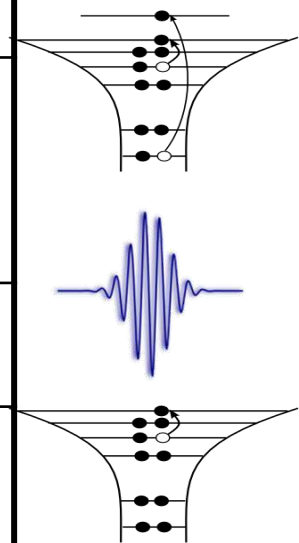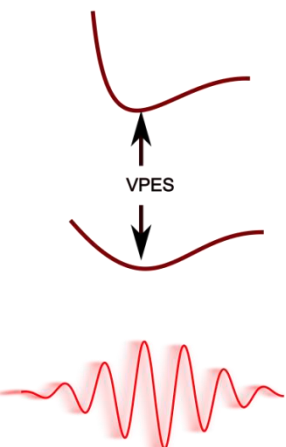
Raman Scattering: Vibrations vs. Electrons –(3)

|	Molecular vibrations	Valence Electrons
Slow systems:	Nuclei /Infrared	Valence electrons/ UV-Vis
Fast system:	Valence electrons/ UV-Vis	Core electrons /X-ray
Direct Probe of slow system:	Infrared	UV-Vis
Impulsive Excitation	Raman	RIXS

VPES
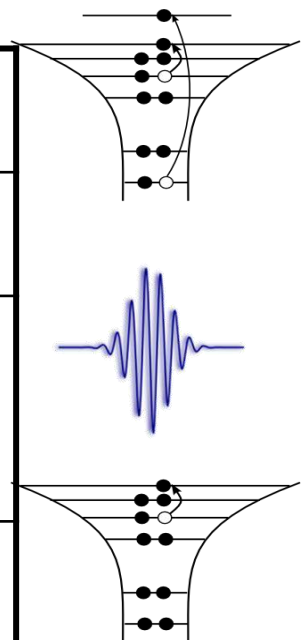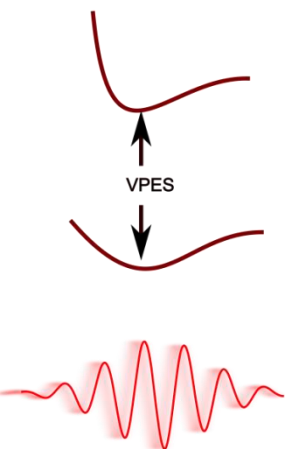
One-Color and Two-Color 1D-SXRS of trans-NMA

Tuning the X-ray pulse to be resonant with different core-edge transitions
Probes delocalized valence excitations perturbed by the selected localized core hole.
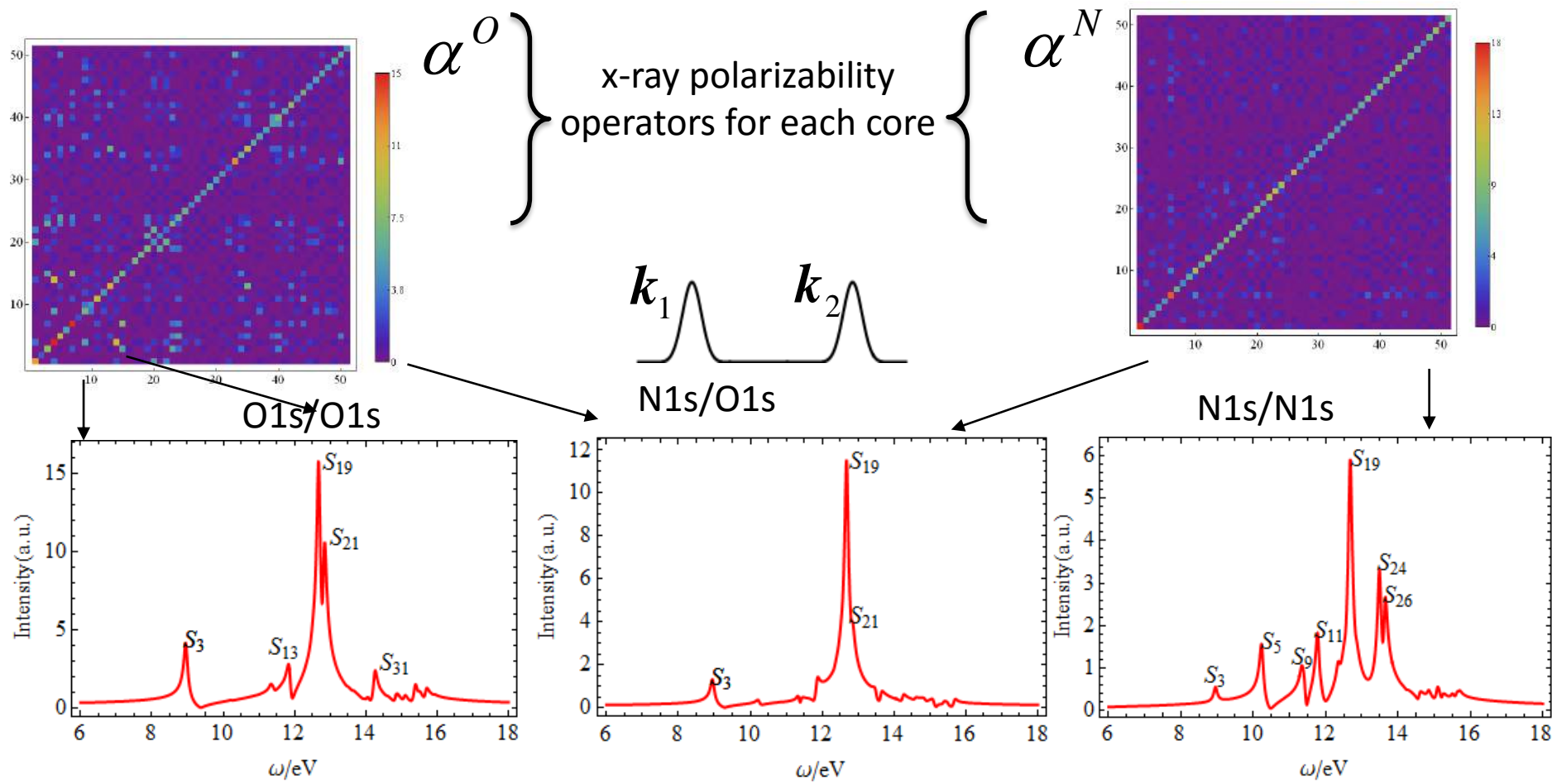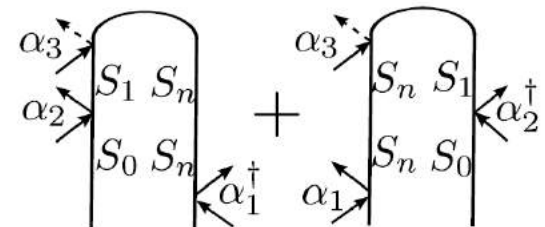
I3P-SXRS of NMA
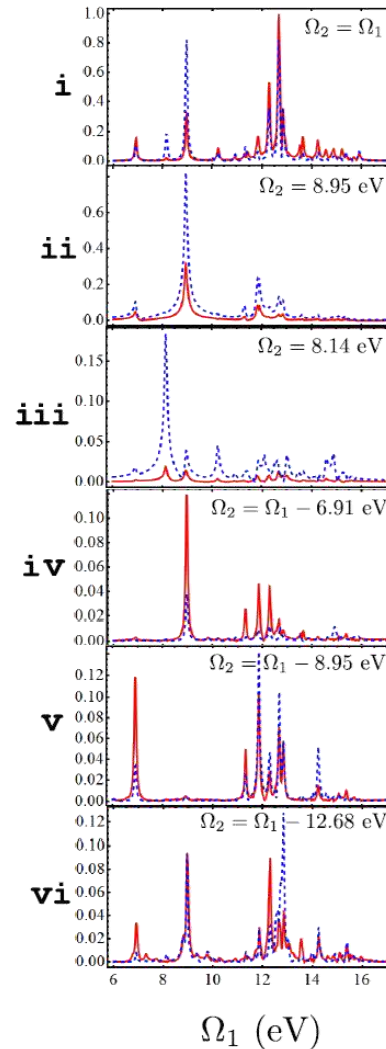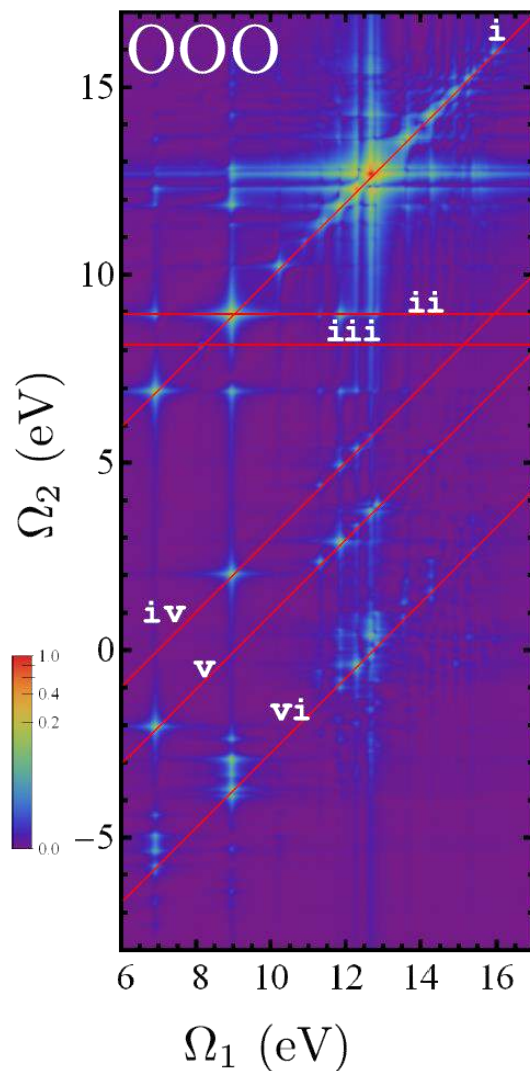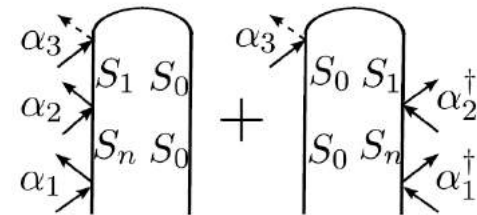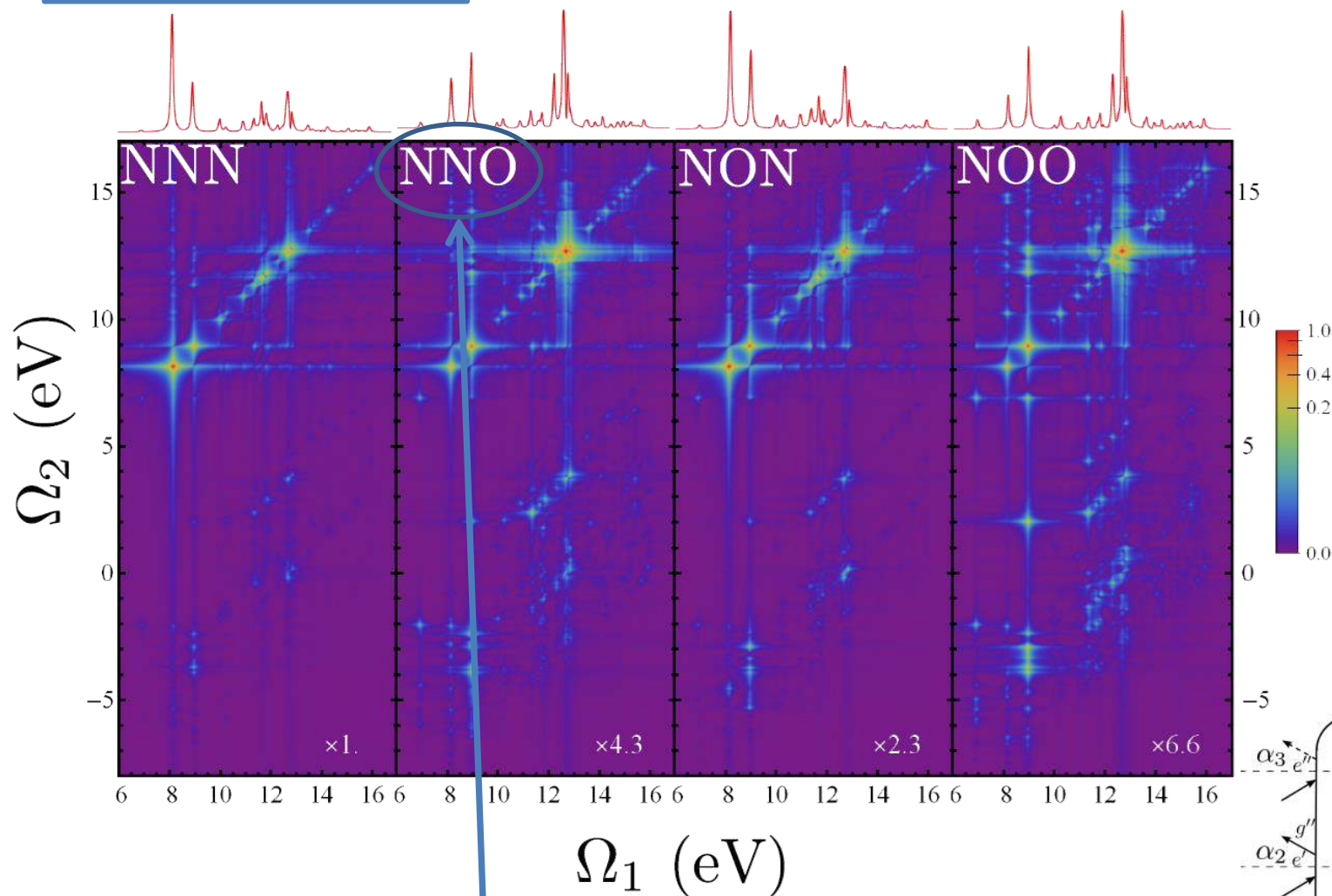
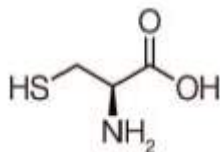x-ray pulse polarizations are all-parallel (VVV)

I3P-SXRS of NMA

pulses1 and 2 tuned to Nitrogen K-edge, pulse 3 to Oxygen K-edge

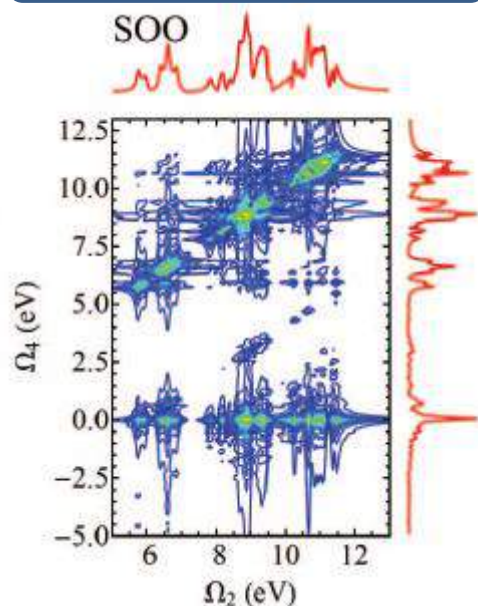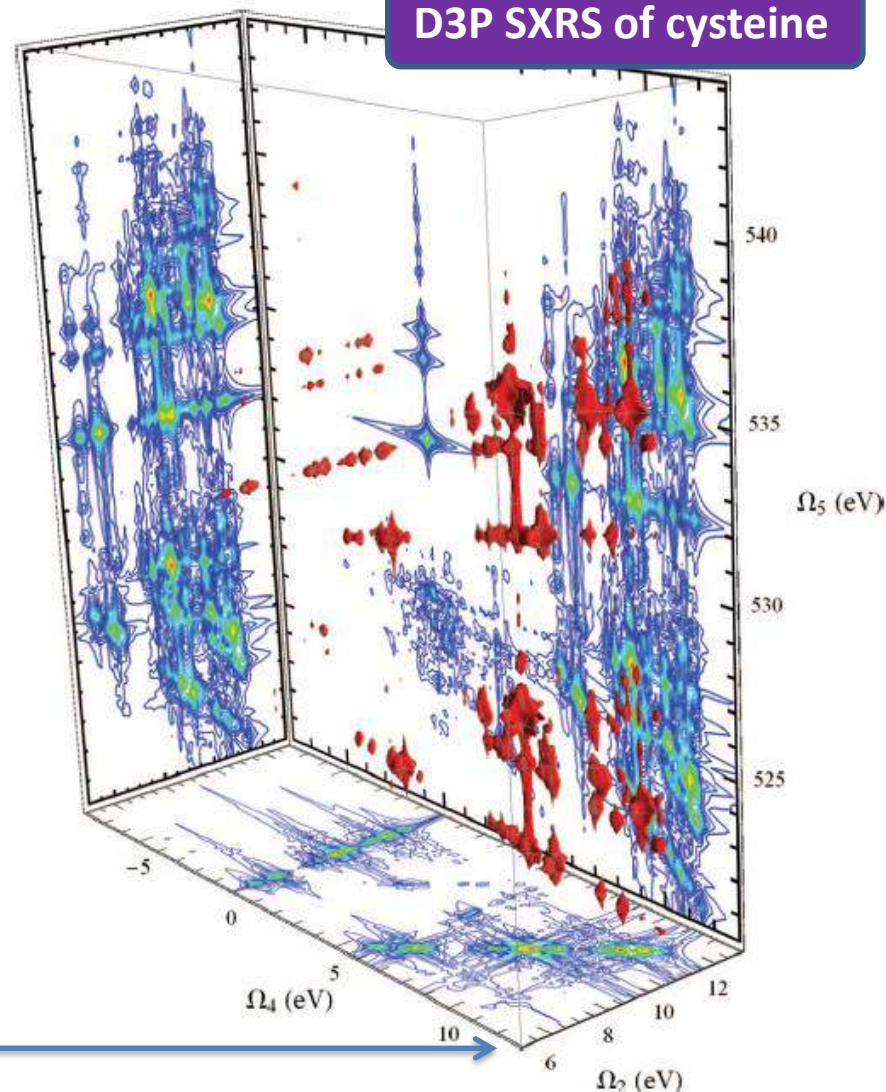# Integrated and dispersed 3-pulse SXRS from cysteine

S – sulfur
O - oxygen

D3P SXRS of cysteine

I3P SXRS of cysteine

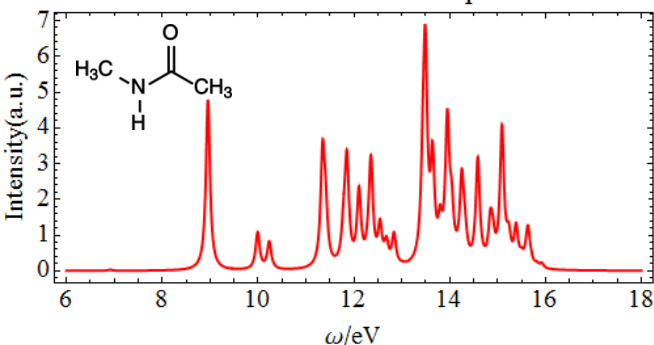By integrating over the dispersed frequency Ω_5 we recover the integrated signal.

$$S_{I3P-SXRS}(\Omega_2, \Omega_4) = \int d\Omega_5 S_{D3P-SXRS}(\Omega_2, \Omega_4, \Omega_5).$$

Direct absorption vs. Raman Scattering

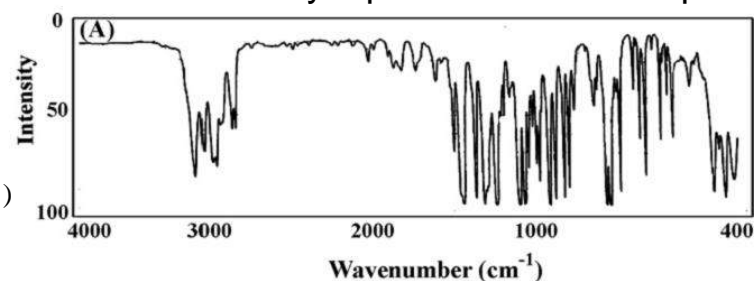**Valence excitations**

Trans−NMA UV absorption

Vibrations

1-methoxynaphthalene IR absorption

Direct absorption, Fermi Golden Rule

$$S_{IR}(\omega) = \sum_{a,c}\left(P(a)-P(c)\right)\left|\mu_{ca}\right|^2 \delta(\omega-\omega_{ca})$$
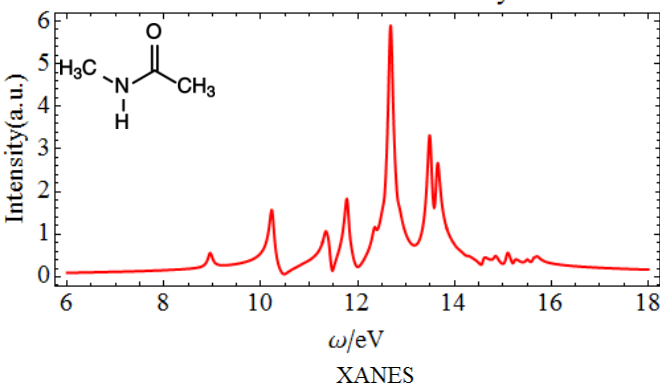

Absorption gives the eigenstate energies (vibrations or valence electron), and their transition dipole moments.
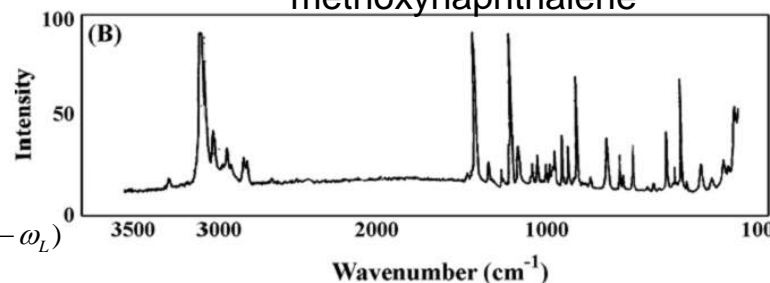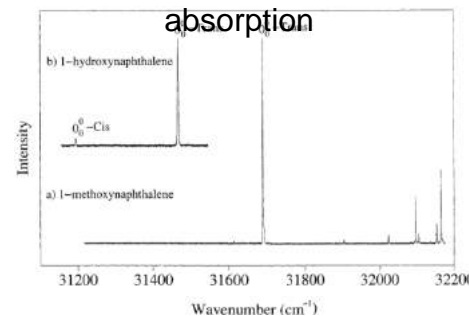
Trans-NMA

Stimulated X−Ray Raman

Raman Scattering Kramers-Heisenberg

$$S_{Raman}(\omega_L,\omega_S) = \sum_{a,b,c} P(a)\left|\alpha_{ca}(\omega_L)\right|^2 \delta(\omega_{ca}+\omega_S-\omega_L)$$
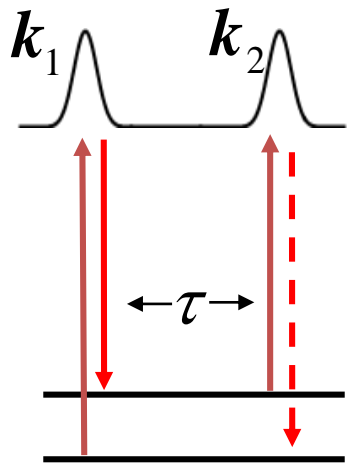
Raman-methoxynaphthalene

UV absorption

XANES

By scattering off high-energy states (valence or core) we study the molecular polarizability

Integrated 2-Pulse Stimulated X-ray Raman

k_1 k_2

$\leftarrow \tau \rightarrow$

• The signal is measured by scanning the interpulse delay rather than the detection frequency

• The observation window is controlled by the pulse bandwidths

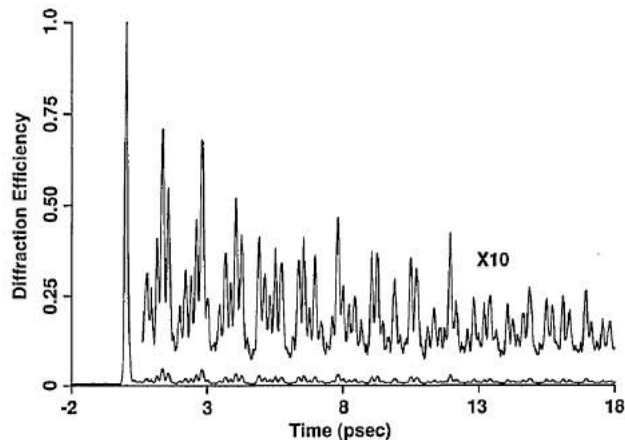Keith Nelson *et al.* α-perylene (1991)

Fourier Transform

Fig. 3. Single-pulse ISRS data recorded from α-perylene with $T < 10$ K and with all pulses linearly polarized parallel to the *b* crystallographic axis. The femtosecond excitation pulses drive several phonon modes whose combined response yields a characteristic beating pattern. The spike at $t = 0$ is a purely electronic response of the crystal to the excitation pulses.
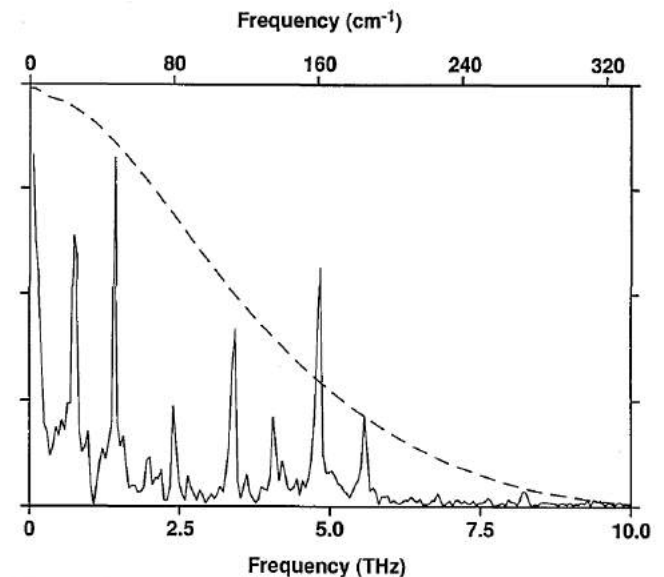
Fig. 4. Solid curve: Fourier transform of the scattering data shown in Fig. 3. The electronic scattering peak at $t = 0$ in the time-domain data was suppressed before the Fourier transform was performed. Dashed curve: Fourier transform of the electronic scattering peak, representing the instrumental response function.

Multidimensional X-Ray Raman Spectroscopy

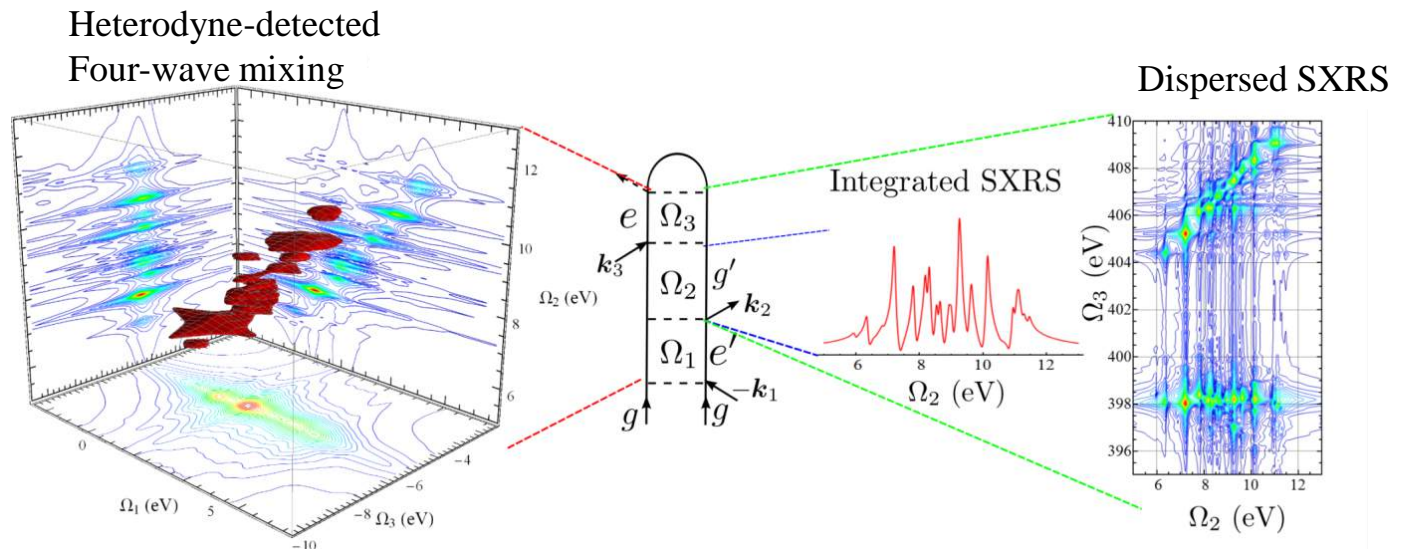| One Dimensional	Two Dimensional	Three Dimensional
Integrated two-pulse Stimulated X-Ray Raman Scattering (I2P-SXRS)	Dispersed two-pulse SXRS	Frequency-Dispersed three-pulse SXRS
	Integrated three-pulse SXRS	Heterodyne-detected four-wave mixing
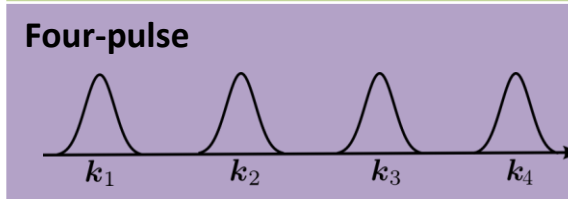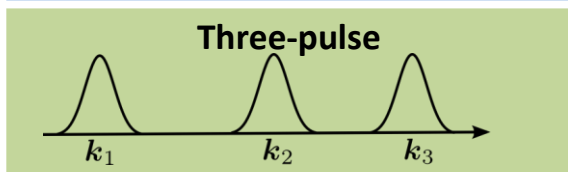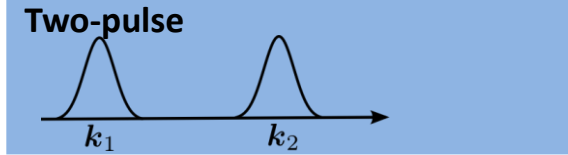
Simulated experiments on the nitrogen K-edge of cysteine. Lower dimensional signals are projections of higher dimensional signals.

Two-pulse k_1 k_2

Three-pulse k_1 k_2 k_3

Four-pulse k_1 k_2 k_3 k_4

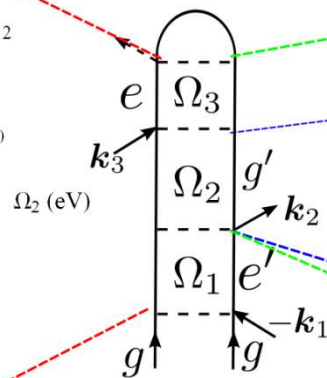Heterodyne-detected Four-wave mixing

Integrated SXRS

Dispersed SXRS

Multidimensional X-Ray Raman Spectroscopy

- Stimulated X-Ray Raman
  - Integrated pump-probe 1D
  - Two-Dimensional X-ray Raman 2D
  - Frequency-resolved pump-probe 2D
  - k_{III} photon echo 3D

3D Photon Echo

Frequency-Resolved SXRS

Integrated SXRS

1D-SXRS

The system interacts twice with the pump and twice with the probe. No phase control is required.

The resonant pump creates a wavepacket of valence-excited states which then evolves for a time τ before the arrival of the probe pulse.

N-Methylacetamide (NMA)

L-Cysteine

The Effective Polarizability: Incorporating the Effects of Pulse Bandwidth

Transition dipole moments between valence (g′) and core (e) states

Jth pulse spectral amplitude

The traditional polarizability which enters the famous Kramers-Heisenberg equation for frequency-domain Raman spectroscopy is modified to account for the finite spectral bandwidth of ultrafast pulses

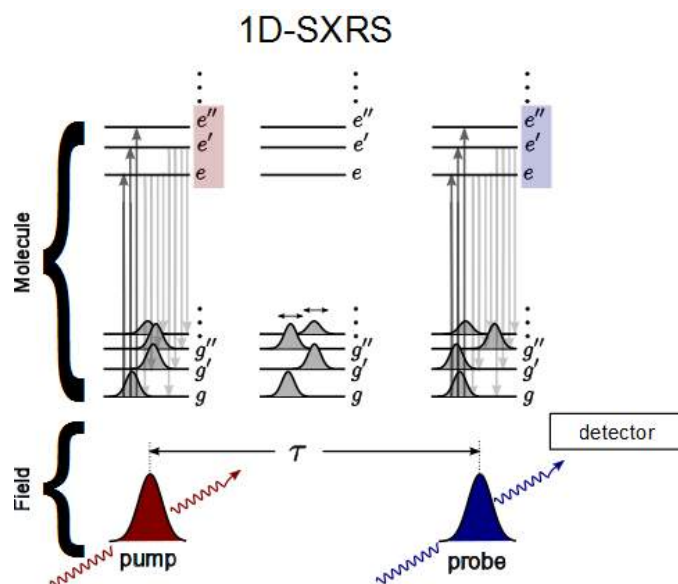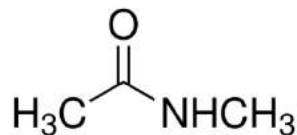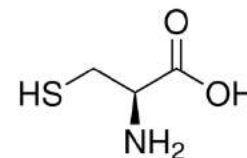$$\alpha_j = \alpha_j{}' + i\alpha_j{}'' = \sum_{e,g',g''} |g'\rangle \frac{V_{g'e}V_{eg''}}{2\pi} \int_{-\infty}^{\infty} d\omega \frac{\mathcal{E}_j^*(\omega)\,\mathcal{E}_j(\omega + \omega_{g'g''})}{\omega - \omega_{eg'} + i\Gamma_e} \langle g''|$$

S1s* ════ 2473.5eV

For frequency-dispersed measurements, we have the frequency-dependent effective polarizability

$$\bar{\alpha}_j(\omega) = \sum_{e,g',g''} |g'\rangle \frac{V_{g'e}V_{eg''}}{2\pi} \frac{\mathcal{E}_j^*(\omega)\,\mathcal{E}_j(\omega + \omega_{g'g''})}{\omega - \omega_{eg'} + i\Gamma_e} \langle g''|$$

O1s* ════ 532.2eV $|e\rangle$

N1s* ════ 404.4eV

α is the integral of α(ω)

$$\alpha_j = \int d\omega\, \bar{\alpha}_j(\omega)$$

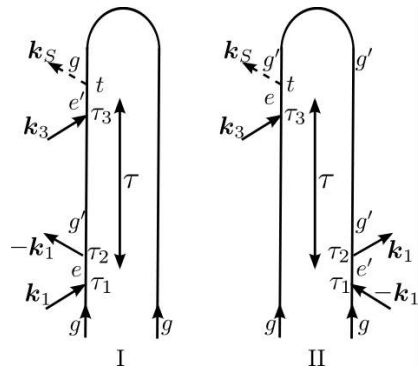════ $|g'\rangle$
════ $|g_o\rangle$

By substituting a delta function for the excitation field and a constant for the de-exciting field, we recover the frequency-domain expression for α.

$$\mathcal{E}_j(\omega) = \delta(\omega - \omega_L);\ \mathcal{E}_j^*(\omega) = 1 \longrightarrow \alpha = \sum_{e,g',g''} |g'\rangle \frac{V_{g'e}V_{eg''}}{\omega_L - \omega_{eg''} + i\Gamma_e} \langle g''|$$

2P-SXRS: Integrated vs. Dispersed Detection

The integrated two-pulse (I2P) signal is one-dimensional and can be written directly from the contributing diagrams.

$$S_{I2P-SXRS}(\Omega_2) = -\sum_{g'} \frac{\alpha''_{2;gg'}\alpha_{1;g'g}}{\Omega_2 - \omega_{g'g} + i\Gamma_{g'}}$$

The polarizability is extended to time-domain experiments, incorporating the pulse spectral envelopes. Only those valence excitations whose energies lie within the pulse bandwidth are impulsively excited.

Another method for extending the 1D-SXRS technique to two dimensions involves sending measuring the spectrum of the transmitted probe pulse rather than its int

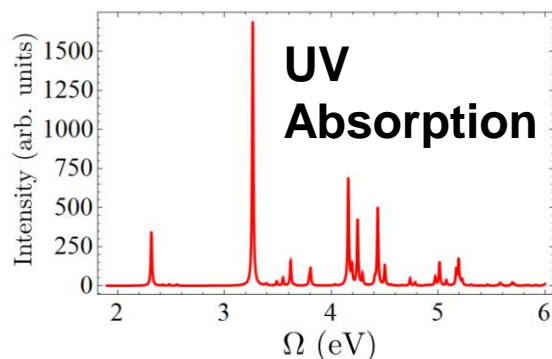$$S_{D2P-SXRS}(\Omega_2, \Omega_3) = \sum_{g'} \frac{i(\alpha_{1;g'g})(\bar{\alpha}_{2;gg'}(\Omega_3) - \bar{\alpha}^{\dagger}_{2;gg'}(\Omega_3))}{\Omega_2 - \omega_{g'g} + i\Gamma_{g'}}$$

which depends on the frequency-dependent resonant polarizability

Porphyrin Heterodimer

Zinc monomer

Nickel monomer

UV Absorption

Core-excited states calculated using restricted excitation window time-dependent
density functional theory (**REW-TDDFT**), which allows for the efficient
~~calculation of core-excited states, and~~

K-edge XANES

Ni1s

Zn1s

L-edge XANES

Ni2p

Zn2p

Intensity (arb. units)

Ω (eV)

Ω (eV)

**Pulse power spectra shown in blue
FWHM of 166 as (10.9 eV)**
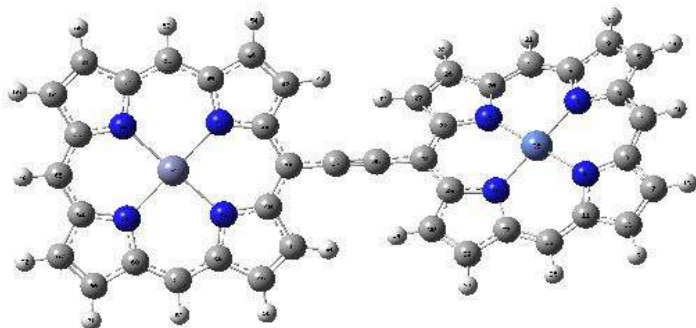
X-ray Raman probes valence-excitations, but through a core-excited intermediate. The same states show up in the UV/visible absorption spectrum, but with vastly

Integrated 2-Pulse Stimulated X-ray Raman

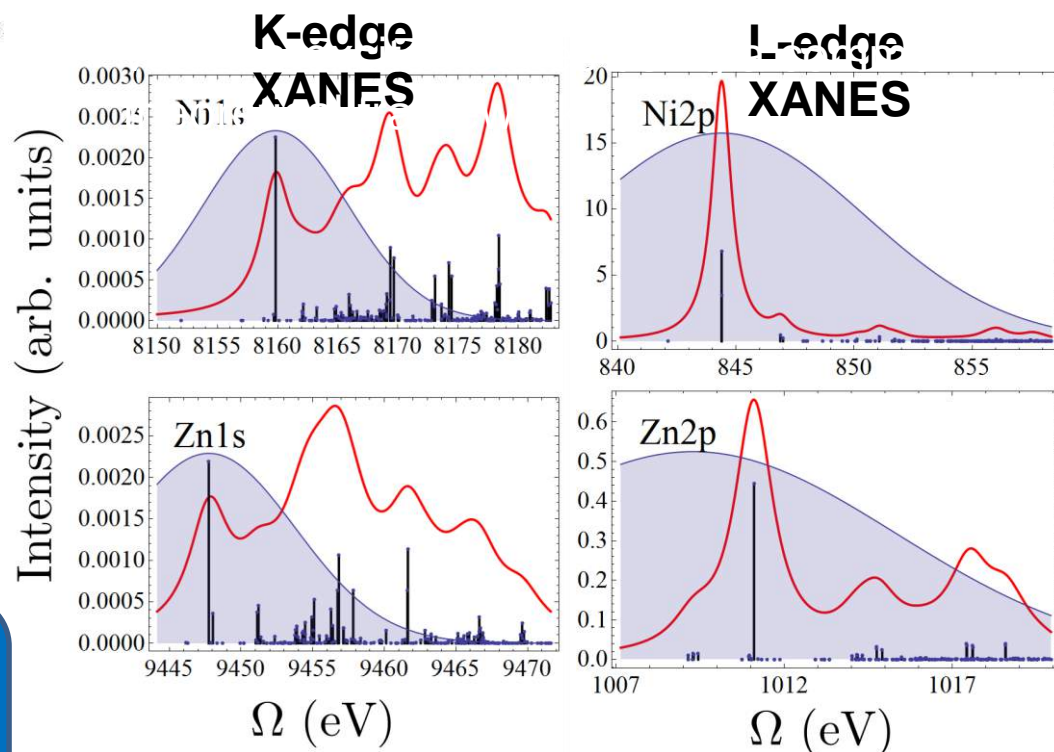The pump pulse creates a valence wavepacket by scattering off a manifold of core-excited states within the pulse bandwidth

This superposition of valence-excited states then evolves during the interpulse delays

The probe pulse then returns the system to the ground state by scattering off of core-excited states. In a two-color setup, these core-excited states are different than those accessed by the pump

choose long delays: core-ionized states are off-resonance
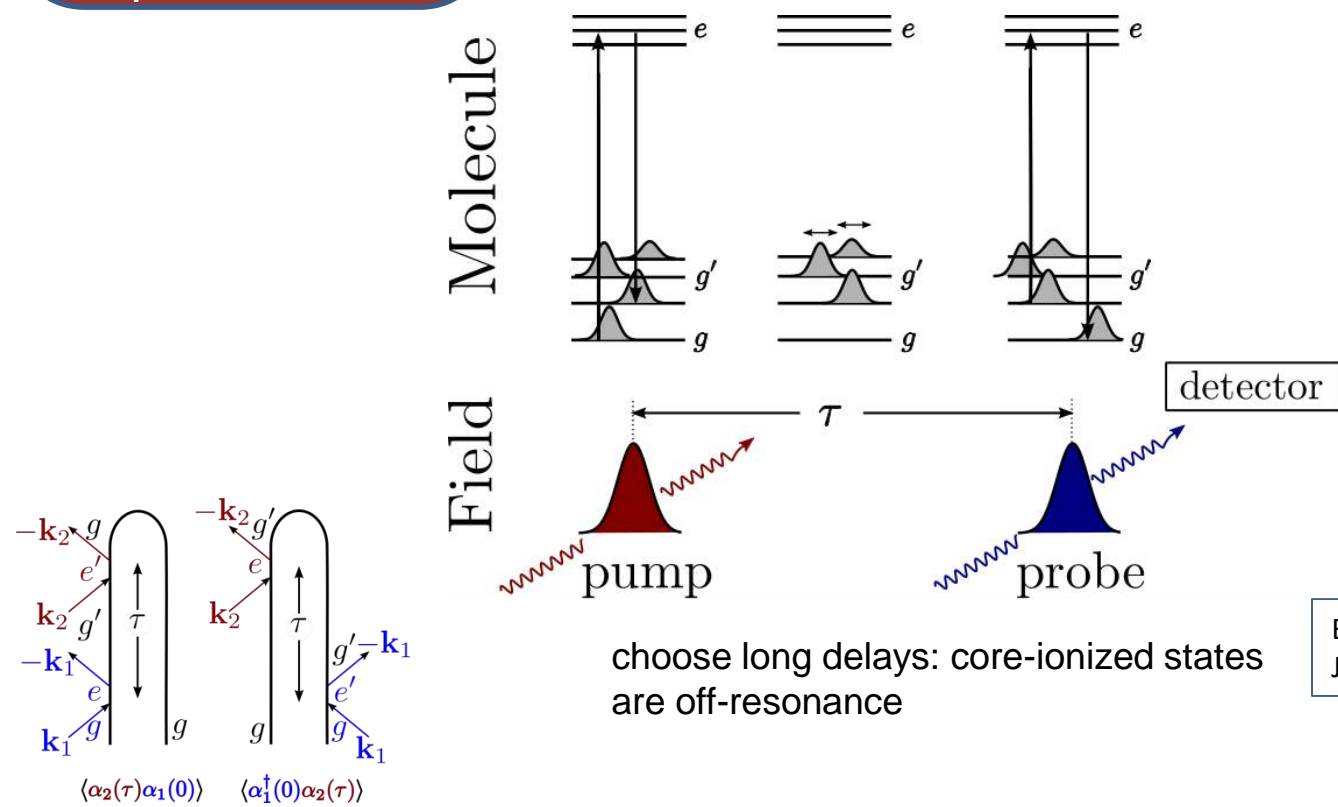
Biggs, Zhang, Healion, and Mukamel; J. Chem. Phys. **136**, 174117 (2012)

$\langle \alpha_2(\tau)\alpha_1(0)\rangle$ $\langle \alpha_1^{\dagger}(0)\alpha_2(\tau)\rangle$

Time Domain:

$$\mathbb{S}_{SXRS}(\tau) = 2\Im\langle \bar{\alpha}_2''(\tau)\bar{\alpha}_1(0)\rangle$$

Frequency Domain:

$$\mathbb{S}_{SXRS}(\Omega) = \sum_{g'} \frac{\bar{\alpha}_{2;gg'}'' \bar{\alpha}_{1;g'g}}{\Omega - \omega_{g'g} + i\Gamma_{g'}}$$

The signal is determined by the effective isotropic polarizability, which is averaged over the finite bandwidth of the excitation pulses.

Real part of the polarizability – responsible for off-resonance Raman scattering.

Imaginary part of the polarizability – goes to zero off resonance.

$$\bar{\alpha}_j = \bar{\alpha}' + i\bar{\alpha}''$$

polarizbility for the jth ultrafast pulse

$$= \sum_{e,g',g''} |g'\rangle \frac{\boldsymbol{\mu}_{g'e} \cdot \boldsymbol{\mu}_{eg''}}{2\pi} \int_{-\infty}^{\infty} d\omega \frac{\mathcal{E}_j^*(\omega)\,\mathcal{E}_j(\omega + \omega_{g'g''})}{\omega + \omega_j - \omega_{eg'} + i\Gamma_e} \langle g''|$$

$$\equiv e$$

$$\equiv g'$$

$$— g$$

Since the I2P-SXRS signal is defined as the change in the integrated intensity of the probe pulse, the probe must be on resonance. Therefore the signal only depends on the imaginary part of the probe polarizability.

One-color SXRS: Pump and Probe at same edge

$$S_{I2P-SXRS} = -\Im\langle\psi_W|\psi_D(\tau)\rangle$$

time-independent window created by probe

time-dependent doorway created by pump

One-color SXRS measures the autocorrelation of the doorway. Only the Zn2p/Zn2p signal exhibits strong low-frequency oscillations indicative of energy transfer. Other on-color signals show only exponential decay.

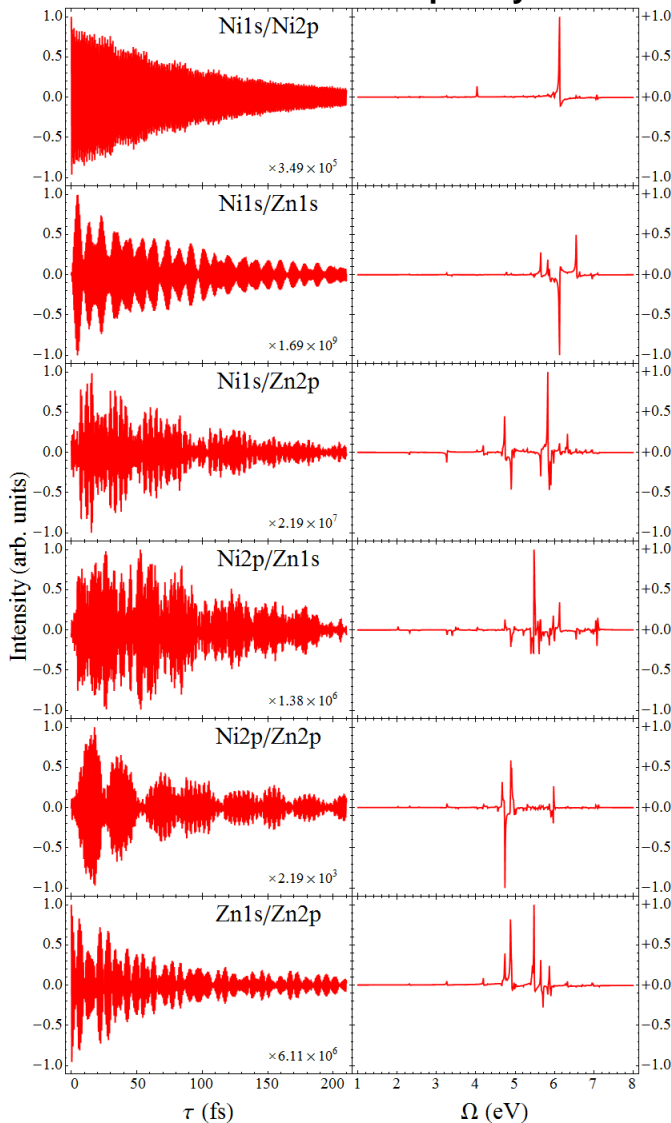**Zinc metal: K-edge, L-edge**
Nickel metal: K-edge, L-edge

One color SXRS from porphyrin dimer
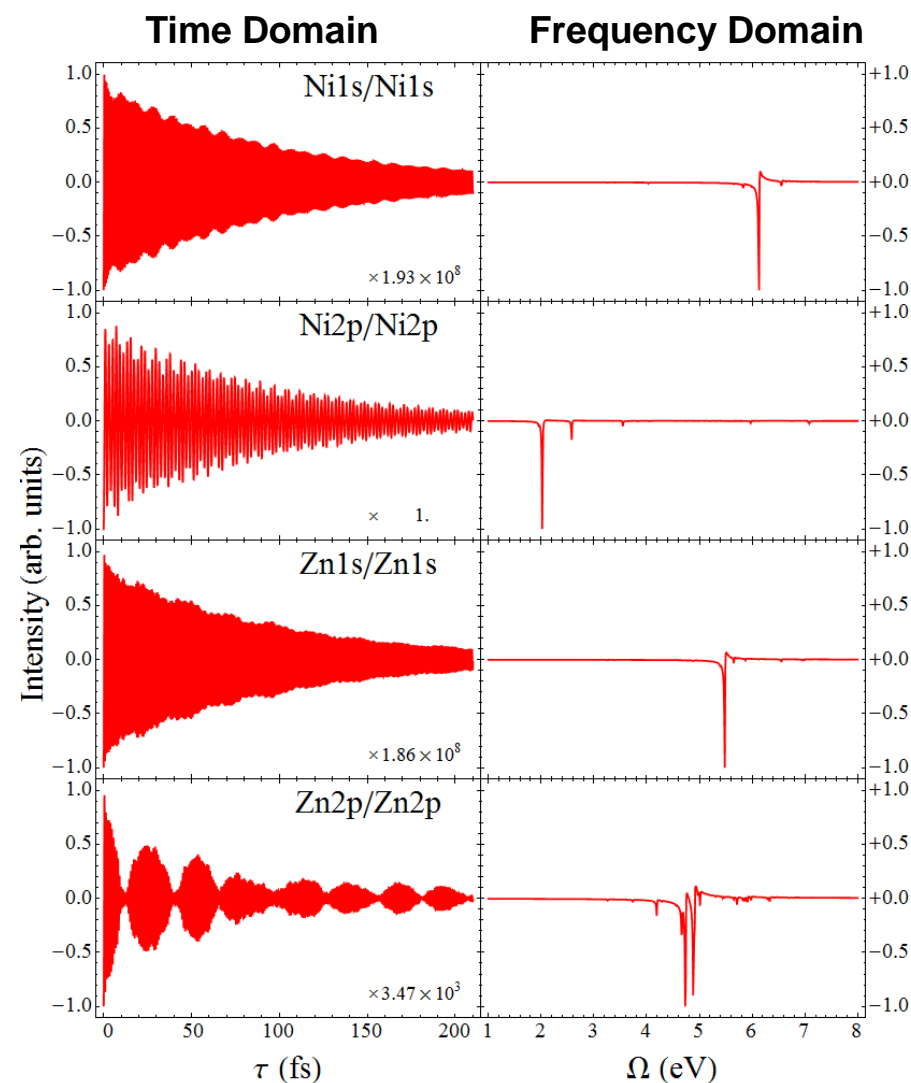
Two-color SXRS

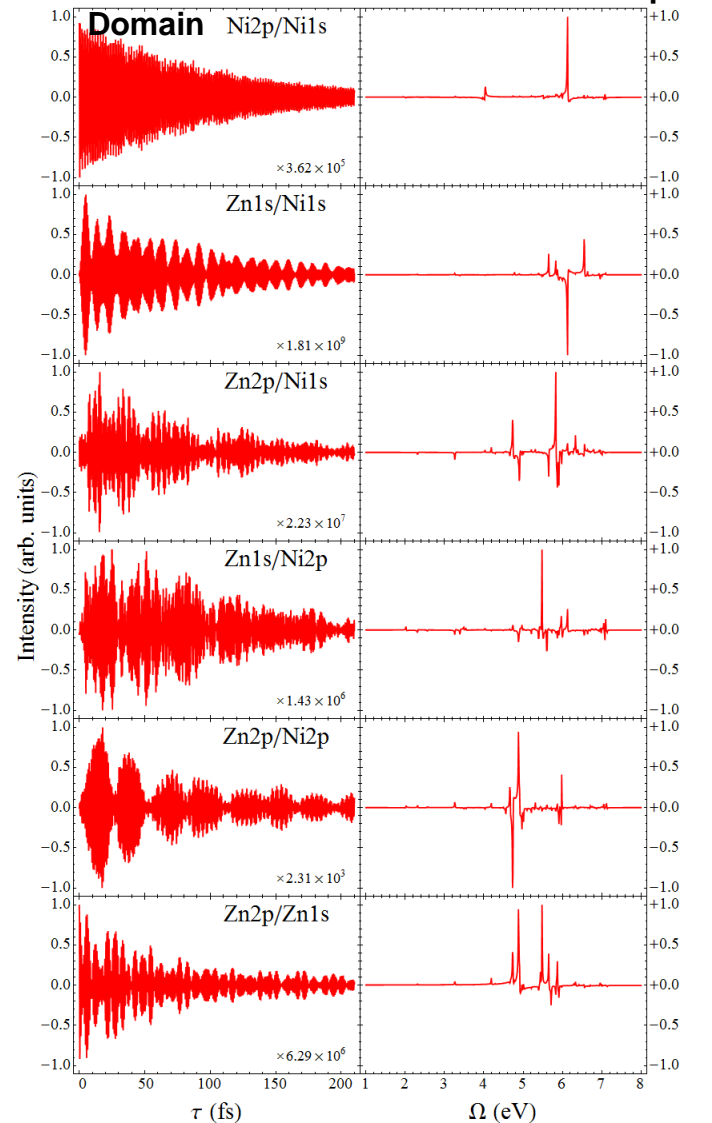**Two-color signals vanish when the two core electrons are not coupled to the same valence manifold. For the porphyrin dimer, a nonzero signal is evidence of energy or charge transfer.**

Switching the order in which the two pulses arrive results in nearly identical signals.
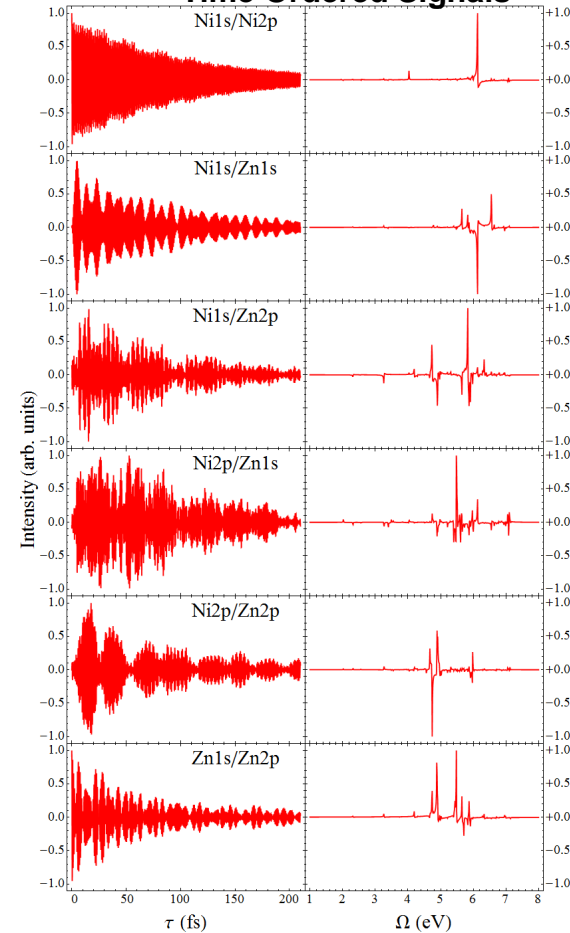
Time-reversal symmetry in 2-color SXRS
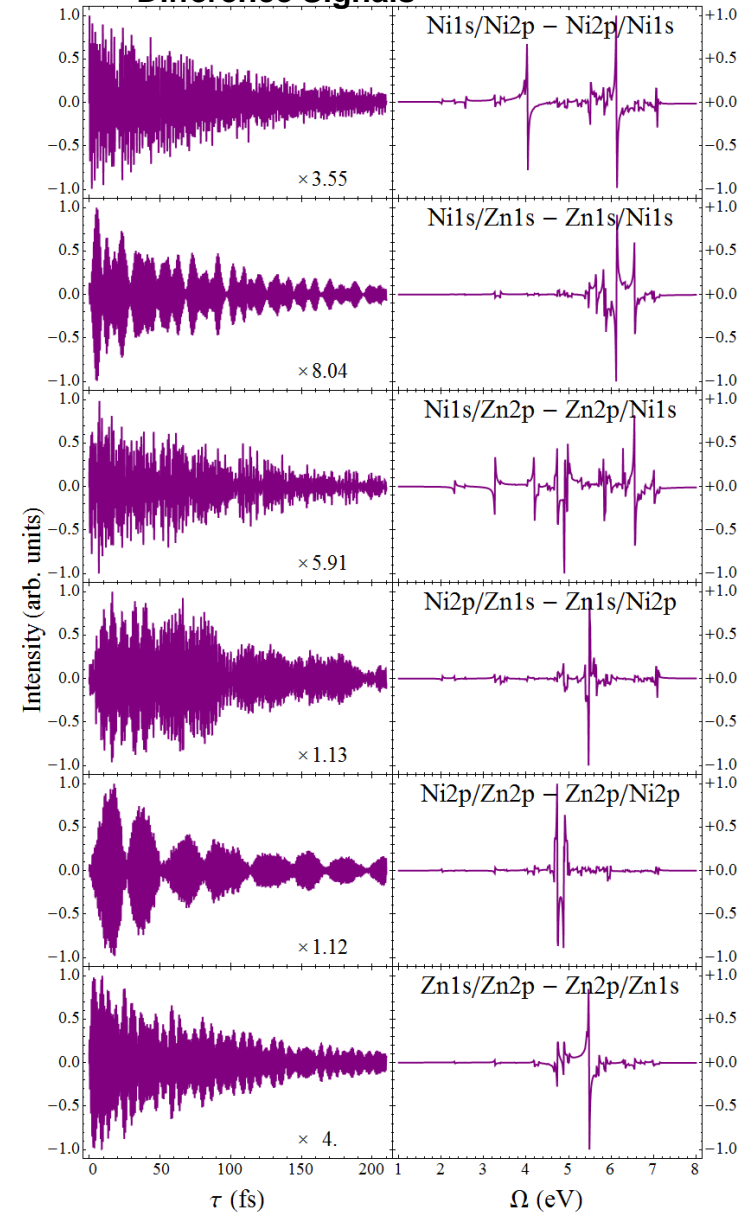
Time Ordered Signals

Difference Signals

In the time domain, the difference signals (in purple) resemble the time-ordered signals (in red). In the frequency domain, the difference signals report upon the interference between the real and imaginary polarizabilities for the two different core edges considered.

$$\mathbb{S}_{\mathrm{Diff}}(\tau) \equiv \mathbb{S}_{SXRS}(\tau) - \mathbb{S}_{SXRS}(-\tau)$$

$$\mathbb{S}_{\mathrm{Diff}}(\Omega) = \sum_{g'} \frac{\left(\bar{\alpha}''_{2;gg'} \bar{\alpha}'_{1;g'g} - \bar{\alpha}''_{1;gg'} \bar{\alpha}'_{2;g'g} \right)}{\Omega - \omega_{g'g} + i\Gamma_{g'}}$$

Natural-Orbital Decomposition

Interaction with the pump creates the doorway, a wavepacket of valence excited states

$$|\psi_D(\tau)\rangle = \sum_{g'} \alpha_{1;g'g_o} e^{-i\epsilon_{g'}\tau}|g'\rangle = \hat{K}(\tau)|g\rangle$$

The time-dependent operator $K(t)$ acts upon the ground state to create the doorway.

$$|g'\rangle = \sum_{ai} C_{ai}^{g'} c_a^\dagger c_i |g\rangle$$

$$\hat{K}(\tau) = \sum_{g,ai} \alpha_{1;g'g_o} C_{ai}^{g'} c_a^\dagger c_i e^{-i\epsilon_{g'}\tau}$$

Valence excitations written in MO basis

A singular value decomposition of provides the most compact representation of the doorway in the space of single excitations.

$c_a^\dagger$ creation operator for virtual orbital a

c_i annihilation operator for occupied orbital i

$$K(\tau) = V(\tau)W(\tau)U^\dagger(\tau)$$

$$|\psi_D(\tau)\rangle = \sum_\xi w_\xi(\tau) c_\xi^\dagger(\tau) d_\xi(\tau) |g\rangle$$

The participation ratio R^{-1} is a useful measure of the degree to which the electron and hole are entangled. When the state is described by a single electron-hole pair, they are not entangled at all and $R^{-1}=1$. Higher values indicate greater entanglement.

Through a rotation of the MO basis, a new set of natural orbitals is achieved which minimizes the number of electron-hole pairs needed to describe the state.
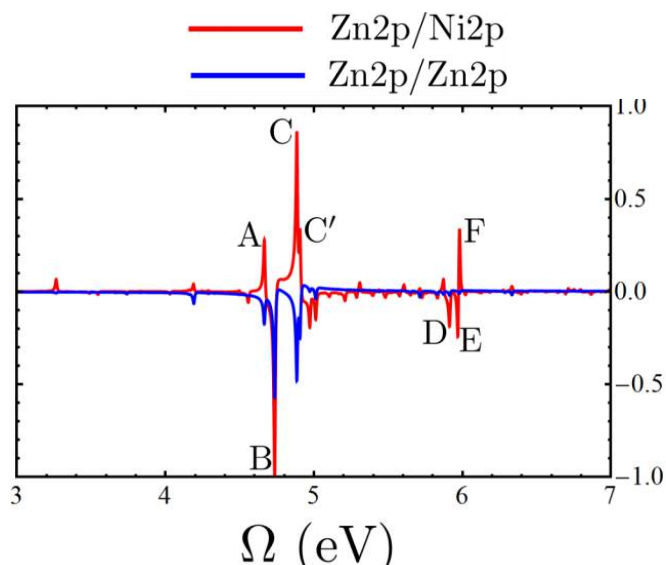
$$c_\xi^\dagger(\tau) = \sum_a V_{a,\xi}(\tau) c_a^\dagger$$

$$d_\xi(\tau) = \sum_i U_{i,\xi}^*(\tau) c_i$$

$$R^{-1}(\tau) = \frac{1}{\sum_\xi w_\xi^4(\tau)}$$

$$\sum_\xi w_\xi^2(\tau) = 1$$

Natural Transition Orbitals for Valence Eigenstates

The eigenstates which show up in the Fourier-Transform spectra are delocalized valence states.

Table 1. Frequencies, participation ratios, and integrated electron and hole densities for the states corresponding to the major peaks in the right panel of Fig. 3.

| Peak	Ω	R^{-1}	hole density Ni monomer	hole density Zn monomer	electron density Ni monomer	electron density Zn monomer
A	4.67	1.57	0.41	0.59	0.38	0.62
B	4.74	2.45	0.37	0.63	0.29	0.71
C	4.89	4.48	0.34	0.66	0.40	0.60
C'	4.91	3.42	0.57	0.43	0.46	0.54
D	5.91	4.51	0.45	0.55	0.44	0.56
E	5.97	1.39	0.92	0.08	0.99	0.01
F	5.98	3.82	0.60	0.40	0.84	0.16
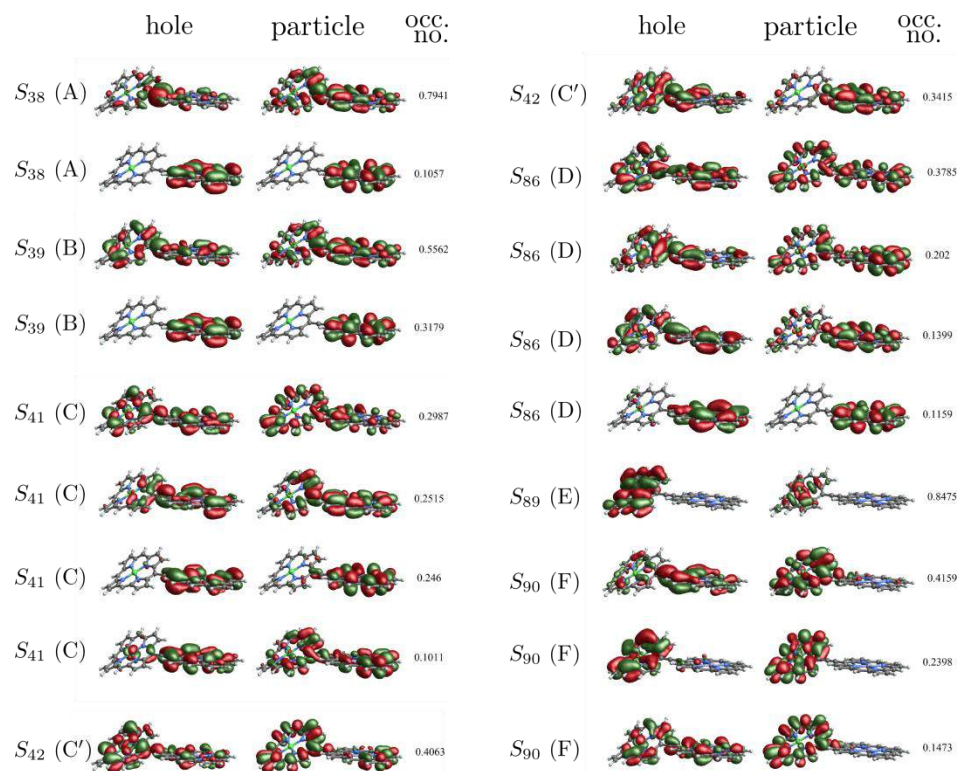
Natural transition orbitals provide the most compact representation of these states. Orbital rotations which result from a singular-value decomposition of the transition density matrices in the space of single excitations
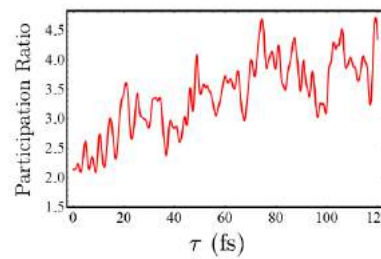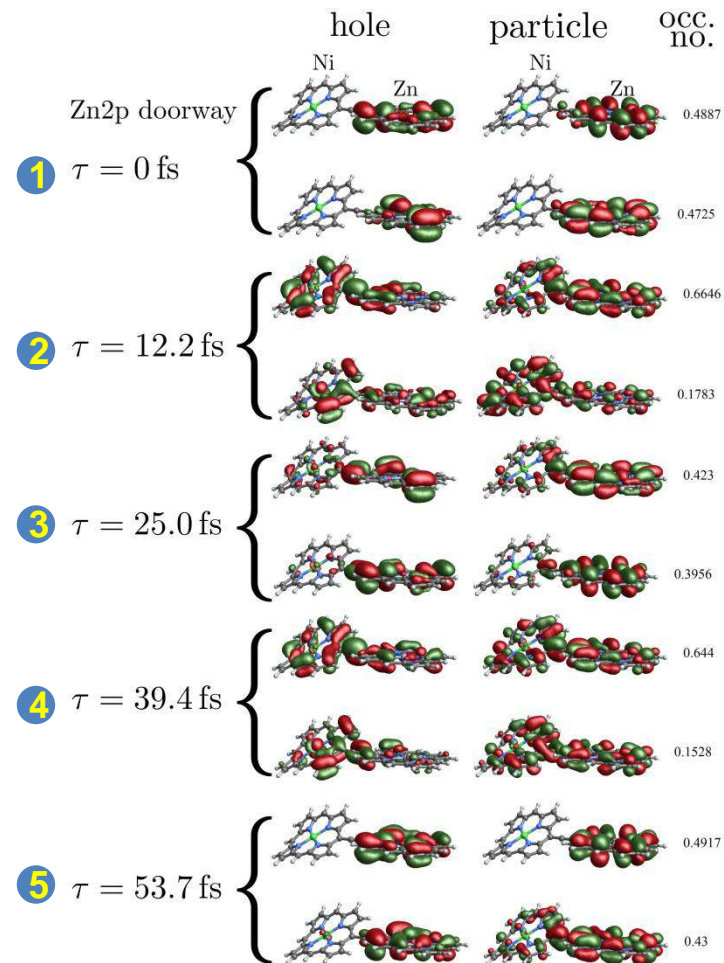
Time-dependent Natural Orbitals for Valence Wavepackets

Zn2p/Zn2p Signal –Time Domain
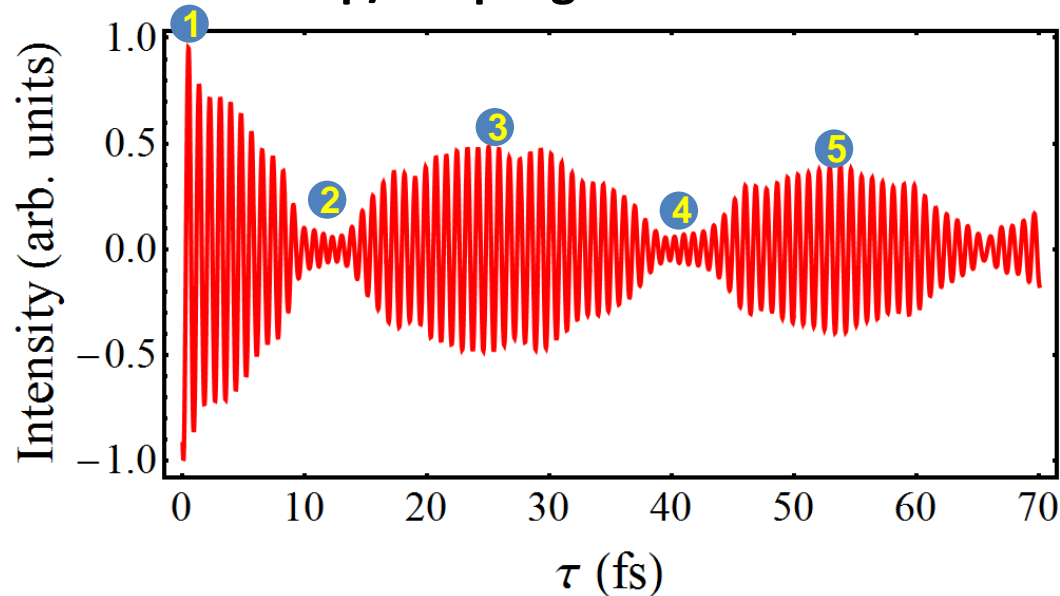
The superposition of delocalized electronic eigenstates resulting from Raman excitation is localized in space. Maxima and minima in this signal correspond to times when the excitation is on the zinc and nickel monomers, respectively.

hole   particle   occ. no.

Zn2p doorway

1    $\tau = 0$ fs   0.4887 / 0.4725

2    $\tau = 12.2$ fs   0.6646 / 0.1783

3    $\tau = 25.0$ fs   0.423 / 0.3956

4    $\tau = 39.4$ fs   0.644 / 0.1528

5    $\tau = 53.7$ fs   0.4917 / 0.43

The electron-hole pairs comprising the wavepacket become increasingly entangled following excitation
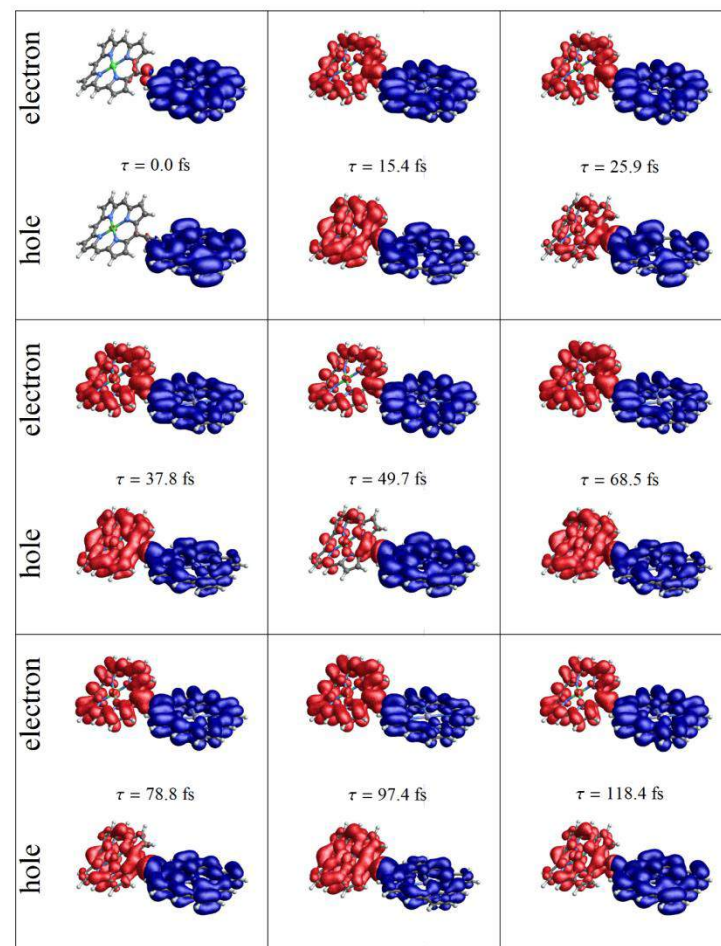
Charge density vs. signal

There is a correspondence between the nonequilibrium charge density and the spectroscopic signal. The electron and hole densities move across monomers together, indicating energy transfer rather than charge transfer.
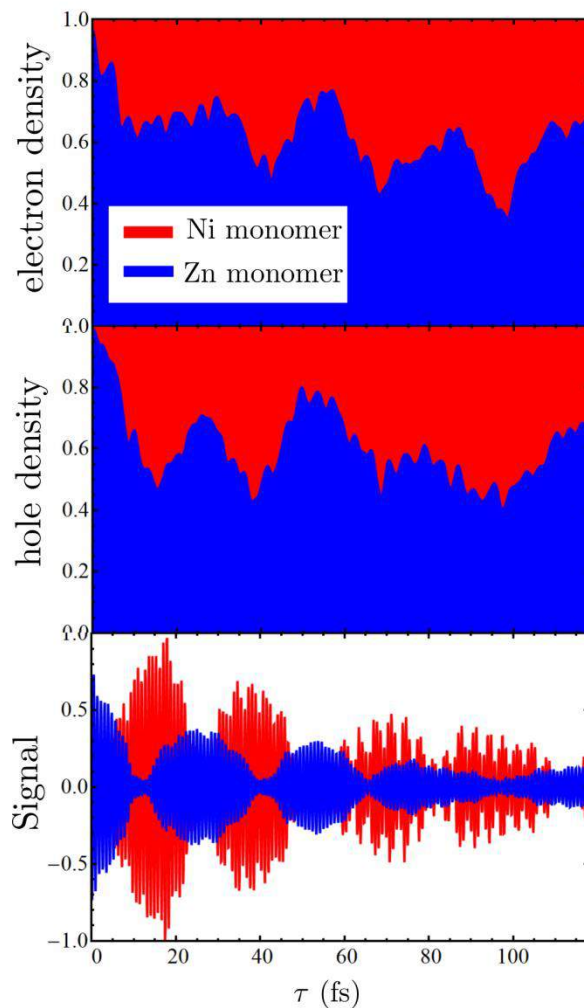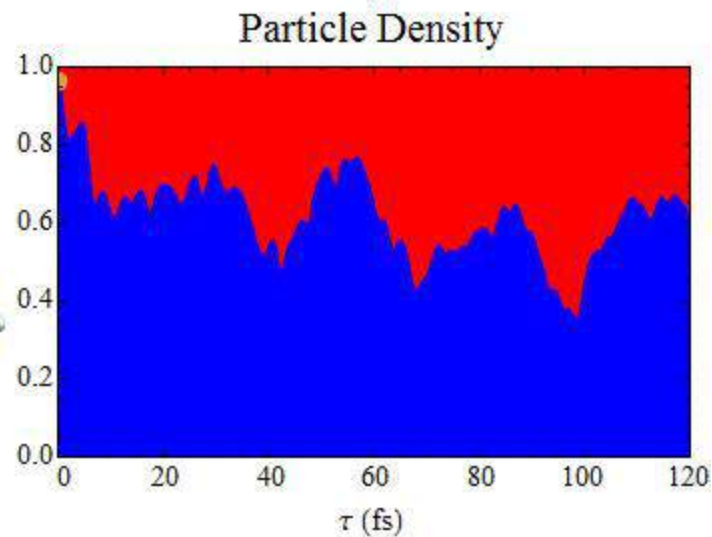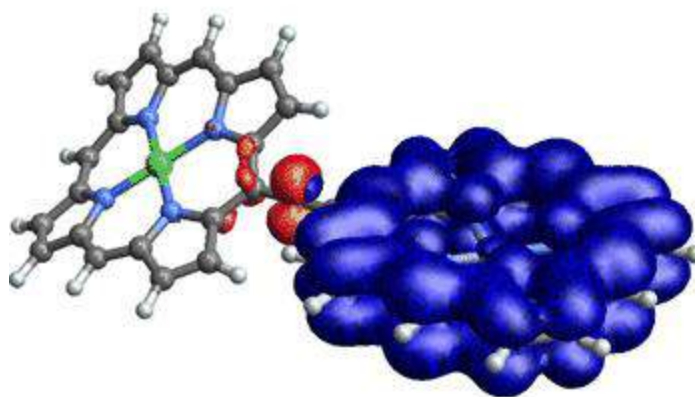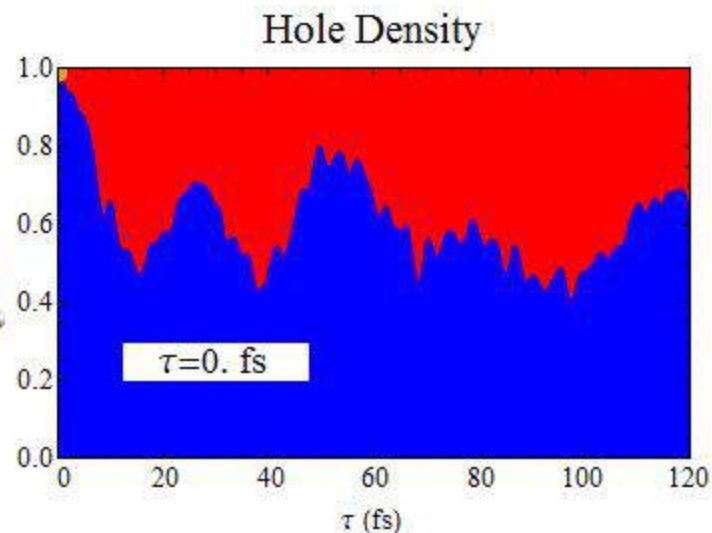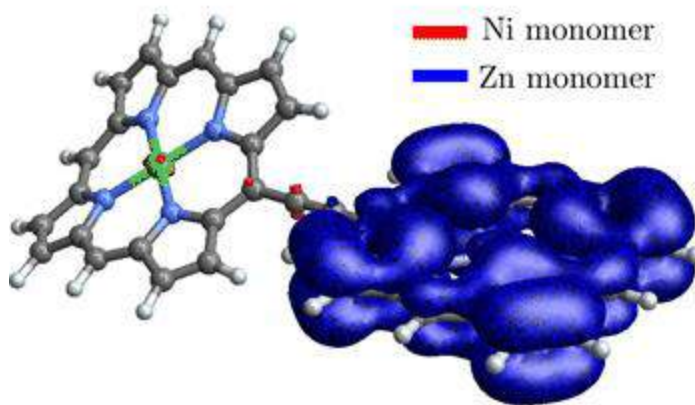

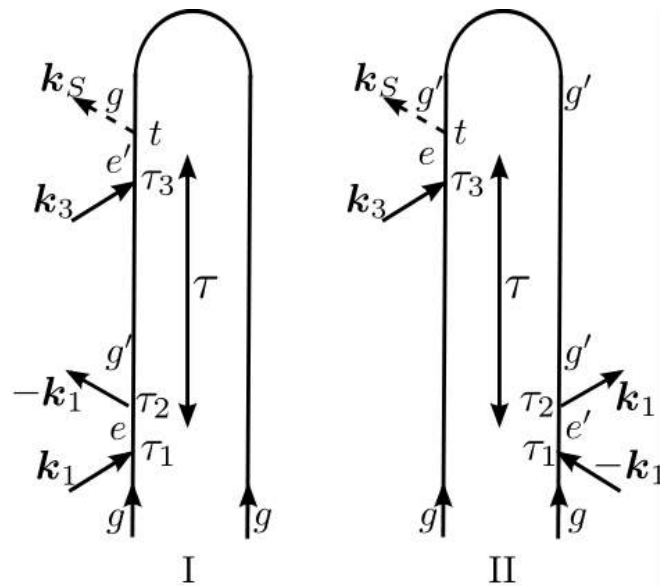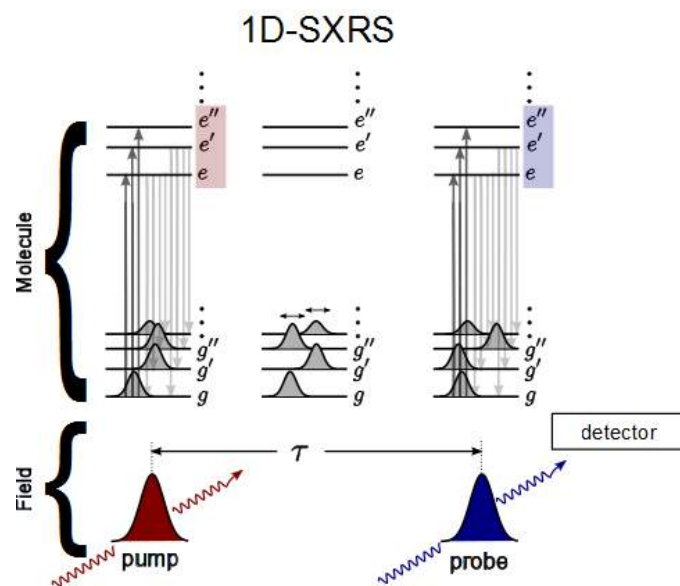Zn2p Raman Wavepacket Densities
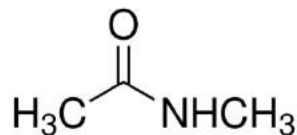
Animation – short simulation
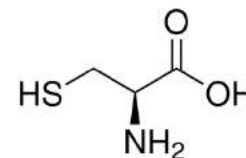
2-Pulse Stimulated X-ray Raman

1D-SXRS

The system interacts twice with the pump and twice with the probe. No phase control is required.

The resonannt pump creates a wavepacket of valence-excited states which then evolves for a time τ before the arrival of the probe pulse.

N-Methylacetamide (NMA)

L-Cysteine

The Effective Polarizability: Incorporating the Effects of Pulse Bandwidth

The traditional polarizability which enters the famous Kramers-Heisenberg equation for frequency-domain Raman spectroscopy is modified to account for the finite spectral bandwidth of ultrafast pulses

Transition dipole moments between valence (g') and core (e) states

Jth pulse spectral amplitude

$$\alpha_j = \alpha_j' + i\alpha_j'' = \sum_{e,g',g''} |g'\rangle \frac{V_{g'e}V_{eg''}}{2\pi} \int_{-\infty}^{\infty} d\omega \frac{\mathcal{E}_j^*(\omega)\,\mathcal{E}_j(\omega+\omega_{g'g''})}{\omega - \omega_{eg'} + i\Gamma_e} \langle g''|$$

For frequency-dispersed measurements, we have the frequency-dependent effective polarizability

$$\bar{\alpha}_j(\omega) = \sum_{e,g',g''} |g'\rangle \frac{V_{g'e}V_{eg''}}{2\pi} \frac{\mathcal{E}_j^*(\omega)\,\mathcal{E}_j(\omega+\omega_{g'g''})}{\omega - \omega_{eg'} + i\Gamma_e} \langle g''|$$

S1s* 2473.5eV

O1s* 532.2eV $|e\rangle$

N1s* 404.4eV

α is the integral of α(ω)

$$\alpha_j = \int d\omega\, \bar{\alpha}_j(\omega)$$

$|g'\rangle$
$|g_o\rangle$

By substituting a delta function for the excitation field and a constant for the de-exciting field, we recover the frequency-domain expression for α.

$$\mathcal{E}_j(\omega) = \delta(\omega - \omega_L); \mathcal{E}_j^*(\omega) = 1 \longrightarrow \alpha = \sum_{e,g',g''} |g'\rangle \frac{V_{g'e}V_{eg''}}{\omega_L - \omega_{eg''} + i\Gamma_e} \langle g''|$$

2P-SXRS: Integrated vs. Dispersed Detection

The integrated two-pulse (I2P) signal is one-dimensional and can be written directly from the contributing diagrams.

$$S_{I2P-SXRS}(\Omega_2) = -\sum_{g'} \frac{\alpha''_{2;gg'}\alpha_{1;g'g}}{\Omega_2 - \omega_{g'g} + i\Gamma_{g'}}$$

The polarizability is extended to time-domain experiments, incorporating the pulse spectral envelopes. Only those valence excitations whose energies lie within the pulse bandwidth are impulsively excited.

Another method for extending the 1D-SXRS technique to two dimensions involves sending measuring the spectrum of the transmitted probe pulse rather than its integrated intensity.

$$S_{D2P-SXRS}(\Omega_2, \Omega_3) = \sum_{g'} \frac{i(\alpha_{1;g'g})(\bar{\alpha}_{2;gg'}(\Omega_3) - \bar{\alpha}^{\dagger}_{2;gg'}(\Omega_3))}{\Omega_2 - \omega_{g'g} + i\Gamma_{g'}}$$

which depends on the frequency-dependent resonant polarizability defined by

- This signal allows us to "open up" the probe polarizability.

- Peaks show which core-excited and valence-excited states are coupled to each other.

- Unlike the integrated signal, contributions from the two contributing diagrams are spectrally removed from each other.

- The 1D-SXRS signal is obtained simply by summing over the dispersed frequency

- Unlike the integrated signal, the frequency-dispersed signal does not vanish when the probe is off resonance. Far from resonance, the system transfers energy from one mode of the field to another.

- By integrating over the dispersed frequency Ω_3, leaving only Ω_2 -the Fourier transform of the delay time- we recover the integrated signal.

$$S_{I2P-SXRS}(\Omega_2) = \int d\Omega_3 S_{D2P-SXRS}(\Omega_2, \Omega_3).$$

N1s pump, N1s probe, L-cysteine
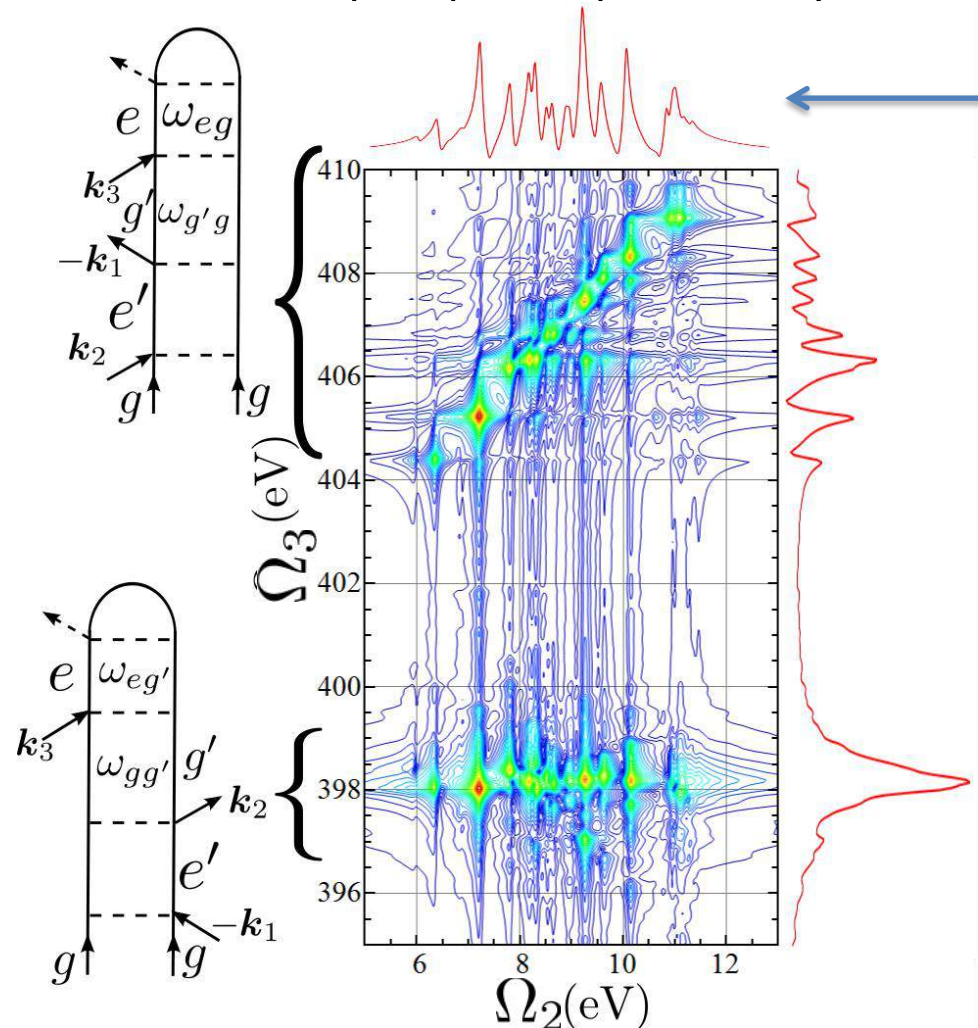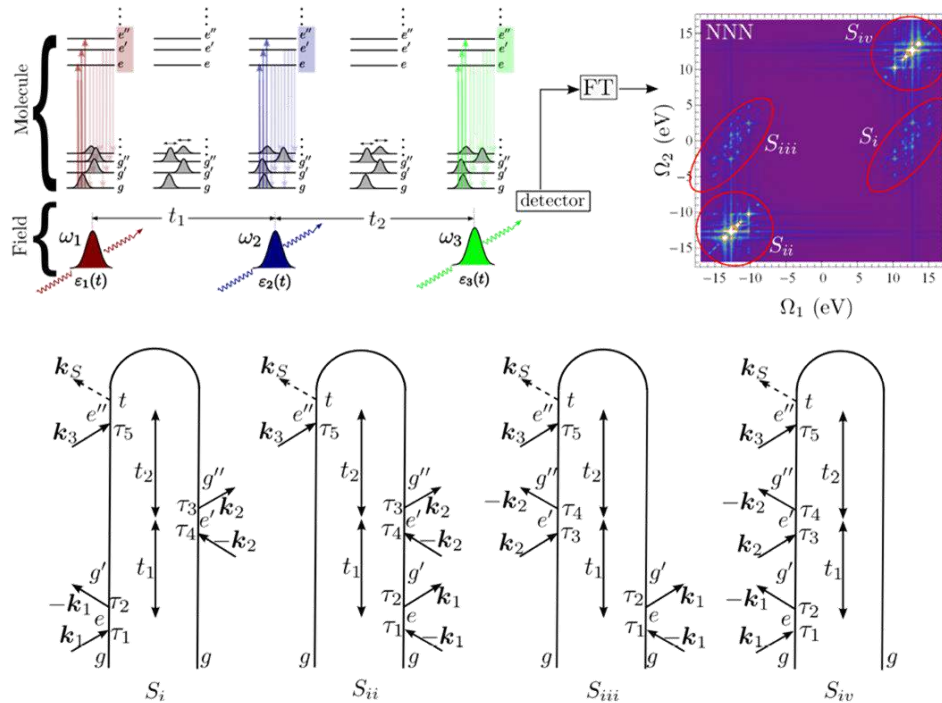
The two-pulse technique is extended by adding another pulse. Now two pulses create and then modify the valence-excited wavepacket that is then detected by the probe. As before, both integrated and dispersed detection are possible.

This signal is dependent on the matrix elements of the polarizability between different valence-excited states.

Ω_2 and Ω_4 are the delay times between the pulses, and both correspond to valence-excited states. Ω_5 is the dispersed frequency and reveals core-excited levels.

$$S_{I3P-SXRS}(\Omega_2, \Omega_4) = \sum_{g',g''} \frac{i\alpha_{1;g'g}}{\Omega_2 - \omega_{g'g} + i\Gamma_{g'}} \left(\frac{\alpha^{\dagger}_{2;gg''}\alpha''_{3;g''g'}}{\Omega_4 - \omega_{g'g''} + i\Gamma_{g'}} - \frac{\alpha''_{3;gg''}\alpha_{2;g''g'}}{\Omega_4 - \omega_{g''g} + i\Gamma_{g''}} \right).$$

$$S_{D3P-SXRS}(\Omega_2, \Omega_4, \Omega_5) =$$

$$\sum_{e,g',g''} \frac{i\alpha_{1;g'g}\alpha^{\dagger}_{2;g,g''}(\bar{\alpha}_{3;g''g'}(\Omega_5) - \bar{\alpha}^{\dagger}_{3;g''g'}(\Omega_5))}{(\Omega_2 - \omega_{g'g} + i\Gamma_{g'})(\Omega_4 - \omega_{g'g''} + i\Gamma_{g'})} - \frac{i\alpha_{1;g'g}\alpha_{2;g'',g'}(\bar{\alpha}_{3;gg''}(\Omega_5) - \bar{\alpha}^{\dagger}_{3;gg''}(\Omega_5))}{(\Omega_2 - \omega_{g'g} + i\Gamma_{g'})(\Omega_4 - \omega_{g''g} + i\Gamma_{g''})}$$
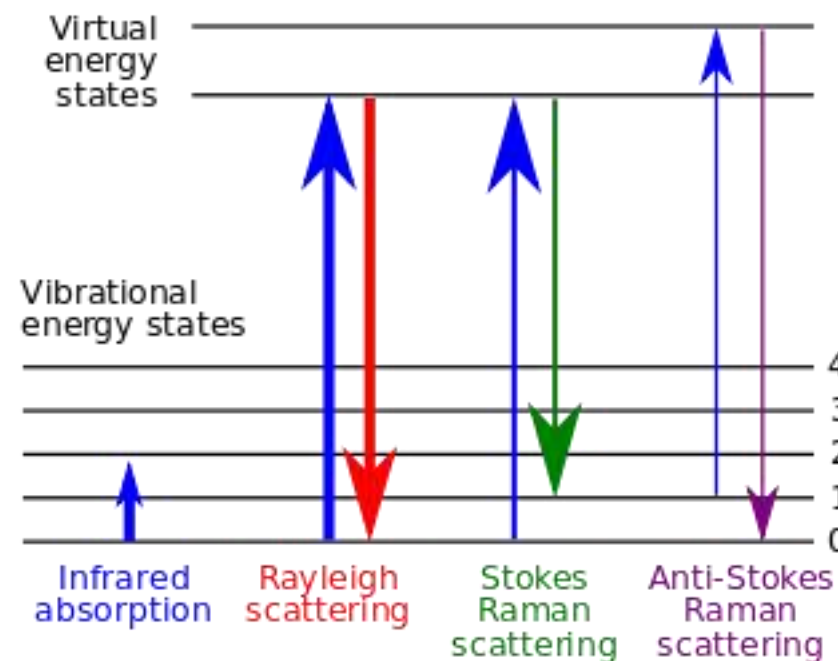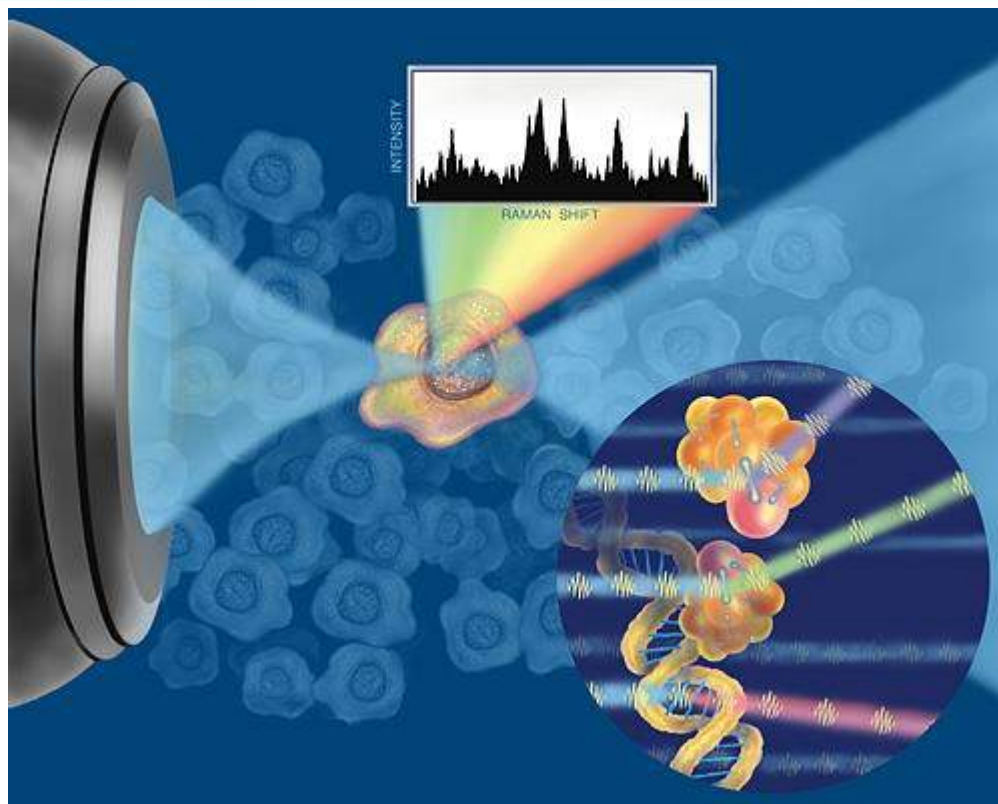
One-Color and Two-Color I2P-SXRS of trans-NMA

Tuning the X-ray pulse to be resonant with different core-edge transitions
Probes delocalized valence excitations perturbed by the selected localized core hole.

α^O

x-ray polarizability operators for each core

α^N

k_1 k_2

N1s/O1s

O1s/O1s

N1s/N1s
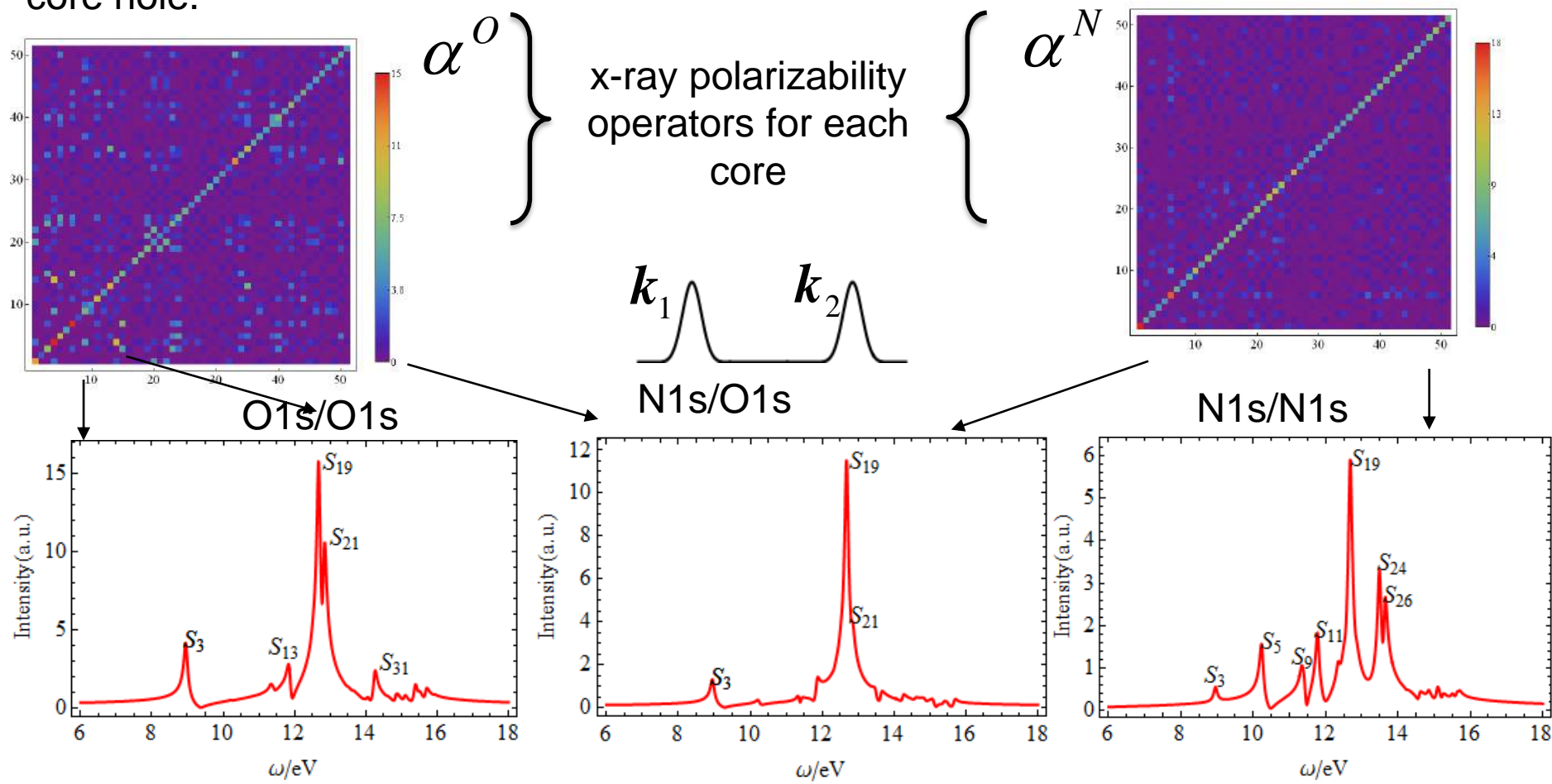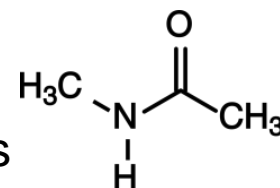
Raman spectroscopy

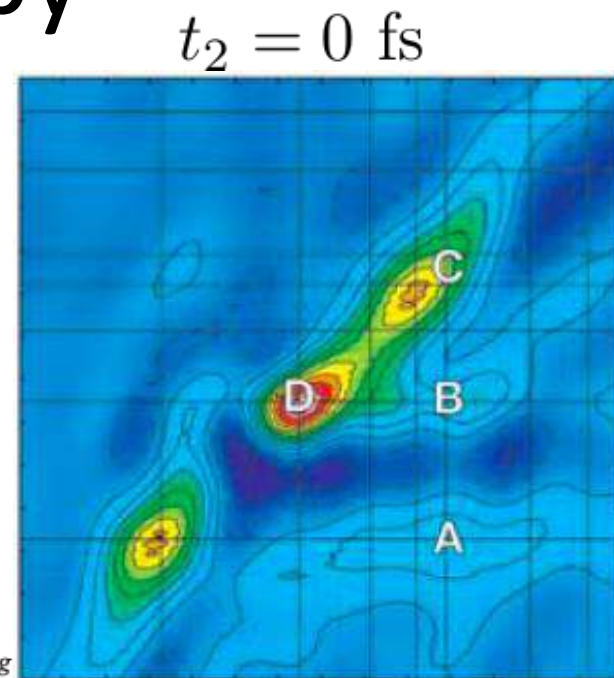

- Ultrafast spectroscopic technique
- Vibrational structures with high temporal 10-fs and spectral $\sim 10 cm^{-1}$ resolution
- Studies of ultrafast electronic dynamics and direct observation of nonstationary vibrational wave-packet motion

Figure (top left) courtesy of T. Huser and D. Taylor UC Davis
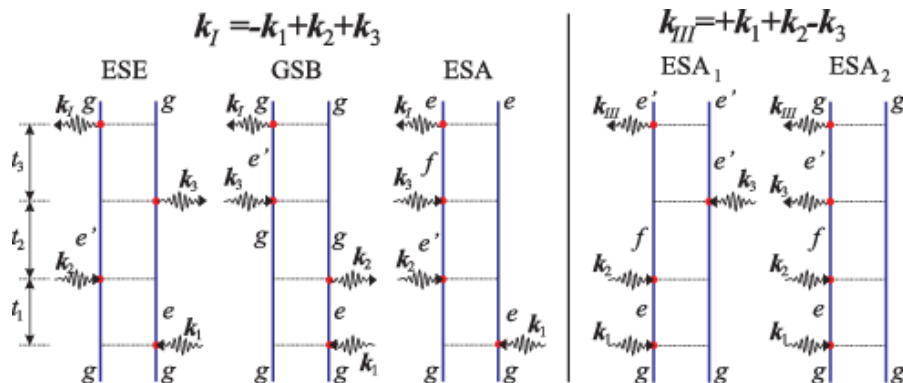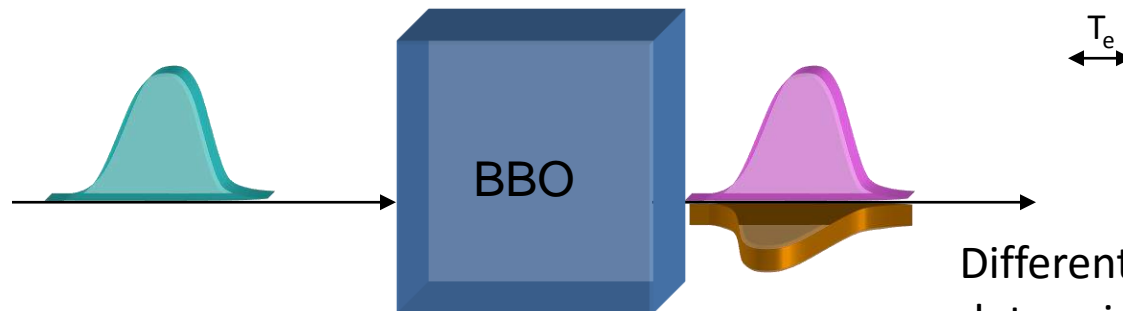
Multidimensional optical spectroscopy
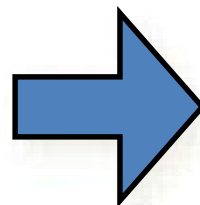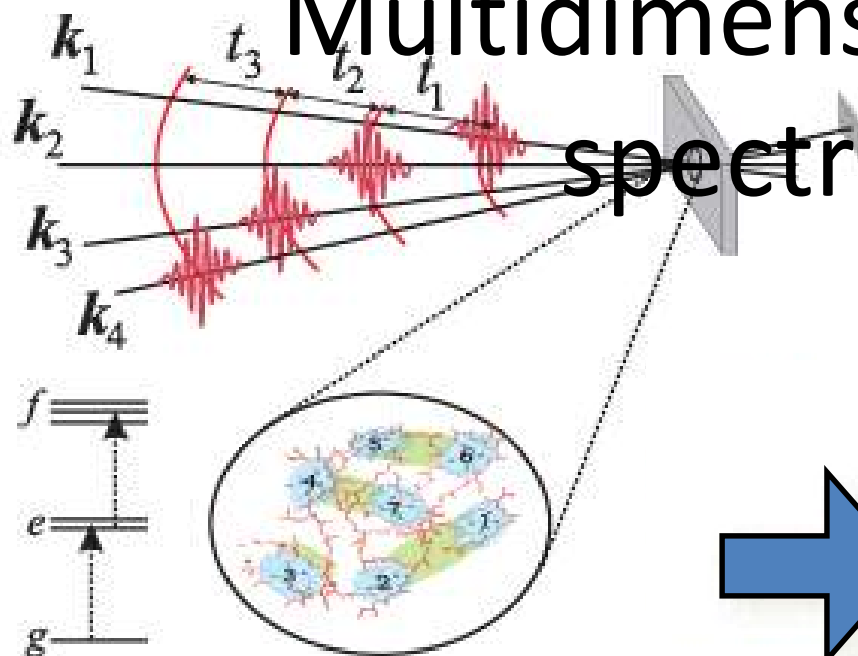
Feynman diagrams

Photon generated through PDC

BBO

T_e

Different group velocity in crystal determines entanglement time $T_e=T_{2e}-T_{1e}$

- Non delayed entangled photon from PDC pairs are time ordered even without a delay
- Classical photon without delay are not time ordered

τ_{12}

$t_2 = t_1 + \tau_{12}$

t_2 [fs]

t_1 [fs]
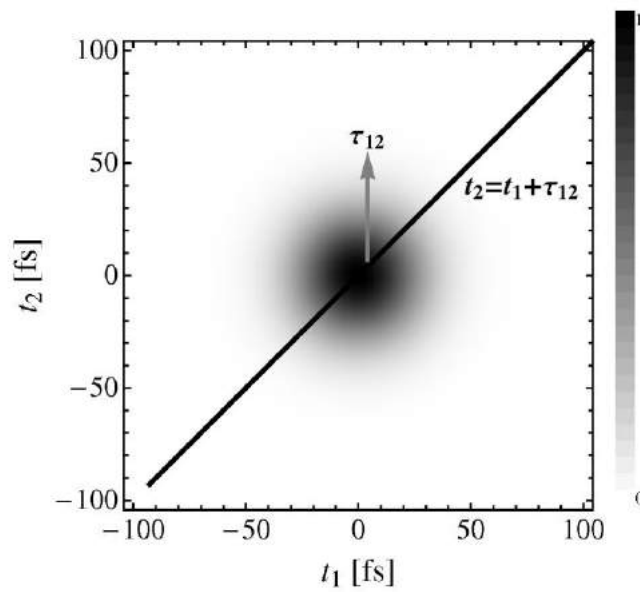
$\langle E(t_1)E(t_2)\rangle$

Photon 2 after Photon 1

Pulsewidth

$\frac{1}{T_e}$

ω_2 [meV]

ω_1 [meV]

T. E. Keller and M. H. Rubin, Phys. Rev. A **56**, 1534 (1997).

$\langle E(\omega_1)E(\omega_2)\rangle$

- Entangled light (parametric down conversion - PDC)

Twin photon state

$$|\psi\rangle = \int_{-\infty}^{\infty} \frac{d\omega_1}{2\pi} \frac{d\omega_2}{2\pi} \Phi(\omega_1, \omega_2) a_{\omega_1}^{\dagger} a_{\omega_2}^{\dagger} |0\rangle$$

Two-photon amplitude

$$\Phi(\omega_1, \omega_2) = A_p(\omega_1 + \omega_2)\text{sinc}\left[\frac{\omega_1 - \omega_p}{2}T_{1e} + \frac{\omega_2 - \omega_p}{2}T_{2e}\right] e^{i\frac{\omega_1 - \omega_p}{2}T_{1e} + i\frac{\omega_2 - \omega_p}{2}T_{2e}} + (T_{1e} \leftrightarrow T_{2e})$$
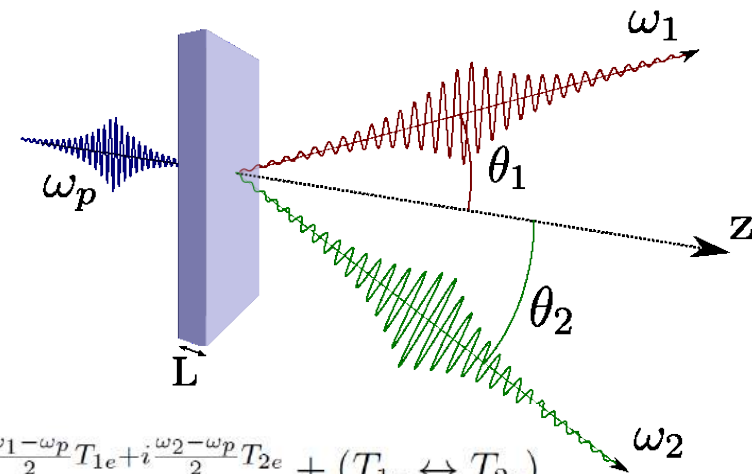
T_{je} time delays acquired by beams during propagation through the nonlinear crystal

$$A_p(\omega) = A_0/[\omega - 2\omega_p + i\sigma_p] \quad \text{Classical pump envelope}$$

$$\langle E^{\dagger}(\omega_d) E^{\dagger}(\omega_a + \omega_b - \omega_d) E(\omega_b) E(\omega_a)\rangle = \Phi^*(\omega_a + \omega_b - \omega_d, \omega_d)\Phi(\omega_a, \omega_b)$$
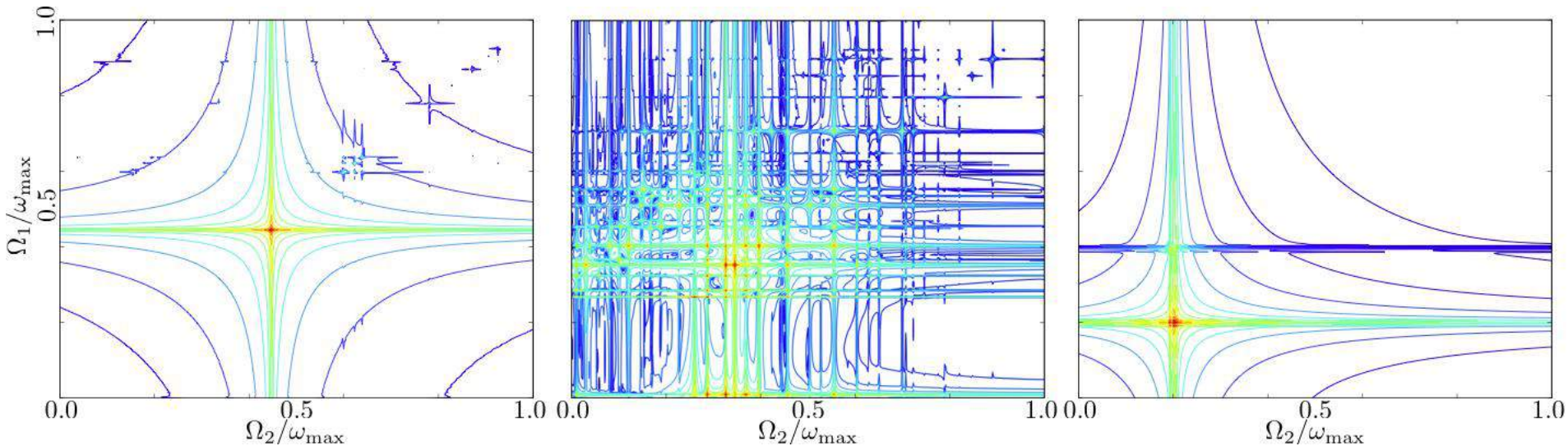
ω_1, ω_2 broad band and $\omega_1 + \omega_2 = \omega_p$ narrowband
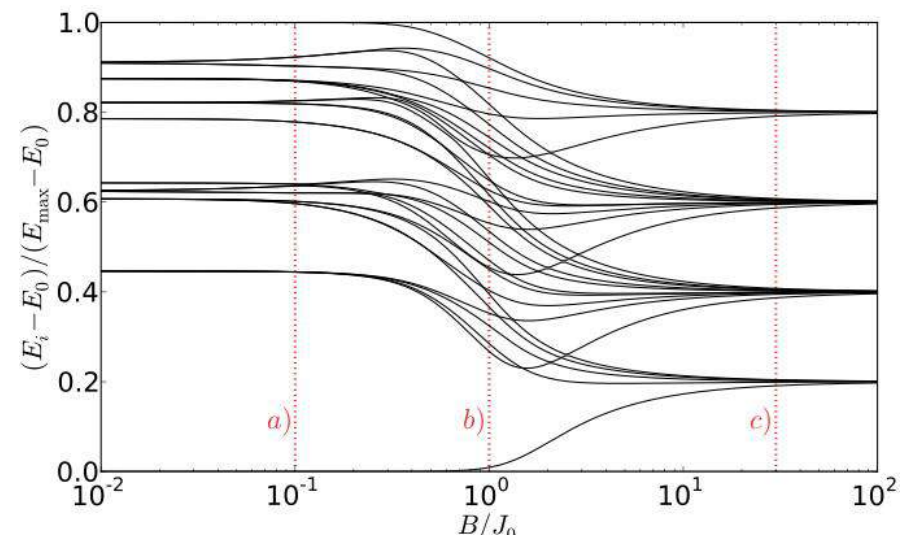
Frequency arguments of different modes are mixed

Spin chains: Phase transitions and critical behavior

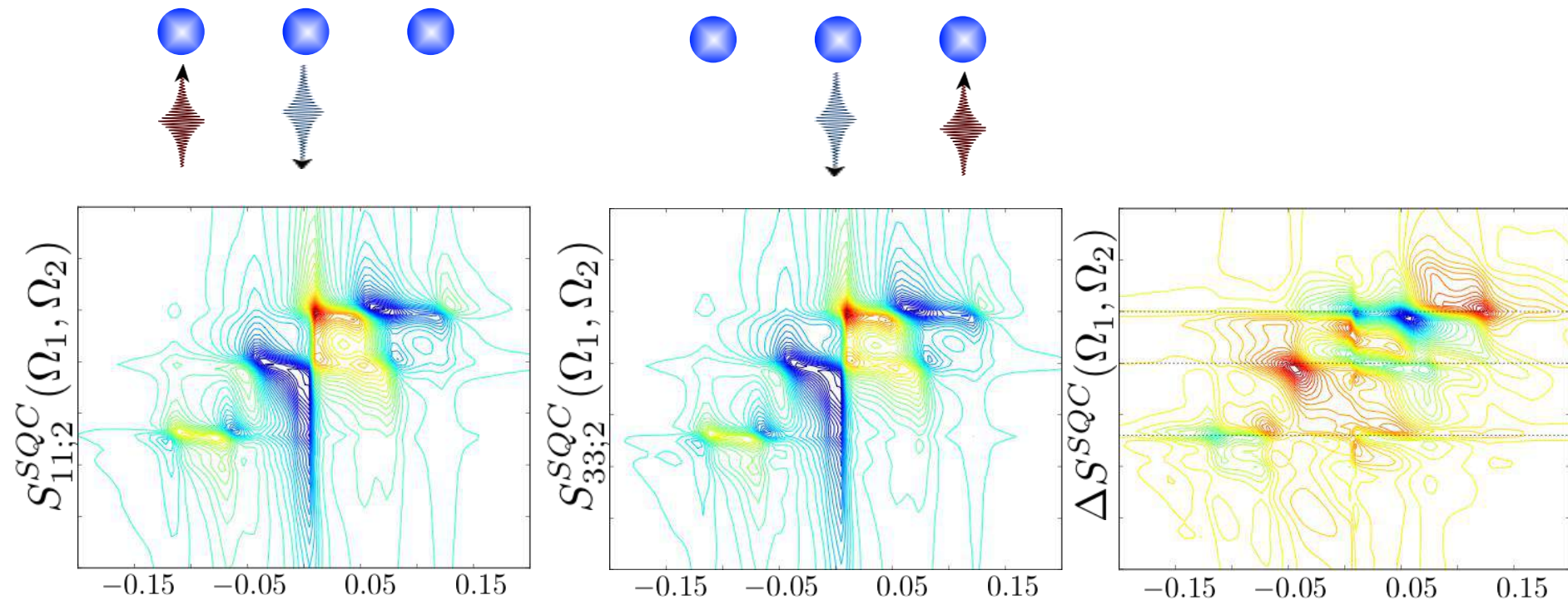Excited state dynamics near quantum phase transitions

$$H = -\sum_{\substack{i,j=1 \\ (i<j)}}^{N} J_{ij}\sigma_x^{(i)}\sigma_x^{(j)} - B\sum_{i=1}^{N} \sigma_y^{(i)}$$

F. Schlawin, M. Gessner, S. Mukamel and A. Buchleitner, Phys. Rev. A 90, 023603 (2014)

Steady State Currents

The two ends of the chain are heated to different temperatures.

In the absence of the temperature gradient, the two excitation schemes yield the same result, and their difference vanishes. Hence, their difference ΔS^{SQC} is a direct probe of the heat current through the chain.

F. Schlawin, M. Gessner, S. Mukamel and A. Buchleitner, Phys. Rev. A 90,

4th order: nonlinearities

Double Quantum Coherence: Identify anharmonic corrections in trap potential
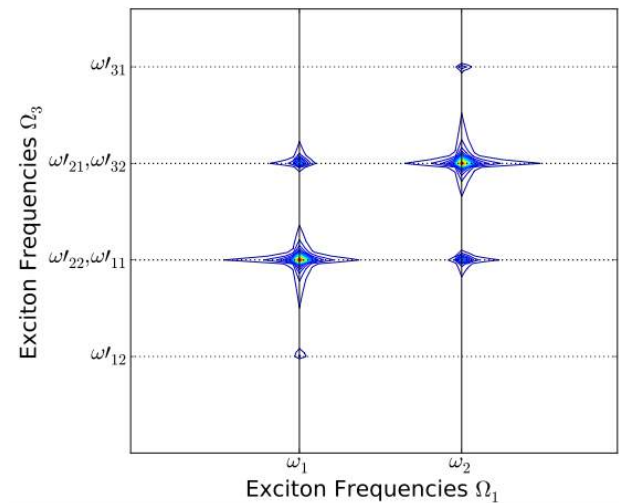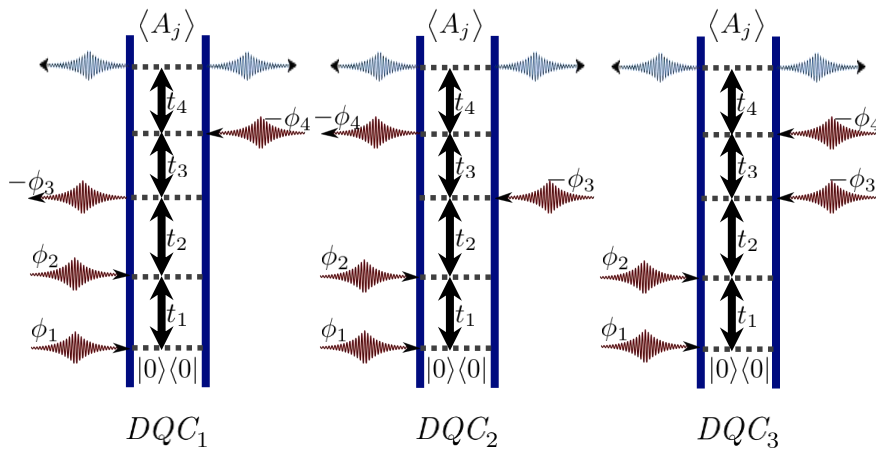
Harmonic trap

In perfectly harmonic trap, resonances are formed by degenerate multiplets.

M. Gessner, F. Schlawin, H. Häffner, S. Mukamel, and A. Buchleitner, New J. Phys. 16, 092001 (2014)

4th order: nonlinearities

Double Quantum Coherence: Identify anharmonic corrections in trap potential
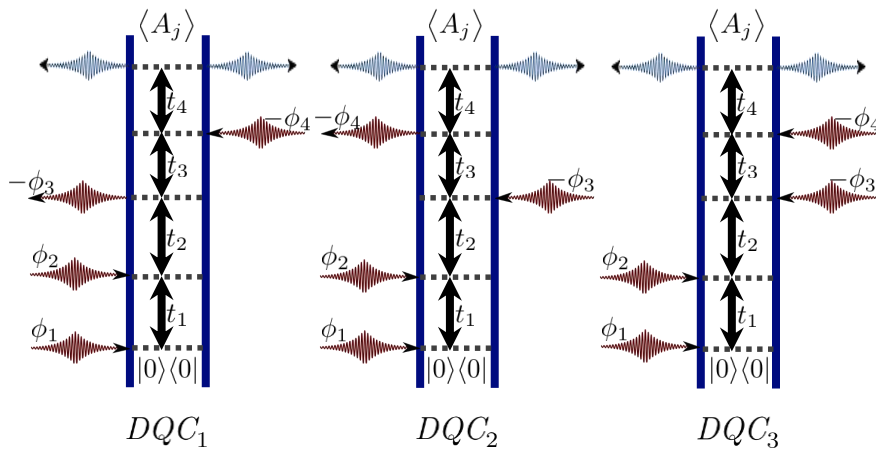
Anharmonic trap

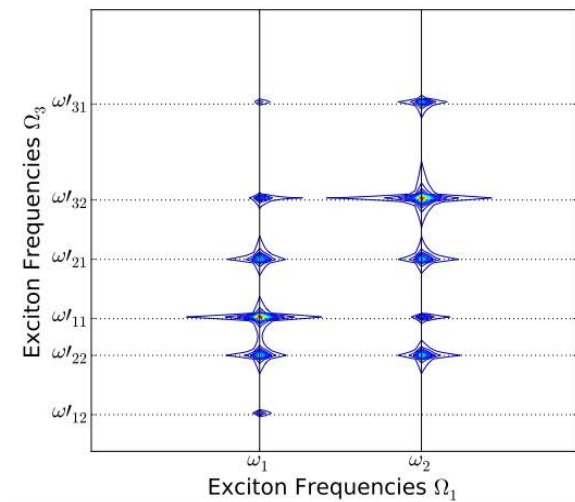Anharmonicity lifts this degeneracy, and the splitting of resonances may be used to measure its strength.

M. Gessner, F. Schlawin, H. Häffner, S. Mukamel, and A. Buchleitner, New J. Phys. 16, 092001 (2014)

4th order: high excitations

Photon Echo: Population decay
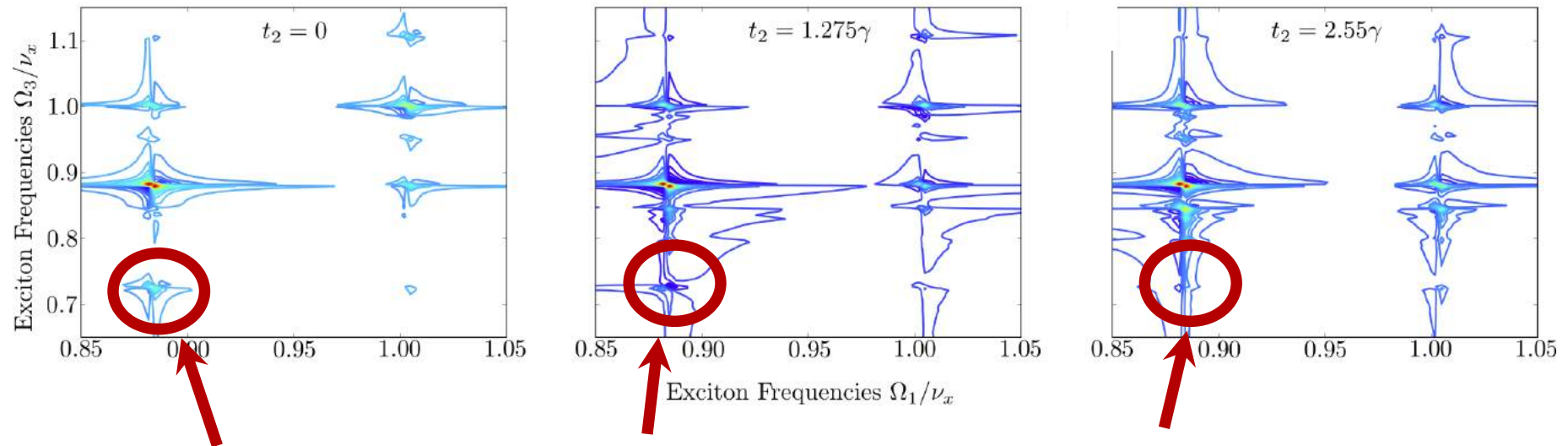
Disappearance of anharmonic resonance between doubly-excited and single-excited state signifies the decay of a phonon into heat bath.

F. Schlawin, M. Gessner, S. Mukamel and A. Buchleitner, Phys. Rev. A 90, 023603 (2014)

Environmental couplings

2D-lineshapes: Identify and quantify different environmental influences
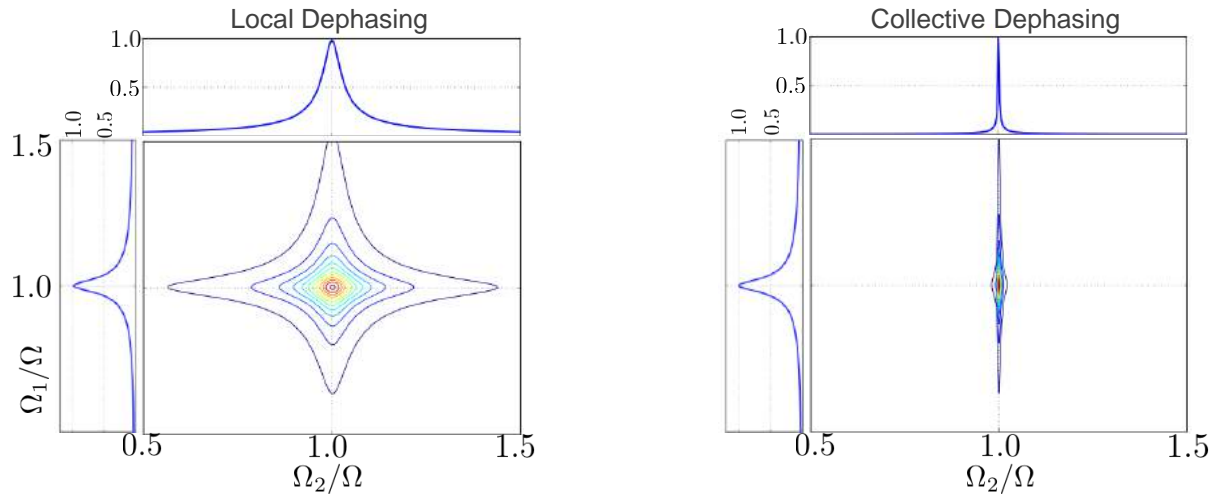
In the case of collective dephasing, the system evolves through a decoherence-free subspace. Hence, the width of the two-dimensional resonance along the corresponding frequency axis vanishes,

M. Gessner, F. Schlawin, H. Häffner, S. Mukamel, and A. Buchleitner, New J. Phys. 16, 092001 (2014)

The Nonlinear Response Function

$$P(t) = Tr[V\rho(t)]$$

$$= P^{(1)}(t) + P^{(2)}(t) + P^{(3)}(t) + \cdots$$

$$P^{(3)}(t) = \int_0^\infty dt_3 \int_0^\infty dt_2 \int_0^\infty dt_1 S^{(3)}(t_3, t_2, t_1)$$

$$\times E(t - t_3) E(t - t_3 - t_2) E(t - t_3 - t_2 - t_1)$$

$$S^{(3)}(t_3, t_2, t_1) = \left(\frac{i}{\hbar}\right)^3 \langle\langle V | \mathscr{G}(t_3) \mathscr{V} \mathscr{G}(t_2) \mathscr{V} \mathscr{G}(t_1) \mathscr{V} | \rho(-\infty)\rangle\rangle$$

t
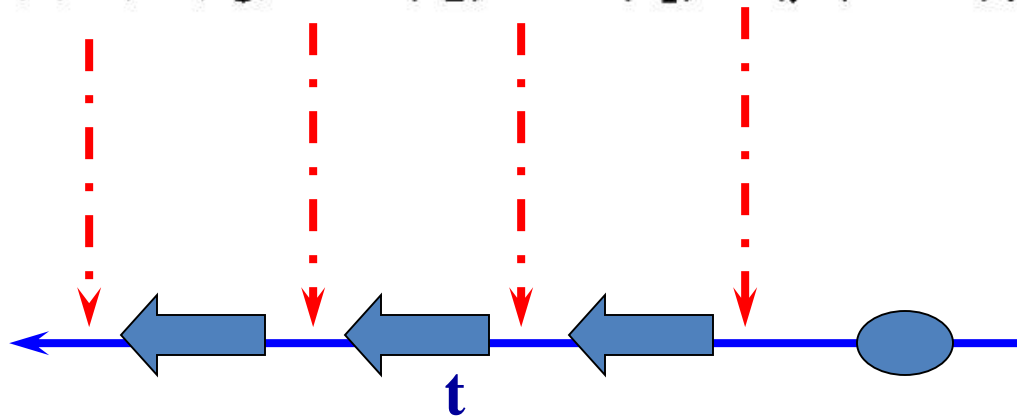
Raman vs. IR Probes: equivalent picture

SRS interaction Hamiltonian:
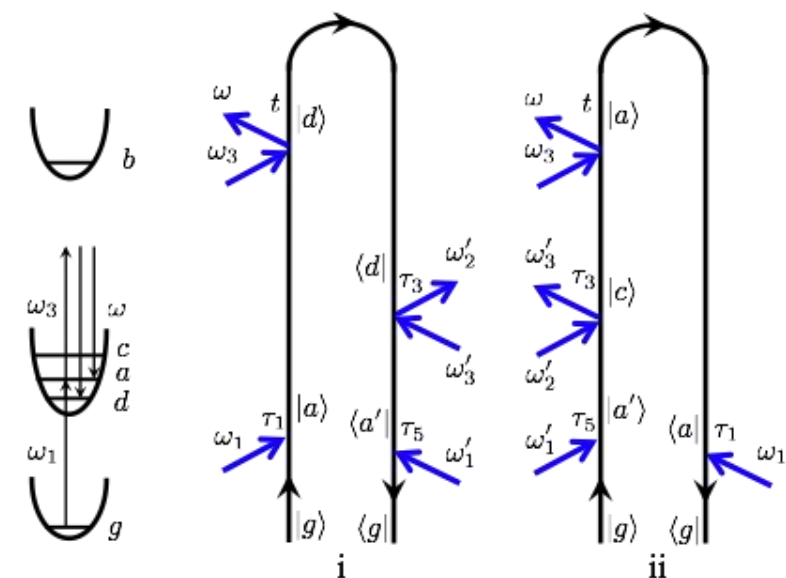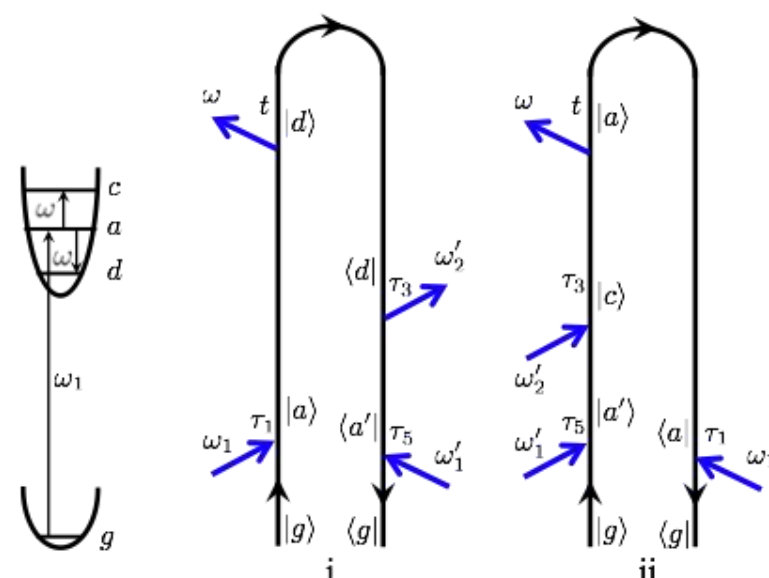
$$H'(t) = \alpha_n \mathcal{E}_2^\dagger(t)\mathcal{E}_3(t) + \mathcal{E}_1^\dagger(t)V_e(t) + H.c.$$

FDIR interaction Hamiltonian:

$$H'(t) = V_N \mathcal{E}_2^\dagger(t) + \mathcal{E}_1^\dagger(t)V_e(t) + H.c.$$

FSRS vs FDIR

$$\alpha_n \to V_n \qquad \omega \to \omega - \omega_3$$

same matter 4-point correlation function:

$$\left\langle V_e G^\dagger(\omega_1) V_n^\dagger G^\dagger(\omega_1 - \omega - \Delta) V_n G(\omega_1 - \Delta) V_e^\dagger \right\rangle$$

K. E. Dorfman, B. P. Fingerhut, S. Mukamel, PCCP 15, 12348 (2013)
B. P. Fingerhut, K. E. Dorfman, S. Mukamel, J. Phys. Chem Lett. 4, 1933, (2013)

W. J. Schreier et. al, Science 315, 625 (2007),
K. Heyne et. al J. Am. Chem. Soc 127, 18100 (2005),
O. Mohammed et. al Science 310, 83 (2005), Angew. Chem. 47, 9044 (2008),
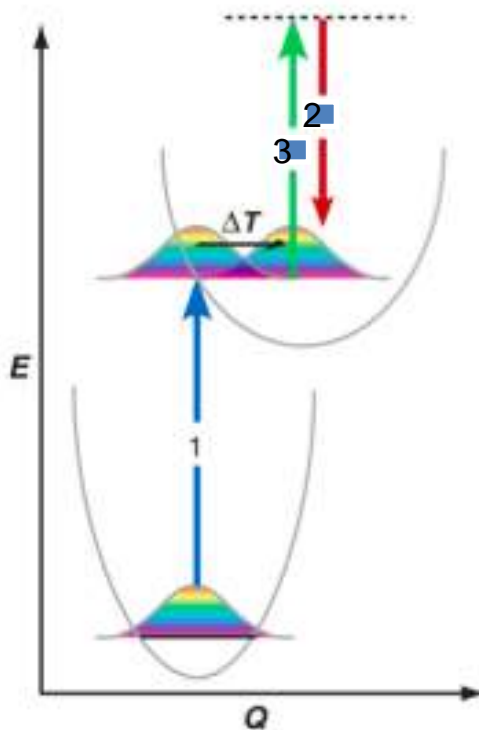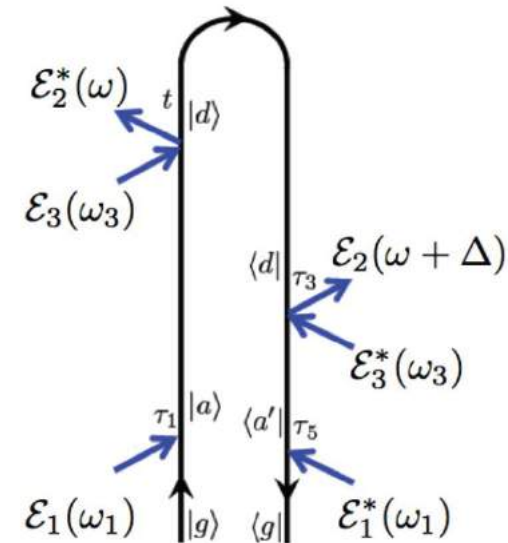J. Phys. Chem. A 113, 5061 (2009).

Time- and Frequency- Resolution in Vibronic Spectroscopy

Δ-Dispersed Signal
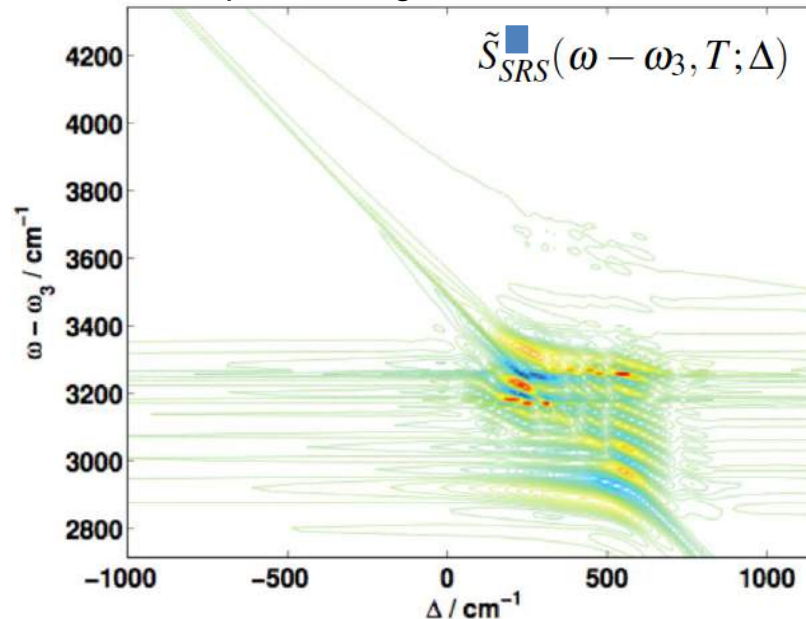
Loop-diagrammatic Ansatz:

$$S_{SRS}(\omega - \omega_3, T) = \mathscr{I} \int_{-\infty}^{\infty} \frac{d\Delta}{2\pi} \mathscr{E}_2^*(\omega) \mathscr{E}_2(\omega + \Delta) \tilde{S}_{SRS}(\omega - \omega_3, T; \Delta)$$

$$\tilde{S}_{SRS}(\omega - \omega_3, T; \Delta) = \frac{2}{\hbar} \int_{-\infty}^{\infty} dt \int_{-\infty}^{t} d\tau_1 \int_{-\infty}^{t} d\tau_3 \int_{-\infty}^{\tau_3} d\tau_5 |\mathscr{E}_3|^2 \mathscr{E}_1^*(\tau_5) \mathscr{E}_1(\tau_1)$$

$$\times \left\langle V_e G^{\dagger}(\tau_3, \tau_5) \alpha_n G^{\dagger}(t, \tau_3) \alpha_n G(t, \tau_1) V_e^{\dagger} \right\rangle e^{i(\omega - \omega_3)(t - \tau_3) - i\Delta(\tau_3 - T)}$$
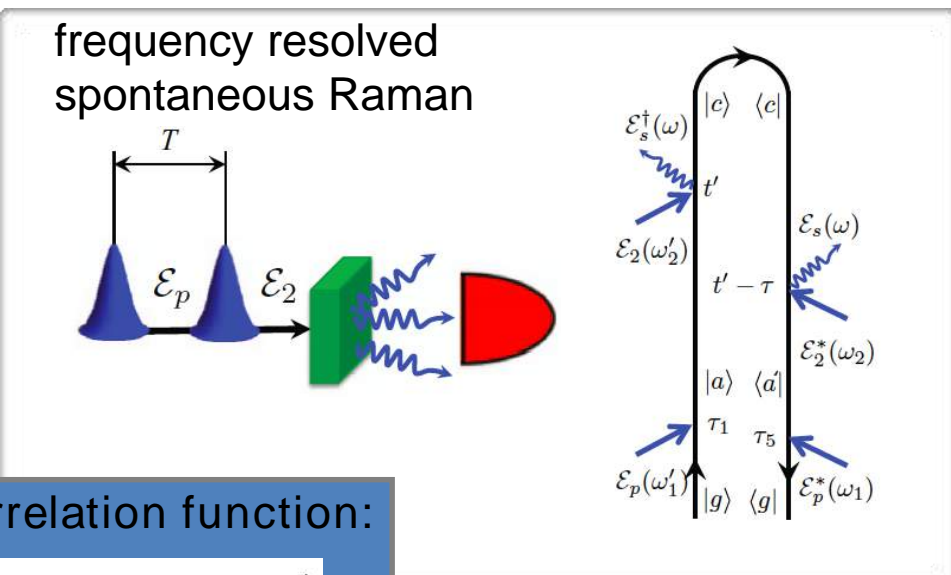
Broadband infrared and Raman probes of excited-state vibrational molecular dynamics;

Simulation protocols based on loop diagrams.

K. E. Dorfman, B. P. Fingerhut, S. Mukamel, Phys. Chem. Chem. Phys. **15**, 12348 (2013).

Off-resonant Raman Probe Techniques

stimulated Raman

frequency resolved spontaneous Raman
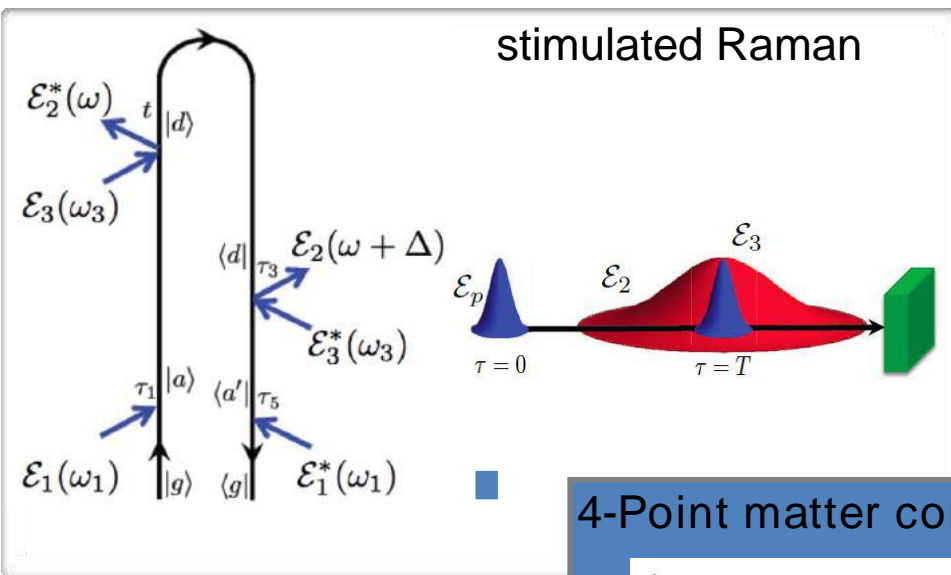
4-Point matter correlation function:

$$\left\langle V_e G^\dagger(\tau_3, \tau_5) \alpha_n G^\dagger(t, \tau_3) \alpha_n G(t, \tau_1) V_e^\dagger \right\rangle$$

time-resolved impulsive stimulated Raman

transient grating impulsive stimulated Raman

K. E. Dorfman, B. P. Fingerhut, S. Mukamel, J. Chem. Phys. 139, 124113 (2013)
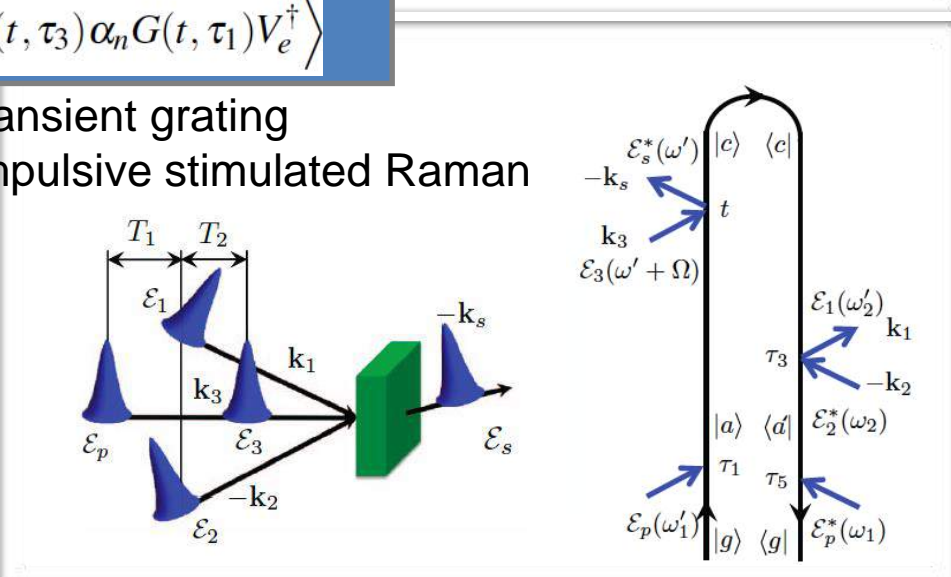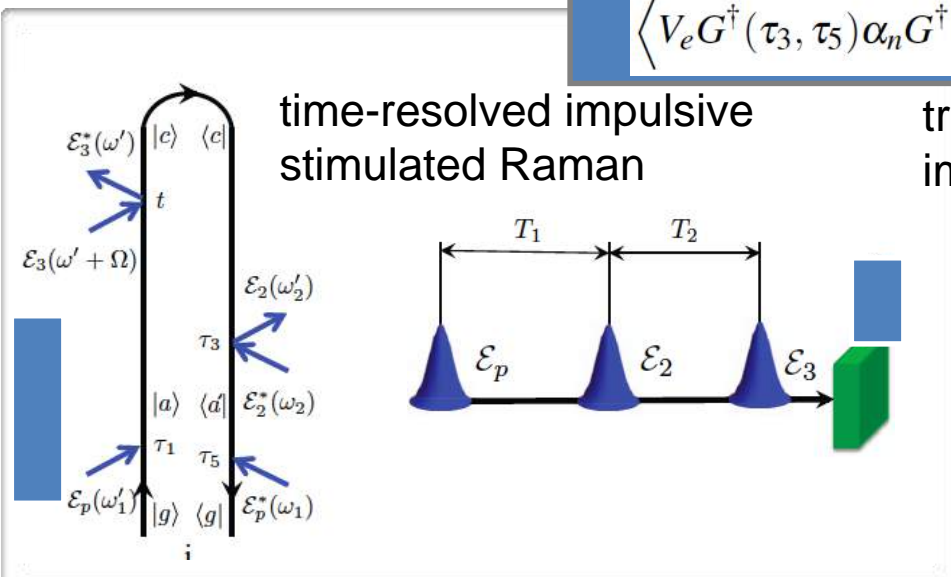
Off-resonant Raman Probe Techniques

Stimulated Raman Signal:
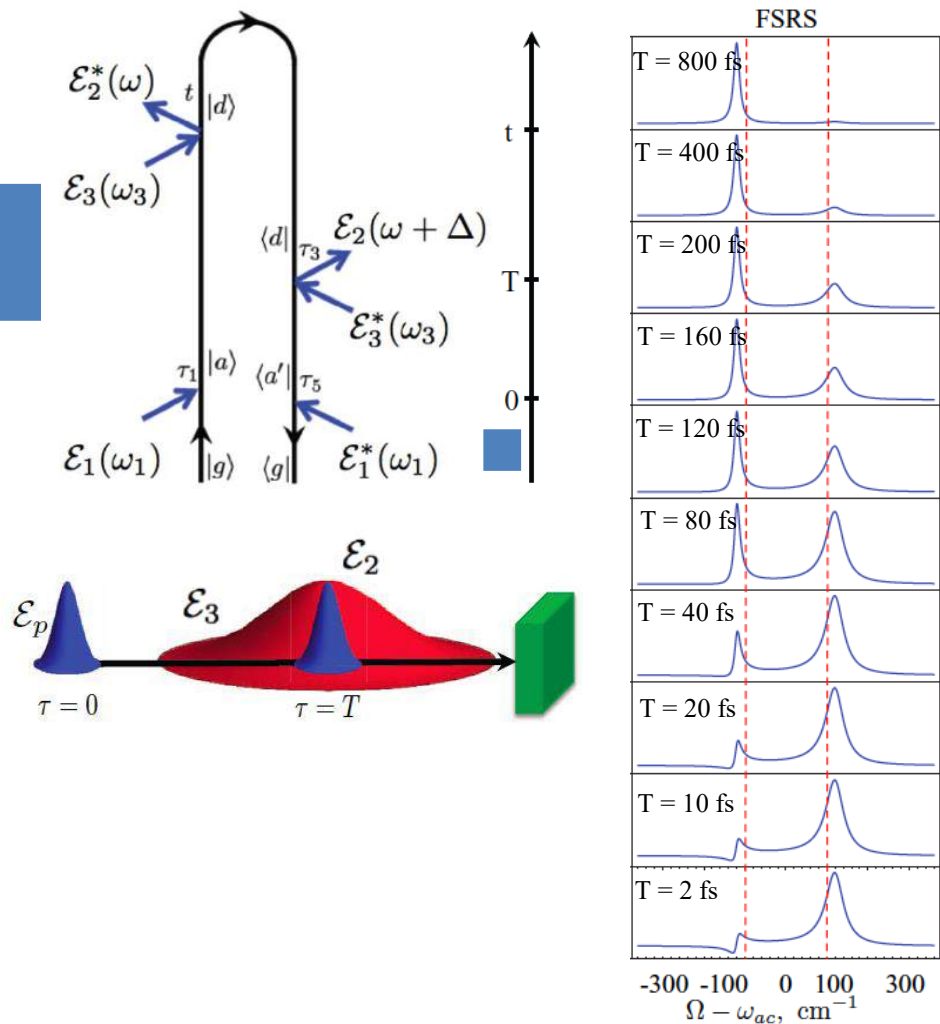
two-state jump model:

$$K_{jump} > \gamma_{ca}$$

• dispersive lineshapes
(broken loop symmetry)

• dynamics broadened transition

K. E. Dorfman, B. P. Fingerhut, S. Mukamel, J. Chem. Phys. 139, 124113 (2013)

Off-resonant Raman Probe Techniques

transient grating impulsive stimulated Raman

Stimulated Raman Signal:

FSRS — TG-ISRS

T = 800 fs
T = 400 fs
T = 200 fs
T = 160 fs
T = 120 fs
T = 80 fs
T = 40 fs
T = 20 fs
T = 10 fs
T = 2 fs

$-300\ -100\quad 0\quad 100\quad 300$
$\Omega - \omega_{ac},\ cm^{-1}$

$-300\ -100\quad 0\quad 100\quad 300$
$\Omega - \omega_{ac},\ cm^{-1}$
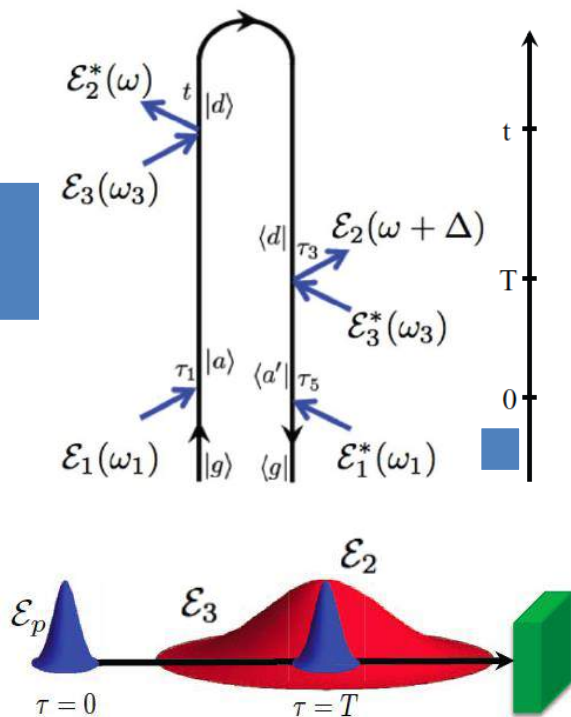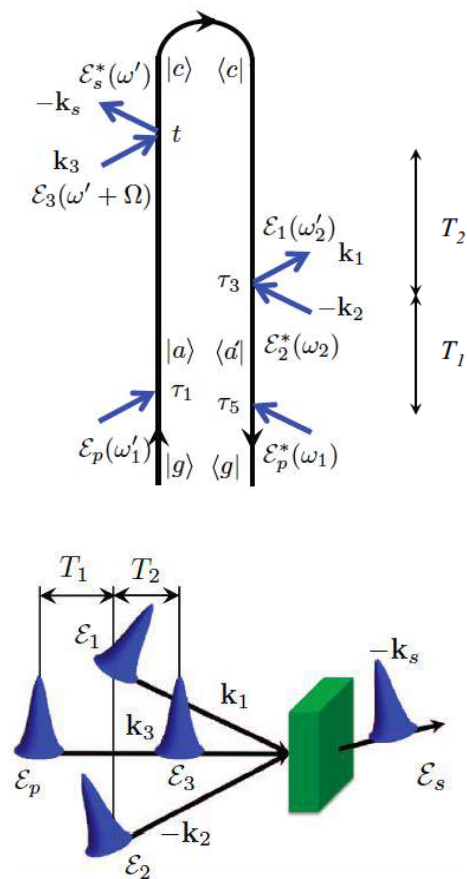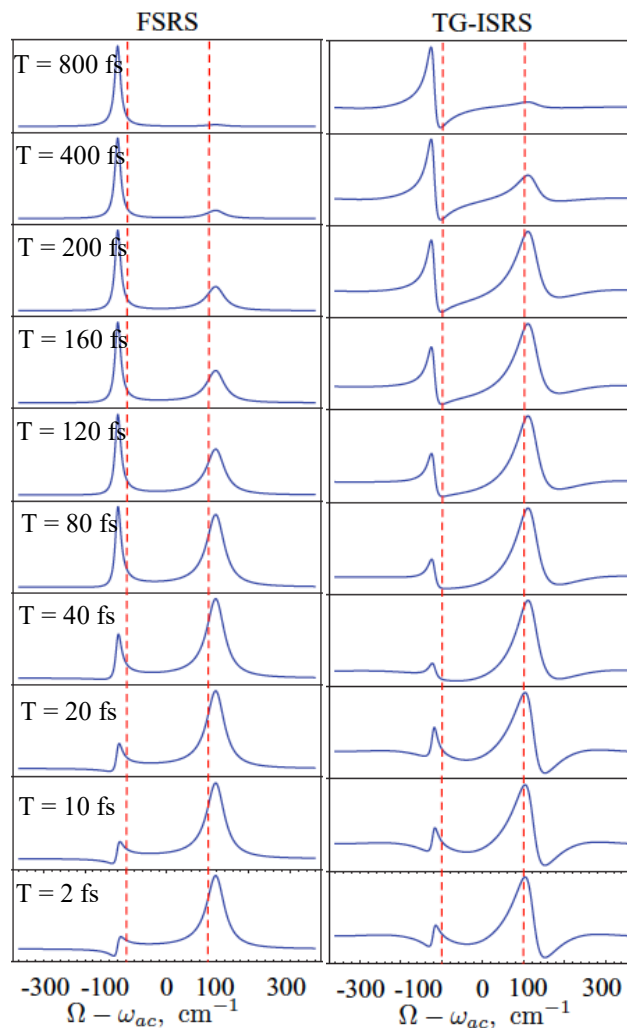
„heterodyne-detected pump-DFWM"

K. E. Dorfman, B. P. Fingerhut, S. Mukamel, J. Chem. Phys. 139, 124113 (2013)

Kraack et al. PCCP 15, 14487 (20

Off-resonant Raman Probe Techniques

probe pulse effects

TG-ISRS

σ = 300 fs

σ = 30 fs

σ = 5 fs

-300 -100 0 100 300

TG-ISRS and FSRS identical for very short pulses

FSRS

TG-ISRS

T = 800 fs
T = 400 fs
T = 200 fs
T = 160 fs
T = 120 fs
T = 80 fs
T = 40 fs
T = 20 fs
T = 10 fs
T = 2 fs

-300 -100 0 100 300
$\Omega - \omega_{ac}$, cm^{-1}

-300 -100 0 100 300
$\Omega - \omega_{ac}$, cm^{-1}

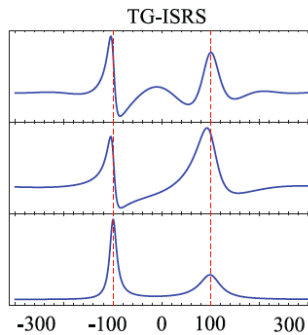$\mathcal{E}_s^*(\omega')$ $|c\rangle$ $\langle c|$

$-\mathbf{k}_s$ t

$\mathbf{k}_3$
$\mathcal{E}_3(\omega'+\Omega)$

$\mathcal{E}_1(\omega_2')$ $\mathbf{k}_1$
τ_3
$-\mathbf{k}_2$

$|a\rangle$ $\langle a|$ $\mathcal{E}_2^*(\omega_2)$
τ_1 τ_5

$\mathcal{E}_p(\omega_1')$ $|g\rangle$ $\langle g|$ $\mathcal{E}_p^*(\omega_1)$

T_2

T_1

T_1 T_2
$\mathcal{E}_1$
$\mathbf{k}_3$
$\mathbf{k}_1$
$-\mathbf{k}_s$
$\mathcal{E}_p$ $\mathcal{E}_3$ $\mathcal{E}_s$
$-\mathbf{k}_2$
$\mathcal{E}_2$

K. E. Dorfman, B. P. Fingerhut, S. Mukamel, J. Chem. Phys. 139, 124113 (2013)
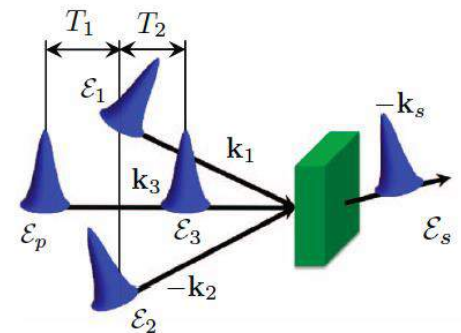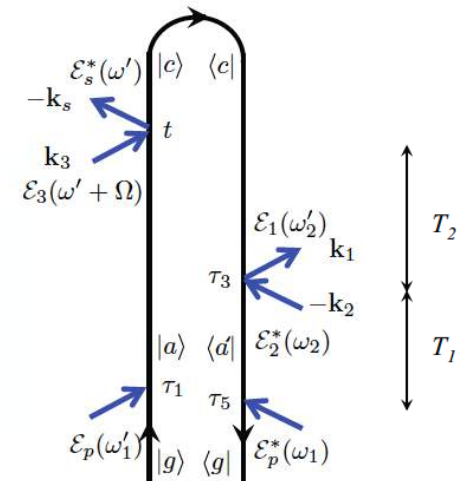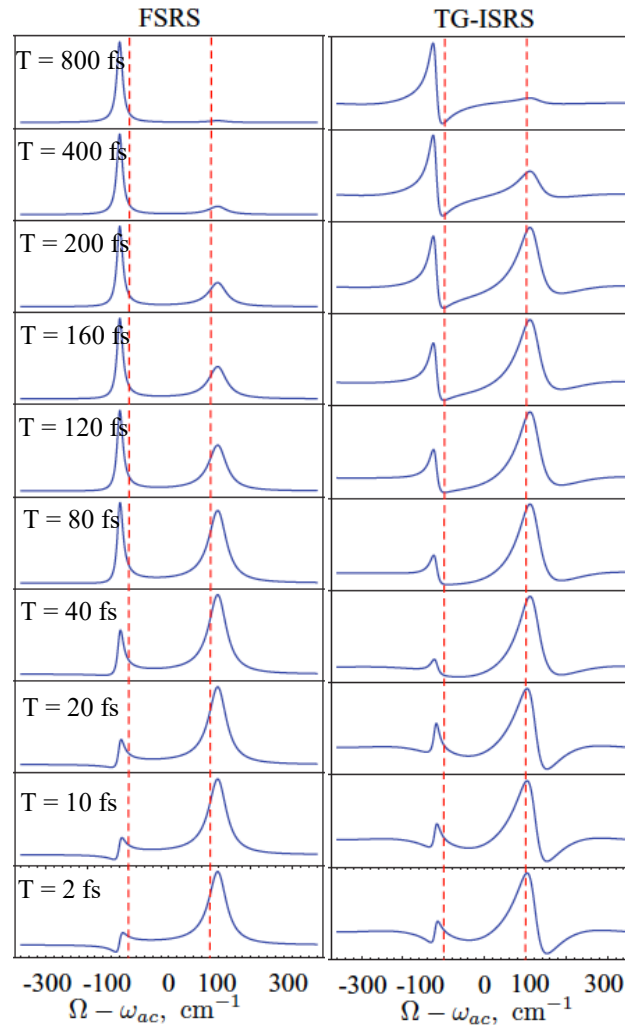
Summary

- **NL spectroscopy**: efficient extraction of specific information by adapted protocols

- applicable in **large systems** where state tomographies fail

- Promising applications:

  - characterization/analysis of **transport** processes
  - measurement of **anharmonicities** of the trap potential
  - detection of couplings to various **environments**

- References:
  New J. Phys. 16, 092001 (2014)
  Phys. Rev. A 90, 023603 (2014)

OCCASIONAL NOTES

Chocolate Consumption, Cognitive Function, and Nobel Laureates
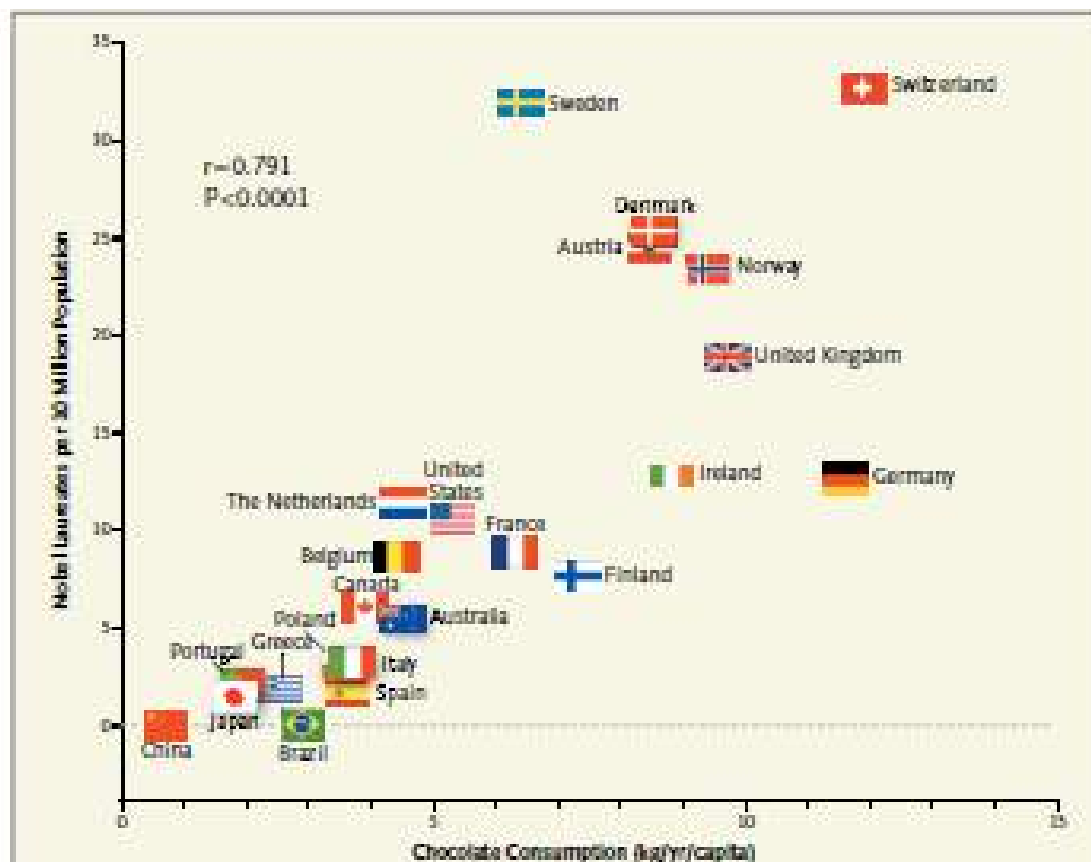
Franz H. Messerli, M.D.

Figure 1. Correlation between Countries' Annual Per Capita Chocolate Consumption and the Number of Nobel Laureates per 10 Million Population.

The principal finding of this study is a surprisingly powerful correlation between chocolate intake per capita and the number of Nobel laureates in various countries. Of course, a correlation between X and Y does not prove causation but indicates that either X influences Y, Y influences X, or X and Y are influenced by a common underlying mechanism. However, since chocolate consumption has been documented to improve cognitive function, it seems most likely that in a dose-dependent way, chocolate intake provides the abundant fertile ground needed for the sprouting of Nobel laureates. Obviously, these findings are hypothesis-generating only and will have to be tested in a prospective, randomized trial.

high temporal and spectral resolution?

LETTERS

Mapping GFP structure evolution during proton transfer with femtosecond Raman spectroscopy

Nature **462**, 200 (2009)

$\Delta\omega\Delta t \approx 500$ *fs cm^{-1}*

vs.

$\Delta\omega\Delta t \approx 5000$ *fs cm^{-1}*
(Fourier uncertainty)
~~*Heisenberg*~~

CIRCUMVENTING HEISENBERG

One of the numerous critical advancements in the field of ultrafast spectroscopy over the past two decades involves the apparent circumvention of the uncertainty principle through femtosecond dynamic absorption spectroscopy (14). In this approach to pump-probe transient absorption spectroscopy, the broadband femtosecond probe pulse is dispersed onto a multichannel detector, resulting in measurement of the full pulse spectrum rather than just its intensity. The time resolution of this technique is only fundamentally limited by the durations of the two pulses initiating the macroscopic polarization in the sample that generates the detected signal. The frequency resolution, conversely, is determined by the lifetime of the induced polarization rather than the pulse duration because the detection step is not time resolved. The simultaneous high time and frequency resolution can then be used to observe electronic signatures of ultrafast chemical reaction dynamics with energy resolution much finer than the bandwidth of the femtosecond pulses used in the experiment.
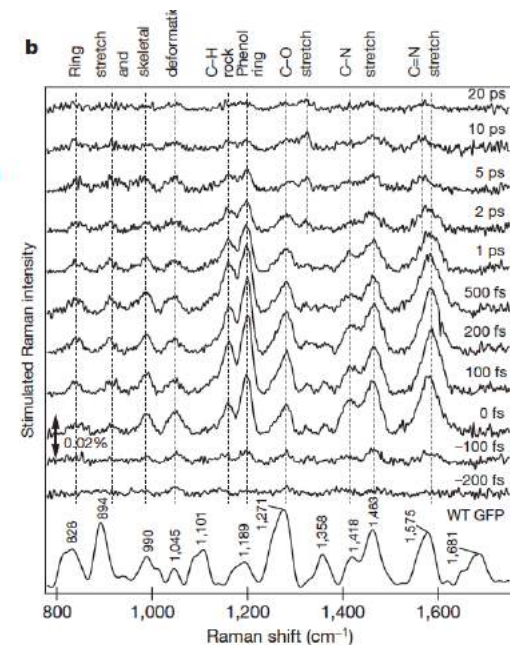
Annu. Rev. Phys. Chem. **58,** 461–88 (2007)

Semi-Classical Simulation Protocol for UV-pump - SRS Probe Signals
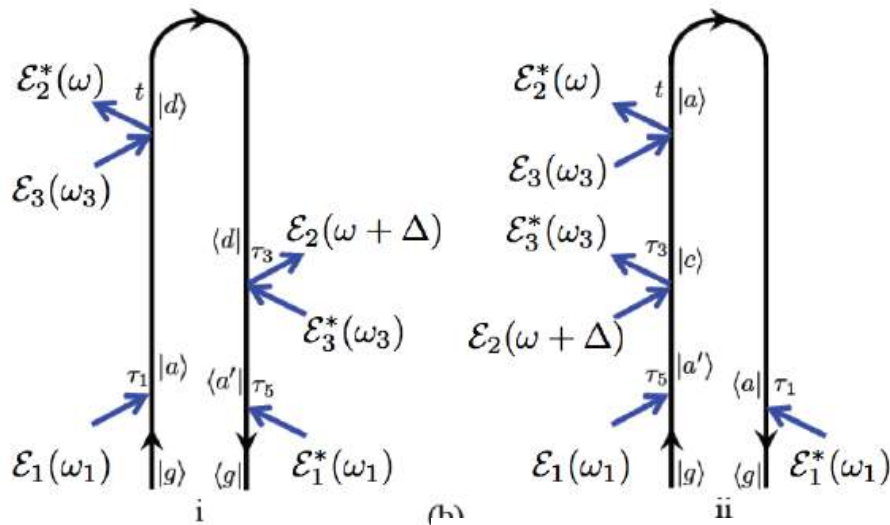
Goals:
- intuitive and simplified description
- restricted to only a few quantum varibles
- suitable for complex non-adiabatic molecular dynamics

→ Recast full-quantum four point correlation function

trajectories of instantaneous frequencies:
→ signal depends on entire pathway in excited state
→ no snapshot of dynamics

$$\tilde{S}_{SRS}^{(i)}(\omega - \omega_3, T; \Delta) = \frac{2}{\hbar} \int_{-\infty}^{\infty} dt \int_{-\infty}^{t} d\tau_1 \int_{-\infty}^{t} d\tau_3 \int_{-\infty}^{\tau_3} d\tau_5 |\mathscr{E}_3|^2 \mathscr{E}_1^*(\tau_5) \mathscr{E}_1(\tau_1)$$

$$\times \left\langle V_e G^\dagger(\tau_3, \tau_5) \alpha_n G^\dagger(t, \tau_3) \alpha_n G(t, \tau_1) V_e^\dagger \right\rangle e^{i(\omega - \omega_3)(t - \tau_3) - i\Delta(\tau_3 - T)}$$

in the form

$$\tilde{S}_{SRS}(\omega - \omega_3, T; \Delta) = -\frac{2i}{\hbar^4} \int_{-\infty}^{\infty} dt \int_{-\infty}^{t} d\tau_3 |\mathscr{E}_1|^2 |\mathscr{E}_3|^2 e^{i(\omega - \omega_3)(t - \tau_3)} e^{-i\Delta(\tau_3 - T)}$$

$$\times \sum_a |\mu_{ag}|^2 e^{-\gamma_a(t + \tau_3)} \left[\sum_c \alpha_{ac}^2 e^{-i\int_{\tau_3}^{t} \omega_{ac}(t')dt'} + \sum_d \alpha_{ad}^2 e^{i\int_{\tau_3}^{t} \omega_{ad}(t')dt'} \right]$$

i

(b)

ii

$\mathscr{E}_2^*(\omega)$ t $|d\rangle$

$\mathscr{E}_3(\omega_3)$

$\langle d| \tau_3$ $\mathscr{E}_2(\omega + \Delta)$

$\mathscr{E}_3^*(\omega_3)$

$\tau_1 |a\rangle$ $\langle a'| \tau_5$

$\mathscr{E}_1(\omega_1)$ $|g\rangle$ $\langle g|$ $\mathscr{E}_1^*(\omega_1)$

$\mathscr{E}_2^*(\omega)$ t $|a\rangle$

$\mathscr{E}_3(\omega_3)$

$\mathscr{E}_3^*(\omega_3)$ $\tau_3 |c\rangle$

$\mathscr{E}_2(\omega + \Delta)$

$\tau_5 |a'\rangle$ $\langle a| \tau_1$

$\mathscr{E}_1(\omega_1)$ $|g\rangle$ $\langle g|$ $\mathscr{E}_1^*(\omega_1)$

t

T

0

Classical Treatment of Isomerization

• At $\tau = 0$, the (slow) reaction is initiated, and the vibrational frequency decays exponentially from an initial value to another, on a timescale t'.

$$\omega_{ca}(t) = \begin{cases} \omega_{ca}^{\text{final}} + e^{-t/t'}(\omega_{ca}^{\text{initial}} - \omega_{ca}^{\text{final}}) & : t \geq 0 \\ \omega_{ca}^{\text{initial}} & : t < 0 \end{cases}$$
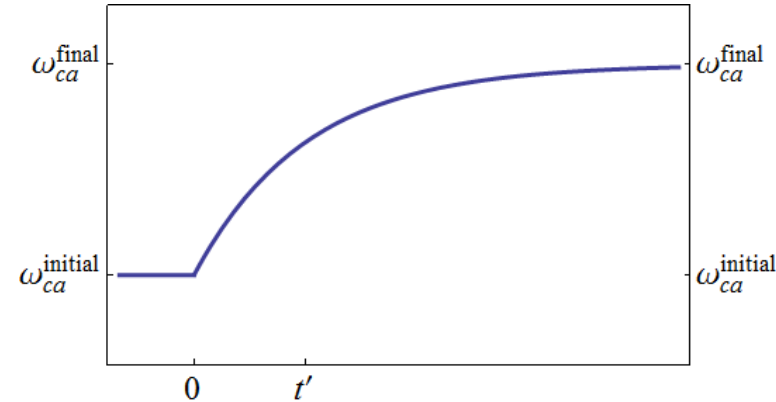
• At $\tau = T$, the polarization is created which decays on a timescale γ_{ca}^{-1}.

$$P^{(5)}(t) = i\theta(t-T)\mathcal{E}_2^2\mathcal{E}_3 \frac{|V_{ab}|^2|V_{cb}|^2}{(\omega_2-\omega_{ab})^2} \exp\left(-i\omega_2(t-T) + i\int_T^t \omega_{ca}(\tau)\,d\tau - \gamma_{ca}(t-T)\right)$$

The detected polarization is not detected simply at $\Omega = \omega_2 - \omega_{ca}(T)$, but depends on the entire frequency trajectory from $\tau = T$ until the polarization decays to zero.

Spectral and Temporal Resolution Revisited

The degree to which the signal detected with a given delay time T gives the vibrational frequency $\omega_{ca}(T)$ depends on the size of t' compared with γ_{ca}^{-1}.

$$t' \gg \gamma_{ca}^{-1}$$

Slow spectral evolution compared with dephasing
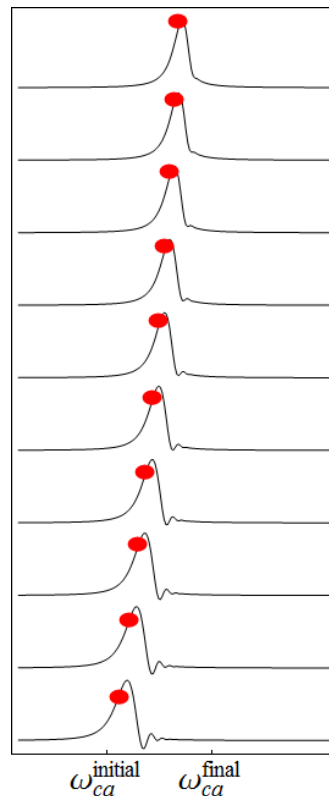
Spectra taken with successively larger values of T

$$t' < \gamma_{ca}^{-1}$$

Spectral evolution faster than dephasing

$\omega_{ca}^{\text{initial}}$ $\omega_{ca}^{\text{final}}$

$\omega_{ca}^{\text{initial}}$ $\omega_{ca}^{\text{final}}$
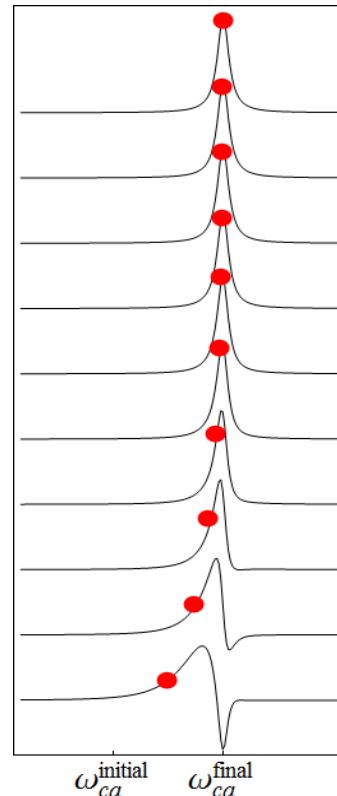
model:
stretched exponential
(non-Gaussian distribution)

peak position:
preceedes time evolution

integrated peak area:
does **not** recover actual time
evolution

dispersive line-shape
(line-width reflects slower
dynamics)

Matter correlations induced by coupling to a light field
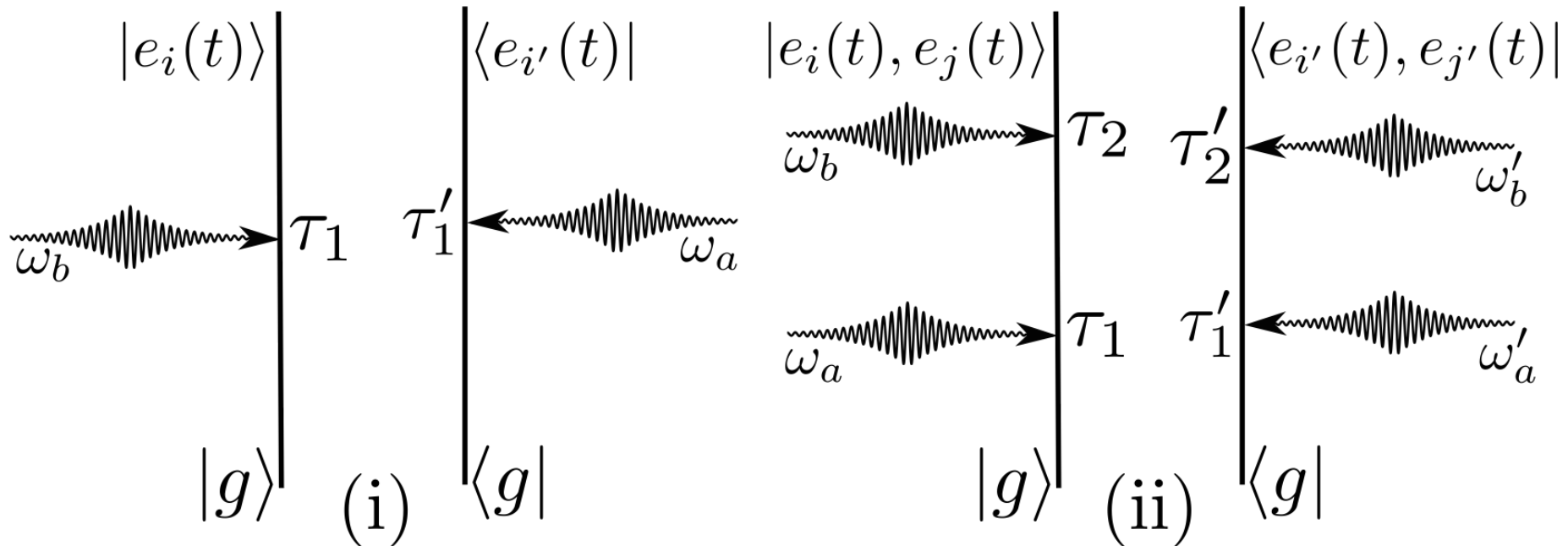
$$\varrho(t)$$

$$\omega_i$$
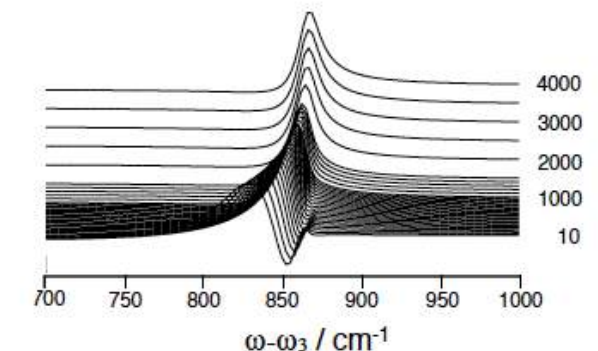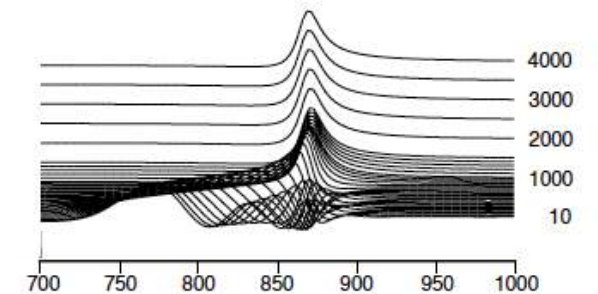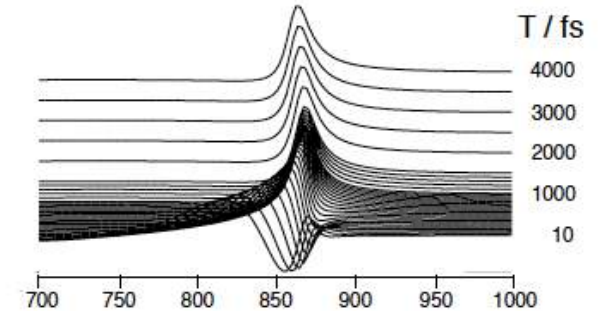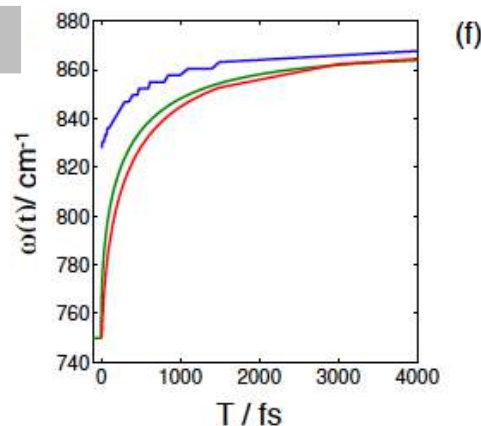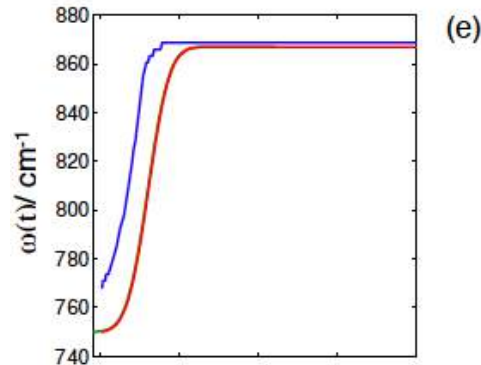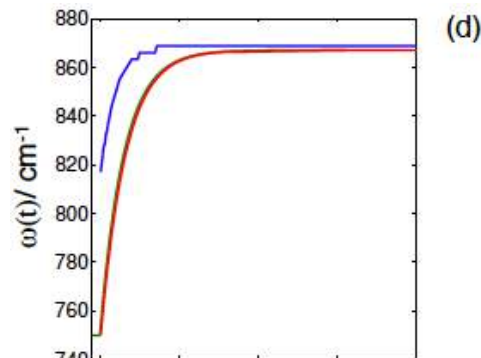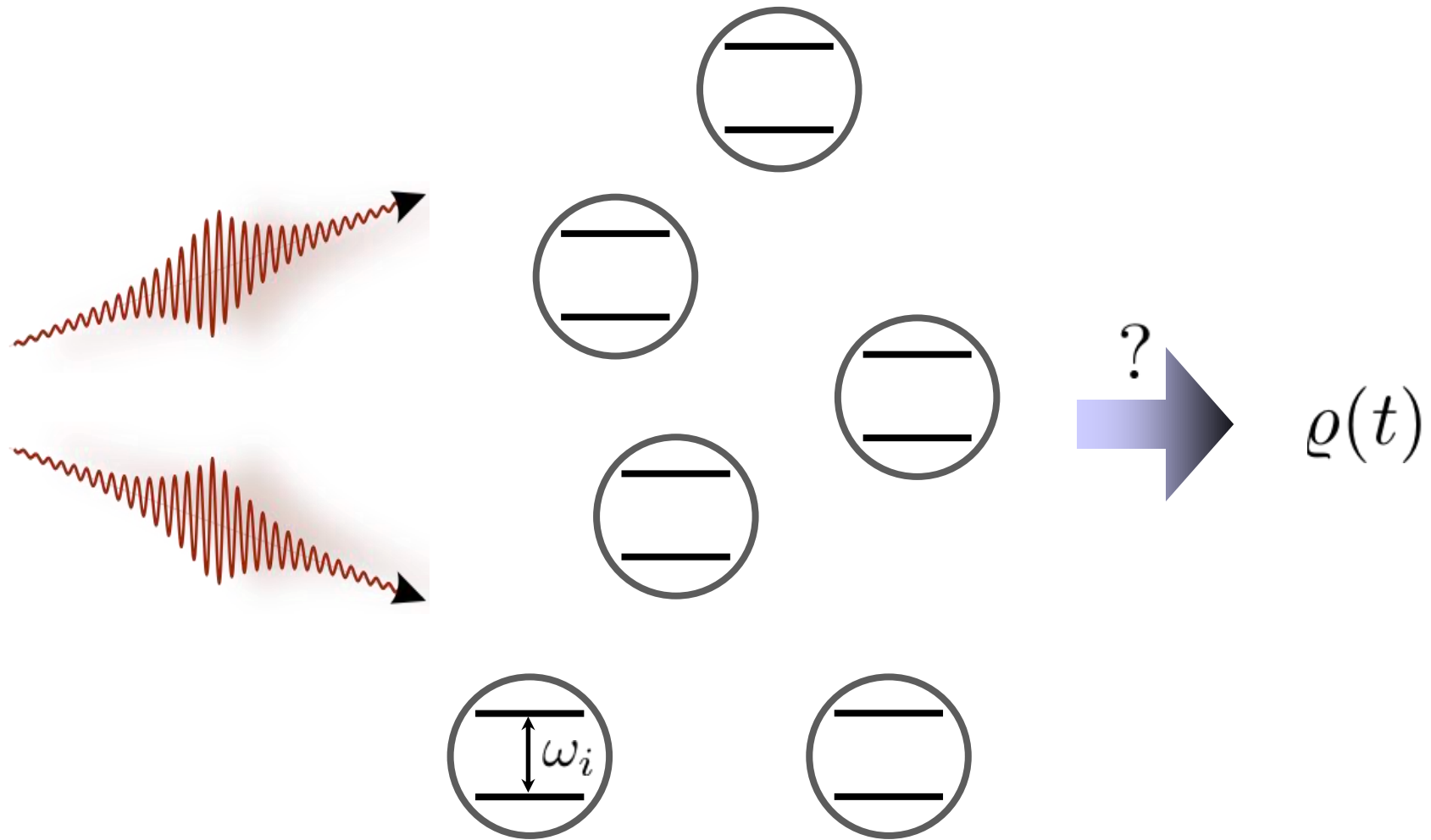
We consider an ensemble of two-level atoms interacting with arbitrary light fields.

Matter correlations induced by coupling to a light field

$$\varrho(t) = \mathcal{T} \exp\left[-\frac{i}{\hbar} \int^t d\tau\, H_{\text{int},-}(\tau)\right] |g\rangle\langle g| \otimes \varrho_{\text{field}}$$
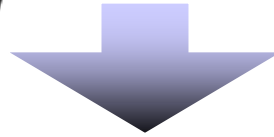

Single- and two-exciton states are given by the two diagrams.

Matter correlations induced by coupling to a light field

$$\varrho(t) = \mathcal{T} \exp\left[-\frac{i}{\hbar} \int^t d\tau \, H_{\text{int},-}(\tau) \right] |g\rangle\langle g| \otimes \varrho_{\text{field}}$$

$|e_i(t)\rangle$ $\langle e_{i'}(t)|$ $|e_i(t), e_j(t)\rangle$ $\langle e_{i'}(t), e_{j'}(t)|$

ω_b τ_1 τ_1' ω_a

ω_b τ_2 τ_2' ω_b'

ω_a τ_1 τ_1' ω_a'

$|g\rangle$ (i) $\langle g|$ $|g\rangle$ (ii) $\langle g|$
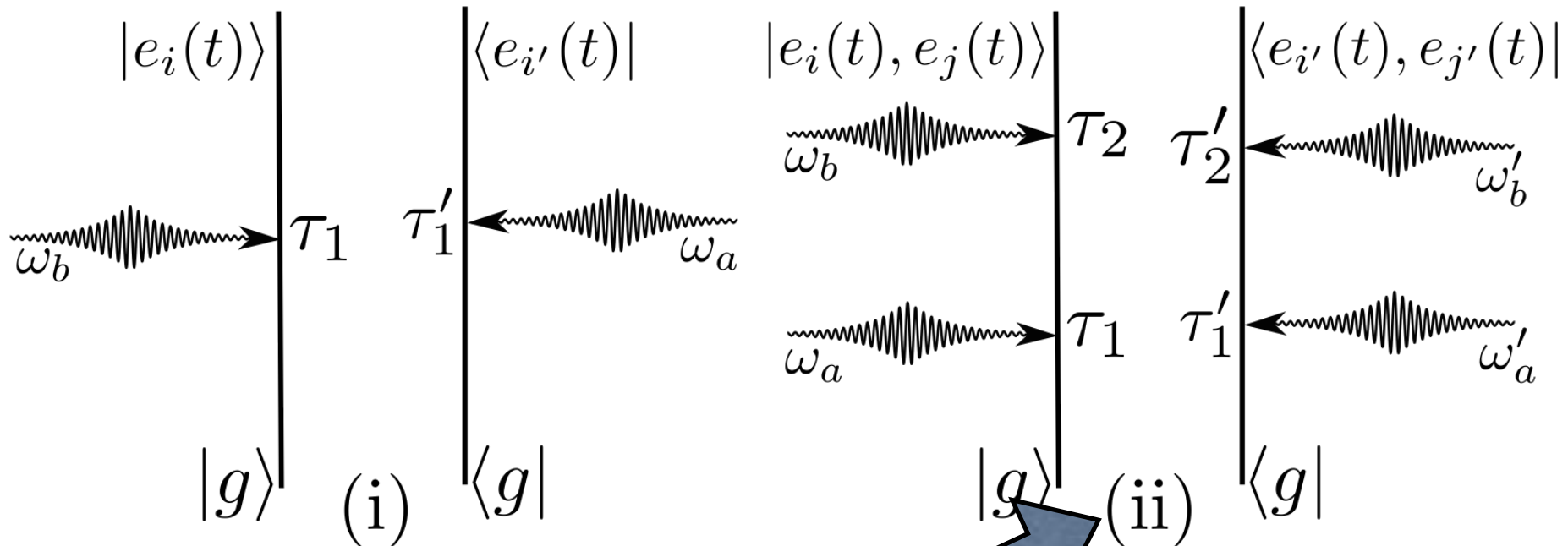
Doubly excited states allow for the discussion of exciton entanglement.

Matter correlations induced by coupling to a light field

The density matrix elements for a single and double-excited states are given by

$$\varrho_{e_i e_{i'}}(t) = \left(-\frac{i}{\hbar}\right)^2 \mu_{g e_{i'}} \mu_{g e_i} e^{i(\omega_{e_{i'} g} - \omega_{e_i g})t}$$

$$\times \left\langle E^{\dagger}(\omega_{e_{i'} g}) E(\omega_{e_i g}) \right\rangle$$

$$\varrho_{e_i e_j, e_{i'} e_{j'}}(t) = \left(-\frac{i}{\hbar}\right)^4 \mu_{g e_{i'}} \mu_{g e_{j'}} \mu_{g e_i} \mu_{g e_j}$$

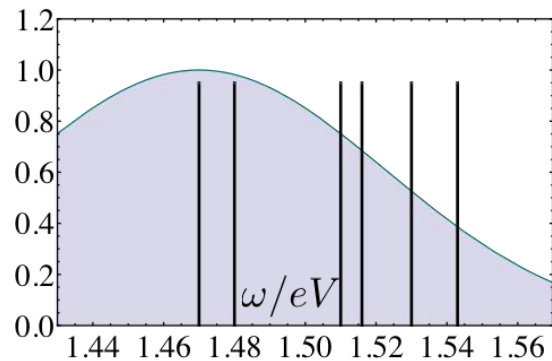$$\times e^{-i(\omega_{e_i g} + \omega_{e_j g} - \omega_{e_{i'} g} - \omega_{e_{j'} g})t}$$

$$\times \left\langle E^{\dagger}(\omega_{e_{i'} g}) E^{\dagger}(\omega_{e_{j'} g}) E(\omega_{e_i g}) E(\omega_{e_j g}) \right\rangle$$
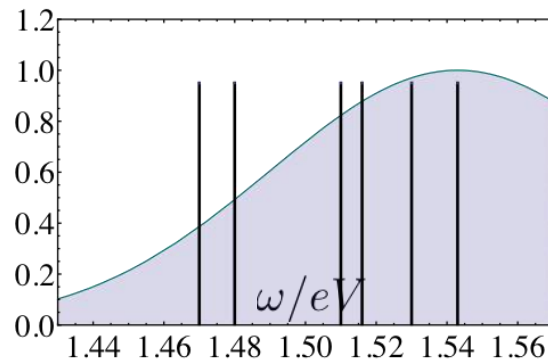
Matter correlations induced by coupling to a light field

The density matrix elements for a single and double-excited states are given by

$$\varrho_{e_i e_{i'}}(t) = \left(-\frac{i}{\hbar}\right)^2 \mu_{g e_{i'}} \mu_{g e_i} e^{i(\omega_{e_{i'} g} - \omega_{e_i g})t}$$

$$\times \left\langle E^\dagger(\omega_{e_{i'} g}) E(\omega_{e_i g}) \right\rangle$$

2-pt correlation function

$$\varrho_{e_i e_j, e_{i'} e_{j'}}(t) = \left(-\frac{i}{\hbar}\right)^4 \mu_{g e_{i'}} \mu_{g e_{j'}} \mu_{g e_i} \mu_{g e_j}$$

$$\times e^{-i(\omega_{e_i g} + \omega_{e_j g} - \omega_{e_{i'} g} - \omega_{e_{j'} g})t}$$

$$\times \left\langle E^\dagger(\omega_{e_{i'} g}) E^\dagger(\omega_{e_{j'} g}) E(\omega_{e_i g}) E(\omega_{e_j g}) \right\rangle$$

4-pt correlation function
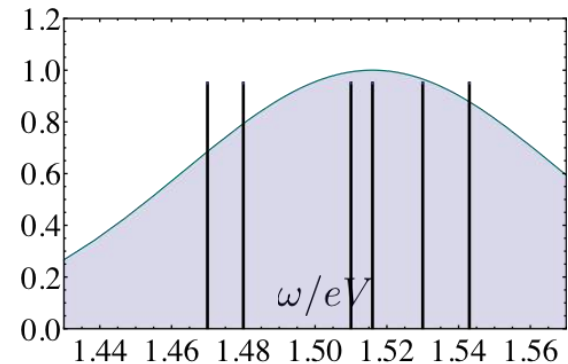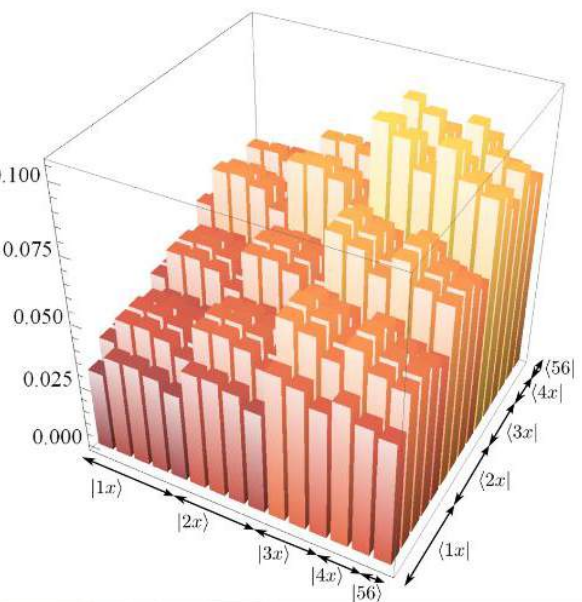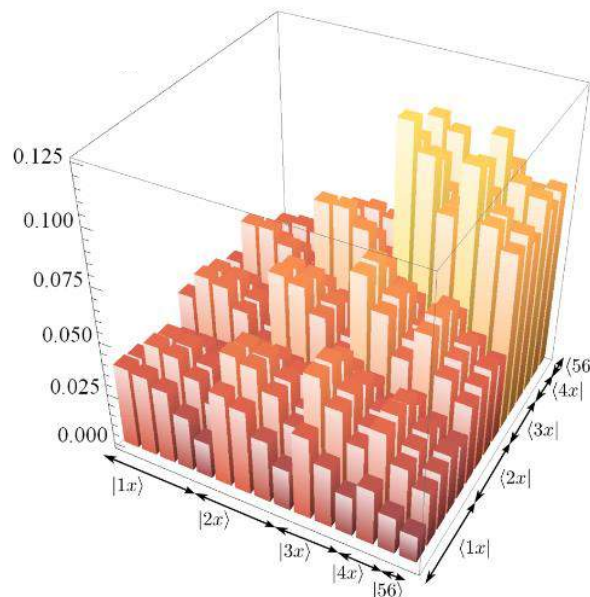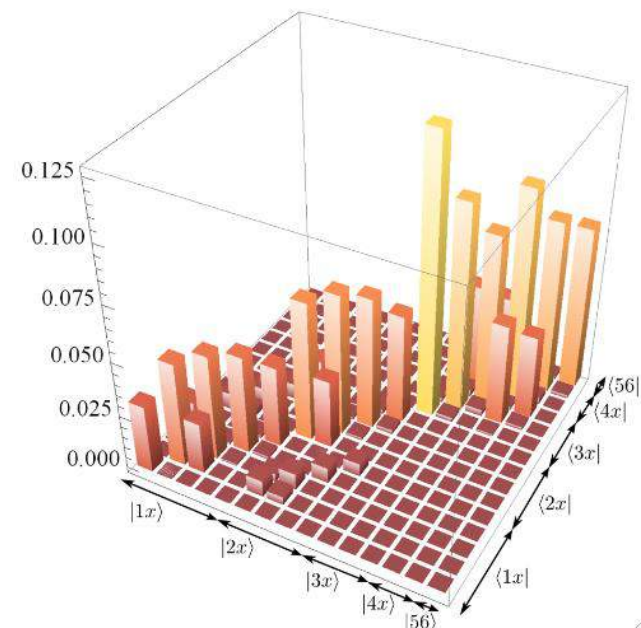
$\omega_0 = 1.4 \ eV$ $\omega_0 = 1.516 \ eV$ $\omega_0 = 1.543 \ eV$
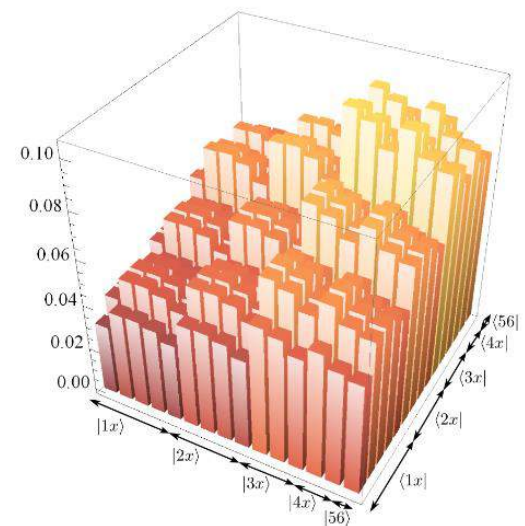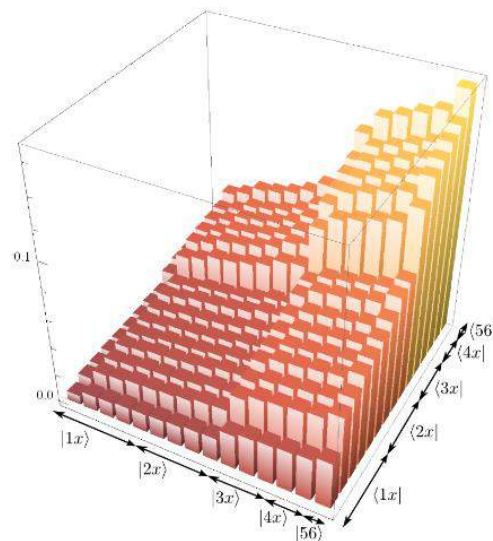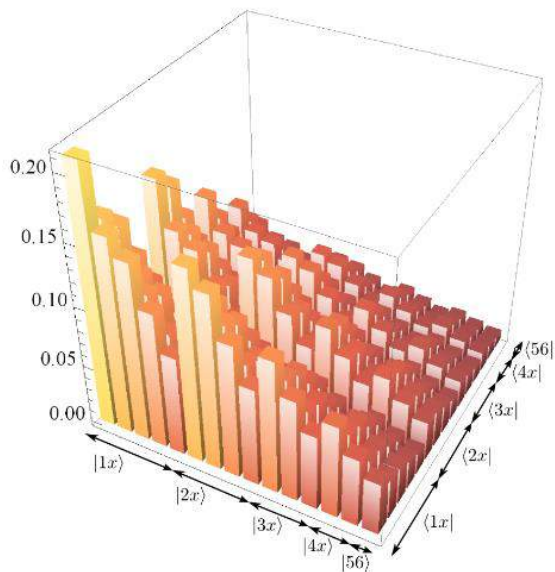
$$A(\omega) \propto \exp\left[-(\omega - \omega_0)^2/2\sigma^2\right]$$
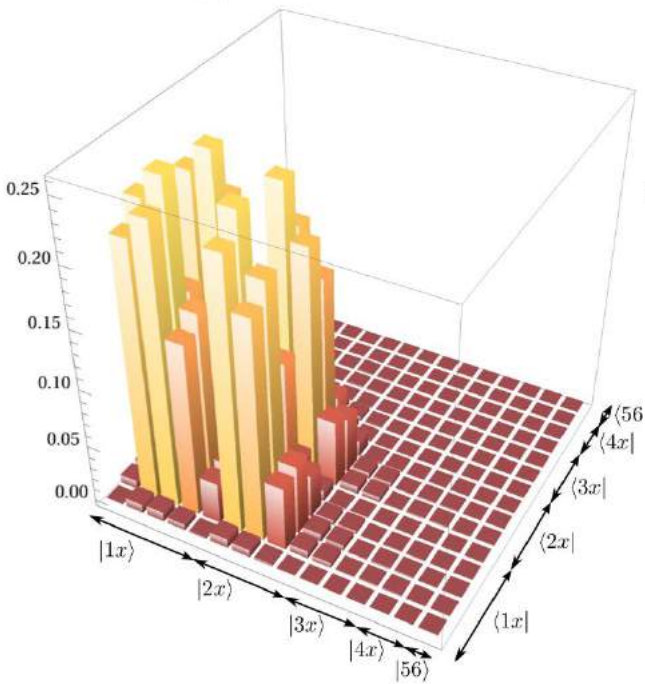
Matter correlations - Gaussian stochastic light

$$\langle E^\dagger(\omega)E(\omega')\rangle = F(\omega)F^*(\omega')C(\omega - \omega')$$

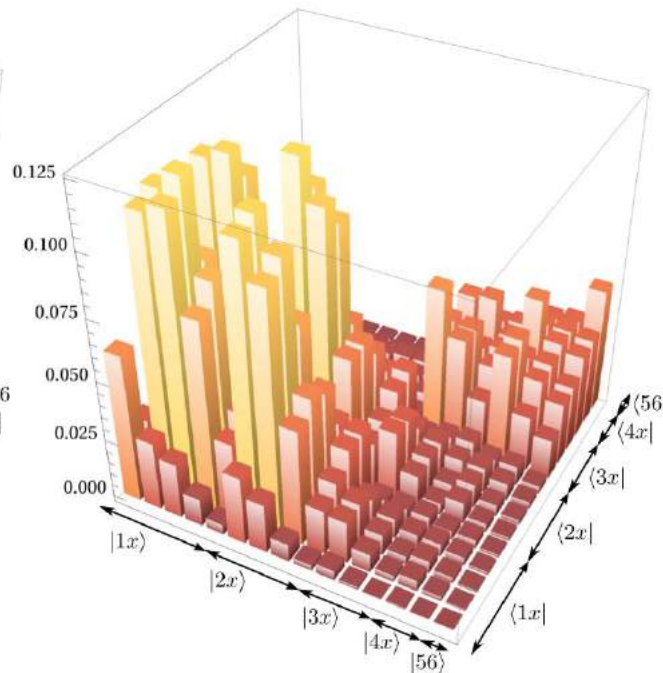$$C(\omega - \omega') = \exp\left[-(\omega - \omega')^2/(2\sigma^2)\right]$$

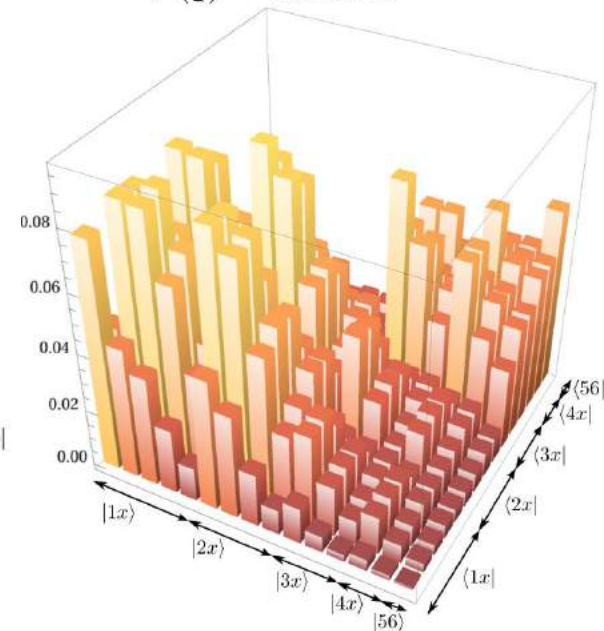# Matter correlations - Squeezed states

$\mathcal{P}(\varrho) = 0.99863$

$\mathcal{P}(\varrho) = 0.383726$

$\mathcal{P}(\varrho) = 0.383955$

Low intensity -the doubly-excited state is almost pure - signature of a dominating two-photon contribution.

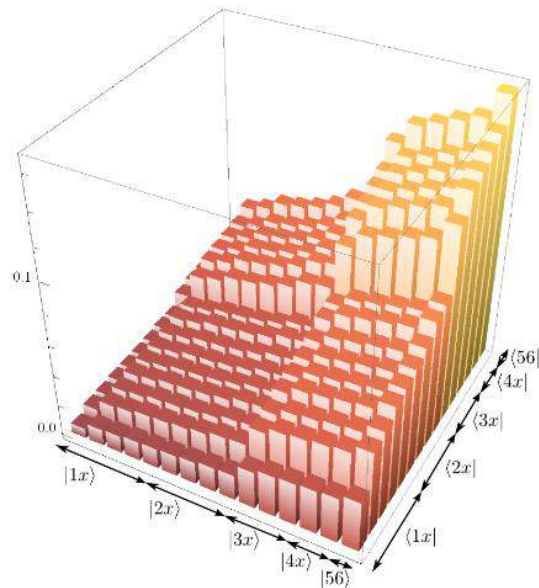As the pump intensity gets increased the broad bandwidth of each beam starts to affect the signal,

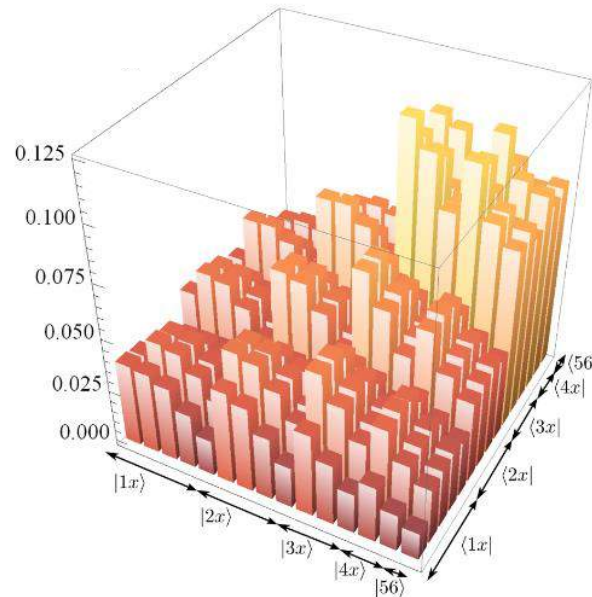As the pump intensity gets increased and the purity of the state decreases.

Matter correlations - comparison

Laser light
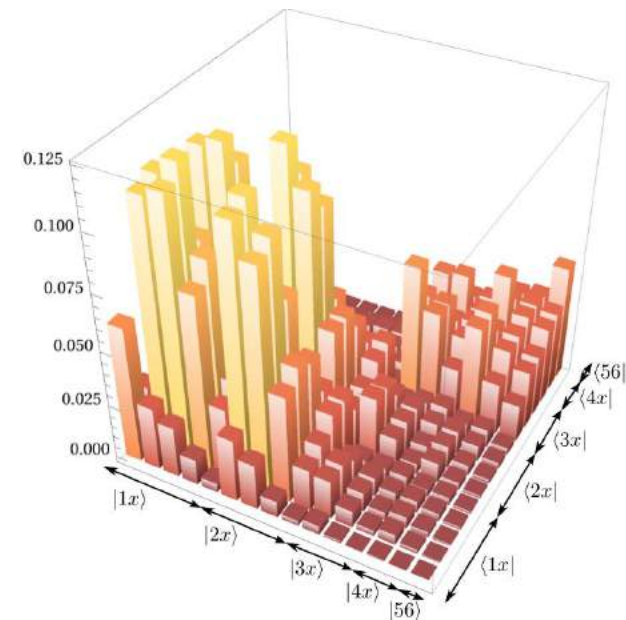

Gaussian stochastic light

Squeezed light

The exciton probability of any double excited state can be traced directly to the overlap of the power spectrum of the pulse; no correlations can be seen $g^{(2)}(0)=1$

For strong stochasticity The off-diagonal elements Are suppressed, only Populations survive, $g^{(2)}(0)=2$

The dominant contribution is coming from the entangled Fock state with autocorrelation contributions due to broad bandwidth of each beam.

Summary

- Two-photon states create entangled, pure states, whereas classical coherent light produces product states, and stochastic light yields incoherent mixtures.

- For a classical light, the interaction with matter does not affect the state of light which thus cannot induce nonclassical correlations in the matter

- The $g^{(2)}$ function of the incoming light fields can serve as an indicator of the ability of the light to induce correlations between the atoms. The differences between single- and two-photon coincidence measurements result from differences between the two-point and the four-point correlation function of the light.

At higher pump intensities, the four-point correlation function of the field shows additional autocorrelation terms:

$$\left\langle E^\dagger(\omega_a') E^\dagger(\omega_b') E(\omega_b) E(\omega_a) \right\rangle$$

$$= \left\langle E^\dagger(\omega_a') E^\dagger(\omega_b') \right\rangle \left\langle E(\omega_a) E(\omega_b) \right\rangle$$

"Coherent contribution" of photon pairs

$$+ \left\langle E^\dagger(\omega_a') E(\omega_b) \right\rangle \left\langle E^\dagger(\omega_b') E(\omega_a) \right\rangle$$
$$+ \left\langle E^\dagger(\omega_a') E(\omega_a) \right\rangle \left\langle E^\dagger(\omega_b') E(\omega_b) \right\rangle$$

Autocorrelation contribution of individual beams; "incoherent contribution"

A. Christ, B. Brecht, W. Maurer and C. Silberhorn (2011)

To describe this, we need to solve the evolution of the electric fields in the Heisenberg picture.
The interaction Hamiltonian in the nonlinear crystal is given by

$$H_{int} = \int d\omega_a \int d\omega_b \Phi(\omega_a, \omega_b) a_1^\dagger(\omega_a) a_2^\dagger(\omega_b) + h.c.$$

$$\Phi(\omega_a, \omega_b) = \alpha A_p(\omega_a + \omega_b) sin\left(\frac{\Delta k(\omega_a, \omega_b)L}{2}\right)$$

A. Christ, B. Brecht, W. Maurer and C. Silberhorn (2011)

Intensity crossover

To describe this, we need to solve the evolution of the electric fields in the Heisenberg picture.
The interaction Hamiltonian in the nonlinear crystal is given by

$$H_{int} = \int d\omega_a \int d\omega_b \Phi(\omega_a, \omega_b) a_1^\dagger(\omega_a) a_2^\dagger(\omega_b) + h.c.$$

$$\Phi(\omega_a, \omega_b) = \alpha A_p(\omega_a + \omega_b) sin\left(\frac{\Delta k(\omega_a, \omega_b) L}{2}\right)$$

proportional to the
pump amplitude

A. Christ, B. Brecht, W. Maurer and C. Silberhorn (2011)

Intensity crossover

Introducing the singular-value decomposition,

$$-\frac{i}{\hbar}\Phi(\omega_a,\omega_b) = \sum_k r_k \psi_k(\omega_a)\phi_k(\omega_b)$$

the solution is given by input-output relations in the Schmidt modes defined by $\{\psi_k\}$ and $\{\phi_k\}$

$$E_{1,k,out} = \cosh(r_k)E_{1,k,in} + \sinh(r_k)E_{2,k,in}^\dagger$$

$$E_{2,k,out} = \cosh(r_k)E_{2,k,in} + \sinh(r_k)E_{1,k,in}^\dagger$$

A. Christ, B. Brecht, W. Maurer and C. Silberhorn (2011)

Intensity crossover

We obtain

$$\left\langle E^\dagger(\omega_a')E^\dagger(\omega_b')E(\omega_b)E(\omega_a)\right\rangle$$
$$= f^*(\omega_a',\omega_b')f(\omega_a,\omega_b)$$
$$+g(\omega_a,\omega_b')g(\omega_a',\omega_b)$$
$$+g(\omega_a,\omega_a')g(\omega_b',\omega_b)$$

with

$$f(\omega_a,\omega_b) = \sum_k \sinh(r_k)\cosh(r_k)(\psi_k(\omega_a)\phi_k(\omega_b) + \psi_k(\omega_b)\phi_k(\omega_a))$$
$$g(\omega_a,\omega_a') = \sum_k \sinh^2(r_k)(\psi_k(\omega_a)\psi_k^*(\omega_a') + \phi_k(\omega_a')\phi_k^*(\omega_a))$$

A. Christ, B. Brecht, W. Maurer and C. Silberhorn (2011)

As the pump intensity is increased, we may not work with a simple two-photon state anymore. Autocorrelation contributions of the individual beams affect the signal, and distort its nonclassical frequency properties

We illustrate this crossover by plotting the field correlation function in frequency domain

$$\langle E^\dagger(\omega_a') E^\dagger(\omega_b') E(\omega_b) E(\omega_a) \rangle$$

vs the pump intensity $|\alpha|^2$

A. Christ, B. Brecht, W. Maurer and C. Silberhorn (2011)
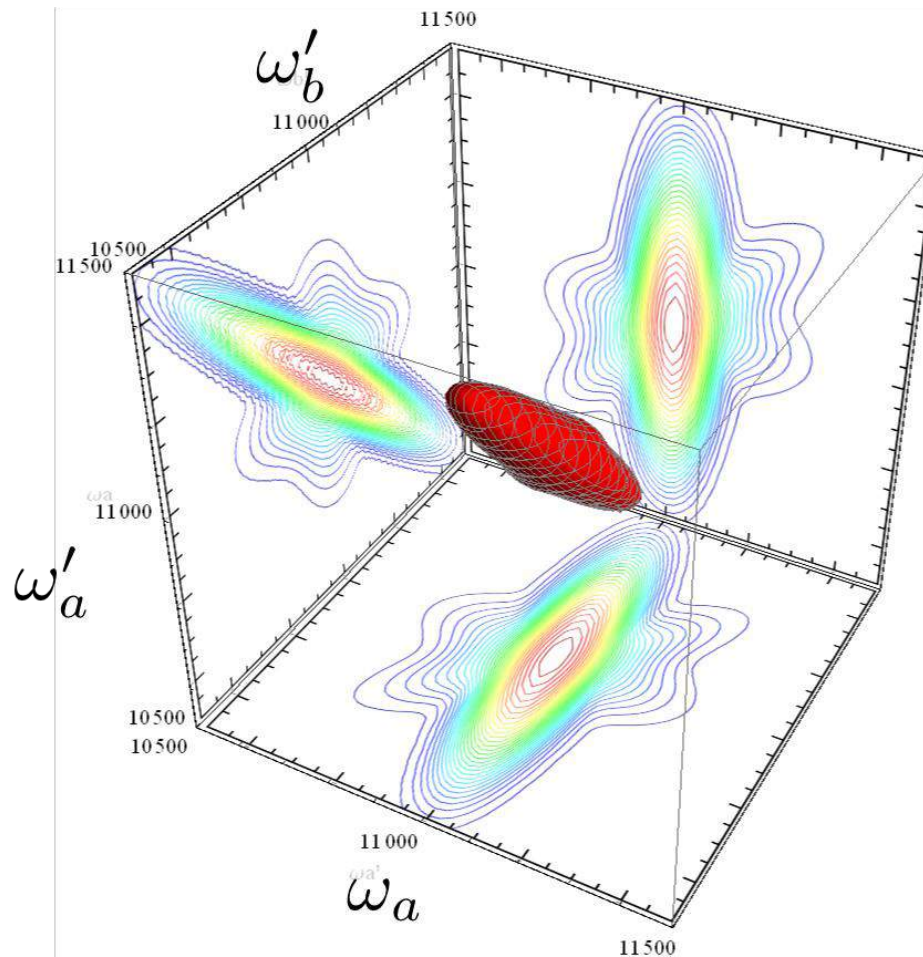
$$|\alpha|^2 = 0.00005$$

$$\langle E^\dagger(\omega_a')E^\dagger(\omega_b')E(\omega_b)E(\omega_a)\rangle$$

Intensity crossover
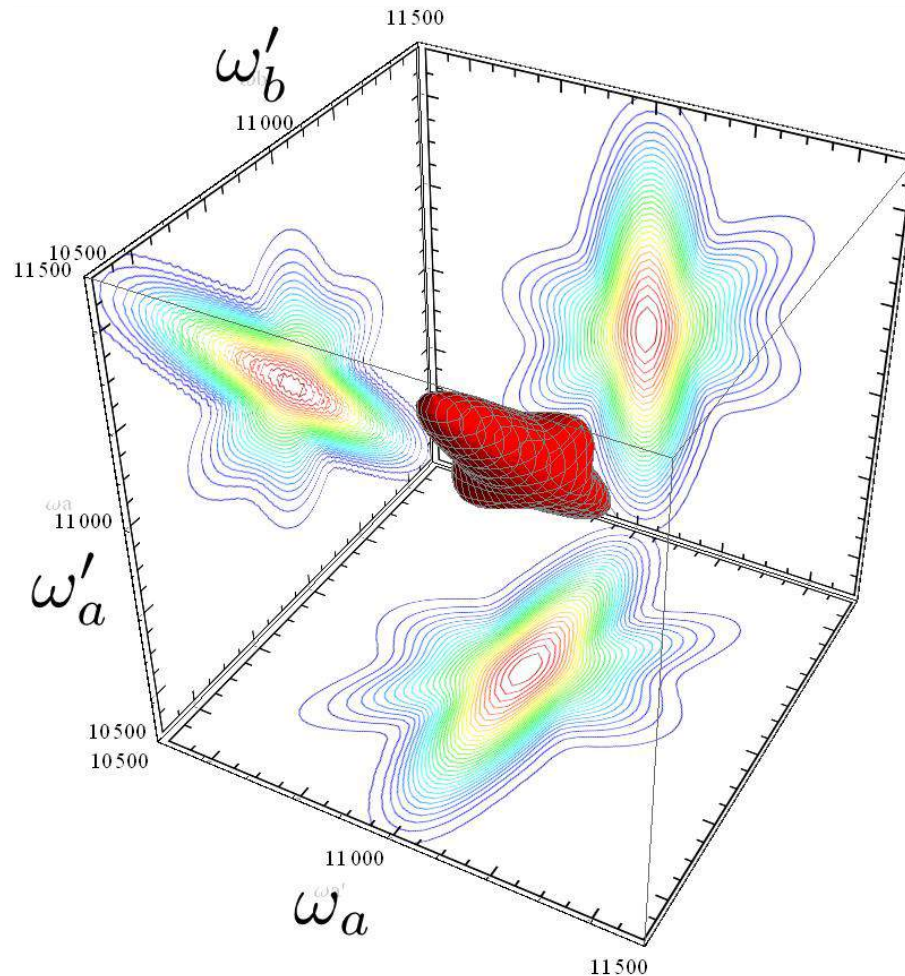
$$|\alpha|^2 = 0.0001$$

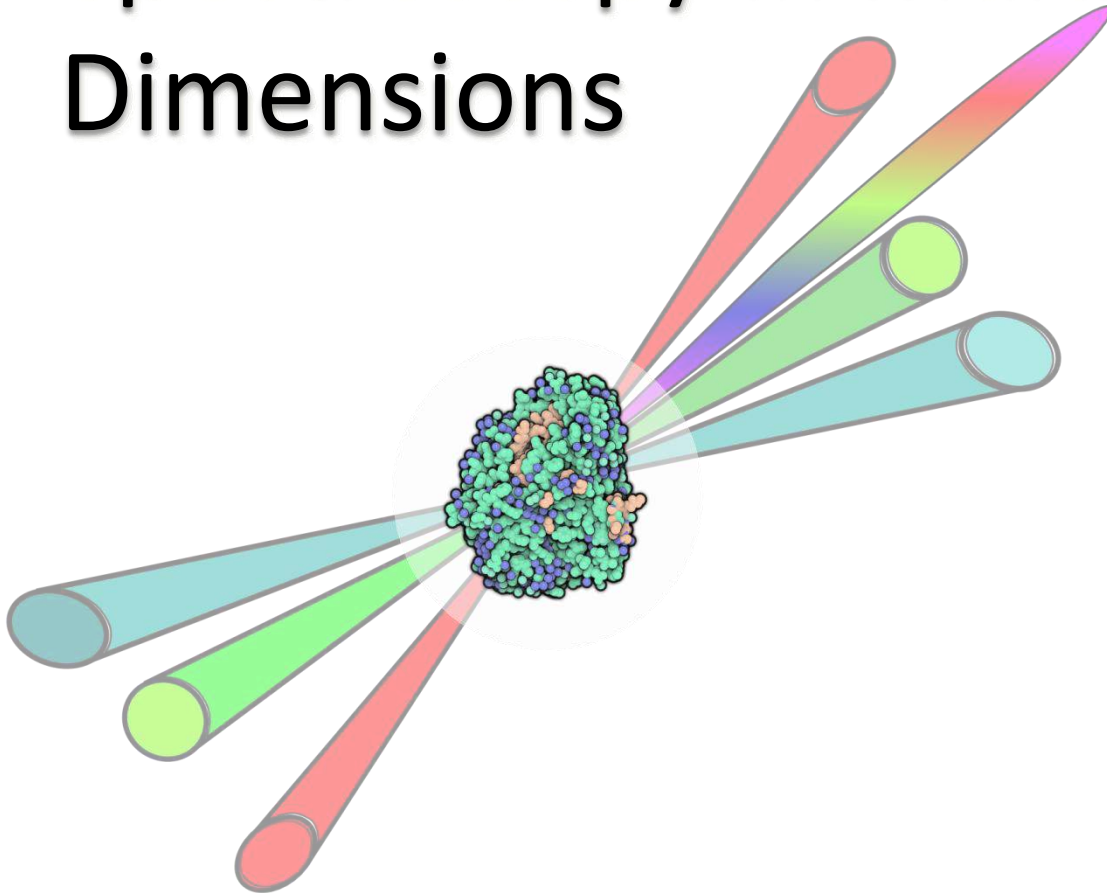$$\langle E^\dagger(\omega'_a) E^\dagger(\omega'_b) E(\omega_b) E(\omega_a) \rangle$$

Intensity crossover

$$|\alpha|^2 = 0.0005$$
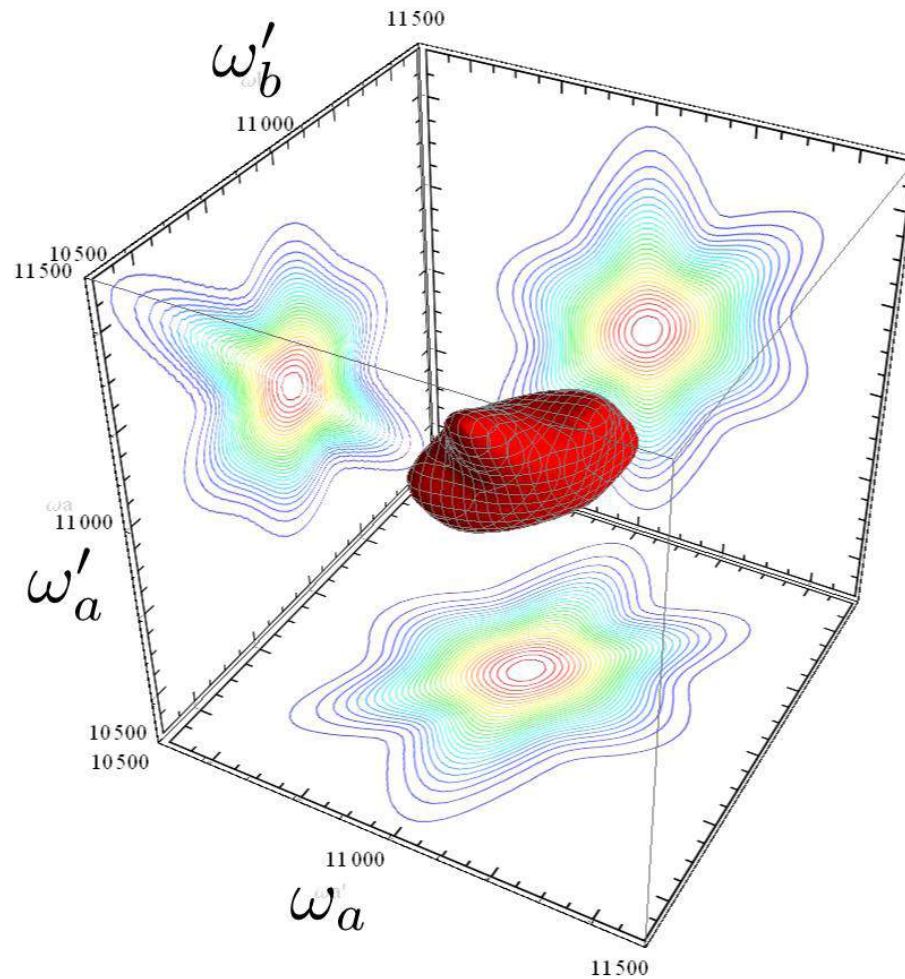
$$\langle E^\dagger(\omega_a') E^\dagger(\omega_b') E(\omega_b) E(\omega_a) \rangle$$

Intensity crossover

$$|\alpha|^2 = 0.001$$
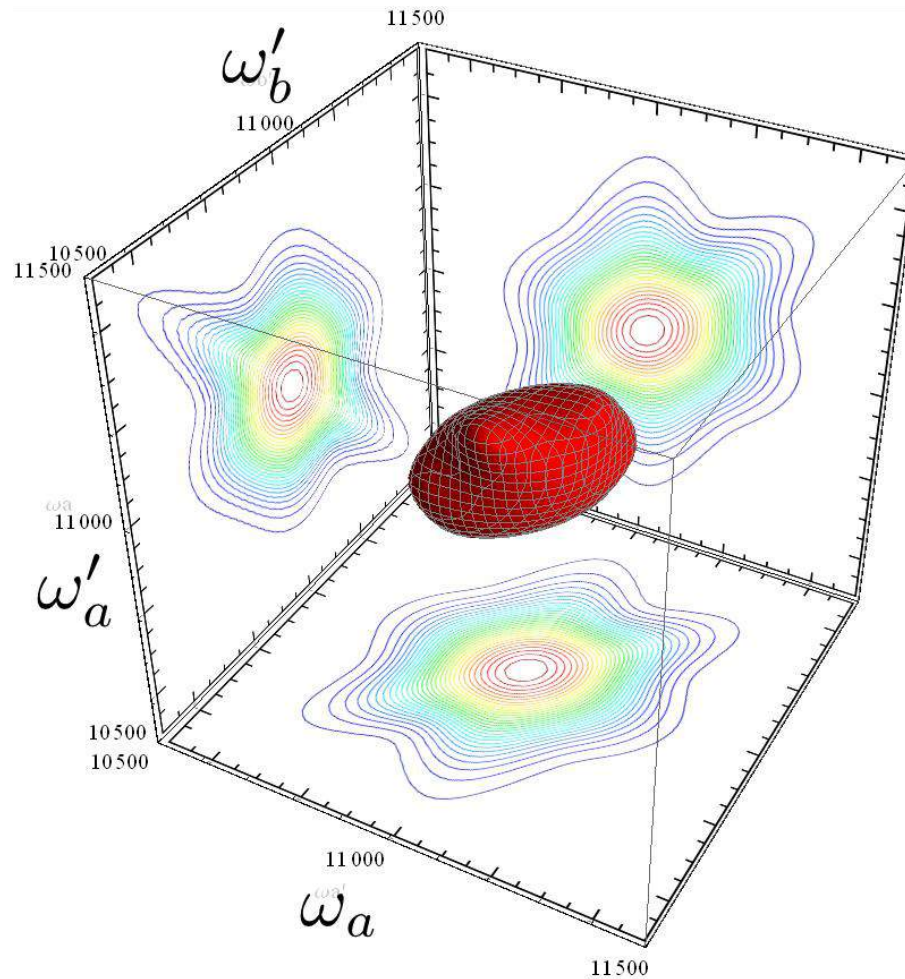
$$\langle E^\dagger(\omega_a')E^\dagger(\omega_b')E(\omega_b)E(\omega_a)\rangle$$

Outline

- Linear scaling of two photon absorption

- Manipulating Two exciton states of molecular aggregates with entangled photons

- Time and frequency resolution in broadband Raman spectroscopy with interferometric detection

- Raman spectroscopy with entangled light and coincidence detection

- Spectral diffusion in photon coincidence measurements

Coherent Nonlinear Optical Spectroscopy in Multiple Dimensions

$$P(\mathbf{r}, t) = P^{(1)}(\mathbf{r}, t) + P^{(2)}(\mathbf{r}, t) + P^{(3)}(\mathbf{r}, t) + ...$$

Nonlinear polarization $\quad P^{(n)}(\mathbf{r}, t) \equiv \langle\langle V | \rho^{(n)}(t) \rangle\rangle \equiv Tr[V \rho^{(n)}(t)]$

$$P^{(n)}(\mathbf{r}, t) = \int_0^\infty dt_n \int_0^\infty dt_{n-1} ... \int_0^\infty dt_1 S^{(n)}(t_n, t_{n-1}, ..., t_1)$$
$$\times E(\mathbf{r}, t - t_n) E(\mathbf{r}, t - t_n - t_{n-1}) ... E(\mathbf{r}, t - t_n - t_{n-1} ... - t_1),$$

$$S^{(3)}(t_3, t_2, t_1) = \left(\frac{i}{\hbar}\right)^3 \langle\langle V | \mathscr{G}(t_3) \mathscr{V} \mathscr{G}(t_2) \mathscr{V} \mathscr{G}(t_1) \mathscr{V} | \rho(-\infty) \rangle\rangle$$
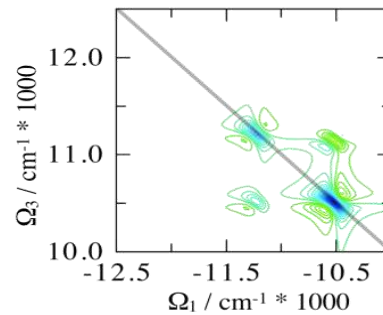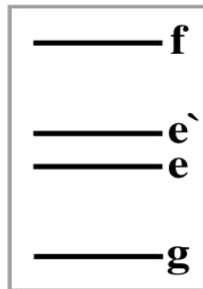
UNIVERSITY of CALIFORNIA · IRVINE

Two-level System

Anharmonic Oscillator
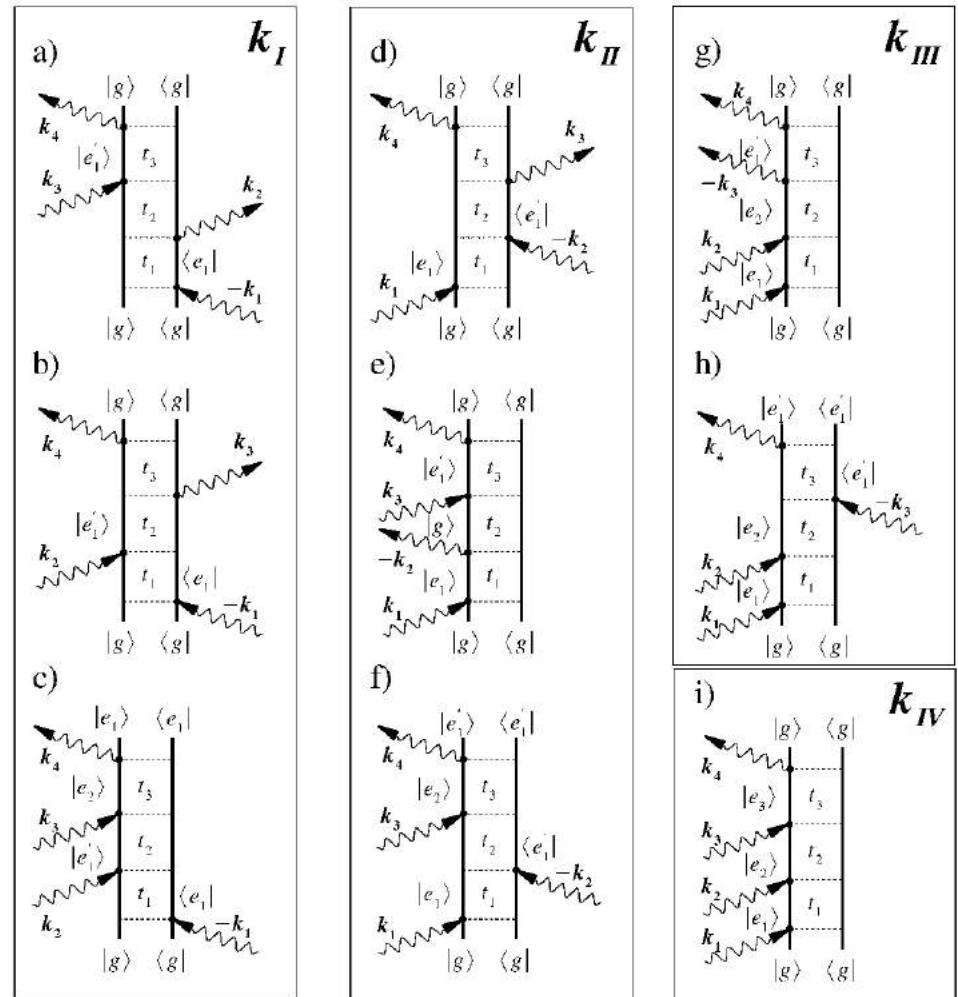
Coupled Two-level Systems

$$\mathbf{k}_I = -\mathbf{k}_1 + \mathbf{k}_2 + \mathbf{k}_3$$

$$\mathbf{k}_{II} = +\mathbf{k}_1 - \mathbf{k}_2 + \mathbf{k}_3$$

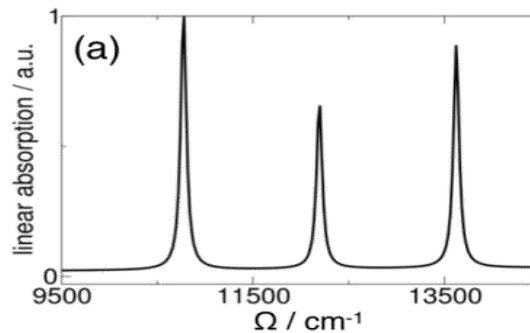$$\mathbf{k}_{III} = +\mathbf{k}_1 + \mathbf{k}_2 - \mathbf{k}_3$$

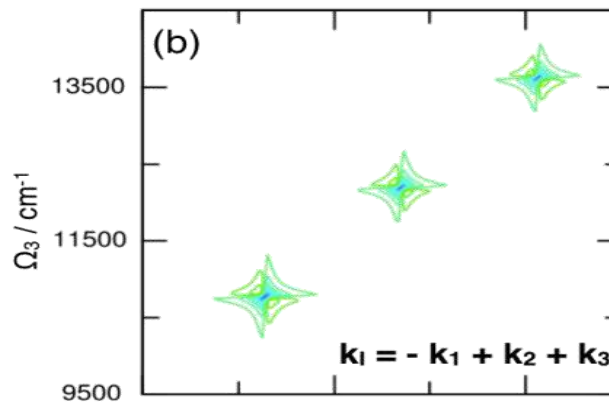$$\mathbf{k}_{IV} = +\mathbf{k}_1 + \mathbf{k}_2 + \mathbf{k}_3$$
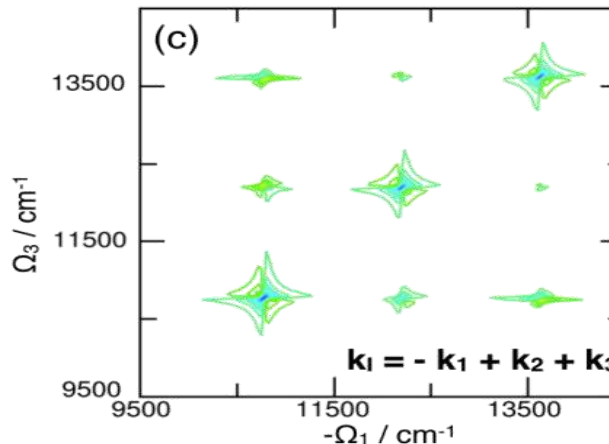
UNIVERSITY of CALIFORNIA · IRVINE

Linear Absorption

Photon Echo of Uncoupled Chromophores

Photon Echo of Coupled Chromophores

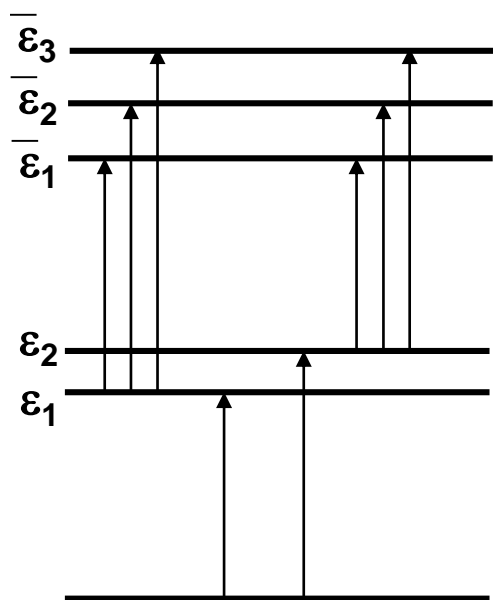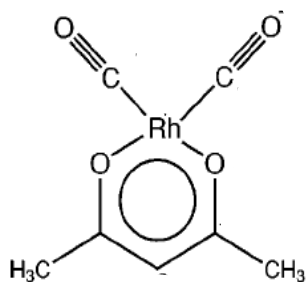
Cross peaks reveal distinct signatures of intermolecular couplings

2D spectra of coupled vibrations
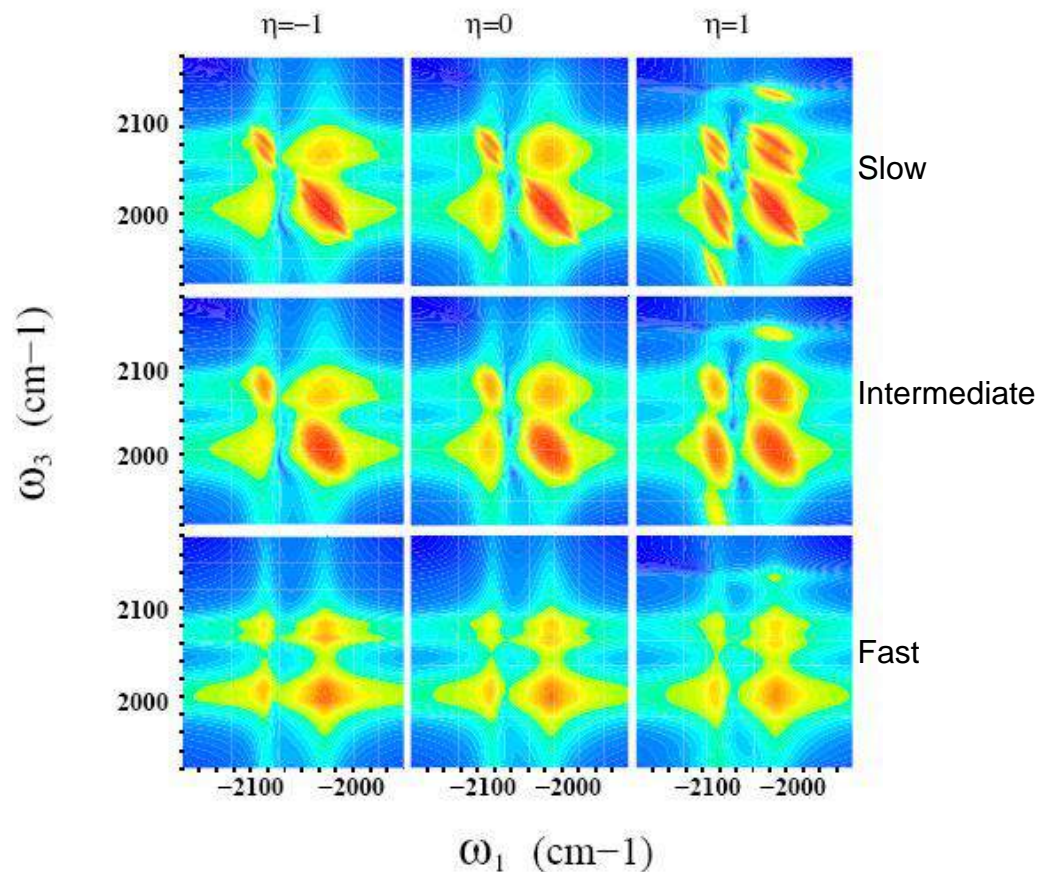
Lineshapes reveal correlated fluctuations

$-1 \leq \eta \leq 1$
$\eta = -1$ Anti-correlated
$\eta = 0$ Uncorrelated
$\eta = 1$ Fully-correlated

$\eta = -1$ $\eta = 0$ $\eta = 1$

Slow

Intermediate

Fast

ω_3 (cm^{-1})

ω_1 (cm^{-1})

$\bar{\varepsilon}_3$
$\bar{\varepsilon}_2$
$\bar{\varepsilon}_1$

ε_2
ε_1

$\varepsilon_1 = 2015$ cm^{-1} $\bar{\varepsilon}_1 = 4015$ cm^{-1}
$\varepsilon_2 = 2084$ cm^{-1} $\bar{\varepsilon}_2 = 4078$ cm^{-1}
                                    $\bar{\varepsilon}_3 = 4153$ cm^{-1}

FSRS with classical field

Classical FSRS with frequency dispersed detection

$$S_{FSRS}^{(c)}(\omega, T) = \mathcal{I} \int_{-\infty}^{\infty} \frac{d\Delta}{2\pi} \mathcal{E}_s^*(\omega) \mathcal{E}_s(\omega + \Delta) \tilde{S}_{FSRS}(\omega, T; \Delta)$$

Frequency dispersed detection. The detection window is a product of two classical field ar

Bare signal contains all the information about the matter

$$\tilde{S}_{FSRS}(\omega, T; \Delta) = \frac{4\pi}{\hbar} \int_{-\infty}^{\infty} \frac{d\omega_1}{2\pi} |\mathcal{E}_p|^2 \mathcal{E}_a^*(\omega_1) \mathcal{E}_a(\omega_1 - \Delta) e^{i\Delta T}$$

$$\times \left[F_i(\omega_1, \omega_1 - \Delta - \omega + \omega_p, \omega_1 - \Delta) + F_{ii}(\omega_1, \omega_1 + \omega - \omega_p, \omega_1 - \Delta) \right].$$

Matter correlation functions read off the diagrams

$$F_i(\omega_1, \omega_2, \omega_3) = \langle V G^\dagger(\omega_1) \alpha G^\dagger(\omega_2) \alpha G(\omega_3) V^\dagger \rangle$$

$$F_{ii}(\omega_1, \omega_2, \omega_3) = \langle V G^\dagger(\omega_1) \alpha G(\omega_2) \alpha G(\omega_3) V^\dagger \rangle$$